CARBON DIOXIDE SEQUESTRATION IN

IN SITU THERMALLY TREATED COAL

AND OIL SHALE FORMATIONS

by

Robert Lee Krumm

A dissertation submitted to the faculty of
The University of Utah
in partial fulfillment of the requirements for the degree of

Doctor of Philosophy

Department of Chemical Engineering

The University of Utah

December 2014

Copyright © Robert Lee Krumm 2014

All Rights Reserved

The University of Utah Graduate School

STATEMENT OF DISSERTATION APPROVAL

The following faculty members served as the supervisory committee chair and members for the dissertation of Robert Lee Krumm .

Dates at right indicate the members' approval of the dissertation.

Milind Deo	, Chair	1/12/2014 Date Approved
Eric Eddings	, Member	1/16/2014 Date Approved
John McLennan	, Member	1/14/2014 Date Approved
Philip Smith	, Member	1/16/2014 Date Approved
Jan Miller	, Member	1/16/2014 Date Approved

The dissertation has also been approved by Milind Deo Chair of the Department/School/College of Chemical Engineering and by David B. Kieda, Dean of The Graduate School.

ABSTRACT

With the consistently growing demand for liquid hydrocarbons there have been new technologies to meet those demands. Some of the new technologies focus on removing a resource from an underground repository using some form of thermal treatment to pyrolyze the material in the formation, either coal or oil shale, to create and produce hydrocarbons. In order to offset some of the carbon dioxide that would be produced in heating underground formations, the possibility of long-term sequestration was investigated for the remnants of said pyrolysis processes.

There are four mechanisms for subsurface storage of CO2: adsorption, mineralization, pore volume storage, and dissolution into the connate water.

Sequestration in a pyrolyzed coal seam relies heavily on the adsorption of CO_2 and is similar in concept to enhanced coal bed methane. Utah Skyline bituminous, Illinois Carlinville bituminous, and Wyoming North Antelope subbituminous coals were pyrolyzed to final temperatures of 325, 450, or 600°C with heating rates of either 10 or 0.1°C/minute. Adsorption isotherms, pore size studies, and permeability measurements were performed on the reacted and unreacted coals. The adsorption of CH_4 and CO_2 on the thermally treated coals increases with treatment temperature and is related to the pore size distributions. Pore size studies found a fraction of the surface area and micro- and mesopores can are attributable to residual tars. Permeability measured on the treated coals generally shows increases with treatment temperature.

Sequestration in a pyrolyzed oil shale demonstrates all four sequestration

mechanisms. Mineralization studies were carried out with a retorted Green River oil shale in the liquid and gas phase. Results of the mineralization study showed that the dissolution of pyrrhotite with siderite was the most prevalent path for CO_2 mineralization. The combined effects of mineralization, pore volume, and adsorption were also simulated and found the most common result to be 40 kg/tonne of CO_2 stored.

To Dr. James “Jimbo” Duane – you taught me the importance of doing more with my life than existing in mediocrity. I would like to also thank you for teaching us the difference between good work and the preferred projectile of orangutans.

“Don’t panic”

Douglas Adams

The Hitchhiker’s Guide to the Galaxy

TABLE OF CONTENTS

Appendices

LIST OF FIGURES

LIST OF TABLES

ACKNOWLEDGEMENTS

First, I would like to acknowledge the sources of funding for these projects, the United States Department of Energy and American Shale Oil, LLC. I would also like to thank my advisor, Prof. Milind Deo, for giving me the opportunity to do this research and for his seemingly endless patience. I would like to list all of the people who were an instrumental help with getting this work done: Clay Jones, Chris Clayton, Dave Wagoner Sr., Ryan Okerlund, Dana Overacker, and my committee. I would like to thank Keith Greaves for his help with the isotherms. Exceptional support was given by Dr. Keith Gneshin, your help and brilliance helped define where this research should go. Dr. Prashanth Mandalaparty, without your input I would have been lost with the geochemistry project. I want to thank Trevor "Boots" Stoddard, Justin "Herbie" Wreidt, and Dr. John McLennan for their auxiliary support. Mostly, I would like to acknowledge my fiancé, Melissa Thies, for being so supportive, especially this last year. We did it.

PART I

CO_2 SEQUESTRATION IN THERMALLY TREATED UNDERGROUND COAL FORMATIONS

LEAD-IN

This is the first part of this two part dissertation. This first part focuses on the potential of CO_2 sequestration in an unmineable coal seam that has undergone pyrolysis. The concept of injection of CO_2 into a pyrolyzed coal seam is similar to that of enhanced coal bed methane. Although both sections in this dissertation focus on CO_2 storage in the remnants of a pyrolysis process, the storage of CO_2 in a spent coal seam differs from storage in a spent oil shale formation in that it relies mostly on the adsorptive capacity of the pyrolyzed material. This section takes special care to address adsorption and present a comprehensive analysis of factors affecting adsorption. Like the later work, this part stands as a unique work related to the other.

CHAPTER 1

INTRODUCTION

The intent of this part in this dissertation is to describe the adsorption of methane and carbon dioxide on a coal that has undergone pyrolysis with slow heating rates. This work supplements the much larger underground coal thermal treatment program underway at the University of Utah. Underground coal pyrolysis is a process similar to *in situ* oil shale production wherein heat is applied to deep coal formations to produce light hydrocarbons. Like enhanced coal bed methane, the injection of CO_2 postthermal treatment can improve hydrocarbon recovery and serves as a means of carbon sequestration. Little information exists pertaining to coals pyrolyzed to temperatures expected with this process. This work specifically examines the development of meso- and micropores and their influence on methane and carbon dioxide adsorption and permeability on thermally treated coals. This work also examines where some of the meso- and micropores reside and the means of their formation. With respect to aforementioned pores, this volume attempts to address the following two questions: "what is the extent of mesopore- and micropore development coals thermally treated at slow heating rates" and "if meso- and micropores are being created, are the developments in the coal matrix or in residual tars?" This volume also attempts to show the relationship between small pores and properties such as surface area, permeability, and adsorption.

This section will give a short background into the UCTT process, the technologies that comprise the process, and how CO_2 sequestration fits into the UCTT process.

Underground Coal Thermal Treatment

Underground coal thermal treatment (UCTT) is a process that uses a heat source to pyrolyze a deep and unmineable coal seam to produce hydrocarbons with higher hydrogen to carbon ratios than the original coal. The UCTT process draws similarities to the *in situ* pyrolysis of oil shale in that both require the use of a heating well to retort the oil shale and a production well to extract the hydrocarbons. UCTT also draws some parallels to underground coal gasification (UCG). The main difference between UCTT and UCG is that with UCTT there would be insufficient oxygen to support gasification reactions and it relies primarily on pyrolysis reactions. An image depicting UCTT can be found in Figure 1.

With increasing environmental regulations, the future of conventional coal utilization (mining and burning) in the United States seems limited. Past reductions on the amount of permissible levels of mercury and sulfur emitted from coal power plants have resulted in expensive retrofits and changing feedstocks. In effort to control the amount of carbon dioxide being emitted, imposed greenhouse gas regulations may make coal economically unattractive.

UCTT, UCG, and enhanced coal bed methane (ECBM) provide alternative means of utilizing coal. All three of the aforementioned processes will be discussed later but what is similar between all three of them is that they do not require mining of the coal.

An advantage of extracting products from coal without mining is that none of these processes combust the coal releasing carbon dioxide. Furthermore the remaining formations after UCTT, UCG[1], and ECBM[2] can be used for long-term CO_2 sequestration.

There are several advantages and disadvantages of UCTT. Two of the advantages

were already mentioned: not combusting the coal and potential for CO_2 sequestration. Other advantages include producing a product with higher hydrogen to carbon ratio, reduced sulfur emissions, and low risk of heavy metal contamination of water. Some of the disadvantages facing UCTT are similar to those facing other *in situ* conversion technologies. These difficulties include the high amount of energy input required for thermal conversion and that not all of the available energy is recovered and the technical challenges associated with the implementation of any new technology. There is also the difficulty of optimizing a pyrolysis process; the products that can be formed vary depending on heating rate, treatment temperature, and residence time.[3, 4]

The UCTT process is targeted for deep and unmineable coal seams that contain high amounts of volatiles. Ideally, the coal used for UCTT should have low water saturations as the removal of the water by heating has an energy cost associated with it. Like *in situ* oil shale production, the heating rates expected with UCTT are very slow, sometimes as slow as a few degrees centigrade per day with pyrolysis reactions coming to completion at the low end of temperatures needed for pyrolysis[5]. Other investigators[6, 7] have previously or are currently working on the technical aspects of underground coal pyrolysis by documenting the nature of the products and physical changes to the coal structure. Expected changes in the coal structure are increases in porosity[7], increases in permeability[8, 9], and a reduction in the hydrogen to carbon ratio.

Role of CO_2 Sequestration to UCTT

Carbon dioxide sequestration plays a crucial role to the UCTT process. If carbon emission regulations come to fruition in the United States, it may be advantageous to offset some of the carbon emitted heating up the coal formation by permanently

sequestering it. This study helps prove the concept that CO_2 could be stored in the pyrolyzed coal.

The pyrolysis of coal results in several changes to the coal. Some of the changes are that the coal could show an increase in meso- and micropores as well as an increase in adsorptive capacity[10]. The purpose of this dissertation is to quantify the changes in meso- and micropores and determine how those changes affect the overall adsorption of methane and CO_2. Some of the other information produced by this study, such as permeability measurements, can be useful in modeling mass transfer during the UCTT process. The main goal of this volume of this dissertation is to provide high pressure adsorption isotherms under reservoir temperatures.

Adsorption Isotherms

Adsorption is significant to the chemical industry and it is often coupled with a desorption step in order to regenerate the adsorbent. Industrial applications of adsorption range from the purification of gases to catalysts to pollution control. Being such an important process, the phenomena of adsorption has been extensively investigated with a myriad of books and papers addressing the topic.[11 12 13 14]

Adsorption is the phenomena by which fluid phase molecules adhere to the surface of a solid phase and is dependent on pressure, temperature, and the composition of the fluid phase. The fluid phase molecule interacting with the solid phase is referred to as the adsorptive, while the solid phase is referred to as the adsorbent. There are two different types of sorption: chemisorption, in which the adsorptive is permanently attached to the solid, and physisorption, where the adsorptive is in a thermodynamic equilibrium between adsorption and desorption. Physisorption is the focus of this

research. The adherence of molecules to the surface is often attributed to Van der Waals or dispersion forces.[15] With physisorption, the sorbate structure can be monolayer, multilayer, or a pore fluid.

Volumetric measurement is one of the most common and the oldest means to measure isotherms.[15] Some of the advantages of measuring isotherms volumetrically are simplicity and that it is a very established method.[16] Disadvantages for volumetric isotherm measurements are that it provides little information about the adsorption kinetics and that it requires a large sample size. Another disadvantage is the longer amount of time required for the adsorptive to come into equilibrium with the adsorbate. Volumetric isotherm measurement provides nearly identical measurements to gravimetric isotherm measurements with the main discrepancies being pressure transducer error at high pressures.[17]

The nature of small pores on the adsorptive, especially with activated carbon[18], can facilitate pore condensation. This phenomena is more noticeable at low temperatures or high pressures.[19] As multiple layers of adsorbate build on the interior surfaces or pores, a critical point is reached corresponding to the overlapping of Lennard-Jones potentials, depending on the size and diameter of the pore, where the pore fills with a condensed liquid. It should be noted that pore condensation occurs below the saturation point of the adsorbate. Pore condensation is the basis for various pore size distribution techniques such as Barrett-Joyner-Halenda[20] (BJH) and density functional theory (DFT).[18] In this study, volumes of small pores are quantified at low pressures and temperatures according to the aforementioned techniques. The effects of small pores are also noticeable when measuring isotherms at high temperatures and pressures[21].

Nature of Pores

It is commonly understood that small pores in carbonaceous material exhibit a slit geometry. Slit geometries are defined as having lengths much longer than diameters. In fact, the aspect ratio (length v. width) is so large that they are often represented as two infinitely long parallel plates.

One feature that makes this work is unique is that it examines the nature of the pores on a coal pyrolyzed with slow heating rates. Pyrolysis products may not completely volatilize from the surface of coal while it is being heated. Products with higher boiling points, and by extension higher carbon numbers, may remain on the surface of the coal. Volatilization of lighter products may result in fractures and small pores in surface tars; similar to cracks in clay after it has dried out. These newly formed pores can serve as adsorption sites thereby increasing the adsorptive capacity of the coal. This works tests the aforementioned hypothesis by implementing a novel technique to estimate the effect of these pores.

If pores can be formed in residual hydrocarbons, the implications would apply to all sorts of *in situ* thermal processes: oil shale, UCG, and of course UCTT. This phenomenon would not be restrictive to CO_2 sequestration but also to mass transfer in the coal[22] and the extraction of pyrolysis products.

Summary

The study of adsorption and the concepts of relating adsorption to pore sizes and determining how the pores exist on thermally treated coals is important not only to the scope of UCTT but possibly to other unconventional resources. A brief description of the UCTT process was given and comparisons were made to other *in situ* processes. Since

UCTT is in its relative infancy relative to processes like *in situ* oil shale and ECBM, lessons learned from the more developed processes can be co-opted to UCTT. The role of CO_2 sequestration to UCTT was outlined and detailed further with an examination into adsorption. This dissertation examines isotherms on coals treated with slow heating rates and the nature of pores with the hope of providing some useful insight into pyrolysis processes that use slow heating rates not just limited to UCTT.

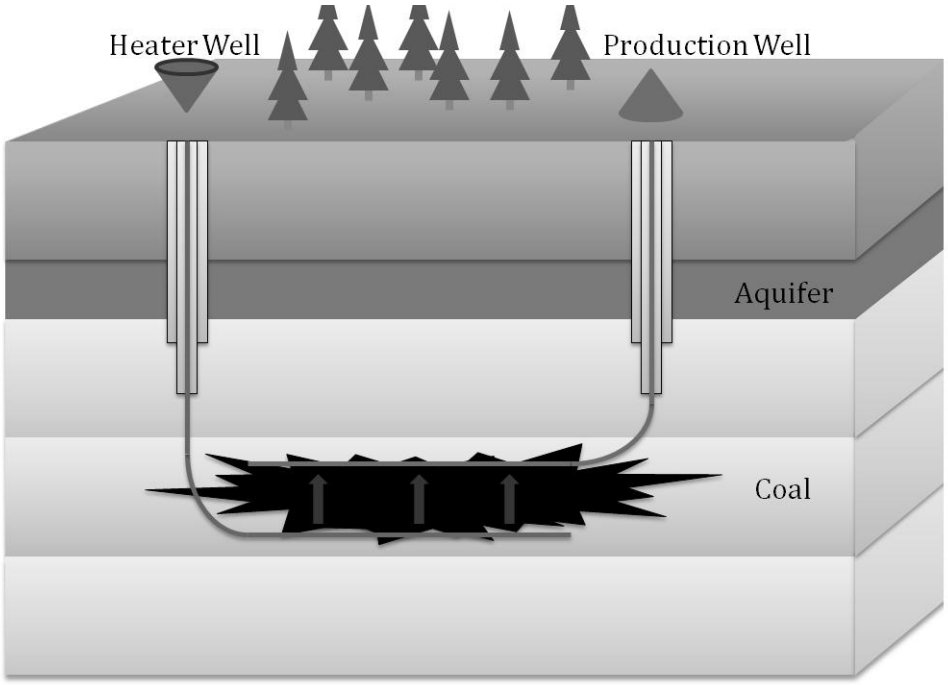

Figure 1: Illustration of the UCTT process showing a directional heater well and a production well in an unmineable coal seam.

CHAPTER 2

LITERATURE REVIEW

Overview

The means by which adsorption is typically characterized is with isotherm measurements, through which the system temperature remains constant while the quantity of the adsorbed phase is measured over a range of pressures. The foundation of adsorption measurements is the work by done by Langmuir.[23] There are essentially two methods[17] for determining adsorption isotherms: gravimetrically[24-29] and volumetrically.[16, 30-32] There is little published material pertaining to isotherm measurements on pyrolyzed coal[33] as it pertains to the UCTT process, however there is extensive isotherm research on fresh coals relating to ECBM recovery.[34-37]

ECBM recovery is an established technology with Amoco filing patents for the process in the 1980s and a pilot plant coming online in the San Juan basin in 1993. ECBM is the process by which CO_2 is introduced to a coal seam via an injection well and methane being recovered with a production well. The ECBM process relies on the adsorbed methane molecules being displaced by the preferentially adsorbed CO_2 molecules.[38] In the effort to improve the ECBM process, there have been copious research efforts regarding isotherms of CO_2 and CH_4 on coal.

Arri et al.[39] performed methane-nitrogen and methane-CO_2 sorption experiments on a wet Fruitland (San Juan basin) coal sample under reservoir temperatures and pressures. Their research was conducted in conjunction with the other works being done

by Amoco regarding ECBM. They found that the extended Langmuir isotherm model fit well for data at pressures less than 1000 psi. The raw data from their experiments show that CO_2 is preferably adsorbed over methane and that methane is preferably adsorbed over nitrogen. Their data also show that, in the presence of high concentrations of nitrogen in the fluid phase, methane will desorb from coal.

The following year, Hall et al.[35] expanded on the research of Arri et al. by taking isotherms on wet Fruitland coal at pressures up to 1800 psi. Hall et al. concluded that the ideal adsorbed solution (IAS) and the equation-of-state (EOS) models provided better agreement with the isotherm data than the Langmuir model.

In 2001, the National Energy Technology Laboratory (NETL) released a report[37] assessing the use of ECBM as a means of geologic sequestration of anthropogenic CO_2. The data presented in the report showed that for a variety of wet coals, CO_2 adsorption is preferred over methane at ratios over 4:1. The data also showed that the CO_2/CH_4 adsorption ratio increases when the coal is dry.

Research published by Bae and Bhatia[40] provided isotherms for methane and CO_2 on Australian coals at high pressures. Their research took into account the effect of swelling at high pressures. The researchers concluded that the excess amount of adsorbed CO_2 and methane can be characterized by the Tóth[41] equation. They also found that for the sake of ECBM, methane recovery efficiency decreases at pressures greater than 10 MPa. The Tóth equation provides a better fit for adsorption for a variety of carbon based adsorbents and for sub-monolayer adsorption.[42, 43] Li et al.[36] provided extensive isotherm measurements on Chinese coals. The data presented by Li et al. agree with data from Bae and Bhatia in that the CO_2 adsorption capacity decreases at pressures exceeding 10 Mpa.

Siemons and Busch[44] volumetrically measured supercritical CO_2 isotherms and addressed some of the complications associated with adsorption measurements in or near the supercritical region. One of the most important considerations with data near the supercritical boundary is to have a good equation of state to determine the density of the CO_2; they concluded that the Span and Wagner[45] equation of state was sufficient. Additionally, Siemons and Busch found that swelling can be a source of error in experimentation.

Ozdemir et al.[46] addressed the issue of coal swelling during isotherm measurements. Ozdemir et al. concluded that the previous isotherm models fail when CO_2 is adsorbed on coal at high pressures and presented an equation to correct for the volumetric effects of swelling.

Activated carbons derived from coals for use as an adsorbent have been thoroughly studied for separation processes ranging from purification of gases to liquid phase extraction.[47-54] The pyrolyzed coals produced by UCTT will have similar properties to activated carbons produced from coal. Data from Yang and Saunders[55] shows that thermal treatment of a Montana lignite and Pittsburgh bituminous increases its adsorption capacity. Moroto-Valer, Tang, and Zhang[10] showed how thermal activation of Anthracites increases its adsorption capacity of CO_2. Moroto-Valer et al. attribute the increase in storage capacity to the increase in microporous surface area. Moroto-Valer et al. also point out that an increase in micropores does not necessarily mean that there will be an increase in CO_2 adsorption capacity but rather the sizes of micropores also plays a significant effect. They evidenced this claim by showing the CO_2 capacity of an activated carbon with a surface area of 540 m^2/g having an adsorption capacity of 65.7

mg-CO_2/g-sorbent and another activated carbon with a surface area of 1071 m^2/g having an adsorption capacity of 40.0 mg-CO_2/g-sorbent. Furthermore, Moroto-Valer et al. showed that pore development is highly dependent on the temperature and duration of thermal treatment; in some instances the microporous surface increases and then decreases with duration of thermal treatment. Gavalas et al.[56] showed micropore volumes before and after pyrolysis for a high volatile bituminous coal and a subbituminous coal. Gavalas et al. used BJH to determine the micropore distribution and measurements were conducted with nitrogen, which has been noted to produce troublesome data when used for this application.[57]

Bae et al.[33] provided limited CO_2 isotherm measurements on coals treated under similar thermal treatment conditions to those used in this research. The pyrolysis conditions for their coal was 500°C for 5 hours with a 30°C/min heating ramp rate. They showed that at low pressures (>0.03 Bar) pyrolyzed coal provides approximately twice the CO_2 adsorption capacity of fresh coals. They also showed that the surface area of the pyrolyzed coals increased by 50-60% over the fresh coals, an effect also seen in early adsorption experiments with the UCTT project.

Current State of the Art of UCTT

Growing global demands for hydrocarbons has driven interest into alternative sources such as oil shale, underground coal gasification (UCG)[58], enhanced coalbed methane (ECBM)[59] and underground coal thermal treatment.[60] UCTT draws many analogues to *in situ* oil shale pyrolysis and underground coal gasification in that they all use heat to recover resources without mining. With increasing regulations on conventional coal operations, UCTT may serve as a viable alternative to recover energy

from this immense resource. The UCTT process is centered on applying heat to a deep, unmineable coal seam to pyrolyze the coal and produce hydrocarbons.[61] Advantages of the UCTT process include producing a product with a higher H:C ratio than the original coal. Similar to ECBM, the remaining coal can be used as a repository for CO_2; since pyrolysis increases the porosity of the coal, it is expected that the storage potential of the remaining material would have an improved CO_2 capacity over that of the fresh coal. Furthermore, the injected CO_2 may also serve the purpose of displacing some of the remaining hydrocarbons.

Some of the advantages of UCTT are the promises of reduced environmental impact as well as providing the potential of a high capacity repository for the storage of anthropogenic CO_2. There are some technical challenges that are also associated with this technology. Fortunately, other means of underground treatment can provide the basis of *a priori* knowledge, and thereby provide a foundation for this technology.

Coal Bed Methane

The term coal bed methane can be used as a definition of the process of extracting light hydrocarbon gas from coal seams or as a reference to the product itself, the proceeding refers to the former. CBM has long been used in the United States as an energy source with an 80 year history[62] and an estimated 749 trillion cubic feet of untapped gas in place.[63] CBM gas is stored primarily via adsorption with some of the gas being stored in the free volume in the coal cleats or as solution gas dissolved in water in the pores of the coal.[64] Gas is usually produced by desorbing from the surface of the coal which is done by reducing the pressure of the reservoir. Desorbed gas migrates to the wellbore through high permeability cleats. Stresses on the coal seam can affect the

permeability of the formation due to the compressive and malleable nature of coal; for example, deeper coals have more hydrostatic stress and typically have less permeability than shallower coals.[65]

ECBM differs from CBM in that a gas, typically CO_2, is injected with the intent of forcibly desorbing the methane from the coal surface and sweeping that methane towards a production well. CO_2 sequestration via ECBM has been touted as feasible means of storing anthropogenic CO_2.[66] In this way, the UCTT process may be more relatable to ECBM than CBM with regards to CO_2 injection post treatment.

Underground Coal Gasification

Underground coal gasification has parallels with the UCTT process in that both attempt to heat a formation of coal *in situ* and remove products. Gasification is the process where a carbonaceous fuel sources is heated and reacted with water and oxygen to produce methane, hydrogen, and carbon monoxide. Underground coal gasification requires a linked network of injector wells and production wells. Injector wells introduce oxygen to a heated formation for the gasification process; connate fluids provide the water. Underground coal gasification dates back to the 1930s in the former Soviet Union[58] and the 1940s in the United States. UCG projects are currently being proposed or implemented worldwide. There are a few issues with UCG such as process economics and the environmental impact, *e.g.*, groundwater contamination.

In situ Oil Shale Pyrolysis

Underground oil shale pyrolysis is similar to UCTT in that both processes involve drilling wells to apply heat to geologic formation to pyrolyze the contents and produce

light hydrocarbons via a production well. *In situ* pyrolysis of oil shale is not a new concept, the origins of this technology date to the 1970s. Despite past technological and economic issues, there has been a resurgence of interest into *in situ* oil shale pyrolysis. New technology such as the Red Leaf "Eco-Shale"[67] hybrid retorting process or the American Shale Oil method of using refluxing oil as a heat transfer medium[68] have reinvigorated prospects. The Unites States is estimated to have over $2x10^{12}$ barrels-worth of oil shale[69] a large portion of which resides in the Green River formation.

With the similarities between oil shale and UCTT there are shared technological difficulties. Some of the issues being addressed with *in situ* oil shale are preventing groundwater contamination[70] and subsidence.[71]

In situ Coal Pyrolysis

There is little information pertaining to the pyrolysis of coal with slow heating rates such as those found with the UCTT process. Bae et al.[33] provided limited CO_2 isotherm measurements on coals treated under similar conditions to those about to be examined in this research. The pyrolysis conditions for their coal was 500°C for 5 hours with a 30°C/min heating ramp rate. They showed at low pressures (>0.03 Bar) that pyrolyzed coal provides approximately twice the CO_2 adsorption capacity of fresh coals. They also showed that the surface area of the pyrolyzed coals increased by 50-60% over the fresh coals, an effect also seen in early adsorption experiments with the UCTT project.

There are a few patents relating to UCTT. Karanikas et al.[6] outline some of the products expected from heating a coal seam *in situ*. Vinegar et al.[8] demonstrated increases in porosity in an *in situ* pyrolyzed coal seam.

The Effects of Meso- and Micropores on Adsorption

Mastalerz et al. [72] investigated the effects of meso- and micropores on coal and how they affect CO_2 sequestration. The authors investigated Danville, Springfield, Buffaloville, Upper Block, and Lower Block coals. All of the coals studied are Pennsylvanian in age and from the Illinois Basin. Vitrinite reflectance for the coals ranged from R_o = 0.52-0.62% and moisture content ranges from 8.74 to 13.29%. Samples from each coal lithotype (vitrian, clarain, and fusain) were manually identified and analyzed for vitrinite, liptinite, inertinite, and mineral matter.

Samples from each coal lithotype were analyzed for meso- and micropores using a combination of low pressure nitrogen and CO_2 isotherms. The measurements were carried out using a Micromeritics ASAP-2020 porosimiter and surface area analyzer. Samples were ground to approximately 250μm and were cone-and-quartered. The authors used the International Union of Pure and Applied Chemistry standards[73] which defines mesopores having an aperature of 2-50nm and micropores having a diameter <2nm. Low pressure nitrogen adsorption measurements were done at 77.35K; CO_2 measurements were done at 273.1K. Samples were off-gassed under vacuum for 960 minutes at 110°C. The minimum equilibration interval was 30 seconds with a pressure tolerance of 5 mmHg. Data from the CO_2 isotherms were regressed with Dubinin-Radushkevich (D-R) and Dubinin-Astakhov (D-A) to determine micropore surface area and micropore volumes, respectively. High pressure CO_2 adsorption isotherms were performed at a commercial laboratory using the methodology outlined by Mavor et al.[30]. All coal samples were allowed to come to moisture equilibrium before isotherms were measured. High pressure adsorption isotherms were done at 17°C. Most of the low

pressure nitrogen adsorption isotherms showed a Type IV pattern with hysteresis occurring at relative pressures between 0.45 and 0.95. It was also found with the low pressure nitrogen measurements that the fusain adsorbs less nitrogen than the vitrain or clarain. Measured BET surface areas ranged from 10 (Springfield-vitrain) to 115 m^2/g (Lower Block-vitrain A). The quantity of nitrogen adsorbed ranged from less than 10 cm^3/g with the Springfield coal to almost 80 cm^3/g with the Lower Block coal. The most prominent mesopores occurred at sizes ranging from 5-10nm. Mastalerz et al. argue that even minor differences in the vitrains [let alone other lithotypes] can have a profound effect on the measures pore volumes and surface areas.

The differences in the adsorptive capacity of the vitrains were also observed in the micropore measurements done with CO_2 as the adsorbate. It was also noticed that the there was an increase in the micropores with an increase in vitrinite content. High pressure CO_2 adsorption measurements showed a correlation between adsorptive capacity and BET/BJH/micropore values. Generally, the more mesopores in the coal sample, the larger amount of CO_2 was adsorbed. After the high pressure experiments, some of the coals were re-analyzed for micropores and mesopores. This postanalysis revealed that the BET surface area and the mesopore volumes both decreased as a result of the coal being exposed to high pressure CO_2. The largest difference was noticed in the vitrain of the lower block coal. Mastalerz et al. conclude that larger amounts of vitrain will cause the coal to have a higher adsorptive capacity; furthermore, the more of the vitrain that is collotelinite, the greater the adsorptive capacity. They also concluded that there is a correlation between the BET surface area, micropore volume, and mesopore volume on the amount of CO_2 that can be adsorbed at high pressures with the highest degree of

correlation being with mesopore volume.

Clarkson and Bustin[21] attempted to identify the correlation between micropore volumes and CH_4 or CO_2 adsorption capacities on coals from the Cretaceous Gates Formation in British Columbia. The coals had large differences in maceral composition and represented three different lithotypes; bright, banded bright, and dull. Samples were crushed and sorted according to mesh size, <60(0.25mm), 60 to 20(0.841mm), 20 to 8(2.38mm), and 8 to 4(4.75mm). The smallest and largest diameters were used for the isotherm analysis. Low pressure isotherms were measured using a Micromeritics ASAP2010 with CO_2 isotherms at 273K. Samples were degassed at 100°C for at least 12 hours. The Dubinin-Radushkevich method was used to correlate the low pressure isotherm to micropore volumes.

Clarkson and Bustin also performed high pressure adsorption measurements using both methane and CO_2 as the adsorbate. The apparatus used was similar in design to that used by Mavor et al.[30] Before the samples were loaded into the isotherm apparatus, the samples were dried in an oven at 110°C. Adsorption isotherms were done on moisture equilibrated coals. The data collected with the high pressure measurements were reduced using the Langmuir equation and the Dubinin-Astakhov equation.

Low pressure adsorption data showed a Type II or a Type IV isotherm with the coals having higher percentages of vitrinite showing less hysteresis than coals with low amounts. From the hysteresis on the low pressure isotherms, the authors were able to conclude that the pores were of a slit shape. The authors also hypothesize that the coal may be swelling due to adsorption even during low pressure measurements. Clarkson and Bustin showed that the BET surface areas are higher for dull coals and lower for the

light and light-banded coals. BJH calculations also showed that the dull coals have larger mesopore volumes than the light and banded coals. It can be implied from the nitrogen adsorption measurements that the mesopores have a significant contribution to the overall surface area of the samples.

The high pressure isotherms showed little difference based on the sieve size used. Clarkson and Bustin also observed that much more CO_2 can adsorb on the coals than methane. The preferential adsorption of CO_2 over methane is a recurring trend in literature.[30, 37] A good fit for the adsorption data was achieved with the Langmuir equation; although a better fit was accomplished with the D-A equation. In their analysis, the authors fail to point that the better fit with the D-A may have been that there are three parameters to fit compared to the two parameters with the Langmuir equation.

Clarkson and Bustin make a case that the meso- and micropore volumes can be used to predict the adsorptive capacity of coal. They noticed that there is an increase in the maximum theoretical adsorptive capacity with an increase in observed micropore volume. This trend held for measurements with both CH_4 and CO_2. Clarkson and Bustin also argue that multilayer adsorption may occur in the mesopores when CO_2 is being used as the adsorbate. Clarkson and Bustin observed that the mesopore and micropore volumes are typically multimodal; therefore building a model to predict adsorption based on pore size distributions must be able to account for these effects.

In another publication, Clarkson and Bustin[74] developed a methodology to model rates of adsorption using data from the aforementioned paper.[21] The purpose of the model was to better describe short-term production in ECBM fields by using a multi-modal description of coal matrix diffusivity. The results of their new model were

verified with comparison to experimental transient adsorption data.

Fick's law can be coupled with adsorption to model intraparticle diffusion in coal, with some inherent limitations.[75] Krishna[22] demonstrated that using the Maxwell-Stefan(M-S) equations coupled with adsorption provides a robust model. At the time, Krishna's work on coupling adsorption with the M-S equations was nonexistent and Clarkson and Bustin based their multimodal model on Fick's law. Earlier models for diffusion in coal assumed a unimodal pore size distribution; Clarkson and Bustin improved on this model by modifying it to account for multimodal pore size distributions.

Clarkson's interest in relating adsorptive capacity to coal rank and micropore/mesopore volumes trace back to his thesis.[76] Clarkson used medium-volatile bituminous coals from the mid-Cretaceous Gates Formation in Northeast British Columbia and a high volatile bituminous coal (HVB) from the Cretaceous Formation in Alberta.

D-A measurements were done at 298K using CO_2 as the adsorptive yielding micropore volumes of 21.7-39.8 cm^3/g and 34.1-49.7 cm^3/g for the Gates and Alberta coals, respectively. BET was also done at 273K. Clarkson found that the BET area increases with vitrinite content and decreases with mineral content. High pressure isotherms also showed similar trends in the adsorptive capacity when compared to vitrinite content. In his thesis, Clarkson postulates that the relatively large amount of micropore volume associated with vitrinite is the reason for the increased storage capacity. He also notes that semifusinite also can contribute to the coal's micropore volume and adsorptive capacity. Clarkson makes the argument that the evolution of micropores may be the result of charring during semifusinite formation; a concept that is

very relevant to UCTT since thermal treatment is by its very nature charring coal.

In his thesis, Clarkson also correlated mesopore volumes to coal ranks under the assumption that mesopores are a primary diffusion pathway for gasses. It should be noted that later research did find that mesopore volume can also significantly contribute to adsorptive capacity.[72] Clarkson found that trends in mesopore volumes are inversely correlated to vitrinite content. He also found that semifusinite contributes to the mesopore volumes. Similarly with micropores and semifusinite, Clarkson theorizes that mesopores are the result of charring.

Amarasekera et al.[77] studied the microporous structure of various ranks of coals. In this paper, the authors emphasize that the removal of water during the off-gassing of the coal sample can collapse the interconnected pore network. Amarasekera et al. also attempt to show a relationship between oxygen containing function groups and adsorption. Their study examined four Australian brown coals with differing concentrations of oxygen-containing functional groups. For comparison, these researchers also used a subbituminous Australian coal and a subbituminous United States coal. Micropore adsorption measurements were done using CO_2 as the adsorbate at 273K. The authors claim that since CO_2 has polar bonds and a large quadrapole moment, CO_2 interactions with coal would make the adsorption isotherms dependent on the chemical composition of the coal. Amarasekera et al. warn against using nitrogen for low pressure adsorption measurements due to a variety of issues such as activated diffusion preventing nitrogen from penetrating the micropores and pore shrinkage. Nitrogen may also not be able to reach isolated micropores where CO_2 can. CO_2 has the ability to solubilize in the coal structure and diffuse through said structure where nitrogen cannot.

Amarasekera et al. report that they were unable to find a relationship between microporous area and the concentration of oxygen containing functional groups. They hypothesize that the surface area may be more related to the maceral variations and woody-material content. The authors also conclude that there is no evidence that specific interactions with functional groups interact with carbon dioxide.

Cai et al.[78] studied pore structure and how it relates to adsorption and flow within bituminous and subbituminous coals from Northeast China. The authors classify adsorption pores as being less than 100nm and transport pores being larger than 100nm. A variety of tests were done on the coals including mercury porosimetry, helium porosity, nitrogen adsorption, high pressure methane adsorption, and small angle X-ray scattering (SAXS). The mercury porosimetry was done on an Autopore III 9420 and the low temperature/pressure nitrogen adsorption measurements were done using a Micromeritics ASAP 2000. High pressure CH_4 measurements were done using a TerraTek IS-100. The TerraTek IS-100 is similar in many respects to the isotherm apparatus used for the experimental measurements presented in this dissertation. SAXS measurements were done using a D/max-2550 with a 10kW rotating anode X-ray generator.

Cai et al. report dull coals have a greater percentage of mesoporosity and less microporosity than bright or banded coals; a trend also affirmed by other literature.[79] The nitrogen adsorption measurements showed that the coals either had a Type II or a Type IV hysteresis loop. The authors also report that the coals with high ash or inertinite contents showed more hysteresis than coals high in vitrinite and low in ash. The hysteresis for the coals being studied was indicative of slit-type or ink bottle shaped pore

structures. Surface areas determined with nitrogen were typically less in coals with high amounts of vitrinite, possible due to complications like those outlined by Amarasekera et al.[77] The nitrogen adsorption measurements also showed that the majority of the micropores were ranged from 1.19nm to 2.34nm for the subbituminous coals and 1.22 to 3.8nm for the bituminous coals. High pressure adsorption measurements for the coals yielded Langmuir volumes ranging from 20.07 m^3/ton to 25.8 m^3/ton (DAF basis).

Cai et al. conclude that coals rich in vitrinite and low in ash have more microporous volume than similar coals with larger amounts of inertinite and ash. The authors also conclude that micropores ranging between ~2 and 5nm have a significant impact on the amount of methane that can adsorb. They also reported that coals with large amounts of macroporosity showed higher permeabilities.

Zhang et al.[80] studied the characteristics of pores in Chinese coals. These investigators studied fifteen coals from the Hedong field in Liulin (Ordos Basin). Coal samples were analyzed for lithotype amounts, facies, composition, and rank. Lithotype and maceral analysis revealed that the coals were from four different types of environments; wet forest swamp, intergradations forest swamp, drained forest swamp, and freshwater peat. The purpose of this study was to relate the effect of coal facies. In this paper, micropores were defined as having a diameter less than 10nm, transition pores (a concept not commonly seen in literature relating to this subject) were defined as having diameters between 10 and 100nm, and mesopores having diameters ranging from 100-1000nm. Macropores were defined as having an aperture greater than 1000nm. The authors also define micro- and transition pores as pores wherein adsorption can occur; mesopores and macropores are defined as transport pores.

In their study, Zhang et al. defined four different facies types. It should be noted here that in geological terms a facies is a definition used to classify rocks in order to differentiate different rock types in a local region. The facies used by the authors were the gelification index (GI), the tissue preservation index (TPI), groundwater index (GWI), and a wood index (WI). The coal facies types used by Zhang were outlined by Diessel.[81] The GI is defined as the ratio of gelation components to nongelation components, or the sum of vitrinite and macrinite divided by the sum of semifusinite, fusinite, and inertodetrinite. The TPI is representative of the tissue degradation and ratio of wood in coal forming plants. The TPI can be written in equation form as the ratio of the sum of telinite, collotelinite, semifusinite, and fusinite to the sum of collodetrinite, macrinite, and inertodetrinite. The GWI is used as an indicator to the level of water at the time of peat accumulation and is defined as the ratio of the sum of gelinite, corpogelinite, mineral content, and vitrodetrinite to the sum of telinite, collotelinite, and collodetrinite. The wood index characterizes coal to the amount of preservation and is the sum of telinite and collotelinite divided by the sum of collodetrinite and vitrodetrinite.

The porosity was measured using mercury and was limited to pores larger than 7.2nm; the porosity ranged from 2.6 to 7.0%. Pore sizes were determined using SAXS, mercury porosity, SEM, and low pressure nitrogen adsorption isotherms. From the aforementioned analyses, it was found that the majority of pores were micropores, followed by transition pores, macropores, and mesopores. The surface area determined by BET was found to range from 0.092 to 20.482m^2/g and was mostly related to the amounts of micropores. Furthermore, it was found that the coal facies was the primary correlation between all pore sizes, such as GWI being found to be an indicator of

porosity. From the facies correlations, it was determined that wet forest swamps were the best coal precursors for coal bed methane and that peat swamps were least favorable.

Zhao et al.[82] also performed studies trying to relate the adsorptive capacity of dry coals and micropore volumes. The porous structures of five unspecified coal samples were determined using a Quantachrome NOVA1000e running low pressure nitrogen isotherms. The surface area and the pore volumes were determined using the Density Functional Theory (DFT) method. High pressure methane isotherms were also measured using the volumetric method. The results of the study by Zhao et al. affirm previous observations that the adsorption of methane on coals can be correlated to microporous surface area.

Mosher et al.[83] simulated the relationship between micro- and mesopores as it pertains to adsorption of methane on coal and shale. Simulations were done using a Grand Canonical Monte Carlo (GCMC) algorithm with the intent of predicting the high pressure adsorption capacity of methane in carbonaceous materials. The model developed by Mosher et al. was simplified to take into account only the effects of pores and not the effects of water saturation or specific functional groups in the coal by assuming the adsorptive was like graphite. The model takes into account the gas phase interactions of the adsorbate as well as gas-solid interactions within the pores themselves. The authors note that there are two main influences that are highly dependent on pore size distribution: the surface area associated of the pore walls and the overlapping force fields in narrow pores.

Mosher et al. cite that the majority of the porous volume in coals falls within the microporous region[79] with high rank coals showing a higher abundance of micropores.

The authors also cite that the mechanisms for adsorption can change with differing pressures; micropores have only single layer physisorption during the pore filling stage where mesopores first show single and multilayer adsorption followed by pore condensation.[84, 85] The authors also emphasize the differences between total gas content, absolute adsorption, and excess adsorption. Total gas content is defined as the sum of the adsorbed and nonadsorbed gas filling pores. Absolute adsorption is the amount of gas present only in the adsorbed state; excess adsorption is defined as the difference between the amount of gas adsorbed per a given volume and the amount of gas adsorbed for the same volume without the effects of the pore walls.

The modeled adsorptive had a "complex" set of ideal pores with slit apertures that were not connected. It should be noted here that for methane, making these assumptions are appropriate, however, for an adsorptive like CO_2, which can easily diffuse through the coal matrix via solubilization, these assumptions may no longer be relevant[77]. The model used a three layer perfect graphite slab to represent the pore walls and each simulation box with a given pore with the dimensions of 4.272nm by 4.932nm in the *x* and *y* directions, respectively. Pore widths were modeled by adjusting the distance between the graphite slabs (*z* direction). Other assumptions used in creating the model was methane being a one-center Lennard-Jones sphere and a rigid graphite structure. Mosher et al. executed simulations at temperatures of 298, 318, and 332K up to pressures of 20 MPa. A total of $1x10^8$ GCMC moves were made for each simulation.

Results of the GCMC simulations by Mosher et al. for micropores ranging from 0.4nm to 9nm show a general trend in that excess adsorption decreases with increases in pore width. The results of the simulations show an increase in excess adsorption

followed by a decrease which the authors suggest is the result of a maximum adsorbed quantity. This is because as pressure increases the amount of energy required to add another molecule to the adsorbed phase approached the amount of energy required for a molecule to desorb into the free phase.

The results of the model by Mosher et al. were validated by comparison to experimental data from Ottiger et al.[86] The coal being used for comparison was Suclis coal from Sardinia, Italy. Micropore distributions were determined using low pressure CO_2 isotherms and the D-A method. The general trends for the simulated adsorption were similar to the experimental results with the simulated excess adsorption being greater than the measured counterparts. Mosher et al. attribute the discrepancy to complications with how the pore size distributions were calculated; the D-A method assumes a Gaussian distribution of pore sizes, where in reality this may not be true. Mosher et al. also point out that since their model assumed ideal graphite slits for pores, the model could not account for some of the effects of functional groups and more complicated pore structures.

Micropore Characterization Using Dubinin-Radushkevich and Dubinin-Astakhov

Adsorption on microporous carbons can often be described using the Dubinin-Radushkevich (D-R) adsorption model,[87, 88] The original Dubinin-Radushkevich applies to microporous solids with a uniform or Gaussian distribution of pores, however, the D-R equation can be modified for non-Gaussian distributions, an example of which is the Dubinin-Astakhov equation,[89] The basis of the D-R and D-A equations (and any multilayer adsorption for that matter) comes from the Polanyi[90] theorem that adsorption

forces act at distances exceeding the radius of a single molecule and said forces are not shielded by the first layer of adsorbate; the propensity for a molecule to adsorb is rather a function of the adsorption potential (*A*) and the volume (*V*) of the adsorbed layer. In its basic form, the D-R equation can be written as:

$$W/W_o=exp[-(RTln(P_o/P)/E)^2] \quad (1)$$

where W is the volume adsorbed, W_o is the micropore volume, R is the ideal gas constant, T is the absolute temperature, E is the potential of the gas molecule with respect to a given adsorbent, and P_o/P is the relative pressure. When performing volumetric isotherm measurements, the amount of gas adsorbed is calculated from the pressure change given a known free volume. Adsorption data can be linearized to the D-R equation by plotting the amount of gas adsorbed versus $log^2(1/(P_o/P))$. The linear portion of the plot is where the D-R equation is applicable and has a slope of $-(RT/E)^2$ with an intercept of $log(W_o)$ thereby providing the micropore volume and the characteristic energy.

Nguyen and Do[91] attempted to improve on the D-R equation for microporous carbonaceous materials. Nguyen and Do assume that adsorption on carbonaceous materials starts with surface layering and finishes with pore condensation. The authors emphasize that a main benefit to their model is that it accounts for overlapping adsorption potentials from opposite walls in a micropore. Furthermore, the overlapping fields not only effect adsorbed gas but also free gas in the pores. From this, it was stated that the phase pressure within the pores differs from the bulk pressure. The pressure within the pores can be estimated according to the Boltzmann distribution:

$$P_p(r)=P\ exp\ (-E_p^g(r)/RT)(2) \quad (2)$$

where $P_p(r)$ is the pore pressure as a function of pore radius, P is the bulk pressure, and

$E_p^g(r)$ is the average energy of the molecules within said pore approximated at the center of the pore. Nguyen and Do provide an excellent explanation for pore condensation:

> …adsorption in pores can be pictured as a process whereby gas phase molecules are drawn into the pore interior. Once inside, they are further pressed against each other as a result of the overlapping potential forces. If the enhanced pressure is beyond the corresponding pressure, the adsorbed phase turns into a liquid (albeit compressed liquid). It is therefore, understood that in some narrow pores, due to the very large enhanced pressures, the adsorbed phase exists as a liquid even at low bulk pressures.[91]

As the bulk pressure increases, larger pores are subsequently filled as the thickness of the adsorbed layer increases to a point where the overlapping fields induce enough enhanced pressure where pore condensation can occur.

The model made by Nguyen and Do uses a modified BET equation which is altered to have dependence on pore size. A threshold for pore filling in their model was defined as the pressure at which half of the radius of the pore is covered with an adsorbate. Nguyen and Do tested their model using low pressure nitrogen adsorption measurements at 77K with a microporous carbon standard to obtain a pore size distribution yielding results agreeable with the known pore size distribution. To test the applicability of the D-R equation, Nguyen and Do examined isotherms over a range of pore sizes and pressures constrained to a material with a uniform pore size. They found that the D-R equation failed to represent single pores but was able to fit data for a distribution of pores. The results of Nguyen and Do's findings show that the D-R equation cannot be used for single pore sizes, furthermore it was argued by Nguyen and Do that the D-R equation would fail to describe a system with a skewed or bimodal pore size distribution.

Scherdel et al.[92] worked on developing a relationship between the three most

commonly used analyses of microporous carbon: Brunauer-Emmett-Teller (BET), Dubinin-Radushkevich (D-R), and t-plot. Many commercially available surface area and micropore analyzers have the option to report data in any of the three aforementioned forms. The authors note that BET is an established method for meso- and microporous materials that also takes into account the effects of multilayer adsorption while D-R can be used for the same purpose but is particularly sensitive to microporous adsorption.

In order to test the relationship between BET and D-R, sorption analyses were performed on carbon based aerogels. Micropore accessibility was varied in the aerogels by pyrolyzing it at temperatures ranging from 1000°C to 2500°C in argon with micropores becoming less accessible with higher treatment temperatures; the meso- and macropore volumes were assumed to be unchanged by thermal treatment. Samples were analyzed using a Micromeritics ASAP 2000 using nitrogen as the adsorptive. The t-plot[93] method was used to differentiate between external surface area and microporous area. The standard reference curve for the t-plot method was determined using principles outlined by Harkins and Jura[94], which follows that the slope of the linearized t-plot is related to the external surface area and the intercept can be used to determine the micropore volume.

Scherdel et al. found that there is an ideal relationship between the volume determined by t-plot and the volume determined using D-R; the difference between the two matching the value for the external surface area of the carbon, meaning that the D-R correlation may be sensitive to external surface adsorption [opposed to pore adsorption]. There was no correlation found between the volume from BET and the t-plot method. The authors experiments also found that the volume determined using D-R can be

correlated to the volume from BET with the BET being equal to 0.91 times the D-R volume. The authors note that the value of 0.91 is similar for different carbon aerogels but caution that the relationship may differ for other carbons.

Carrasco-Marin et al.[95] studied the applicability of the D-R equations using CO_2 as the adsorptive on activated carbons. The authors give three examples of comparisons of the BET surface areas for carbonaceous material with nitrogen (77K) and CO_2 (273K). For activated carbons with little burn-off the apparent surface area with CO_2 is often larger than that measured with nitrogen because the narrow constrictions often associated with microporosity often restrict the ability of nitrogen to diffuse at the low temperature at which measurements are conducted. With increasing burn-off, the surfaces measured by nitrogen and CO_2 become similar because some of the pore constrictions are removed. With activated carbons with moderate to high amounts of burn-off, the nitrogen surface area may be larger than the CO_2 surface area. This may be in part due to wider micropores and more heterogeneous microporosity. Due to the heterogeneity in activated carbons (and chars); the authors state that the original D-R equations have limited applicability. To account for heterogeneity, adjustments to the D-R equation can be made, such as dividing terms into partitions for multiple pore sizes or using the Dubinin-Astakhov method. The main difference between the Dubinin-Radushkevich equation and the Dubinin-Astakhov (D-A) equation is the exponential factor of 2 being changed to *n*, wherein *n* represents the magnitude of variation in the energy distribution from which an inference can be made about the pore size distribution.

Carrasco-Marin et al. studied a series of four activated carbons. The first series being from pyrolyzed olive pits, the second from lignite coal, and the other two activated

carbons prepared from subbituminous coals. All of the activated carbons were examined with low pressure isotherms using nitrogen and CO_2 as the adsorbate. Mercury porosimetry and helium densities were also determined. The BET equation was used in conjunction with the nitrogen adsorption measurements while the D-R and D-A equations were applied to the CO_2 isotherms. For all samples, the exponential factor in the D-A equation reduced with increases in the amount of burn off. The authors also found that the D-A equation was better suited for activated carbons with a lot of burn off when using CO_2 as the adsorbate.

Pore Characterization Using Density Functional Theory

Density Functional Theory (DFT) is another means of characterizing pores in microporous solids. One of the drawbacks to more conventional methods of micropore characterizations based on classical thermodynamics is that they fail to accurately describe pore condensation in very small pores. Another method used for pore size determination, the D-A and D-R equations, have the drawback of assuming that the pore size distribution is Gaussian which is only acceptable for porous materials that are known to have uniform structures such as molecular sieves and fails to accurately describe materials with heterogeneous pore sizes such as coal chars. Other pore characterization techniques, such as the Everett and Powell method, work well for small pore sizes but not for larger pore sizes.

DFT can be summarized as the process of simulating adsorption using statistical thermodynamics for a specific adsorptive and adsorbate taking into account fluid-fluid as well as fluid-solid interactions. Particle size distributions (PSDs) can be determined by simulating adsorption over a range of pore sizes and then fitting theoretical simulations to

experimentally obtained adsorption isotherms.

One of the first mentions of using DFT for pore size distributions in carbons comes from Lastoskie et al.[18]. Using a combination of molecular dynamics, Monte-Carlo simulation, and density functional theory, Lastoskie et al. demonstrated that it is possible to calculate sorption properties like heat of adsorption and adsorption isotherms using what the authors deem an "independent pore model."

The model developed by Lastoskie et al. uses a three step procedure. The first step is to define the interaction potentials for fluid-fluid and fluid-solid interactions. The second step is to use statistical mechanics to calculate sorbent properties for a given pore size. The final step is to calculate the overall sorbent property for a given temperature and pressure for a variety of pore sizes, shapes, and surfaces.

In the DFT model, pores are represented by semi-infinite plates with infinite lateral boundaries to represent pores with apertures featuring large aspect ratios. The model presented by Lastoskie et al. assumes that there is no pore connectivity and that there are no active functional groups on the surface of the pore. Fluid-fluid interactions are accounted for using the Lennard-Jones 12-6 potential; fluid-solid interactions are accounted for using the Steele potential. The external potential is the combination of the Lennard-Jones potential and the Steele potential. The unknowns from the Lennard-Jones equation and the Steele equations were chosen to provide the best fit for activated carbon (Vulcan) using low pressure nitrogen measurements at 77K. The specific surface area for the carbon was determined using the t-curve method. The authors noted that there was difficulty reconciling the chosen parameters for the Lennard-Jones and Steele equations when comparing low and high pressure measurements. The authors attribute this to the

anisotropy of nitrogen and the nonuniform interaction that it has with graphite. To model a carbonaceous structure with varying pore sizes, Lastoskie et al. proposed that an array of pores be accounted for using a gamma distribution of a log normal distribution.

By relating pressure and pore width, Lastoskie et al. report that it is possible to determine a pore size distribution for the solid material by modeling multiple pores sizes and reducing the residual from fitting the DFT method. Three different carbons were used to test this method, all of which were degassed at 300°C under vacuum before measurements were conducted. It was found that the DFT method provided a good agreement with the isotherm measurements and that it succeeded in determining the pore size distributions for the carbons. The DFT model used by Lastoskie et al. is commonly referred to as the Non-Local Density Functional Theory (NLDFT); it is still commonly used. Furthermore, there are currently a multitude of variations to NLDFT for various applications.[96]

Dombrowski et al.[97] expanded on the work of Lastoskie et al. for NLDFT applied to activated carbons using argon as the adsorbate. The authors claimed that there was a need to expand NLDFT to argon because nitrogen may not be suitable in all situations due to its quadrapole moment or because of possible interactions between nitrogen and the surface of the adsorptive. Four different Aldrich activated carbons were measured using both argon and nitrogen at 77K; 16155-1, 4021-s, Saran, and coconut char. Since the boiling point of argon is 87K, Lennard-Jones parameters had to be defined for argon as a super-cooled liquid and as a solid; however, the authors chose to emphasize a model using super-cooled argon parameters. Measurements were conducted using a Coulter Omnisorp 100.

Dombrowskie et al. report that they were able to find good agreement between the argon pore size distributions and the PSDs determined using nitrogen with the discrepancies between the measurements being attributed to nitrogen's polar moment.

Jagiello and Thommes[98] compared using nitrogen, argon, CO_2, and hydrogen as the adsorbing gas in NLDFT measurements. Like Dombrowski et al., Jagiello and Thommes point out some of the shortcomings of using nitrogen for NLDFT measurements such as nitrogen being slow to diffuse in carbon which could hinder its adsorption in pores smaller than 7Å. Jagiello[99] had previously published work suggesting that smaller micropores could be accessible to CO_2 molecules when adsorbed at 273K. Four activated carbons were examined by Jagiello and Thommes in this work: ACF10(Kynol), ACF10(Osaka Gas), ACF15(Osaka Gas), and the coal based F400(Calgon Carbon). Adsorption measurements were carried out using a Quantachrome Autosorb 1 MP and a Quantachrome NOVA 4200. All samples were off-gassed for 12 hours at 520K under vacuum. Nitrogen, hydrogen, and argon measurements were performed at 77K while CO_2 measurements were done at 273K.

The results of the NLDFT computations from Jagiello and Thommes for hydrogen showed that hydrogen is best used for pores smaller than 10Å. However, they note that nitrogen and CO_2 can easily be applied to pores falling into the mesopore classification as well as stating that CO_2 is more easily used for carbons as the point where adsorption becomes statistically relevant occurs at a higher absolute pressure than hydrogen, nitrogen, or argon. Pore size distributions using nitrogen and argon yielded similar results but it was assumed that the argon measurements were more accurate due to the lack of nonadsorption surface interactions that may be present in the nitrogen

measurements. Hydrogen measurements had an early peak for very small pore sizes. Overall, the authors claimed that the results using the different gasses were consistent with the exception of some gasses working better for some pore sizes than others. They also mentioned that CO_2 should be sufficient for most micropore sizes.

Neimark et al.[100] improved on the NLDFT with a model commonly referred to as Quenched Solid Density DFT (QSDFT). QSDFT accounts for "geometrical inhomogeneities" by using a roughness parameter which the authors claim may be more accurate for carbonaceous material because of the complexity of the pore structures therein. Another pitfall of the NLDFT method is that it can be hard to differentiate between the completions of simulated surface layers and pore filling. An example given by the authors is the adsorption of nitrogen on carbon. The completion of the first simulated monolayer occurs at the same relative pressure as that needed to fill a pore about 10Å in diameter. This will result in an incorrectly low value for the number of pores around 10Å.

QSDFT is different from NLDFT in that it is multicomponent and accounts for the solid in the fluid-fluid interaction calculations. The surface heterogeneity is accounted for by a roughness factor which the authors claim is better than more rigorous models because it sufficiently and accurately accounts for pore shape heterogeneities. Similar to previous researchers, Neimark et al. report that the PSD determined using argon should be more accurate than the one determined with nitrogen.

Using QSDFT, Neimark et al. were able to show that their model did not exhibit some of the erroneous steps found with NLDFT when simulating adsorption on carbon surfaces. When applied to measured adsorption isotherms on activated carbons, the

QSDFT provided an excellent agreement with the laboratory data. Furthermore, the missing pore volumes associated with the simulated surface monolayer were diminished from which the discrepancies could have large implications in the characterization of activated carbons and by extension, the pyrolyzed coals produced by the UCTT process.

Characterization of microporous carbons using density functional theory is generally accepted to be the state-of-the-art and is widely accepted.[96] It can be used with a variety of adsorbents and is constantly being improved to be applicable to more surfaces and adsorptives.

Mechanisms on Adsorption on Coal

Gaseous molecules can adsorb on the surface of coal following a mechanism similar to that proposed by Langmuir[23], which follows that the adsorbate condenses on the surface to eventually form a uniform monolayer, or the gas can adsorb in multiple layers following the theory of Brunauer, Emmett, and Teller (BET).[11] Langmuir adsorption assumes that there are a fixed number of adsorption sites with equal spacing and equal energies that can only adsorb one molecule at a time. BET, which is an extension of the Langmuir model, improves on the Langmuir model by allowing treating adsorbed molecules as sites for other molecules to adsorb. Variations of the aforementioned adsorption models can be modified to account for heterogeneous coal surfaces[41, 101] in which some sites are more preferential than others. The preferential nature of the sites is usually associated with the functional groups on the coal surface. Coal also can absorb a gas which can be best described as the dissolution of a gas into the coal lattice.[102] None of the aforementioned sorption mechanisms account for the phenomena of pore filling. Pore filling or pore condensation is another sorption

mechanism which has been described by Dubinin. The confining nature of micropores can result in overlapping force fields as described by Polyani.[90] More details about Dubinin pore filling mechanisms are specified later. Gaseous components can also dissolve into tars within the coal. All of the aforementioned sorption mechanisms are illustrated in Figure 2.

Different governing equations have differing best uses; for example, if one was attempting to characterize a microporous solid for a pore size distribution, it would be useful to use the Dubinin-Radushkevich equation, but if a solid has an abundance of mesopores, it would be useful to use the Barrett-Joyner-Halenda (BJH) method. The industry standard for adsorption measurements on coal are commonly described by the Langmuir equation, even though it is generally understood that the assumptions used in the derivation of the Langmuir equation do not hold true and sometimes do not provide the best fit to experimental data.

Chaback et al.[103] measured high pressure (up to 11 MPa) adsorption isotherms at 46°C for nitrogen, methane, and CO_2 on wet bituminous coals. Chaback et al. found that the Langmuir equation was well suited to describe the experimental results for not only the pure components but also their mixtures. Previous investigators have made several attempts at pinpointing the primary adsorption mechanism on coal. Clarkson et al.[104] applied several of the aforementioned adsorption theories to high pressure methane and low pressure CO_2 adsorption measurements on coal. Clarkson et al. examined Langmuir, BET, and Dubinin adsorption theories and found that a three parameter Dubinin pore filling model best fit the methane and CO_2 adsorption measurements. Clarkson et al. determined that the assumptions used for the Langmuir theory do not apply to adsorption

on coal, namely, the assumption that surface of the adsorbant exhibits homogenous sorption potential.

Martin-Martinez et al.[105] studied the adsorption of CO_2 on activated anthracites presorbed with n-nonane. It was assumed during the measurements that the n-nonane filled the pores of the activated carbon preventing CO_2 pore filling in those pores. There was not any discussion about the possibility of CO_2 dissolution into the n-nonane. Heating the activated carbons to different temperatures removed the nonane from certain pore sizes. By selectively making some micropores inaccessible to CO_2, Martin-Martinez et al. were able to determine the adsorption in micropores produced a curved isotherm at low relative pressures and that the shape of the pore has a noticeable effect on CO_2 adsorption.

The dissolution of CO_2 into the coal structure can even change the nature of the pores of a coal due to swelling. Larsen[102] studied the effects of dissolved CO_2 on coal properties. Larsen states that CO_2 can act as a plasticizer that can help in the rearrangement of the coal structure, which in turn can affect the adsorptive and permeability properties of the coal.

Factors Effecting Adsorption on Carbons

There are a multitude of factors that can affect the adsorptive capacity of coals and activated carbons. Ozdemir[106] outlines several major factors effecting the adsorptive capacity on coals: 1) Coal rank, 2) Temperature, 3) Moisture content, 4) Coal swelling. Since coal is being thermally treated, there are two additional factors affecting adsorption: 5) Treatment temperature and 6) Heating rate.

Effects of Coal Rank

There have been a multitude of adsorption studies on various coals of different ranks and compositions. Rank and composition can affect adsorption with various functional groups[107] and variations in mesopore/micropore distributions (discussed elsewhere). Bustin and Clarkson[108] studied gas content and gas saturation for several Australian, Canadian, and United States coals. Bustin and Clarkson took volumetric isotherm measurements similar to Mavor et al.[30] and fit the resulting data to the Langmuir adsorption model. In addition to studying adsorption capacities, Bustin and Clarkson also performed micropore characterization. Bustin and Clarkson were not able to find a correlation between adsorption capacity and composition/rank. Furthermore, Clarkson and Bustin were not able to correlate adsorption to microporous surface area.

Garner et al.[109] also studied adsorption capacities on coals of various ranks for the purpose of CO_2 sequestration. Garnier et al. found a slight correlation between adsorptive capacity and microporous surface area and mineral content but were only able to make a weak relationship between adsorptive capacity for CO_2 and rank. This relationship can be summarized as anthracites and meta-anthracites generally have more adsorptive capacity than subbituminous and medium volatile bituminous which have more adsorptive capacity than high volatile bituminous coals. When the adsorbate is changed to methane, the trends between adsorptive capacity changes, for example, the subbituminous coal adsorbs much less methane than CO_2.

Effects of Temperature

It is generally accepted that underground reservoirs are isothermal[110-112], however, with thermal treatment there are bound to be thermal gradients in the reservoir affecting

the local adsorption capacity of the gasses on coal. It is safe to make the generalization that increases in temperature reduce the amount of adsorbed gas. Increases in temperature decreasing the volume of adsorbed gas has been commonly reported in literature for coals.[113, 114]

Effects of Moisture Content

Clarkson and Bustin[31] investigated the effect that moisture has on CO_2 adsorption on coals. Moisture on coal can be treated as another adsorbed gas phase; to model the isotherms with more than one adsorbing component, Clarkson and Bustin used the extended Langmuir equation which is a multicomponent form of the standard Langmuir. Clarkson and Bustin dried their coals at 110°C overnight and then 24 hours at the isotherm temperature or they equilibrated them with moisture at 30°C in a manner similar to Levy et al.[115] Measurements were performed using an apparatus similar to Mavor et al.[30] Clarkson and Bustin found that for wet coals the amount of CO_2 that is adsorbed is higher for bright and banded bright coals than dull coals.

Krooss et al.[114] volumetrically measured isotherms on dry and moisture equilibrated Pennsylvanian coals using both CO_2 and methane as the adsorbate. Coals were moisture equilibrates according to ASTM D 1412-93[116] or dried in a heated air cabinet followed by vacuum desiccation in the sorption measurement apparatus at 105°C. Krooss et al. were able to show that the moisture equilibrated coals have less adsorption potential than dry coals for both methane and CO_2. This was because the water was occupying adsorption sites that methane and CO_2 require.

Švábová et al.[117] studied the effects of moisture on the kinetics of CO_2 adsorption on coal. Samples were high volatile bituminous coals sourced from the Upper Silesian

Basin and lignite from the North Bohemian Basin. Expeimental data were fitted using the Dubinin-Radushkevich model. Švábová et al., like Krooss et al., noticed a decrease in the adsorptive capacity in the presence of moisture. Švábová et al. also found that the rate of adsorption of CO_2 is less with the moisture equilibrated coals than the dry coals.

Effects of Coal Swelling

The swelling of coals is a common result of adsorption, especially with CO_2, and is a well documented phenomena. This swelling with adsorption and shrinkage with desorption can change the permeability in a coal formation. Wang et al.[118] experimented with coal swelling with a binary mixture of methane and CO_2 for the sake of ECBM. To test the coal swelling, flush tests were performed using large pieces of coal and a tri-axial pressurized coal holder. The flush tests started with equilibrating the coal with methane first, then reducing the pressure releasing methane to simulate gas production, then injecting a sweeping flow of CO_2 to simulate CO_2 ECBM. Wang et al. found that the changes in permeability as a result of coal swelling was directly related to the confining stress and the hydrostatic pressure on the coal block when flowing either methane or CO_2. Increases in pressure increase the swelling thereby reducing the permeability.

Mazumder et al.[119] also studied the change in permeability in coals from the injection of CO_2. Mazumder measured permeability and strain on coal in a core holder initially saturated with methane and then flushed with CO_2. The authors observed that CO_2 causes more swelling than methane as a result of the CO_2 dissolving into the coal matrix thereby causing a loss of permeability.

Pan and Connell[120] attempted to develop a model for adsorption induced coal swelling. Pan and Connell identify two competing forces which determine the net change

in volume of the coal: the swelling due to adsorption/dissolution and the compression of the coal matrix from pore pressures. The model developed by Pan and Connell was validated against the coal swelling data of Levine[121] with decent agreement.

Effects of Treatment Temperature

There is little published work pertaining to the adsorption of either methane or CO_2 on thermally treated coals. The treatment and activation of coal derived activated carbons should provide similar insight into the adsorptive properties of coals thermally treated by UCTT. Maroto-Valer[10] et al. showed the effects of different activation temperatures on the adsorptive characteristics of activated charcoal derived from anthracite. Maroto-Valer et al. activated Pennsylvanian anthracite in the presence of steam at treatment temperatures ranging from 700-890°C with temperature hold times of 2 to 3.5 hours. Coals treated to higher treatment temperatures showed higher adsorptive capacities (N_2) than lower temperature counterparts. Micropore area increased with time up to the 3 hour mark and decreased thereafter; mesopore areas increased gradually with treatment time.

Effects of Heating Rate

Differing heating rates can have effects on the yields of volatiles removed from the coals. The results of a variety of coal carburization experiments have been tabulated [57]. Generally, in carburization experiments the heating rates being investigated are much faster than what would ever be attainable by UCTT. Some general trends may be extrapolated from the aforementioned carburization experiments; Van Krevelen et al.[122] were able to show that heating with slower rates results in more devolatilization at lower

temperatures, it could therefore stand to reason that lower heating rates would result in more surface area and adsorptive capacity in thermally treated coals due to the removal of a larger amount of volatiles.

Originality of This Work

This work investigates small pores in coals that have been pyrolyzed at slow heating rates. There currently is little information about the products of coals that underwent *in situ* pyrolysis. This work focuses on surface area analysis, pore size distributions, and permeability on coals treated with slow heating rates similar to what would be encountered with the UCTT program. This work also attempts to show a relationship between the pore size distributions of pyrolyzed coal and adsorptive capacity. Additionally, this work attempts to determine the effects of residual hydrocarbons on surface area and pore size distributions.

The two most significant pieces of information from this research are that high pressure adsorption isotherms such as these will be the most useful in estimating the storage capacity of pyrolyzed coal seams. The other very important concept is with pores on thermally treated coals, some of the increases in the observed pore volumes after pyrolysis could in fact be the result of residual hydrocarbons.

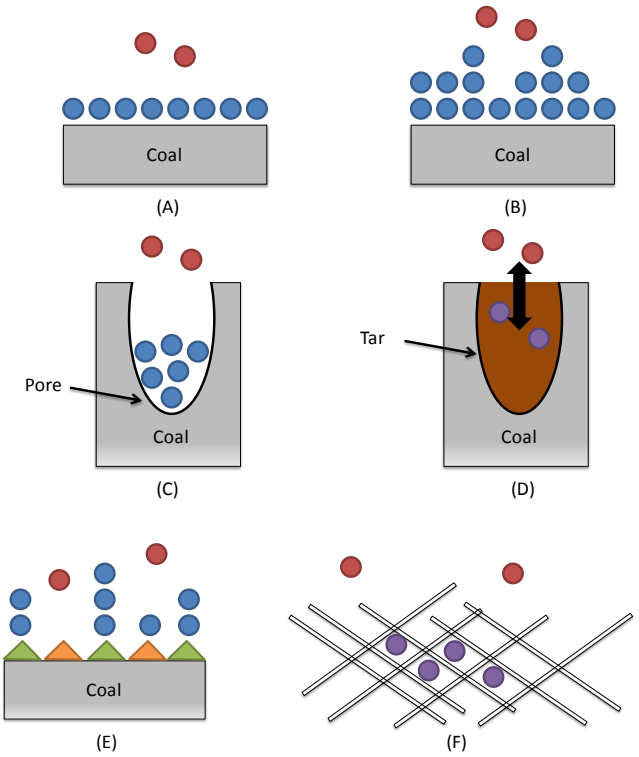

Figure 2: Illustration of sorption mechanisms for coal. (A) Langmuir adsorption. (B) BET adsorption. (C) Pore condensation akin to Dubinin models. (D) Dissolution into residual tars. (E) Heterogeneous surface adsorption. (F) Dissolution into coal matrix. Red spheres represent the gaseous (free) phase, blue spheres represent the adsorbed phase, and purple spheres are dissolved phase.

CHAPTER 3

EXPERIMENTAL APPARATUS AND METHODOLOGY

Several different pieces of equipment were used during this study and are discussed in detail in this chapter. The procedure used for sampling, storage, and experimentation is also disclosed in this chapter. With the information presented in this chapter, it should be possible for other researchers to replicate the experiments and repeat the results.

Sample Storage and Selection

Three different coals were examined in this study: a Utah bituminous coal from the Skyline Mine near Helper Utah, an Illinois bituminous coal from the Carlinville mine, and a Powder River Basin (subbituminous) coal from the North Antelope mine near Gillette, Wyoming. In the following text, the individual coals will be referred to by the mine from which they were sourced. These coals were chosen for different reasons. The Skyline coal was chosen primarily for its high levels of volatile matter and relatively low sulfur. The Skyline coal was also chosen to retain consistency between this work and the work of a colleague. Skyline coal is representative of a lot of the bituminous coals in Utah. The Carlinville coal was chosen to represent some of the high sulfur bituminous coals near the northern Appalachians. The North Antelope coal was chosen to further diversify the scope of this study; Powder River Basin coals have some interesting

properties such as very low sulfur and very high moisture contents. All three of the aforementioned coals can be found in shallow mineable formations or in deep unmineable seams that would make them a target candidate for underground coal thermal treatment.

All of the coals used for this study were delivered to the University of Utah already crushed to chunks approximately 20mm in diameter. The coals were sampled and cone and quartered before being stored in opaque airtight containers in a climate controlled room. Approximately 5kg of each coal was procured for experimentation. Elemental, heating value, moisture, ash content, and volatile analysis were provided by Huffman Labs in Golden Colorado. The results of the analyses performed by Huffman Labs can be found in Table 1 and Table 2.

Some of the major differences between these coals are easily noticed in Table 1. The Skyline coal and the North Antelope coal both have carbon amounts less than 1% while the Carlinville coal is approximately 4% sulfur. It can also be seen that the Skyline coal has the highest amount of volatile material and the North Antelope has the smallest amount. Conversely, the North Antelope coal had the highest amount of moisture while the Skyline coal had the least.

Experimental Equipment

Pyrolysis Apparatus

Pyrolysis of the coal samples was done using a 64mm clamshell-style tube furnace 24 inches (61cm) in length. The tube furnace was a Thermo Scientific Lindberg Blue. The furnace was controlled using an Omega CN1504 programmable process controller. Power was supplied to the heaters by a 240V three phase wall outlet passing

through a 30 ampere solid state relay.

The reactor for pyrolysis was 2.5 inch (64mm) O.D. 314 stainless steel tube 183cm in length. A long protrusion was cooled with a fan and served to condense out some of the oils produced during heating. Plumbers unions were attached to both ends of the reactor in order to make loading and unloading the tube furnace easier. With the use of sequentially reducing fittings, the ultimate diameter on the inlet was made to be 0.25 inches (6mm). A 0.25 inch Swagelok tee facilitated the injection point for gas and mounting point for a k-type thermocouple that ran longitudinally through the reactor to the center of the heated zone. Gas was supplied from a k-size cylinder through the appropriate regulator and controlled with a calibrated rotometer.

When situated in the tube furnace, 4 feet of the reactor protruded on the downstream side of the furnace. Reducing unions were used to adapt the larger pipe to 1inch (2.5cm) stainless steel tube 61cm in length. This smaller diameter tube was fed into a hole in the laboratory fume hood. Inside the fume hood, the tube is attached to a glass oil trap with silicone tape. A 0.5inch diameter (12mm) polytetraflouroethylene (PTFE, aka. Teflon) tube connected a bunghole stopper in the decanter to a 10 liter plastic jug that served as a scrubber. Another length of tube and another 10 liter container served as the second scrubber. Scrubbing the effluent of pyrolysis experiments aids in removing some of the sulfurous and foul-smelling compounds. Figure 3 is a process flow diagram for the pyrolysis apparatus.

Adsorption Apparatus

The isotherm measurement apparatus was identical in design to that used by Mavor et al.[30] The apparatus used by Mavor et al. was a volumetric/manometric type.

The advantages of a volumetric/manometric apparatus are as follows[15]: 1) Simplicity, volumetric measurements do not require complicated or expensive equipment. 2) Data reduces well if the mass of the sorbent is known and the calibration is maintained. Disadvantages of volumetric/manometric measurements are: 1) Volumetric measurements require more material than other measurement techniques. 2) A long time may be required for the adsorption system to come to equilibrium. 3) Volumetric measurements give little insight into the kinetics of adsorption.

The isotherm apparatus used custom machined reference and sample cells rated to 690 bar at 100°C. The reference cells and the sample cells were made out of polished stainless steel. Using polished material reduces the amount of adsorption in the apparatus thereby reducing experimental error[15]. All fittings and connections in the apparatus are from Autoclave Engineers and are 0.25 inches (approx 6mm). Fittings and tubing used for the apparatus are rated to over 690 bar. High pressure needle valves were used to contain pressure. Pressure was monitored using Honeywell TJE pressure transducers with an effective range from 0 to 690 bar. The voltage outputs from the pressure transducers were transmitted to a custom TerraTek signal conditioner and from there to a Dell Optiplex 755 personal computer via serial cable and data acquisition card. Pressure readouts were recorded using TerraTek software, Isotherm Legacy. Isotherm legacy was built using the LabVIEW (National Instruments) software package.

Three identical reference cell and sample cell isotherm systems were used in parallel. Due to the long time necessary for the isotherm system to come to equilibrium (hours to days per data point), running three isotherm measurements simultaneously was more efficient. A schematic of a single reference cell and sample cell system can be

found in Figure 4.

All of the isotherm measurement units were placed in a custom-made stainless steel bath filled with Xiameter. Xiameter is a Dow-Corning silicone based fluid and was used because of properties such as low vapor pressure and high temperature stability. The temperature of the bath was controlled using a VWR 1122s immersion heater/circulator.

Supporting Equipment

Surface area analyzer. A surface area analyzer was used to determine the pore size distributions of the fresh and pyrolyzed coals. The instrument used for these measurements was a Micromeritics Tristar II surface analyzer. This instrument is capable of a multitude of surface analysis and is conceptually similar to the adsorption apparatus previously mentioned in that is has a reference cell and sample cell and relies on adsorption of the analysis gas. Since there are issues with using nitrogen as the adsorptive for surface measurements on coal chars[123], CO_2 was chosen as the analysis gas. Some of the preliminary measurements performed using nitrogen at 78K provided nonrealistic results with negative adsorption values; other researchers have noticed a similar phenomena using argon as the adsorptive.[33] Measurements were performed using CO_2 as a noncondensing adsorptive at 0°C at P/Po values ranging from 0.01 to 1. Micromeritics software included with the surface analyzer was able to regress the data. Although the software included a multitude of analysis techniques, a custom procedure was written for the analysis of the samples and was based on the procedure for analyzing an activated carbon except for more data points being added in the low P/Po range. The Micromeritics software produced a variety of information useful to this study such as

BET surface area analysis, BJH mesopore distributions, DFT micropore distributions, and Dubinin-Radushkevich micropore areas. Samples for surface area analysis were dried in a vacuum oven for at least 1 week at 80°C. The sample tubes for the surface area analyzer were custom made out of 3/8 inches (approximately 9.5mm) borosilicate glass 10cm in length. Approximately 150 to 250mg of sample was weighed out for each analysis. Since the samples have such a high surface area, it was decided that this amount should be used in accordance with the Tristar II user's manual.

Sohxlet extraction. Sohxlet extraction[124] is a commonly used analytical method for removing material that is not easily dissolved in the solvent. This is accomplished by distilling a solvent and refluxing the hot solvent through a thimble containing the sample. Once the fluid level in the sample level reaches a certain volume, a siphon is triggered and the solvent/solute mixture is drained into a boiling flask where the solvent is again distilled. The sohxlet extraction process ensures that pure solvent is flushed through the sample thereby increasing the amount of solute that can be extracted.

Samples for sohxlet extraction were ground to approximately 105 microns (140 mesh) using a SPEX shatter box. Acetone was used as the solvent phase for the sohxlet extractions. Acetone was found to be a good solvent for removing residual pyrolysis tars after a screening of various solvents; aggressive solvents such as pyridine were avoided as to not damage the overall coal structure[125]. The surface area and pore size distribution was determined on the acetone treated samples in order to determine what fraction of the surface area can be attributed to the coal structure and what is attributed to residual tars. Three identical sohxlet extraction apparatuses were used to remove residual hydrocarbons from the coal samples. The volume of the sohxlet extractor was 250 ml. Samples

underwent extraction for 8 hours; this duration was determined to be sufficient to remove the vast majority of residuals. Sample amounts used for extraction were approximately 5 grams; enough sample for extra analysis.

Thermogravimetric analysis. Thermogravimetric analysis (TGA) was used to determine the amount of time for pyrolysis of the coals to come to completion for a given temperature. TGA was done using a TA Instruments Q600. The Q600 was able to provide mass losses versus temperature and time as well as heat fluxes. The same heating rates that were used in the larger tube furnace were also used with TGA. The Q600 uses a dual balance mechanism where one balance is for reference and the other for sample; both balances are equipped with thermocouples to determine differential temperature. Samples were placed in a 0.25 inch (~6mm) quartz sample cup about 3 millimeters deep. Sample amounts for analysis are usually around 15mg. A tube furnace was used to heat the samples to a maximum of 1000°C with a heating rate of 20°C/minute. A sweeping flow of nitrogen at 50 cm^3/min is used to remove volatilized products. For the samples used, heating rates of 0.1 or 10°C per minute were used with ultimate temperature of 325, 450, or 600°C with a final hold time of at least 24 hours.

Permeability measurements. Permeability was measured on the fresh and pyrolyzed samples using a TerraTek tight rock analysis (TRA) pressure decay permeability analyzer. The permeability analyzer is conceptually similar to the Gas Research Institute (GRI) method[126] but more closely resembles the tight rock analysis methods of Handwerger et al.[127] The permeability apparatus consisted of a sample cell and a reference cell with a pressure transducer. Helium was used as the analysis gas. When performing measurements, the reference cell was pressurized with 6.8 bar of

helium which was then released into the sample cell. The transient pressure data were analyzed with the TerraTek software and permeability was calculated. Approximately 30 grams of sample was required for permeability measurements. Samples were crushed and sieved to a Taylor sieve fraction between 12 and 20 (1.4 and 0.85mm, respectively). By crushing the samples, the effects of high permeability cleats and thermally induced fractures are neglected. Samples for permeability measurements were off gassed in a vacuum oven for 36 hours at 80°C.

Experimental Methods

This section is devoted to describing sample preparation, procedures, and calculations used over the course of this study. Since this study used a variety of techniques ranging from simple extraction to complex computer simulations, the goal of this section is to provide a thorough yet concise description of techniques used.

Pyrolysis Sample Preparation

Coal samples that were to be pyrolyzed in the previously discussed tube furnace apparatus required little preparation. Approximately 300 grams of crushed coal was weighed out into two quartz troughs, 5cm diameter and about 30cm in length. The troughs were carefully placed into the section of the stainless steel tube that was going to be in the heated zone of the tube furnace. Once loaded, the stainless steel tube was carefully moved to the furnace to avoid any shifting of its contents. With the tube situated, the feed and effluent lines were attached and the pyrolysis experiment was ready to proceed.

Coal Pyrolysis and Sampling

Pyrolysis of the coal in tube furnace began by setting the nitrogen sweep gas to a flowrate of 170 standard liters per hour (6 SCFH). The low flow rate ensured that no small coal particles would be blown from the quartz trough; however, using a flowrate that is too low could cause plugging in the scrubber system and inefficient removal of volatiles.

The thermal controller was programmed with the ramp-soak profile for the given pyrolysis experiment. The soak times for the pyrolysis experiments were determined using thermogravimetric analysis. Ramp rates of either 10 or 0.1°C per minute were used. If the ramp rate was 10°C/minute, the corresponding hold time after the sample reached its ultimate temperature was 24 hours, likewise if the sample was being heated at a rate of 0.1°C/minute the hold time would be 4 hours. Once thermal treatment was completed, the pyrolysis apparatus was allowed to cool naturally to room temperature. Only after the system cooled off was the nitrogen sweep gas turned off; this was done for safety reasons. The system was disassembled and the samples were carefully removed to avoid any spilling. After a final weight of the sample was measured, the coals were placed into mason jars and sealed under vacuum to prevent oxidation. Mason jars were found to be an effective alternative to more traditional laboratory glassware for storage; for one, they can be sealed under vacuum and secondly, they are only about one fifth the cost.

The pyrolysis apparatus was cleaned after each experiment. Due to the overwhelmingly foul odor of some of the produced tars, it was important to do the cleaning in a well ventilated area. It was also important (it always is) to wear the

appropriate personal protective equipment during cleanup because some of the pyrolysis tars produced are carcinogenic.[128]

Ultimate pyrolysis temperatures of 325, 450, and 600°C were chosen as likely temperatures encountered with UCTT. Multiplying the different treatment temperatures with the different heating rates for three different coals plus three unreacted coal samples resulted in 21 samples overall (Table 3).

Isotherm Sample Preparation

Samples for isotherm measurements were ground to approximately 105 microns (140 mesh) using a SPEX shatter box. A small particle size is beneficial when taking adsorption measurements as it reduces amount of time required for the isotherm step to come to equilibrium. As the ratio of internal surface area to external surface area of coals is about 100:1, the effect from surface area changes on adsorption due to grinding is minimal[30]. All samples were dried in a vacuum oven at 80°C for at least 36 hours to ensure that all moisture was removed from the coal[129]. Removing the moisture from the coal is important as moisture can have a great effect on adsorption[31]. After the coal samples were dried, they were resealed in mason jars under vacuum. About 200 grams of sample was prepared for each isotherm measurement.

Isotherm Measurement and Sampling

Coals for the isotherm measurement had two small samples removed before loading the bulk of the material into the sample cell. These smaller samples were about 5 grams each and were for surface area analysis with and without sohxlet extraction. Samples were loaded into the cell with a funnel. It was important to get good packing of the sample in the cell to reduce the overall free volume. Packing was done by vigorously

tapping the side of the sample cell with a rubber mallet while pouring in the sample. The difference in the weights of the Mason jar before and after loading the sample provided the mass of sample used. After filling, the cell was sealed with vacuum grease on the inside contact surfaces and nickel antiseize on the threads to ensure easy disassembly. The sample cell was attached to the rest of the apparatus and immersed in the Xiameter bath at either 50 or 70°C. The system was allowed to come to equilibrium over 2 days for each temperature change.

Before individual adsorption measurements were done and between switching the adsorptive gas, the system was flushed multiple times with 69 bar (1000 psig) of helium to remove any residual gas. After the final helium flush, pressure was removed from the system and the pressure transducers were allowed to come to equilibrium for at least 15 minutes.

The sample cell was calibrated for free volume four different times using helium. First the valve between the reference cell and the sample cell is closed, next the reference cell was charged with 69 bar (1000 psig) of helium. After the system came to equilibrium, *id est* the values read from the pressure transducers read level, the pressure values were recorded and the valve between the vessels was opened. After letting the system come to equilibrium, the final pressure values were recorded and pressure removed from the system.

The pressure transducers were rezeroed between each different gas and measurement temperature. Isotherm measurements followed a similar procedure as the free-volume calibration except the pressure of the gas charge in the reference cell increases for each step. For all the adsorption isotherms, nine pressure steps were taken.

The values of the pressure charge for CO_2 and CH_4 measurements can be found in Table 4.

CP grade methane and Coleman grade carbon dioxide were used for the isotherm measurements with delivered tank pressures of 172 bar and 56 bar, respectively. Methane charges to the reference cell with pressures greater than the tank pressure required the use of a gas booster pump. Since this apparatus was not capable of handling super critical isotherm measurements, the CO_2 pressure was not boosted above tank pressure. It is important to notice that the incremental differences in the first few pressure steps are smaller than the latter pressure steps; this is because when it comes time to fit the adsorption data to a fitting equation *e.g.*, Langmuir, the greatest rate of change in adsorption is at lower pressures and defines the curvature of the adsorption plot.

Unlike the calibration steps, the pressure was not removed from the sample cell until the end of the experiment; for example, after the first pressure step, the equilibrium pressure in the sample cell could be 2.1 bar, this would be the initial pressure for the next step. Pressures were always recorded after the system came to equilibrium. Some of the adsorption measurements could take quite a long time for equilibrium to be reached, typically on the order of hours. With this in mind, a measurement schedule was employed wherein the pressure step was done early in the morning and another one in the late afternoon, allowing for a minimum of 12 hours between pressure steps.

Measurement on each sample involved two different gasses (CO_2 and CH_4) at two different measurement temperatures (50°C and 70°C) thus resulting in four isotherm measurements for each sample (Table 5). Measurement temperatures were chosen as

reasonable approximates of unmineable coals at *in situ* temperature.

Each adsorption measurement took about 1 week to complete; for a complete matrix of measurements about 1 month was required. Between measurements, the system was flushed multiple times with helium. Temperature changes were allowed 2 days to come to equilibrium. After the final isotherm measurement was completed, the system was depressurized and removed from the temperature bath to cool. Once cool, samples were removed from the sample cell and two more 5 gram splits were taken for surface area analysis and sohxlet extraction. Samples were taken after analysis to determine if high pressure exposure to methane and CO_2 had any effect on the pore structure.

Isotherm Calculations

Calibration of the apparatus. Calibrating the isotherm measurement apparatus was a multistep process beginning with calibrating the pressure transducers and then calibrating the free volume of the reference and sample cells.

A hydraulic dead weight tester was used to calibrate the pressure transducers. The hydraulic calibrator had a piston and a given amount of weight placed on top of said piston; the resulting pressure was applied to the pressure transducer. The pressure transducer outputs a voltage that corresponded to the amount of pressure. Using different pressures and recording the voltages, a linear regression was used to determine the relationship between voltage and pressure.

The next step in calibrating the isotherm apparatus was determining the amount of empty volume in each of the reference cells and sample cells. The reference cell was filled first with helium and the pressure recorded. Then the valve between the sample

cell and the reference cell was opened. Once the pressure reached steady state, the pressures in both cells was recorded. This was similar to free volume measurements mentioned elsewhere. Measurements were repeated four times with stainless steel billets of a known volume, V_b, being placed in the sample cell. Knowing the volume of the billets and using the real gas law, the volumes of both the sample cell and the reference cell was determined algebraically.

$$V_{He}^{S} = V_{ref} + V_{sample} - V_{He}^{free} \tag{3}$$

wherein V_{He}^{S} is the adsorbed volume of helium, which is assumed to be zero. V_{ref} is the volume of the reference cell, and V_{sample} is the volume of the sample cell. V_{He}^{free} is the free volume of the helium, which can be determined using the following equation:

$$V_{He}^{free} = \frac{m_{He}}{p_{He}M_{He}} RTZ(p,T) \tag{4}$$

Here m_{He} is the mass of helium in the system, p_{He} is the pressure of the system, M_{He} is the molecular weight of helium, R is the gas constant, T is the temperature in Kelvin, and Z is the compressibility of helium as a function of temperature and pressure.

Although there are analytical expressions for determining the compressibility of helium, compressibility was determined using REFProp9. REFProp9 is a NIST property calculation software that was chosen because of its ability to calculate the compressibility of multicomponent mixtures as an Excel macro without the use of iterative calculation.

Solving the following equation algebraically yields the volumes of both the sample call and the reference cell:

$$\begin{bmatrix} \frac{p_{refE1}}{Z_1T} - \frac{p_{refE2}}{Z_2T} & \frac{p_{sampleE1}}{Z_1T} - \frac{p_{sampleE2}}{Z_2T} \\ \frac{p_{refF1}}{Z_1T} - \frac{p_{refF2}}{Z_2T} & \frac{p_{sampleF1}}{Z_1T} - \frac{p_{sampleF2}}{Z_2T} \end{bmatrix} \begin{bmatrix} V_{ref} \\ V_{sample} \end{bmatrix} =$$

$$\begin{bmatrix} 0 \\ V_b\left(\frac{p_{sampleF1}}{Z_1T} - \frac{p_{sampleF2}}{Z_2T}\right) \end{bmatrix} \quad (5)$$

where p_{refE1} and p_{refE2} are the pressures in the reference cell before and after the helium is released into the sample cell, respectively. Also, $p_{sampleE1}$ and $p_{sampleE2}$ are the pressures in the sample cell before and after the release of pressure, respectively. The subscript *E* denotes that the measurement for the empty sample cell, likewise the subscript *F* denotes a sample cell with billets. Z_1 and Z_2 are compressibilities calculated relative to p_{ref} or p_{sample}. Equation 3 is solved four times with the four sets of pressure measurements with and without the billets. Values for V_{ref} and V_{sample} are averages and uncertainties are determined. A desirable uncertainty is less than ±0.2cm^3.

Free volume calculation. The determination of the free volume of the sample cell with a sample in it is similar to the calculation of the empty volume except the volume of the material inside the sample cell is unknown. Helium was used in determining the free volume and measurements were repeated four times. Equation 3 was solved for V_b, except in this instance V_b refers to the volume of the coal rather than the volume of the billets. Equation 4 can be used to determine the free volume:

$$V_{free} = V_{sample} - V_{coal} = -V_{ref}\frac{\frac{p_{ref1}}{Z_1T} - \frac{p_{ref2}}{Z_2T}}{\frac{p_{sample1}}{Z_1T} - \frac{p_{sample2}}{Z_2T}} \quad (6)$$

Here V_{free} is the free volume and V_{coal} is the volume of the coal occupied by the coal sample.

Adsorption calculations. The amount of gas that adsorbed was determined by mass balance. Since the volume of the reference cell is known and the pressure in the reference cell is known, the number of moles of gas in the reference cell can be

calculated using the real gas law. The mass of the gas in the reference vessel was calculated using the following equation:

$$M_{ref} = \rho_{ref} V_{ref} = V_{ref} \frac{p_{ref} \widehat{M}}{RTZ_{ref}} \quad (7)$$

wherein M_{ref} is the mass of the gas in the reference cell, ρ_{ref} is the density of the gas in the reference cell, $\widehat{M}$ is the molecular weight of the gas, and Z_{ref} is the compressibility of the gas. For a multicomponent gas, the gas molecular weight can be calculated knowing the composition of the gas and using:

$$\widehat{M} = \sum_{i=1}^{n} M_i x_i \quad (8)$$

where M_i is the molecular weight of gas component *i* and x_i is the molecular fraction of component *i* in the gas.

The mass adsorbed on the samples is equivalent to the difference in mass in the reference cell and sample cell before expansion and the mass in both the sample call and reference cell after expansion:

$$M_{ads2} = M_{ads1} + V_{ref} \frac{p_{ref1} \widehat{M}}{RTZ_{ref1}} + V_{free} \frac{p_{sample1} \widehat{M}}{RTZ_{sample1}} - V_{ref} \frac{p_{ref2} \widehat{M}}{RTZ_{ref2}} - V_{free} \frac{p_{sample2} \widehat{M}}{RTZ_{sample2}} \quad (9)$$

The volume of gas adsorbed per the mass of adsorbent was determined using the following:

$$G_{ads} = \frac{M_{asd2} Z_{SC} R T_{SC}}{MW_{ads2} p_{SC}} 0.04464 \quad (10)$$

wherein G_{ads} is the amount of gas adsorbed per unit mass. MW_{ads2} is the molecular weight of the adsorbed gas. The subscript *SC* refers to standard conditions of 0°C and 1 bar. The constant 0.04464 is the conversion from standard cm^3/g to moles adsorbed per kilogram of coal.

Equation 7 does not account for the volume of the sorbed phase and was modified

to account for this change in volume as follows[130]:

$$n_2 = n_1 \frac{\rho_s - \rho_{f1}}{\rho_s - \rho_{f2}} \left(1 - \frac{\rho_{f2}}{\rho_s}\right)^{-1} \left[V_{ref} \left(\frac{p_{ref1}}{Z_{ref1}RT} - \frac{p_{ref2}}{Z_{ref2}RT}\right) + V_{free} \left(\frac{p_{sample1}}{Z_{sample1}RT} - \frac{p_{sample2}}{Z_{sample2}RT}\right)\right] \quad (11)$$

In Equation 9, n_2 is the number of moles of gas adsorbed at the end of the step, n_1 is the number of moles adsorbed from the previous step, ρ_s is the density of the sorbed phase, ρ_{f1} is the density of the free gas at the end of the previous step, and ρ_{f2} is the density of the free gas at the end of the step. Equation 8 was used with Equation 9 to convert from number of moles to gas adsorbed per unit mass.

Langmuir fit. In order to model the injection of CO_2 into a thermally treated coal seam, the experimental isotherms were fitted to an equation that represents the amount adsorbed as a function of pressure. The International Union of Pure and Applied Chemistry (IUPAC) has guidelines for classifying different adsorption isotherms, of which there are six different types. The isotherm type observed from these measurements is a Type 1 or a Langmuir isotherm.[131] A Type 1 isotherm is characterized by having increasing gas storage capacity until a plateau is reached. Type 1 isotherms are typically seen with microporous solids showing micropore filling but no multilayer surface adsorption.[26] The Langmuir equation used to represent a Type 1 isotherm can be found below:

$$m(p,T) = m_\infty(T) \frac{b(T)p}{1+b(T)p} \quad (12)$$

wherein $m(p,T)$ is the predicted amount of mass adsorbed as a function of temperature and pressure, $m_\infty(T)$ is the maximum theoretical amount of gas that can be adsorbed, and $b(T)$ is the Langmuir fitting parameter. Although the details of the thermodynamics involved in deriving Equation 10 will not be discussed, it is important to list the

assumptions used in said equation:[26]

1. Adsorption only occurs on a fixed number of sites
2. Monolayer adsorption
3. All sites are energetically equivalent
4. There are no interactions between adsorbed molecules.

The experimental data were fitted to the Langmuir equation using least squares minimization in MATLAB R2009b. The Langmuir equation can also be expanded to account for multiple components:

$$m_i(p_i \dots p_N, T) = m_{i\infty}(T)\frac{b_i p_i}{1+\sum_{k=1}^{N} b_k p_k}, i = 1 \dots N \quad (13)$$

m_i is the mass adsorbed of component *i*, p_i is the partial pressure of component *i*, $m_{i\infty}$ is the maximum theoretical amount of i that can be adsorbed, and b_i is the Langmuir parameter for component *i*.

Injection simulations. Injection simulations were done to show the effect of changes in the adsorptive capacity of the thermally treated coal on the recovery of methane and the storage of CO_2. Injection simulations were done using the Computer Modelling Group (CMG) software GEM. This software can be used to model enhanced recovery processes in heterogeneously fractured structures. GEM is useful for modelling CO_2 enhanced oil recovery, water-alternating-gas (WAG), and enhanced coal bed methane (ECBM) operations. The ECBM packages in GEM were found to be the most useful as it shares many similarities with what would be found in a postthermal process CO_2 injection scenario: dual porosity modeling, multicomponent adsorption, injection and production controls.

The domain used for the injection simulations was 100 meters in length, 100

meters laterally, and 9 meters deep. A dual porosity/ dual permeability model was used to represent heterogeneous flow paths through the system. Cleats and thermally induced fractures would have high porosity and permeability compared to the remaining material. Experimentally determined adsorption values and permeability values were used for the coal matrix.

Due to lack of information, some default values were used. Fracture permeability was defined as four Darcy's. Pore compressibility was defined as 1.45E-7. The default relative permeabilities were used as well as the matrix density. Adsorption of CO_2 and desorption of CH_4 were modeled using the multicomponent Langmuir equation, which is common practice for these types of simulations but does have its shortcomings[132, 133], particularly resulting from the values used in the equation being from single component isotherms. Due to a lack of resources, multicomponent isotherms were unattainable and are a possibility for future work.

An injector well was placed in one corner of the domain and a producer well was positioned in the opposite corner. The wells were perforated through the entire zone. The injector well was rate controlled and the producer well was pressure controlled. The injector well introduced $6000m^3$ of CO_2 per day while the production well operated with a minimum bore hole pressure of 2.75 bar. Rate control refers to a set rate of injected fluid while pressure control refers to the well head pressure controlling the rate of production. No-flow boundary conditions were used at the domain boundaries. The simulation was performed over a 1 year time span.

Table 1: Analysis performed by Huffman Labs on the coals used. All values are reported on a percentage by weight basis except for the Higher Heating Value (HHV).

	Skyline	Carlinville	North Antelope
Loss on Drying (105°C)	3.18	9.65	23.69
Ash (750°C)	8.83	7.99	4.94
C	70.6	64.67	53.72
H	5.41	5.59	6.22
N	1.42	1.12	0.78
S	0.53	3.98	0.23
O (by diff.)	13.21	16.65	34.11
Volatile Matter	38.6	36.78	33.36
Fixed Carbon	49.39	45.58	38.01
HHV (BTU/lb)	12606	11598	9078

Table 2: Elemental analysis of the sampled coals' ashes. Values reported in percentage of weight of the ash.

Element	Skyline	Carlinville	North Antelope
Al	14.52	17.66	14.78
Ca	6.11	1.87	22.19
Fe	5.09	14.57	5.2
Mg	1.39	0.98	5.17
Mn	0.02	0.02	0.01
P	0.59	0.11	1.07
K	0.57	2.26	0.35
Si	60.89	49.28	30.46
Na	1.41	1.51	1.94
Si	2.33	2.22	8.83
Ti	0.88	0.85	1.3

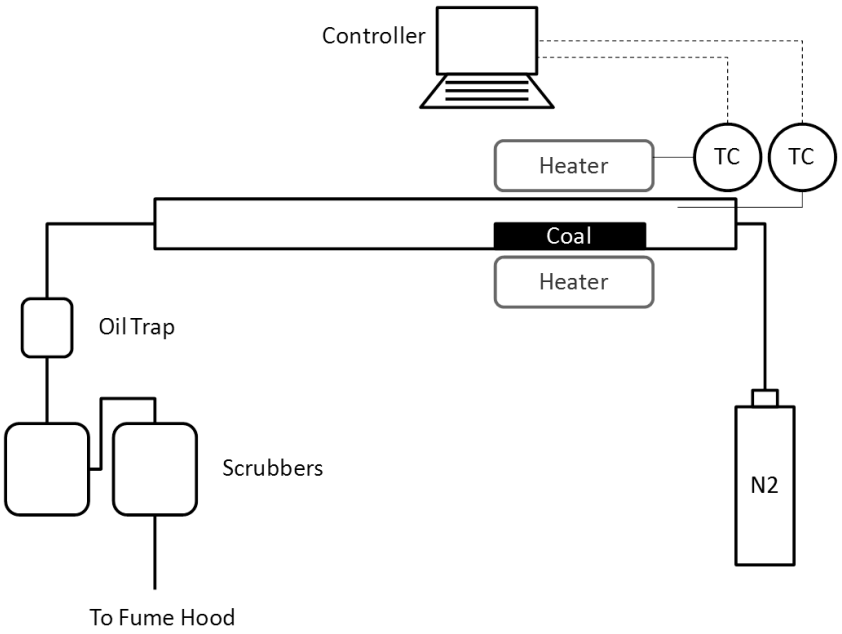

Figure 3: Schematic of the tube furnace used for producing the coal samples. The furnace has an internal diameter of 2.5 inches and a heated length of 2 feet. There is a 4 foot unheated section to facilitate cooling of the oils and gasses. An oil trap collects a portion of the produced oil for later analysis. The tube furnace has a programmable controller with an automatic shut off feature. The produced gasses from the furnace are flowed through two water scrubbers and vented directly inside a fume hood.

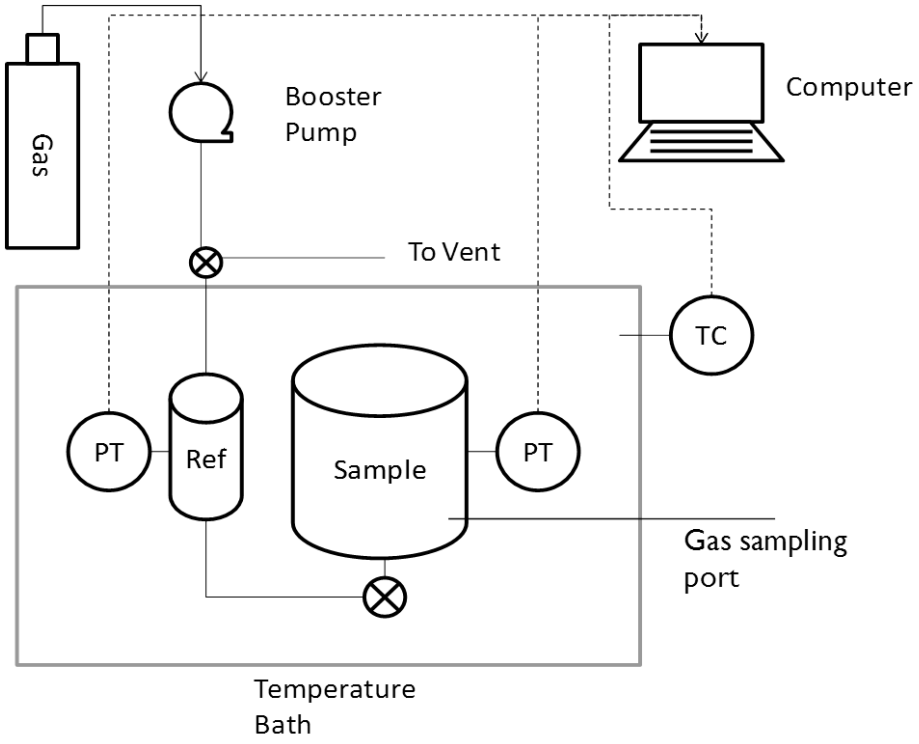

Figure 4: Schematic of a single sample cell and reference cell used for measuring isotherms. The isotherm apparatus at TerraTek has three identical sample cell and reference cell systems. Having three systems running in parallel allowed for more efficient measurement.

Table 3: Summary of all of the coal samples prepared for analysis

Skyline		**Carlinville**		**North Antelope**	
Unreacted, Dry		Unreacted, Dry		Unreacted, Dry	
325°C @ 10°/min.	325°C @ 0.1°/min.	325°C @ 10°/min.	325°C @ 0.1°/min.	325°C @ 10°/min.	325°C @ 0.1°/min.
450°C @ 10°/min.	450°C @ 0.1°/min.	450°C @ 10°/min.	450°C @ 0.1°/min.	450°C @ 10°/min.	450°C @ 0.1°/min.
600°C @ 10°/min.	600°C @ 0.1°/min.	600°C @ 10°/min.	600°C @ 0.1°/min.	600°C @ 10°/min.	600°C @ 0.1°/min.

Table 4: Reference cell charges for isotherm measurements with CO_2 and CH_4

Pressure Step Number	CO_2 (bar)	CO_2 (PSIG)	CH_4 (bar)	CH_4 (PSIG)
1	3.4	50	6.9	100
2	6.9	100	13.8	200
3	10.3	150	27.6	400
4	13.8	200	55.2	800
5	20.7	300	82.8	1200
6	27.6	400	137.9	2000
7	34.5	500	206.9	3000
8	41.4	600	275.9	4000
9	55.2	800	344.8	5000

Table 5: Experimental matrix for isotherm measurements on each sample

	Adsorptive	
Temperature	CO_2	CH_4
50°C	1	3
70°C	2	4

CHAPTER 4

PORE SIZE DISTRIBUTIONS

The main purpose of this chapter is to present the results of the BET surface area measurements and pore size distributions for the Skyline, Carlinville, and North Antelope coals. The mass losses of the coals from thermal treatment are also included in this section.

The role of pore size distributions are a critical element of this dissertation. The pore sizes were found to correlate well with surface area, adsorption, and permeability. Since changes in pore distributions were the result of thermal treatment of the coal, attempts were made to develop a relationship between the pore sizes and final treatment temperature and heating rate. It was also hypothesized that some of the residual hydrocarbons remaining after thermal treatment could be a location for additional pore development.

Mass Losses from Pyrolysis

Coals from the Carlinville mine in Utah, the Carlinville mine in Illinois, and the North Antelope mine in Wyoming were pyrolyzed in a tube furnace in an anoxic environment. The coals were heated to final temperatures of 325, 450, or 600°C with heating rates of 10 or 0.1°C per minute. As part of the pyrolysis procedure, masses of the coals were recorded before and after each experiment.

The results for the mass losses for the coals can be found in Table 6. The results

in Table 6 are reported on a dry basis as a percentage of the dry weight. Reporting values on a DAF (dry, as-free) basis was done to help with comparison, the North Antelope coal contained a lot more moisture compared to the Skyline and Carlinville coals.

This study was not concerned with the either the kinetics of pyrolysis or the products; therefore, a proximate analysis of the pyrolysis products was not performed. Further, due to the large quantity of coal needed for isotherm measurements, setting up a sample loop to capture a representative sample would have proven technically troublesome. There is some existing literature pertaining to coal pyrolysis with slow heating rates[6, 9, 134, 135] where general trends should be applicable to this work.

From the results presented in Table 6, it can be seen that the Carlinville coal had the least amount of mass loss while the North Antelope presented the greatest. A general trend in the data can also be easily noticed; higher treatment temperatures resulted in larger mass loss. The effects of heating rate are not as conclusive. The Skyline and Carlinville coals, both bituminous, generally showed larger mass losses with slower heating rates, while the North Antelope coal (sub bituminous) showed more mass loss with faster heating rates. It is a possibility that the faster heating rate caused a quick buildup of pressure that may have blasted off small coal particles.

Surface Area Analysis

Surface area analysis was done on all of the coals using a Micromeritics Tristar II surface analyzer. All of the samples were pretreated at 80°C under vacuum for at least 36 hours to remove any volatiles. CO_2 was used as the analysis gas because there have been issues reported using nitrogen or argon.[33, 123] A custom program was written for the Micromeritics machine based on the “full isotherm for pore size distribution” program

built into the software. The main differences between that program and the program used in this study was the use of CO_2 instead of nitrogen, more measurements at lower pressures, and including Dubinin-Radushkevich and BJH into the calculations.

The contribution of residual hydrocarbons to the surface area of the coals after pyrolysis was examined. After screening several different solvents, it was found that acetone was best suited for this analysis. Acetone is a mild solvent that was effective at removing the residual hydrocarbons without being so aggressive that it would alter the overall structure of the coal. Solvent treatment was done using Dean-Stark extraction. Dean-Stark has the advantages of using a continuously recycled hot solvent to better remove components with low solubility.

Samples were collected before and after high pressure isotherm measurements were performed. This was done in order to determine if exposure to CH_4 or CO_2 at high pressures would have any change on the pore size distributions or the amount of pores in the residual hydrocarbons.

BET Surface Area Analysis

The BET surface area analysis of the fresh and thermally treated coals revealed some of the changes in the surface area of the coal. Brunauer, Emmett, and Teller expanded on the classic Langmuir adsorption model for multilayer adsorption. It should be noted that the surface area measurements presented henceforth were done with CO_2. Carbon dioxide surface areas generally tend to be larger than surface areas measured with nitrogen. This difference is due to the higher affinity of CO_2 for chars than nitrogen. Carbon dioxide was required for these measurements because nitrogen surface area measurements can produce erroneous results.[123]

Skyline Coal

Surface area measurements on the Skyline coals can be found in Figure 5. For the Skyline coal, the surface area increased with treatment temperature. There seems to be little dependence on the heating rate with this particular coal. Coals treated to 325°C showed similar surface areas regardless of heating rate, but had surface areas less than that of the untreated coal. The coal treated with the faster heating rate to 450°C showed more surface area than the same coal treated to the same final temperature with a slower heating rate. The coal treated with the faster heating rate to 600°C showed less surface area than its counterpart treated with a slower heating rate.

Solvent extraction on the Skyline coals was done to remove any pores made of residuals and to remove residuals from the interior linings of pores in the coal matrix. Solvent extraction on the unreacted Skyline coal showed a pronounced increase in the measured surface area. The coals treated to 325°C showed an increase in the surface area with solvent extraction.

The values seen with the extraction on coals thermally treated 325°C are still less than the solvent extracted unreacted coal. The coal treated to 450°C with a heating rate of 0.1°C/min showed a slight increase in surface area, while the coal treated to the same temperature with a heating rate of 10°C/min showed a slight decrease. The coals treated to 600°C showed decreases in the surface area after solvent extraction, regardless of heating rate.

Carlinville Coal

Surface area measurements on the Carlinville coals can be found in Figure 6. The trends in the surface area measurements for the Carlinville coals were similar to that

observed with the Skyline coals. Carlinville coals showed increases with thermal treatment temperature. The coals treated to 325°C showed similar surface areas regardless of heating rate. Coals treated to 600°C also showed similar surface areas independent of heating rate but not too different than the unreacted coal. The coal treated to 450°C with a heating rate of 10°C/min showed slightly higher surface area than the coal treated to the same final temperature at a rate of 0.1°C/minute.

Surface area analysis after solvent extraction on the Carlinville coals also showed similar trends to the Skyline coals. Coals treated to 325°C and 450°C showed increases in the measured surface area after solvent extraction. The coal treated to 600°C with a heating rate of 0.1°C/min had an increase in surface area after solvent extraction while the coal treated to the same temperature but with the faster heating rate showed a slight reduction in surface area.

The unreacted Carlinville coal showed a slight decrease in surface area similar to the Skyline coal. The coal treated to 325°C with a heating rate of 0.1°C/minute showed a decrease in surface area after solvent extraction less than that of the unreacted Carlinville coal but greater than that solvent extracted Carlinville coal. A heating rate of 10°C/minute and a final treatment temperature of 325°C showed a large increase in surface area after solvent extraction.

There are a few differences between the surface area measurements of the Skyline and Carlinville coals. One of the starkest differences is the influence of residual tar on the coals treated to 325°C. Both coals showed similar surface areas, but solvent extraction revealed that residual tars were filling pores with the 10°C/minute experiment and tars were negligible with the 0.1°C/minute experiment.

North Antelope Coal

Like the Skyline and the Carlinville coals, the North Antelope coals also showed increases in surface area with increasing treatment temperatures (Figure 7). The North Antelope coals treated to 325°C showed similar surface areas regardless of heating rate; similar to the Carlinville coals treated to the same temperature and all having similar surface areas compared to their respective unreacted coals. The North Antelope coal treated to 450°C with the faster heating rate showed a greater increase in surface area than the coal treated to the same temperature with a slower heating rate. The coals treated to 600°C also showed similar surface areas regardless of heating rate.

The nature of the surface areas of the coals can be misleading as observed with the coals being subjected to solvent extraction. Unlike the Skyline and Carlinville coals, both North Antelope coals treated to 325°C showed increases in surface area after solvent extraction meaning that for these treated coals, residual tars were blocking access to surface area. The coal treated to 450°C with a heating rate of 0.1°C/minute showed an increase in surface area after solvent extraction while the coal treated to the same terminal temperature with a faster heating rate showed little difference. North Antelope coals treated to 600°C both showed significant decreases in surface area after extraction but with the coal treated with a heating rate of 10°C/minute retaining more surface area.

The surface area measurements on the unreacted and thermally treated North Antelope coals definitively show the effects of different heating rates. More nonresidual residing pores can be found with coals treated with a faster heating rate while the effects of thermo-plastic deformation and surface area in residual tars are more prevalent with a slower heating rate. Slower heating rates are more likely to be encountered with the

UCTT process. If UCTT were applied to North Antelope coals, one would anticipate that most of the increase in surface area would be due to residual tars.

Pore Size Distributions

Pore size distributions were done using a combination of two different methods. density functional theory (DFT)[18] was used to characterize micropores (<20Å) and Barrett-Joyner-Halenda (BJH)[20] was used for pores larger than 20Å. The BJH analysis encompassed most of the mesopore range (20Å-500Å) as well as some of the smaller pores in the macropore range (>50Å). Pore size distributions were performed alongside the BET surface area analysis, albeit over a much larger range of pressures. Pore sizes were measured using a Micromeritics Tristar II using CO_2 as the adsorbate at 273.15K.

There is a small gap in the data provided by the two aforementioned methods. This discontinuity usually occurs between 20Å and 30Å. The discontinuity in the data is easily recognized as a sudden dip in the pore size distributions within the aforementioned range. With this in mind, it is important to interpret the area preceding the discontinuity independently from the area following the discontinuity. Furthermore, since the methods used for micropores and mesopores are different, there may be discrepancies of the estimated pore volumes and the true pore volumes.

Pore volumes from DFT and BJH were plotted together to provide an *ab ovo* approach for pore sizes measureable using the Tristar II with CO_2. Like the surface area measurements, pore size distributions were also done on solvent extracted coals to determine the effects of residual hydrocarbons.

Skyline Coal

The pore size distributions for the untreated and thermally treated Skyline coals can be found in Figure 8. Pore volumes increased with treatment temperature after 325°C. Like the surface area for the coals treated to 325°C being less than that of the fresh coal, there is a slight reduction in pore volumes from that of the unreacted coal over the entire range of pores measured. This reduction in pore volumes occurred regardless of heating rate. Coals treated to 450°C showed an increase in the mesopore ranges for both heating rates with a larger increase in mesopores. Coals treated to 450°C with a heating rate of 0.1°C/min showed little increase in micropores while the coal treated to the same temperature with a heating rate of 10°C/min showed a noticeable increase. Both coals treated to 600°C showed large increases over the entire range of measured pore sizes. The coal treated to 600°C with a heating rate of 10°C/min showed larger increases in the micro- and mesopore regions than the coal heated with a rate of 0.1°C/min.

Solvent extraction on the untreated and thermally treated Skyline coals showed interesting results with pore size distributions. Sohxlet extraction on the untreated Skyline coal showed increases in both meso- and micropore volumes. The increase in pore volumes implies that some tar filled aforementioned pores. Solvent extraction on the coal treated to 325°C with a heating rate of 0.1°C/min found increases in the mesopore range larger than that of the solvent-extracted untreated coal but showed little difference with respect to micropores. Extracted Skyline coal treated to 325°C with a heating rate of 10°C/min showed meso- and micropores volumes still less than that of the untreated coal. The fact that removing residual hydrocarbons did not increase the pores

size distributions for this coal implies that another mechanism, such as plastic deformation, is responsible for this reduction.

Solvent extraction on the coal treated to 450°C with a heating rate of 0.1°C/min showed slight increases in both the micro- and mesopore ranges while extraction on the same coal treated to the same temperature with a heating of 10°C/min showed negligible change in the mesopore region and a decrease in the micropore region. This difference demonstrates some of the competing kinetics occurring between plastic deformation and pore development in the coal matrix and remaining tars. The effects of plastic deformation at 450°C are overacted by pores created via pyrolysis. With the slow heating rate, it is likely that eluted tars begin filling pores slightly reducing their volume, while with the faster heating rate, most of the tars in the mesopore region have completely volatilized but some tar remained creating abundances of micropores.

This idea of kinetic competition for pore development with Skyline coal is further justified after examination of the solvent extracted coals treated to 600°C. With the coal treated to 600°C at 10°C/min, there is little change in the mesopore distribution but an increase in the micropore distribution; this is similar to the coal treated to 450°C with the same heating rate. However, regarding the coal treated to 600°C with a heating rate of 0.1°C/min, there is an increase in the micropores and a large decrease in the mesopores after solvent extraction, meaning that some of the mesopores in this sample are in tars. The interpretation of the solvent extraction on the thermally treated Skyline coals is summarized in Table 7.

Sometimes an analogy with a common household item is useful in explaining an otherwise abstract concept. For coals undergoing slow pyrolysis, it is mentally beneficial

to compare the process to something else that undergoes deformation when heated, cheese. Swiss cheese works well for this mental depiction as it has naturally occurring small and large pores to represent the initial pores in the coal. As the cheese is heated, it softens and some of the original pores are reduced in size or completely closed off; this is like heating the Skyline coal to 325°C. Once a certain temperature is reached, components volatilize creating internal pressure causing bubbles that eventually burst. If the heating rate is fast enough, some of these bubbles set but if the heating rate is slow, some of these bubbles are still subject to closure from plastic deformation. Oil that separated from the cheese collects on the surface and in the pores. Now imagine that this oil can dry out and by doing so creates even more pores; this is akin to pores developing in the residual tars of the coal only to have the porous media washed away with solvent extraction.

Carlinville Coal

The pore size distributions on the Carlinville coals showed some major differences when compared to the Skyline coal. While the Skyline coal showed large increases in the range greater than 20Å, the Carlinville coal showed more changes in the micropore region. Pore size distributions for the untreated and thermally treated Carlinville coals can be found in Figure 9. The shift between the largest pore abundances between these two coals is not great and is likely the result of differences in the original coal matrix structure. With the unreacted Carlinville coal, the largest amount of pore volume occurs around 20Å with solvent extraction showing increases in both the micro- and mesopore regions. Like the Skyline coal, pore volumes tend to increase with treatment temperature. The Carlinville coal treated to 325°C with a heating rate of

0.1°C/minute had pore size distributions almost identical to the untreated coal even after solvent extraction, implying that little physical change occurred in the coal structure. Carlinville coal treated to 325°C with a heating rate of 10°C/minute showed an increase in the high micropore/ low mesopore region with solvent extraction showing only slight differences. The coal treated to 450°C with a heating rate of 10°C/minute showed a shift into the mesopore region with the largest increase around 20Å. The increase in this coal remained after solvent extraction but shifted into the micropore region. The coal treated to 450°C with the slow heating rate had a large increase over the entire range of pore sizes after solvent extraction. Both coals treated to 600°C showed a significant increase across the entire pore distribution with solvent extraction increasing those pore volumes.

This trend seems to be universal across all the coals and shows that at low pyrolysis temperatures pore changes are largely dominated by plastic deformation. When the unreacted coals were treated with acetone extraction, a large increase in the micropore region was observed, implying that pre-existing hydrocarbons were blocking these pores. Solvent treated coals heated to 325°C showed increases in the micro- and mesopore regions but both were still less than the solvent extracted untreated coal. This lends credibility to the hypothesis of small pores swelling shut at lower treatment temperatures. The North Antelope coal treated to 450°C with the fast heating rate showed a net increase over that of the unreacted coal and coals treated to 325°C; solvent extraction caused little change in pore volumes.

The coal treated to 450°C with the slower heating rate also showed an increase in pore volumes but less than that of the coal treated with the faster heating rate; also, there was more pore volume after solvent extraction. The trend of the coals treated to 450°C

with the faster heating rate showing little change in pore volumes after solvent extraction occurred with all coals; the trend of coals treated to 450°C with the slower heating rate universally showed increases in pore volumes after solvent extraction. These trends occurring with coals treated to 450°C are illustrative of competing pore-changing processes occurring near this temperature. At this temperature, the coal is softened and a combination of rapid expulsion of pyrolysis gases and explosive particle ejection are evident with fast heating rates. Softening and expansion of pores is seen with the slower heating rate, but these pores soon filled with produced tars only to be revealed with solvent extraction.

Even though the trends at 450°C seem transient across all coal types in these experiments, the results of the pore size distributions on coals treated to 600°C seem more coal-type dependent. The North Antelope coals treated to 600°C showed large increases in the micropore and mesopore regions but solvent extraction proved that a significant portion of these increases were in residual hydrocarbons. While this is similar to the Carlinville coals, it differs from the Skyline coal where pores were obstructed by residual hydrocarbons.

There are some common trends between changes in pore size distributions with certain treatment temperatures/rates; there are also some discrepancies with other temperatures and rates. These discrepancies seem related to the coals used in these experiments and support the fact that in an actual implementation of UCTT it will be important to perform these same measurements on the coal being used to better estimate pore sizes.

Surface Area and Pore Size Distributions after High-Pressure Isotherm Measurements

All coals had surface area and pore size distribution measurements after high pressure isotherm measurements (Chapter 5). The results of these analyses showed negligible change in the pore structure and surface area providing little additional information. The postisotherm studies did solidify that the porous structures in the coals were hardly changed from exposure to adsorptive gasses at high pressures and temperatures.

Dubinin-Radushkevich Micropore Surface Areas

The Dubinin-Radushkevich (D-R) method was used to help estimate the surface areas of micropores in these coals. The D-R measurements were performed alongside the BET surface area measurements and pore size distributions. There was little to be gained from the DR measurements on these coals; the D-R measurements were similar to the BET surface area measurements except they showed slightly larger micropore surface areas. The differences between D-R measurements and BET measurements were more pronounced with coals after solvent extraction; this is because the calculations used in D-R measurements rely more on lower pressure measurements to account for micropores, whereas BET analysis used a wider range of adsorption measurements. If solvent extraction revealed more micropores, than the expected result would be a higher estimation of micropore surface area. Coals that showed larger increases in micropore surface areas after solvent extraction showed higher D-R surface areas.

Implications for Modeling Particle Pyrolysis

The results of the pore size distributions have multiple implications on the modeling of coal pyrolysis at slow heating rates. In addition to different heating rates and final temperatures having effects on the kinetics of pyrolysis, complications now arise in the modeling of mass transfer and adsorption on a particle with changing pore sizes. The effects of permeability are investigated in a later chapter but can be summarized: increasing temperatures increases the permeability of the coal. Further, the changes in micro- and mesopores can also affect how pyrolysis products adhere to the coal surface. It is acknowledged that a single lumping coefficient could be employed to approximate these effects.

Conclusions

The results of the surface area analysis showed that surface area increases with terminal treatment temperature. It is important to restate that the surface area measurements performed here were done with CO_2 and not with nitrogen due to aforementioned reasons. Solvent extraction with acetone was used to determine what fraction of the surface existed in residual hydrocarbons on coals. Untreated Skyline coal showed an increase in surface area after solvent extraction while the Carlinville and North Antelope coals showed a decrease. The increase for the Skyline coal implied that tars were blocking access while the other coals showed that tars attributed to surface area.

All of the coals treated to 325°C showed decreased or similar surface areas compared to the unreacted coal. In most cases, it was determined that the pyrolysis residuals blocked surface area sites. Coals treated to 450°C showed increases in surface areas and in most cases solvent extraction showed little change or a slight increase. Coals

treated to 600°C exhibited the largest increase in surface area but solvent extraction on these coals showed mixed results depending on heating rate and coal source. The Skyline and North Antelope coals treated to 600°C showed decreases in surface area after solvent extraction, implying that a large portion of the surface area in these coals was in evolved hydrocarbons. The Carlinville coal treated to 600°C with a slow heating rate showed an increase in surface area after extraction meaning tars were blocking access to pores even with the high final temperature.

Pore size distributions of the coals were performed with DFT and BJH to account for the changes in microporous and mesoporous regimes. The pore size distributions were done concurrently with the surface area measurements and likewise used CO_2 as the analysis gas. Similar to the surface area analysis the pore volumes trended to increase with the extent of thermal treatment. Some trends were noticed for all coals:

- Coals treated to a terminal temperature of 325°C showed similar or lesser pore volumes than the unreacted coals likely due to thermo-plastic deformation.
- Solvent extraction on coals treated to 325°C showed increases in meso- and micropore volumes but still less than solvent extracted unreacted coals.
- Coals treated to 450°C with a heating rate of 10°C/minute showed little change after solvent extraction.
- Coals treated to 450°C with a heating rate of 0.1°C/minute showed increases in pore volumes after solvent extraction.
- Coals treated to 600°C showed increases in pore volumes.

- Solvent extraction on coals treated to 600°C showed differing results depending on heating rate and coal source.

From these trends it was evident that there were competing mechanisms for pore changes. There is the softening of the coal causing reductions in pore abundances, expansion of pores or expulsive ejection with fast heating rates, residual hydrocarbon deposits restricting access to pores, and the evolution of micro- and mesopores in residual hydrocarbons. To better aid in the conceptualization of pore changes, the Swiss cheese analogy was presented. With the heating of aforementioned cheese, one would expect that the pre-existing pores would soften and collapse. With increasing heating rates, evaporation of moisture in the cheese causes the formation of bubbles and pores. Depending on the heating rate, grease would either be quickly removed or would accumulate in new pores with solvent extraction revealing these pores.

Dubinin-Radushkevich micropore surface area analysis was done on all coals but the results from said analysis revealed little as they were similar to the BET surface areas. D-R analysis of the coals showed more surface area than BET analysis which was attributed to the different calculations used for each method.

BET, pore size distributions, and DR measurements were performed on the coals after high-pressure isotherm measurements. These measurements showed little change from the material before isotherm measurement.

These analyses had many implications for modeling the pyrolysis of coal with slow heating rates. The competing pore-changing mechanisms imply that a kinetic approach may be needed to thoroughly model these coals, although it is accepted that a "fudge" factor could be used account for these phenomena. It had been documented that

mesopores attribute to permeability and since it was shown that mesoporosity changes with treatment temperature, the changes in permeability may be accounted for (Chapter 6).

The most important things that can be taken from this section are how pore-volumes and surface areas increase with treatment temperature. In subsequent chapters it will be shown how pore size distributions, which are inherently related to treatment temperature, can affect properties such as permeability and high-pressure storage capacity.

Table 6: Percentage mass losses from pyrolysis. Results reported on a dry basis.

Thermal Treatment	Skyline	Carlinville	North Antelope
325 @10°C/min	8.09	4.34	20.97
450 @10°C/min	25.48	17.78	34.3
600 @10°C/min	30.3	25.66	41.98
325 @0.1°C/min	11.25	7.23	23.66
450 @0.1°C/min	19.15	17.2	25.06
600 @0.1°C/min	31.58	26.54	29.64

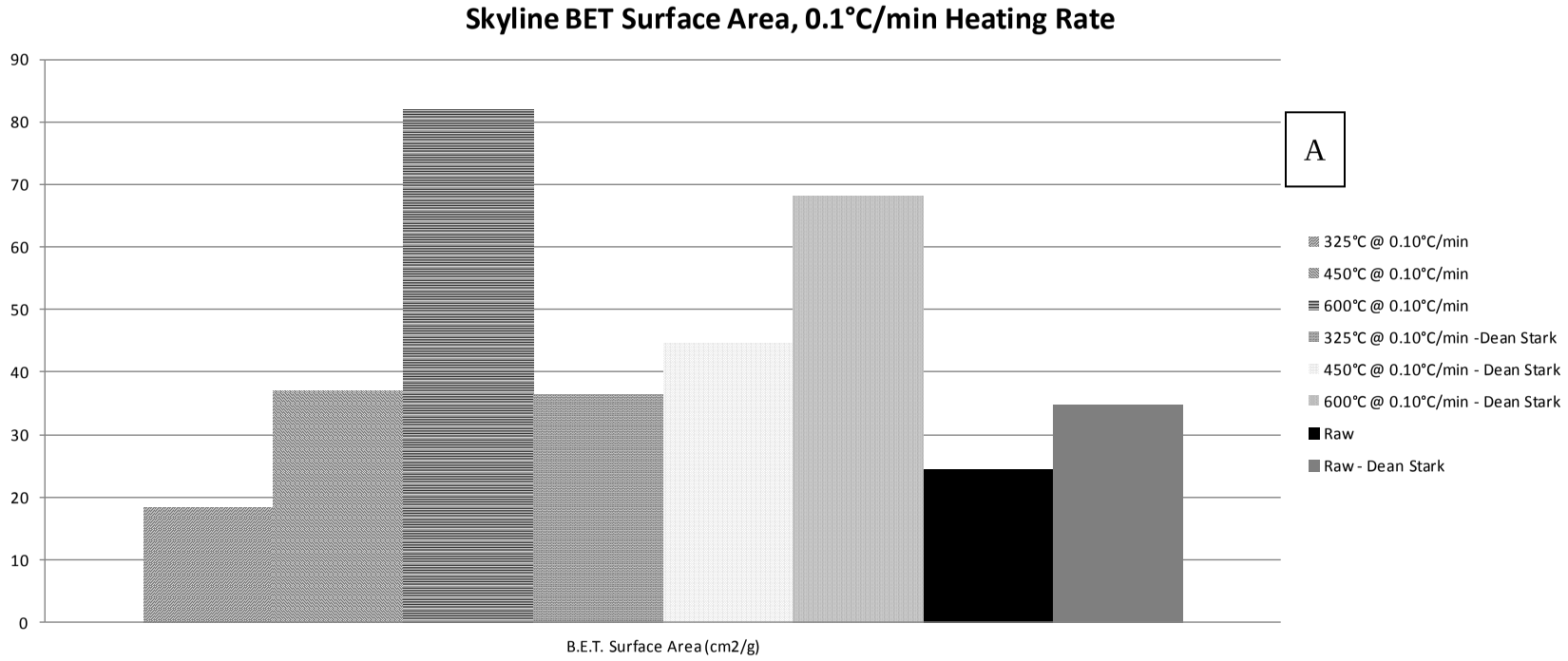

Figure 5: BET surface area measurements on the Skyline coal. A) Shows the coals treated with a 0.1°C/minute heating rate. B) Shows results using a 10°C/minute heating rate. Measurements were done on the untreated and thermally treated coals with and without solvent extraction. Measurements were performed using CO_2 as the adsorbate.

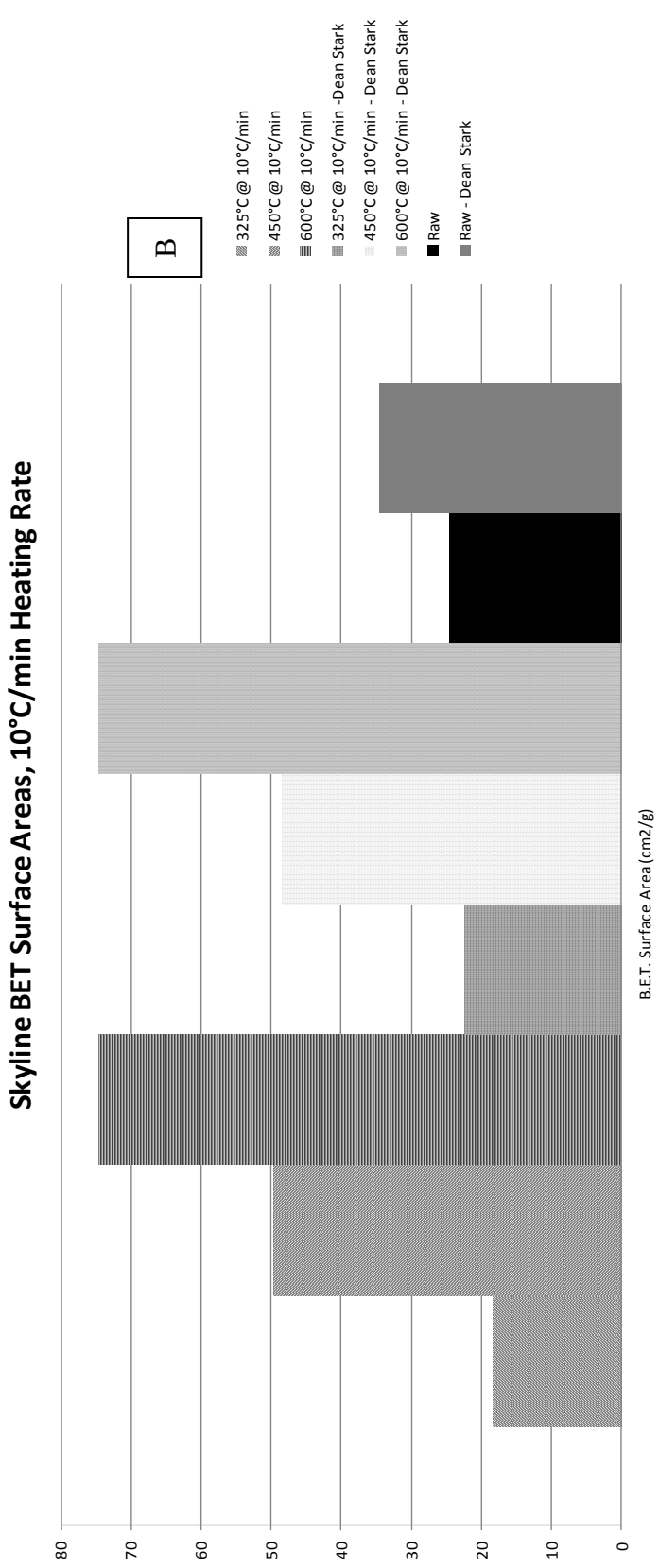

Figure 5 continued

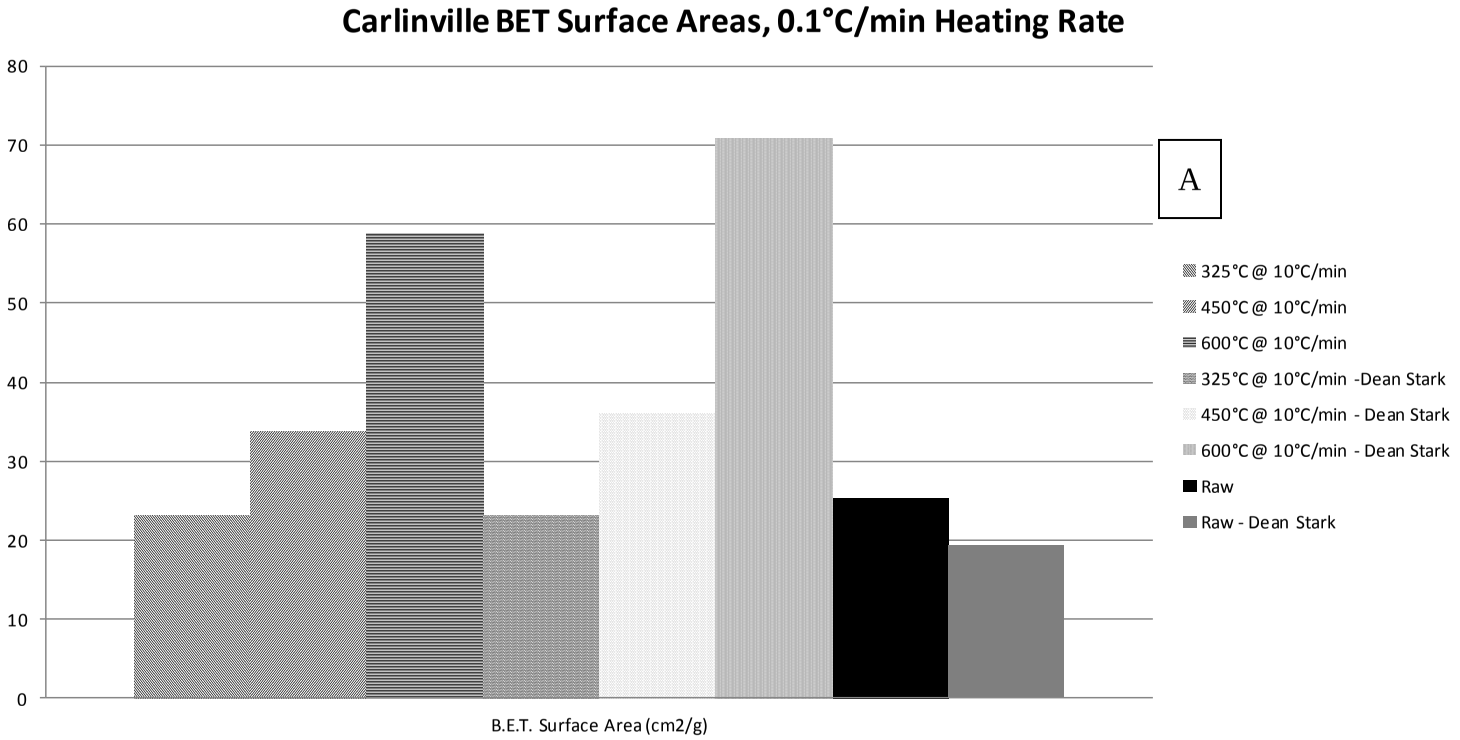

Figure 6: BET surface area measurements on unreacted and thermally treated Carlinville coal. A) Shows coals heated at 0.1°C/minute. B) The results with a 10°C/minute heating rate. All coals were subjugated to Dean-Stark solvent extraction with acetone. CO_2 was used as the adsorbate.

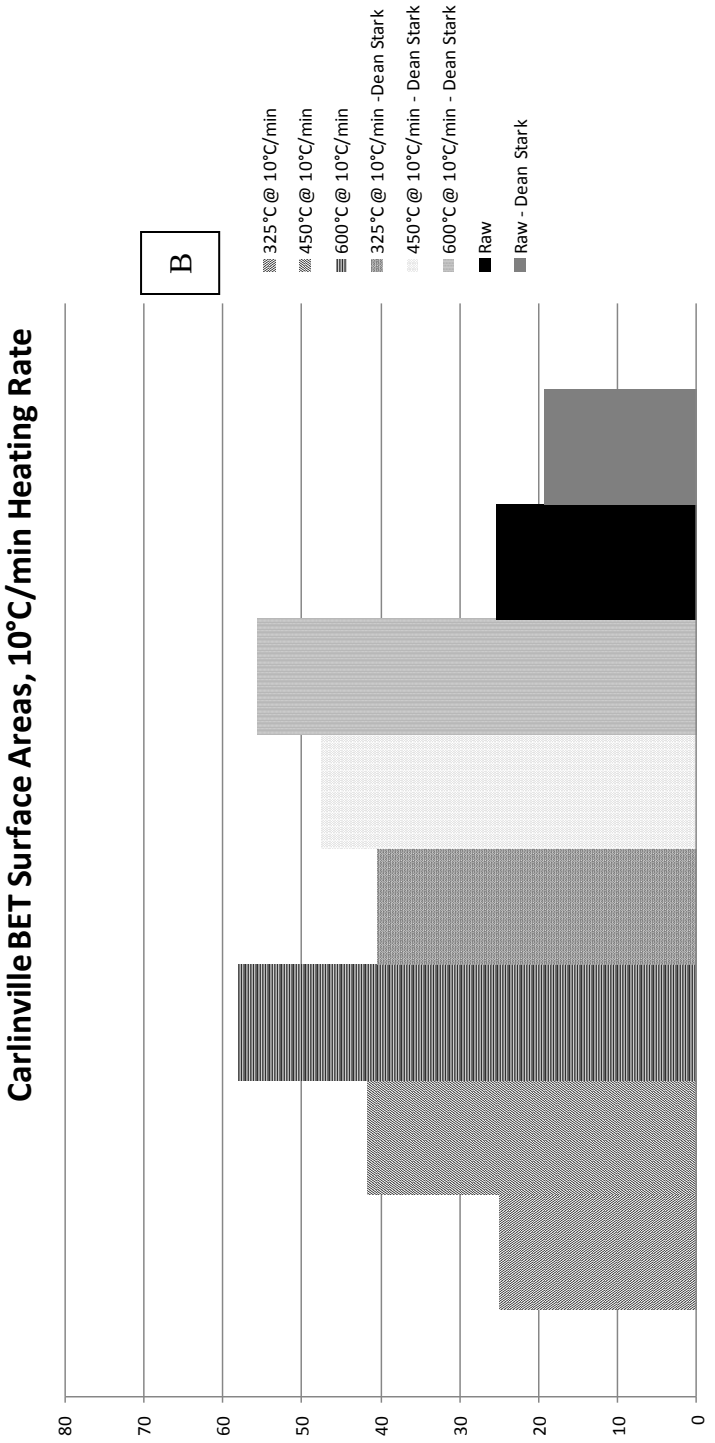

Figure 6 continued

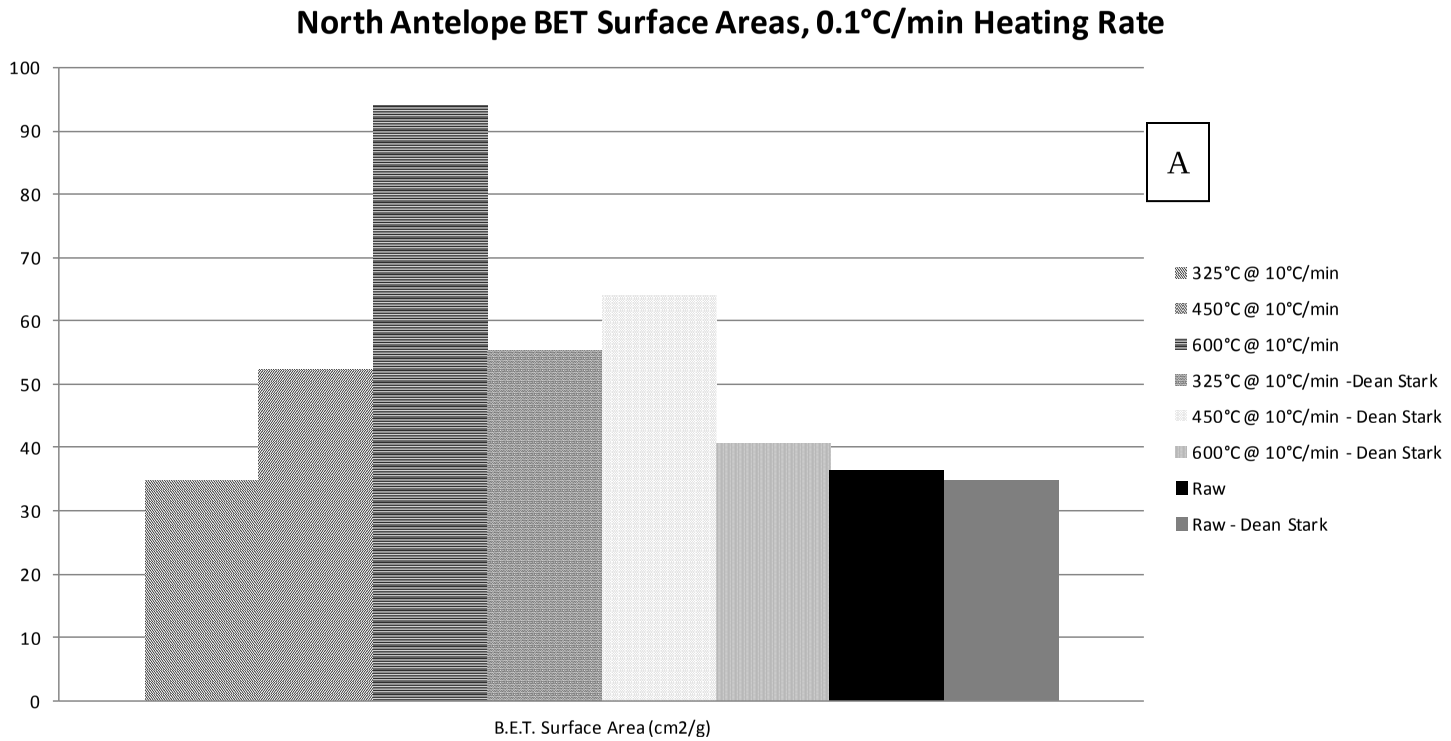

Figure 7: BET surface areas measured with CO_2 on untreated and thermally treated North Antelope coals. A) Shows coals heated at 0.1°C/minute. B) Shows the surface areas for coals treated with a 10°C/minute heating rate. All coals underwent solvent extraction with acetone to determine the effect of residual hydrocarbons on pore size.

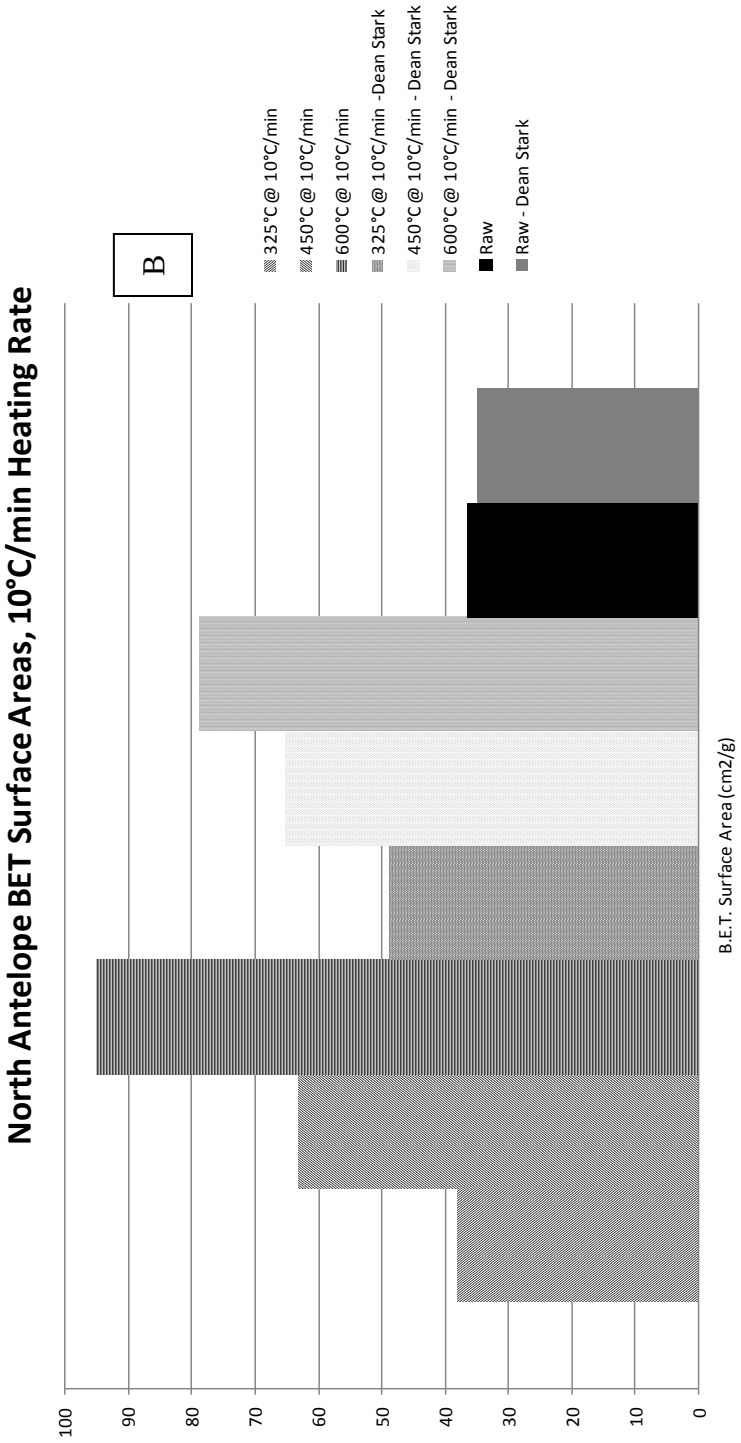

Figure 7 continued

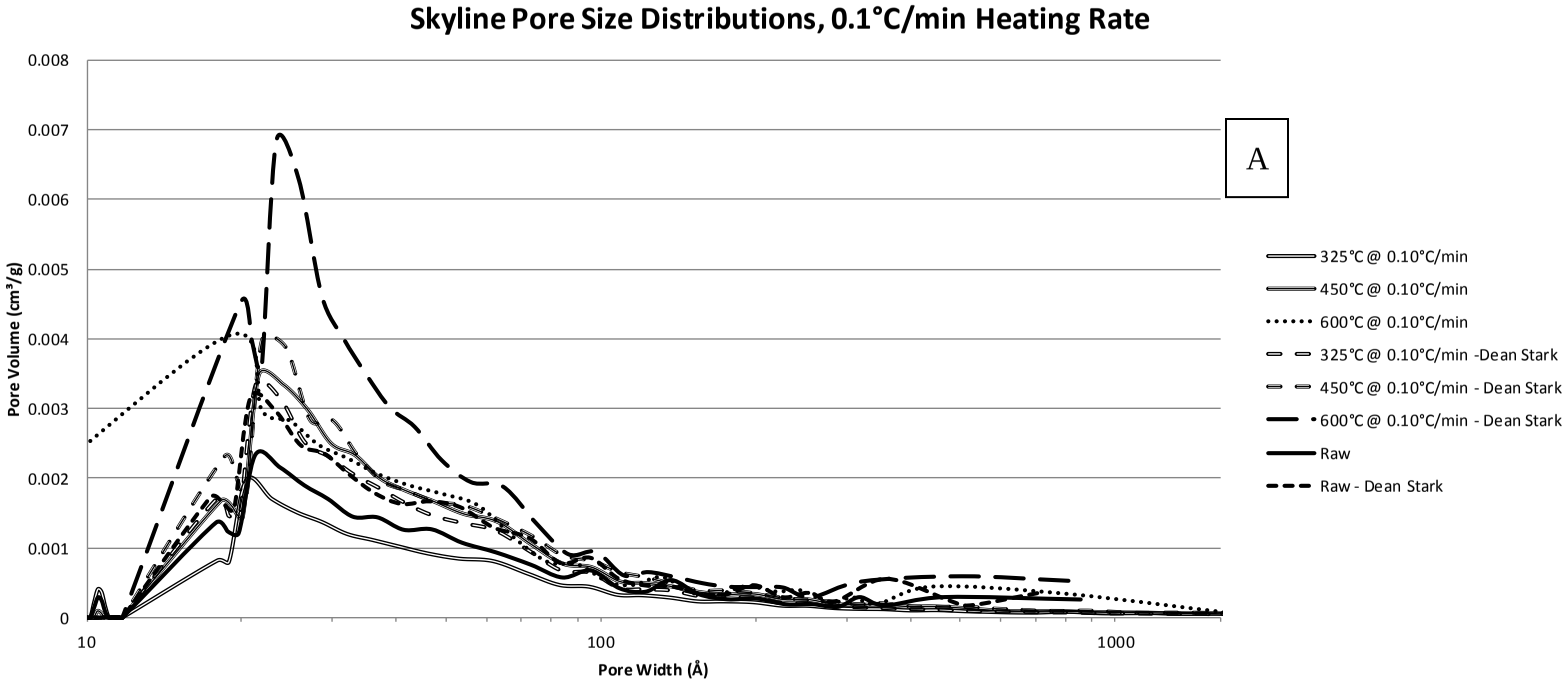

Figure 8: Pore size distributions for the unreacted and the thermally treated Skyline coal. A) Shows coals heated at 0.1°C/minute. B) Shows the pore size distributions for Skyline coals heated at 10°C/minute. Solvent extraction (Dean-Stark) was used to determine effect of residual hydrocarbons on pore sizes.

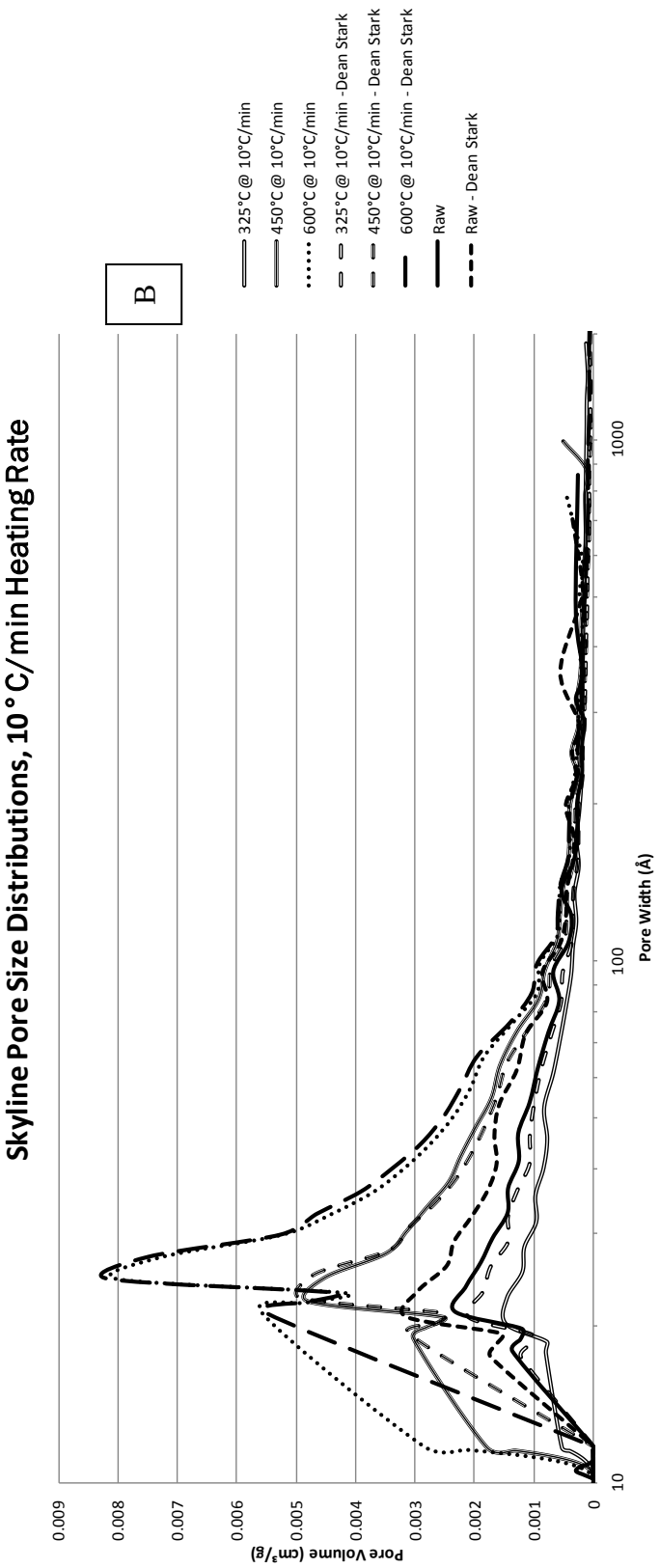

Figure 8 continued

Table 7: Interpretation of pore size development of Skyline coals after solvent extraction

Thermal Treatment	Micropores	Mesopores
325°C @ 0.1°C/min	plastic shrinking	plastic shrinking
450°C @ 0.1°C/min	net increase / tar filling	net increase / tar filling
600°C @ 0.1°C/min	net increase / tar filling	exist in tar
325°C @ 10°C/min	plastic shrinking	plastic shrinking
450°C @ 10°C/min	net increase / tar filling	net increase / no tar
600°C @ 10°C/min	net increase / tar filling	net increase / no tar

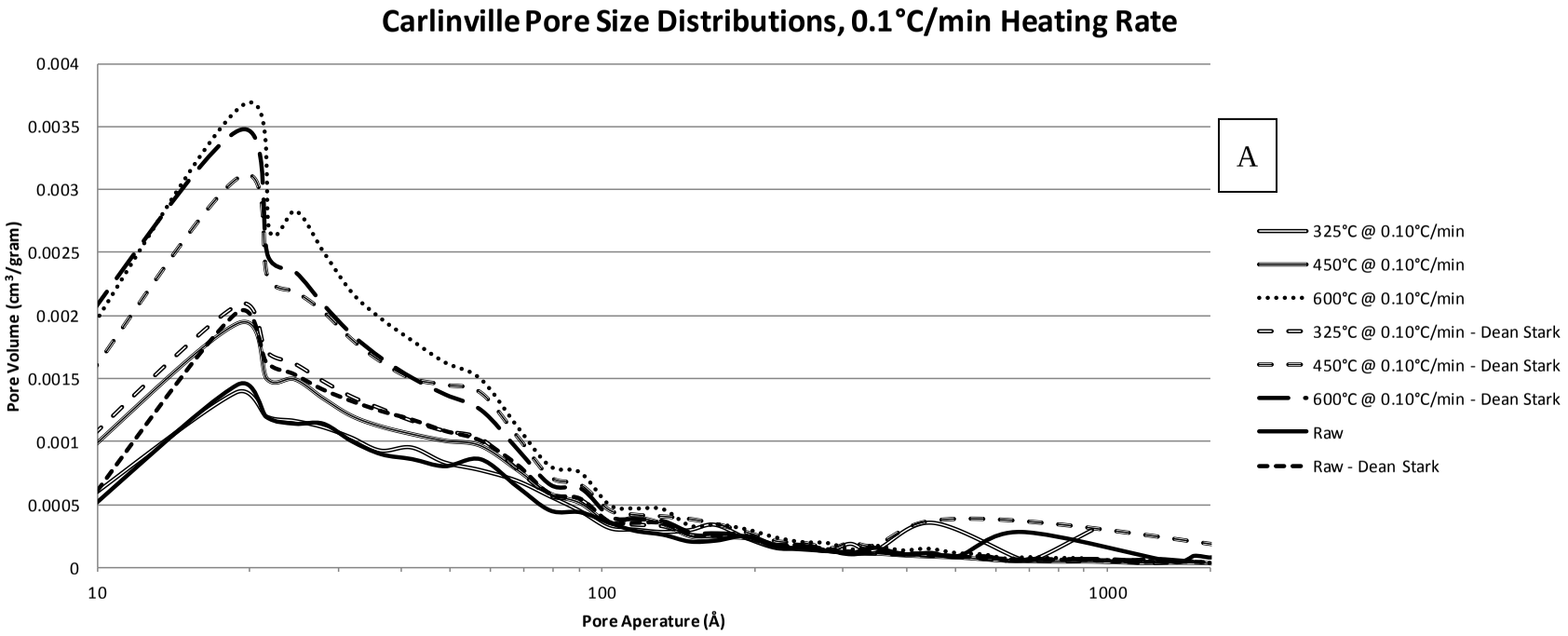

Figure 9: Pore size distributions for the unreacted and the thermally treated Carlinville coal. A) Shows pore size distributions for coals heated at 0.1°C/minute. B) Shows Carlinville heated at 10°C/minute. Solvent extraction (Dean-Stark) was used to determine effect of residual hydrocarbons on pore sizes.

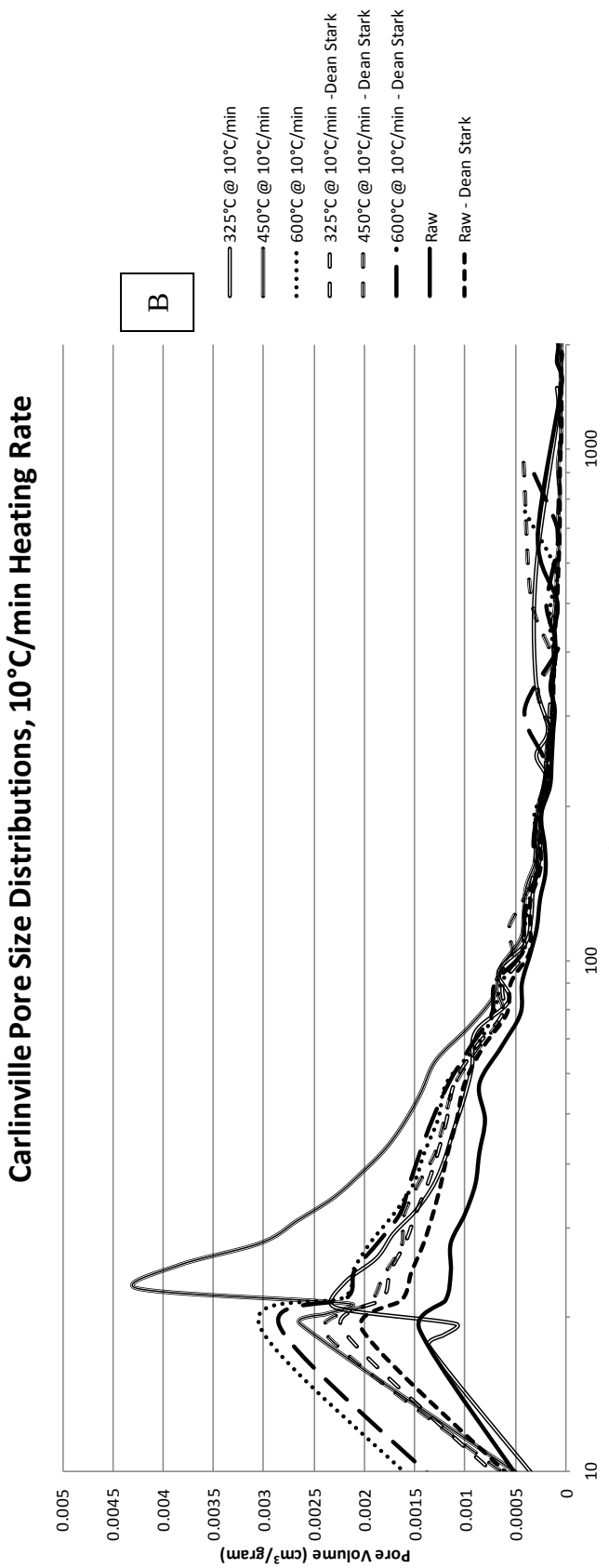

Figure 9 continued

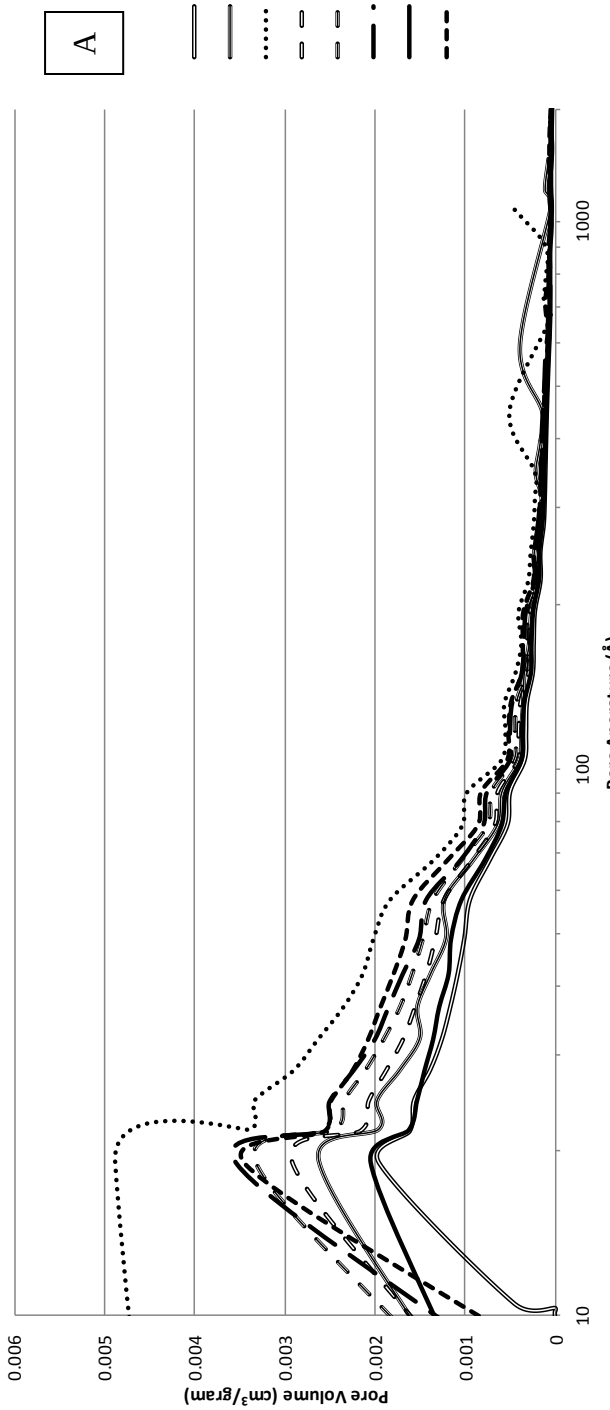

Figure 10: Pore size distributions for the unreacted and the thermally treated North Antelope coal. A) Pore size distributions for the unreacted and the thermally treated North Antelope coals heated at 0.1 °C/minute. B) Pore size distribution for North Antelope coal heated at 10 °C/minute. Solvent extraction (Dean-Stark) was used to determine effect of residual hydrocarbons on pore sizes.

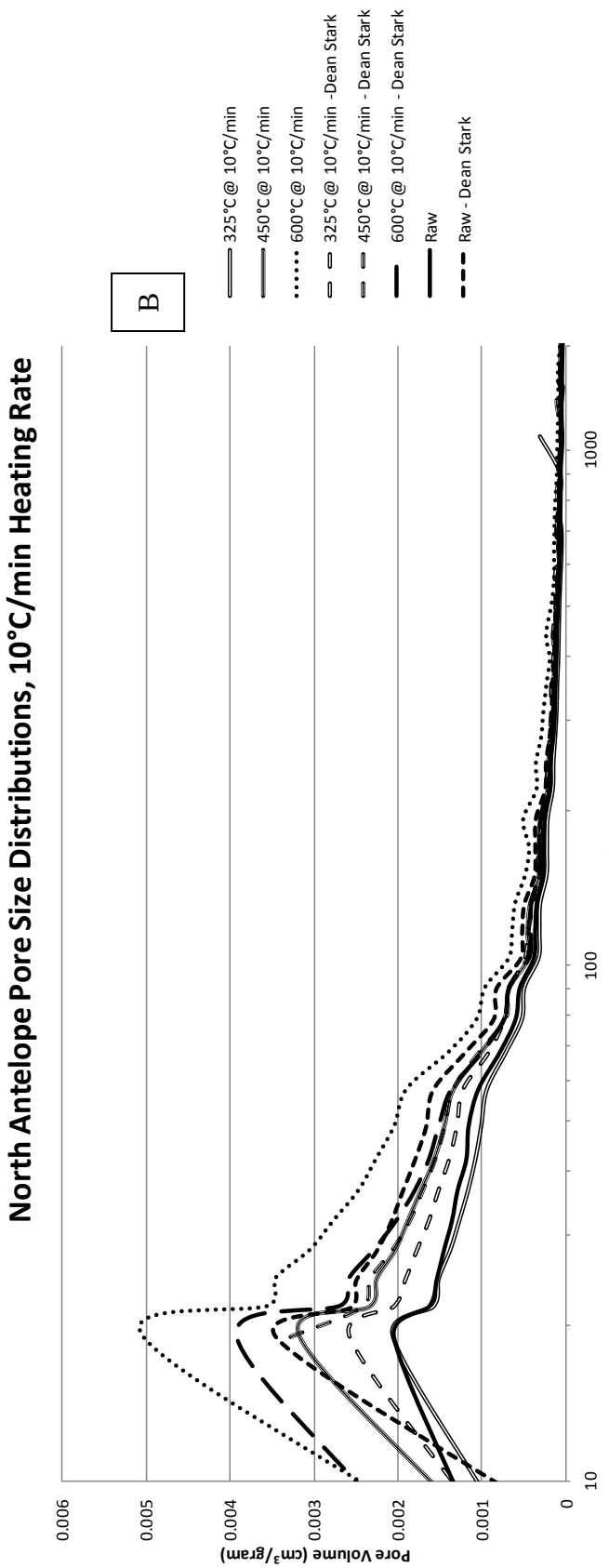

Figure 10 continued

CHAPTER 5

ISOTHERM MEASUREMENTS

High pressure isotherm measurements are critical to the UCTT project. These measurements can be used to estimate the CO_2 storage potential of a thermally treated coal seam. The results of these measurements were used to help model the injection of CO_2 in this study. Measurements were performed on the equipment similar to that used by Mavor et al.[30] located at TerraTek (a Schlumberger company) in Salt Lake City, UT. Isotherm measurements were performed at temperatures of 50 or 70°C with CH_4 or CO_2.

Results of the isotherm measurements were fitted to the Langmuir equation fully knowing that the assumptions of the equation do not accurately describe the physical nature of the adsorbed phase; the Langmuir equation, however, is often used in industry to describe adsorption of coal and shale. The Langmuir equation is often used to model adsorption in reservoir simulators and decently fits adsorption data. In this study, the results of 84 individual isotherms were presented with each individual isotherm requiring about 1 week to perform. Isotherms were plotted with the various terminal treatment temperatures with the heating rate at which they were treated alongside the isotherm of the untreated coal.

It was hypothesized that there is a relationship between the adsorptive capacities of the coals and the thermal treatment temperature. This relationship was further hypothesized to be related to the pore size distributions in the coal. Like the pore size

distributions, there were some unilaterally recognized trends in the isotherm data. In this chapter, an attempt was made to develop a relationship between adsorptive capacity and coals thermally treated with slow heating rates.

Adsorption Isotherm Measurements

Skyline Coal

Like the surface area measurements and pore size distributions, the high pressure isotherm measurements of the Skyline coal showed trends dependent on the treatment temperature but not so much with heating rate. For each of the coals used in this study, there are eight unique plots. Each plot shows the three thermally coal samples treated at a given heating rate plus the untreated coal for comparison. The results of the adsorption isotherm measurements for the fresh and thermally treated Skyline coal (heat rate of 0.1°C/minute) can be found in Figure 11; adsorption isotherms for the Skyline coal treated with a heating rate of 10°C/minute can be found in Figure 12.

High pressure isotherms for the thermally treated coals showed similar trends to what was observed with the pore size distributions and surface area measurements. Isotherms on coals treated to 325°C showed less adsorptive capacity than the fresh coals and capacity of the coals increased with treatment temperature. The adsorptive capacity of the coals increased with treatment temperature. The effect of heating rate on adsorptive capacity is less pronounced than with the pore size distributions. As expected, the adsorptive capacity for CO_2 exceeded that of CH_4 and volume adsorbed decreased with measurement temperature.

Adsorption values were fitted to the Langmuir adsorption equation which provides theoretical maximum adsorptive capacities and curvature of the isotherm. The

Langmuir equation defines the adsorbed phase as a single layer; with coals this is not the case. The Langmuir equation, however, does fit the adsorption data with a good degree of agreement and is commonly used to model adsorption on coals. The R^2 value from the linear regression fitting data to the Langmuir equation was at least 0.97 and very commonly 0.99 or better. Langmuir fitting parameters treated coals can be found in Table 8 and Table 9; in these tables the units of $V\infty$ is in moles adsorbed per kilogram, β is in 1/bar. In the following section, the correlations between meso- and micropores and the $V\infty$ terms for all the coals will be examined.

Carlinville Coal

The isotherms measured on the Carlinville coals showed trends very similar to those shown by the Skyline coals. The measured values of the adsorbed gas on the Carlinville coals were of similar orders of magnitude as the Skyline coals. For the sake of not having the majority of this section filled by figures, the isotherm plots for the Carlinville coals were placed in Appendix B (Figures 43-44).

Like the Skyline coals, the Carlinville coals treated to 325°C showed capacities rarely greater than unreacted coal. Also like the Skyline coal, the Carlinville coals showed increases in capacity with the extent of thermal treatment temperature. As expected, the capacity for CO_2 exceeded that of methane and adsorptive capacity decreased with measurement temperature.

North Antelope Coal

Isotherms on the unreacted and thermally treated North Antelope coals showed trends identical to that of the Skyline and Carlinville coals; coals treated to 325°C

showed reduced capacity compared to the unreacted coal and adsorptive capacity increased with final treatment temperature. Also like the previous coals, the North Antelope coal showed little difference in capacity with either heating rate.

Correlations with Pore Size Distributions

One of the main hypotheses of this dissertation is that there exists a relationship between the final treatment temperature and adsorptive capacity; a relationship which is bridged through the pore size distributions of the coals. Throughout this work, similar trends were noticed with several different analytical techniques. For example, the BET surface area measurements showed increases with thermal treatment temperature and that the surface area of the coals treated to 325°C were less than that of the unreacted coals. Pore size distributions showed increasing abundances of small pores with treatment temperature and coals treated to the lowest temperature exhibited pore volumes less than that of the unreacted coals. Permeability measurements (later section) also showed that there are increases with treatment temperature and that the measured permeabilities of the 325°C coals were less than that of the unheated coals. The aforementioned trends with the coals seem universal regardless of heating rate or the coal used; ergo, it should stand to reason that they are all related. Trends were related with the pore size distributions because the PSDs are the most encompassing characteristic of the coal surface. PSDs account for small pores where capillary condensation can occur affecting the adsorptive capacity, the surface area of small pores affecting overall surface area, and the abundance of large pores which affect permeability.

Maximum theoretical adsorptive capacities from the Langmuir equation ($V\infty$) were plotted against the measured pore volumes in the either the micropore or mesopore

range. If pore condensation is prolific in high pressure measurements, then the relationship would be a simple volume to volume comparison. Since determining the fraction of pores that were filled via pore condensation in the high pressure measurements was not done, it is hard to assume that all pores were filled by this mechanism.

The Skyline coals showed a definite relationship between adsorptive capacity and meso- and micropores. This relationship held true for both CO_2 and CH_4 with both measurement temperatures. The relationship between adsorptive capacity and mesopore abundance was stronger for the Skyline coals than with the micropore volumes. The relationship between pores and capacity for CO_2 on Skyline coals can be found in Figure 13. Little relationship between pores and adsorption was found for the Carlinville coals. North Antelope coals, like the Skyline samples, also showed relationships between adsorptive capacity and micro- and mesopores. However, unlike the Skyline coals, the relationships of either pore types to adsorptive capacity were nearly equal.

It is generally accepted that both mesopores and micropores attribute to adsorption. From this analysis, it was determined that for thermally treated coals there is more of a dependence on mesopores but the contribution of the micropores should not be neglected.

Because of this work, it may be possible to at least estimate the adsorptive capacity of a thermally treated coal seam with only a few laboratory isotherm measurements. There is also a cost and time benefit to these analysis. Before, if one wanted to thoroughly model gas potential or sequestration capacity of a thermally treated coal seam, they would have to perform a multitude of isotherm measurements. Adding

the effects of treatment temperature gradients in a coal seam further necessitates the need for more isotherm measurements by adding another degree of complexity. Now only a few isotherm measurements need to be performed and correlated to DFT/BJH pore size distributions. From the correlation between pyrolyzed coal and pore size distributions, adsorptive potential could be inferred from pore size distributions. For comparison, PSDs are an order of magnitude less expensive and require only a day to perform compared to weeks for full isotherms.

Conclusions

High pressure isotherms were measured on unreacted and thermally treated Skyline, Carlinville, and North Antelope coals. Isotherms were measured at temperatures of 50 and 70°C using methane or carbon dioxide. In total, 84 isotherms were measured in order to provide an extensive analysis of the adsorptive capacity of thermally treated coals. Isotherms were fitted to the Langmuir equation fully knowing the limitations of aforementioned model but were done so to retain consistency with industry standards. All thermally treated coals showed similar trends in the isotherm measurements:

- Adsorptive capacity of the coals decreased with increasing measurement temperature.
- Measured adsorptive capacities of carbon dioxide were greater than methane.
- Most coals treated to 325°C showed less adsorptive potential than untreated coals.
- Adsorption potential increased with final treatment temperature.
- Little relationship between high pressure adsorption and heating rate.

Since the trends observed with the adsorption measurements were similar to other trends like surface area, pore size distributions, and permeability (later chapter) it was hypothesized that all of the aforementioned trends in properties could be related to treatment temperature through one measurement. Since various pore sizes have been documented to affect surface areas, adsorption, and permeabilities, it was determined that this measurement should also be used as the means of relating measured properties to treatment temperature. Correlations were developed between the Langmuir maximum theoretical adsorptive capacity and mesopores or micropores. It was found that a stronger correlation exists with mesopores but the influence of micropores should not be neglected.

The implications of correlating adsorptive capacity to pore size distributions means that fewer of the relatively expensive and time consuming high pressure isotherms would be required for characterizing a thermally treated coal seam.

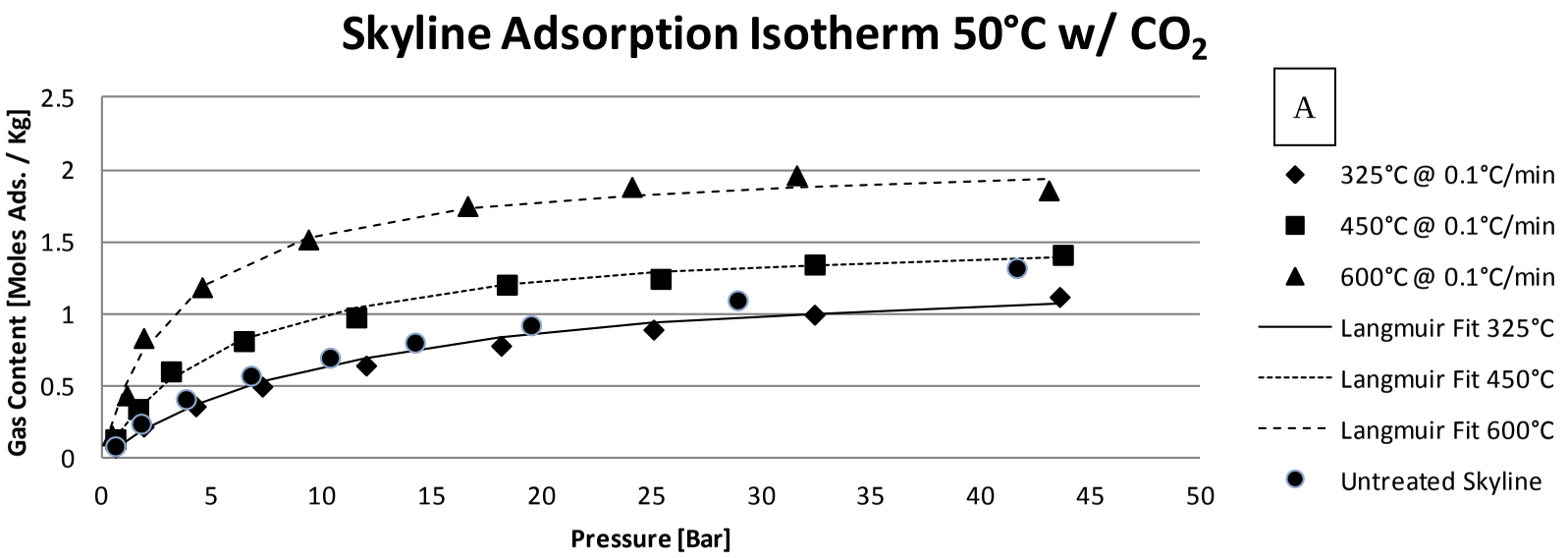

Figure 11: Adsorption isotherms for thermally treated Skyline coal heated at 0.1°C/minute. A) CO_2 isotherms measured at 50°C on coals heated with a rate of 0.1°C/minute. B) CH_4 isotherms measured at 50°C on coals heated with a rate of 0.1°C/minute. C) CO_2 isotherms measured at 70°C on coals heated with a rate of 0.1°C/minute. D) CH_4 isotherms measured at 70°C on coals heated with a rate of 0.1°C/minute.

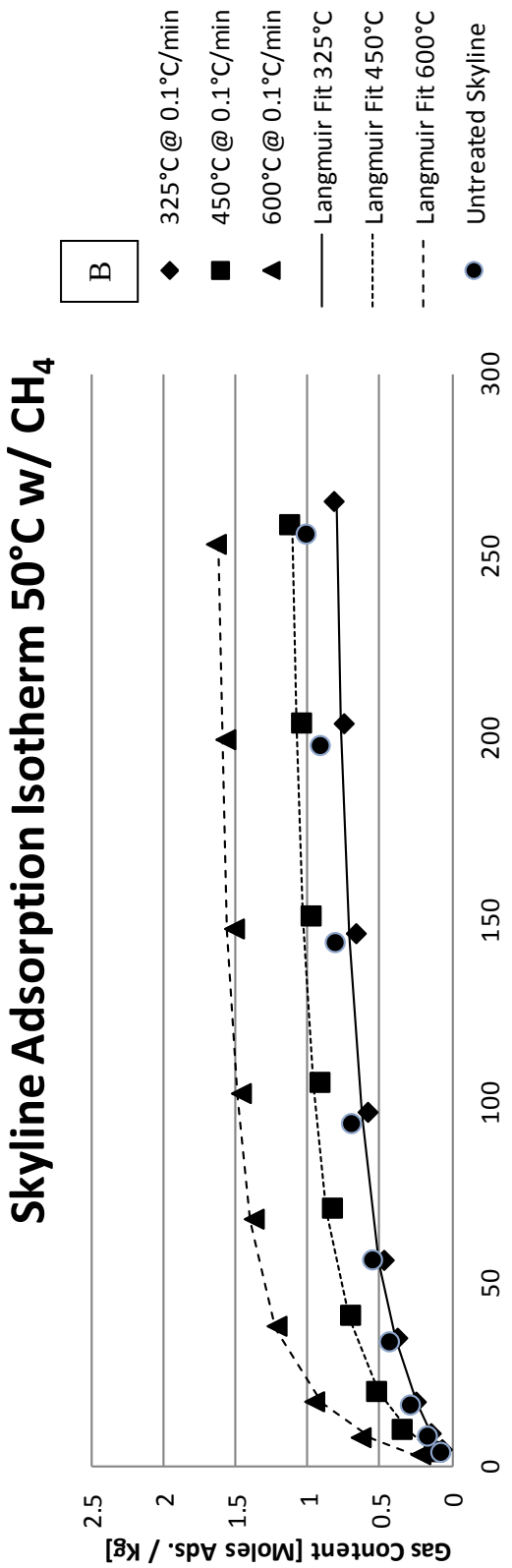

Figure 11 continued

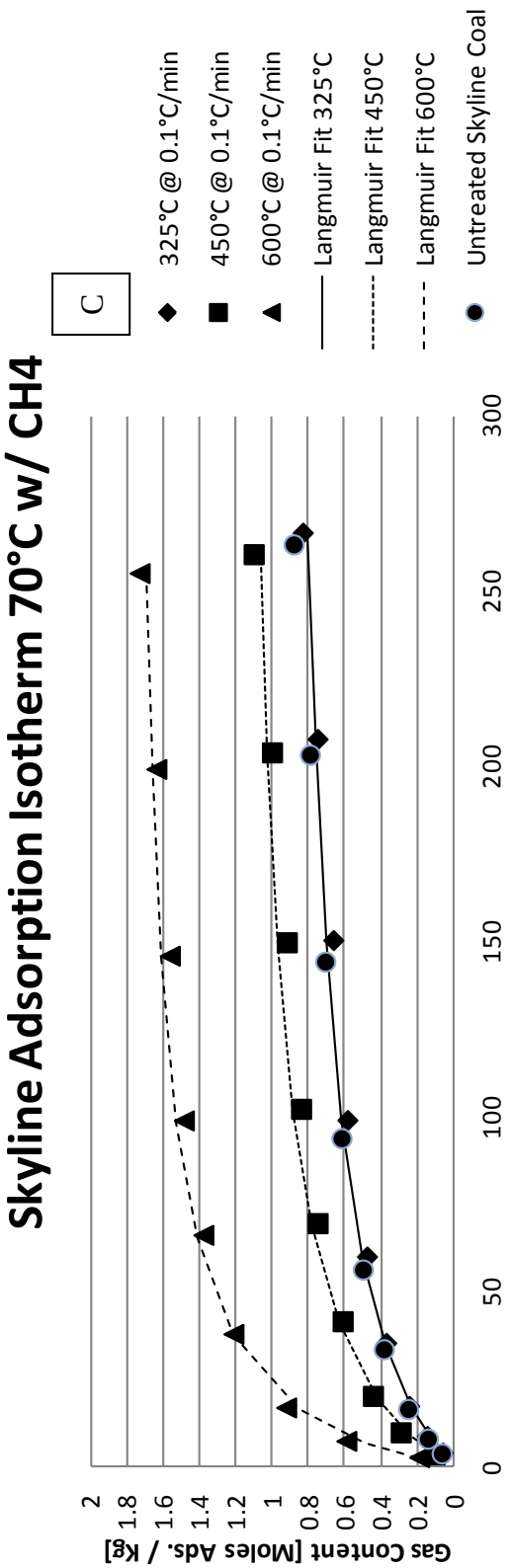

Figure 11 continued

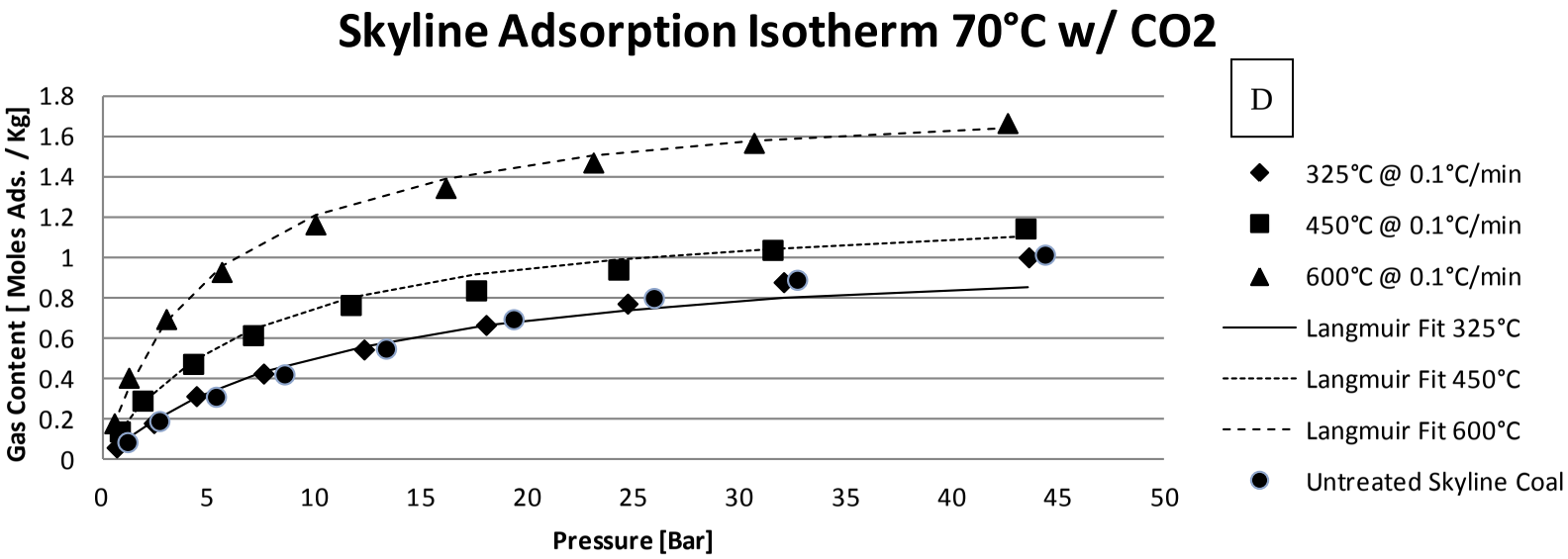

Figure 11 continued

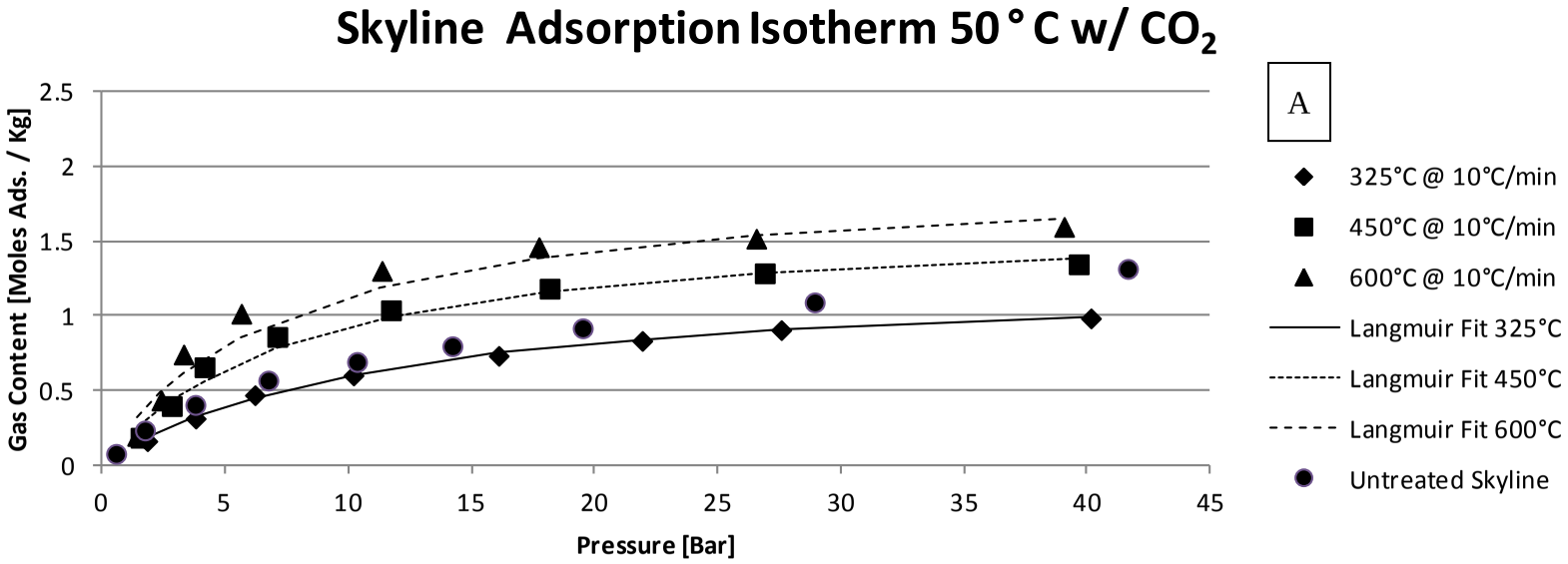

Figure 12: Adsorption isotherms for thermally treated Skyline coal heated at 10°C/minute. A) CO_2 isotherms measured at 50°C on coals heated with a rate of 10°C/minute. B) CH_4 isotherms measured at 50°C on coals heated with a rate of 10°C/minute. C) CO_2 isotherms measured at 70°C on coals heated with a rate of 10°C/minute. D) CH_4 isotherms measured at 70°C on coals heated with a rate of 10°C/minute.

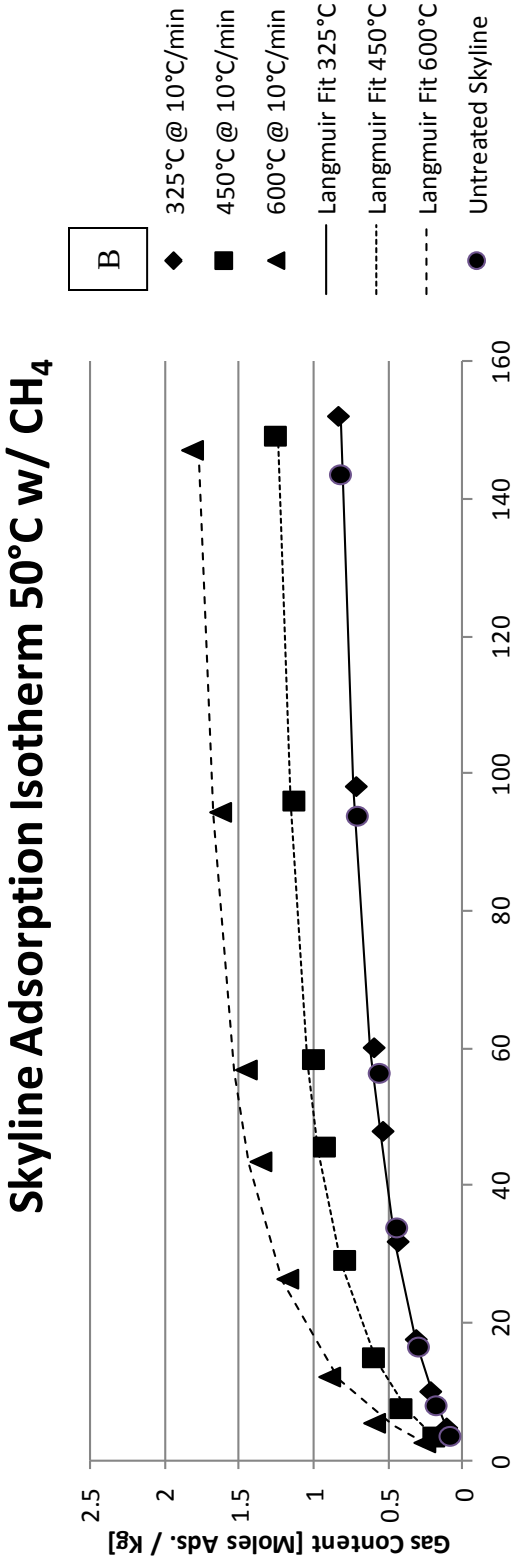

Figure 12 continued

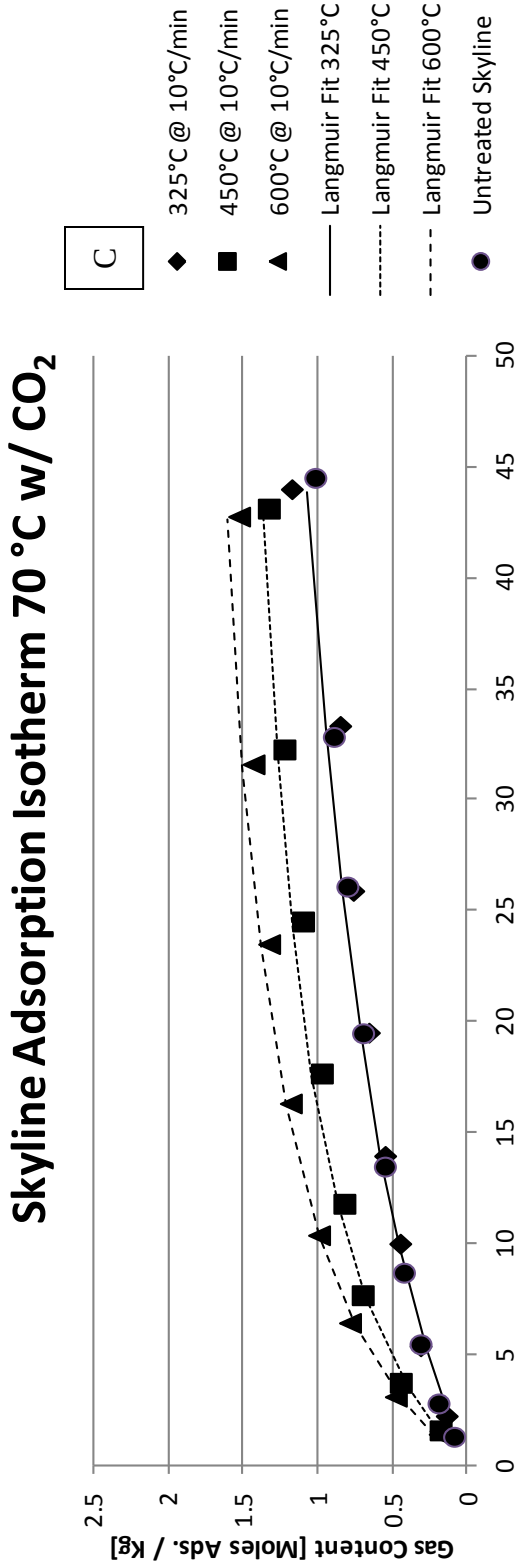

Figure 12 continued

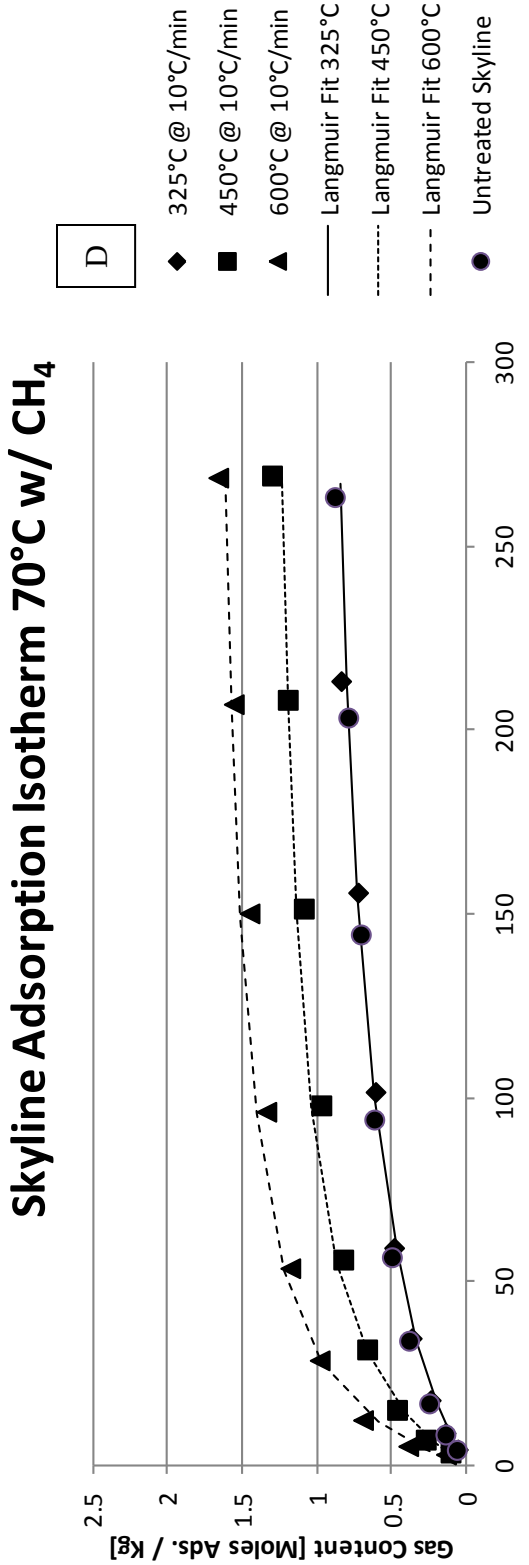

Figure 12 continued

Table 8: Langmuir fitting parameters for isotherms on coals thermally treated with a 10°C/minute heating rate. V∞ is in moles adsorbed per kilogram, β is in 1/bar.

Coal	*Langmuir Fit*	*CH_4 @ 50°C*	*CH_4 @ 70°C*	*CO_2 @ 50°C*	*CO_2 @ 70°C*
Skyline	V∞	1.174	0.885	1.590	1.213
	β	1.972E-02	2.425E-02	8.600E-02	6.490E-02
325@10	V∞	1.034	1.072	1.267	1.742
	β	2.473E-02	1.341E-02	8.938E-02	3.561E-02
450@10	V∞	1.404	1.393	1.666	1.742
	β	4.884E-02	2.952E-02	1.237E-01	8.366E-02
600@10	V∞	1.957	1.742	1.947	1.990
	β	6.289E-02	4.434E-02	1.392E-01	9.679E-02

Table 9: Langmuir fitting parameters for coals treated with a 0.1°C/minute heating rate. V∞ is in moles adsorbed per kilogram, β is in 1/bar.

Coal	*Langmuir Fit*	*CH_4 @ 50°C*	*CH_4 @ 70°C*	*CO_2 @ 50°C*	*CO_2 @ 70°C*
Skyline	V∞	1.174	0.885	1.590	1.213
	β	1.972E-02	2.425E-02	8.600E-02	6.490E-02
325@10	V∞	1.034	1.072	1.267	1.742
	β	2.473E-02	1.341E-02	8.938E-02	3.561E-02
450@10	V∞	1.404	1.393	1.666	1.742
	β	4.884E-02	2.952E-02	1.237E-01	8.366E-02
600@10	V∞	1.957	1.742	1.947	1.990
	β	6.289E-02	4.434E-02	1.392E-01	9.679E-02

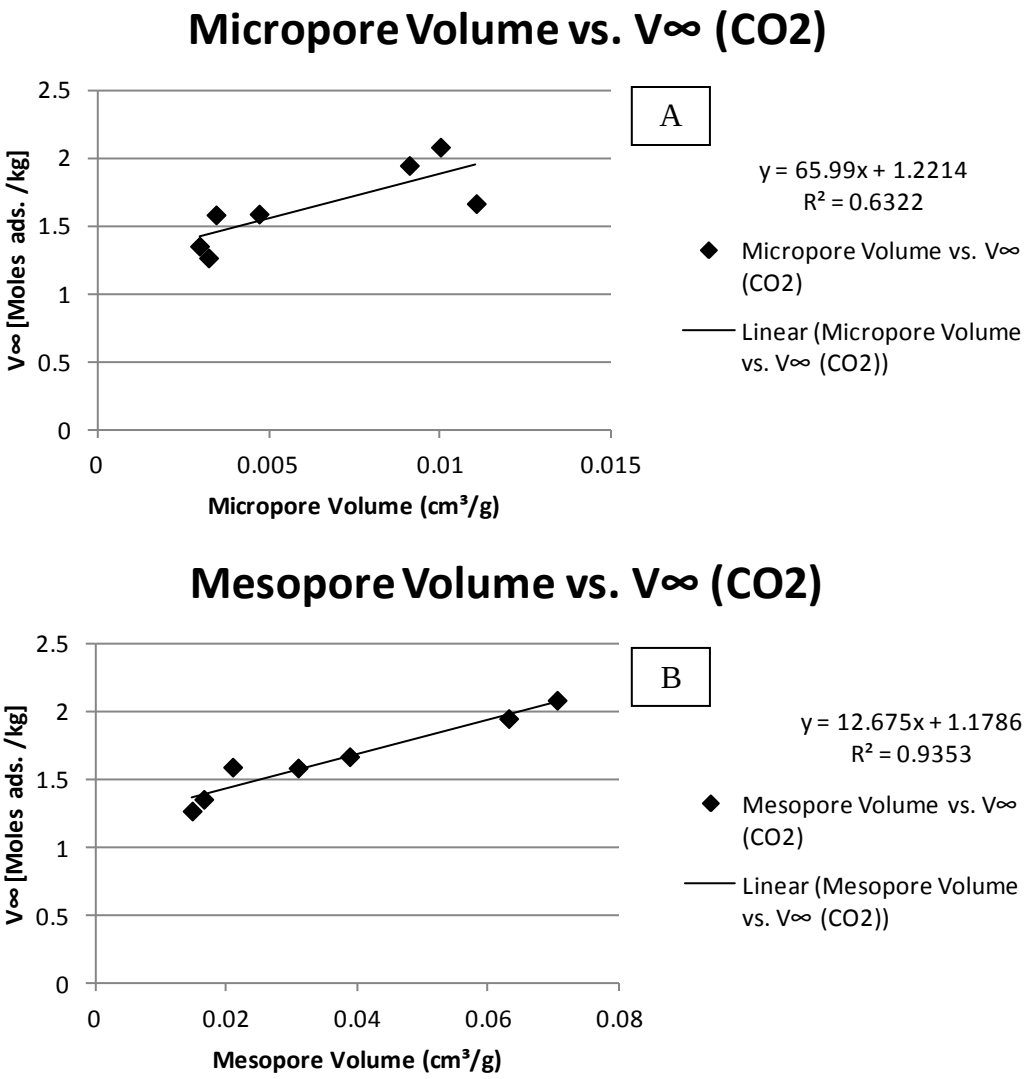

Figure 13: Relationships between maximum theoretical adsorptive capacity and the amounts of mesopores and micropores for the Skyline coal. The relationships presented in this figure were for CO_2 isotherms measured at 50°C, however, the trends held for other temperatures and for measurements using methane. A) Shows the relationship between micropores and adsorptive capacity. B) Shows the relationship between capacity and mesopores. The relationship with mesopores has a stronger linear correlation that with micropores

CHAPTER 6

PERMEABILITY MEASUREMENTS

The purpose of this chapter is to report the permeability of the fresh and pyrolyzed coals used in this study. A general trend was noticed where the permeability increases with the extent of thermal treatment. The development of certain pores during the pyrolysis process is the reason for the increase in permeability.

Permeability Measurements

The method used to determine the permeability on the fresh and pyrolyzed coal samples is the Tight Rock Analysis (TRA) procedure developed by Handwerger et al.[127] TRA permeability analysis claims to provide better matching to field data than other methods like that from the Gas Research Institute (GRI). The permeability measurements were done at TerraTek (a Schlumberger company) using a proprietary piece of equipment. There are two different methods for determining permeability as outlined by the TRA procedure; pressure decay and pulse decay. Pulse decay uses cylinders of rock under confining pressure. Pulse decay has the advantages of taking the measurement under confinement but has the disadvantage of not being as precise as the pressure decay measurements. Pressure decay measurements are performed on crushed rock samples without a confining stress. Pressure decay has advantage of being more precise but also encounters the possibility of false measurements from off gassing of the sample or microcracks in the sample structure.

The mathematics behind the permeability measurements are outlined by Cui et al.[136] but are not all inclusive to the "black box" calculations used by the TerraTek permeability analyzer. The basis of the mathematical model is Darcy's law with Fickian diffusion for flow into a sphere:

$$\Phi \frac{\delta \rho}{\delta t} + (1 - \Phi) \frac{\delta q}{\delta t} = \frac{1}{r^m} \frac{\delta}{r} (r^m \frac{\rho k}{\mu} \frac{\delta p}{\delta r}) \quad (14)$$

where Φ is the porosity of the rock, t is time, ρ is the density of the fluid, q is the adsorbate density, r is the radius, m is used for different sample shapes (0 for slabs, 1 for cylinders, and 3 for spheres), k is the permeability, μ is viscosity, and p is the pressure.

Cui et al.[136] noted that the effects of adsorption can greatly skew the results of the permeability measurements and need to be accounted for. With highly adsorptive materials like coals and activated carbon, not accounting for adsorption will result in an underestimation of the permeability. The effects of adsorption were minimized by using helium as the analysis gas and performing the tests at room temperature at relatively low pressures.

Permeability Results

Permeability measurements were done using TerraTek equipment on fresh and pyrolyzed coals using the TRA analysis method. Additional to the TRA analysis method was allowing the samples to thoroughly dry and degas before analysis by placing them in a vacuum oven at 80°C for 36 hours. Transient pressure data were analyzed using TerraTek software which has its foundation in the works by Cui et al.[136] The results presented are the averages of two permeability measurements.

Permeability analysis of the raw Skyline, Carlinville, and North Antelope coals found initial permeabilities of 0.505, 1.145, and 0.269μD, respectively. The results of the

permeability measurements on the thermally treated skyline coal can be found in Table 10.

From Table 10, a general trend is evident in that the permeability of Skyline coal increases with the final treatment temperature. Cai et al.[78] reported some of the effects of pore size distributions on the transport of natural gas through Chinese coals. Cai et al. classified pores smaller than 100nm as adsorption pores and pores larger than 100nm as transport pores. Zhang et al.[80] also studied the effects of various pore sizes on methane transport in Chinese coals. Like Cai et al., Zhang et al. classified transport pores as having apertures larger than 100nm. In Chapter 4, the effects of thermal treatment on pore size distributions were discussed.

The results shown in Chapter 4 show that there is an increase in the abundances of micro- and mesopores with increases in treatment temperature. With the works of Cai et al. and Zhang et al. relating transport to pores of a certain size, it stands to reason that the results for thermally treated coal can also be related to pore sizes. Since thermal treatment conditions directly affect pore sizes, this relationship can be expanded to *permeability can be related to thermal treatment conditions via pore size distributions*.

The trend of final treatment conditions increasing permeability is easily noticed when treatment conditions are plotted against each other (Figure 14). It should be noted that for all of the permeability figures in this chapter the error bars are the standard deviation of the measurements. Another interesting parallel between the permeability of Skyline coal and the pore size distribution can be seen in Figure 14; just like surface area and pore size distributions, values for permeability for coal samples thermally treated to 325°C show a slight *decrease* from the values of the unreacted coal. This similar trend

stands as further evidence that there is a concrete relationship between pores and permeability with thermally treated coals.

The trend of thermal treatment increasing permeability is not noticeable with the Carlinville coal. Most of the measured permeabilities on thermally treated Carlinville coal resulted in values less than that of the unreacted coal. The two samples that showed overall increases in permeability were treated to 450°C at 10°C/minute or treated to 600°C at 0.1°C/minute.

There are several explanations as to why the Carlinville coal could lose permeability with thermal treatment. The Carlinville coal is bituminous which can plastically deform when undergoing pyrolysis. If the interconnection between small pores in the coal is not maintained, one would expect to see a decrease in the permeability. Lee et al.[137] reported on a collapse of mesopores in an Illinois No. 6 undergoing pyrolysis with fast heating rates under pressure. It should be noted for the sake of comparison that the Carlinville coal is also from Illinois. It is possible that the same collapse in mesopores and even large pores is being seen with the permeability results for the Carlinville coal. Numerical values for Carlinville permeability can found in Table 11. A plot comparing all the data points from the Carlinville coal can be found in Figure 15.

Permeability measurements for the North Antelope coal show similar trends to the Skyline coal. Increases in thermal treatment temperature result in increases in permeability. The similarities between the Skyline coal and the North Antelope coal are stark. Numerical values for permeability can be found in Table 12.

The similarities between the Skyline and North Antelope coals are even more

noticeable when permeability is plotted versus treatment temperature (Figure 16). The results for the North Antelope coal show increases in permeability over that of the unreacted coal for all treatment temperatures, although coals treated to 325°C show little improvement rather than a decrease in permeability. Like the Skyline samples, the North Antelope coal treated with the faster heating rate had higher permeability at 450°C than the sample treated with the slower heating rate; however, at 600°C, the inverse is true. This identical relationship implies that the influence of heating rate on permeability cannot be neglected. There is the possibility, in terms of permeability improvement, of devolatilization and plastic deformation counteracting each other. Devolatilization would cause an increase in permeability while plastic deformation could cause decreases in permeability.

The results of the permeability measurements have implications on the transport of fluids trough an in situ pyrolyzed coal formation. It should be stated, however, that these measurements were conducted with helium which does not easily adsorb. In an actual scenario, the thickness of adsorbed species such as CH_4 and CO_2 could reduce the observed permeability of the system.

If one were to model the UCTT process *ab ovo usque as mala* they would have to take into account not only a dual permeability of a matrix and cleat coal system but also the transient change in permeability of the matrix resulting from plastic deformation and devolatilization.

In an actual UCTT operation, depending on the coal, it can be expected that the permeability of the coal will increase with treatment temperature and that the permeability of the whole formation will change. Increases in treatment temperature

could improve the extraction of hydrocarbons as well as increase the rate that CO_2 permeates the coal matrix.

Conclusions

Permeability measurements were performed on unreacted and thermally treated Skyline, Carlinville, and North Antelope coals. Permeability measurements were done using the TRA method outlined by Handwerger et al.[127] Skyline and North Antelope coal showed nearly identical trends in respect to permeability changes versus treatment temperature and heating rate. The Carlinville coal showed decreases in permeability which may have been the result of the collapse of meso- and macropores due to plastic deformation.

A relationship was established between the permeability of pyrolyzed samples and the treatment temperature, a relationship that is better unified when relating either to pore size distributions. Development of transport pores during pyrolysis could increase the rate that pyrolysis products are produced and increase the rate that a CO_2 plume could permeate a reservoir.

Again, the relationship between pore sizes to other petrophysical properties of pyrolyzed coal is noticeable. This relationship could be extrapolated to other underground thermal processes as well. The implications of this study may also be relatable to unconventional resources such as oil-from-shale plays. Although a unifying theory between pore distributions and permeability/adsorption may seem untenable, the effects of these small pores cannot be neglected when referring to coal seam formations.

Table 10: Results of the permeability measurements on the unreacted and thermally treated Skyline coal

Sample	Test #1 (μD)	Test #2 (μD)	Avg (μD)
Raw Skyline	0.497	0.513	0.505
Skyline 325°C @ 10°C/min	0.412	0.414	0.413
Skyline 450°C @ 10°C/min	1.047	1.044	1.0455
Skyline 600°C @ 10°C/min	1.023	1.01	1.0165
Skyline 325°C @ 0.1°C/min	0.435	0.437	0.436
Skyline 450°C @ 0.1°C/min	0.779	0.783	0.781
Skyline 600°C @ 0.1°C/min	1.619	1.546	1.5825

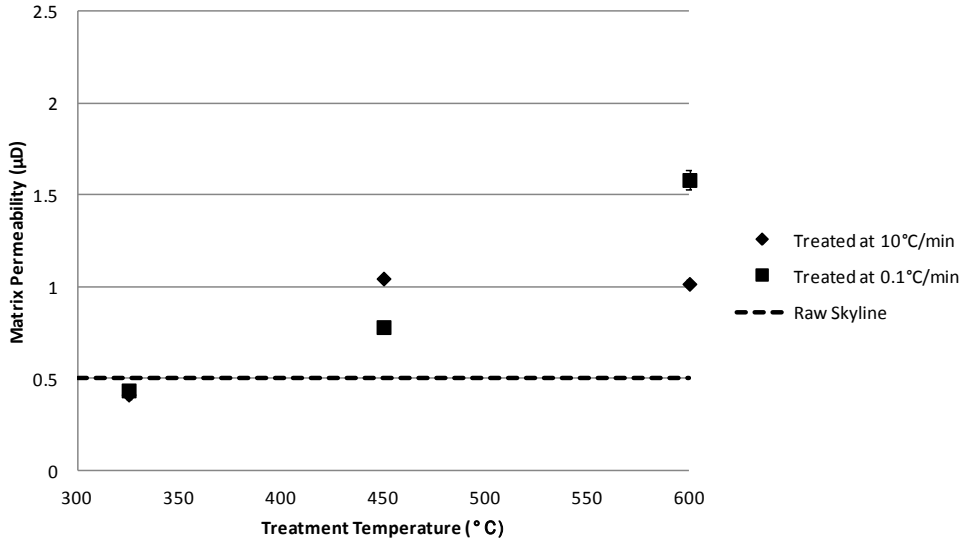

Figure 14: Permeability vs. treatment temperature for the Skyline coal. Permeability generally increases with treatment temperature. The error bars are the standard deviation of the measurements.

Table 11: Results of the permeability measurements on the unreacted and thermally treated Carlinville coal.

Sample	Test #1 (μD)	Test #2 (μD)	Avg (μD)
Raw Carlinville	1.173	1.117	1.145
Illinois 325°C @ 10°C/min	0.664	0.582	0.623
Illinois 450°C @ 10°C/min	2.351	2.228	2.2895
Illinois 600°C @ 10°C/min	0.887	0.703	0.795
Illinois 325°C @ 0.1°C/min	0.661	0.652	0.6565
Illinois 450°C @ 0.1°C/min	0.824	0.753	0.7885
Illinois 600°C @ 0.1°C/min	1.6	1.42	1.51

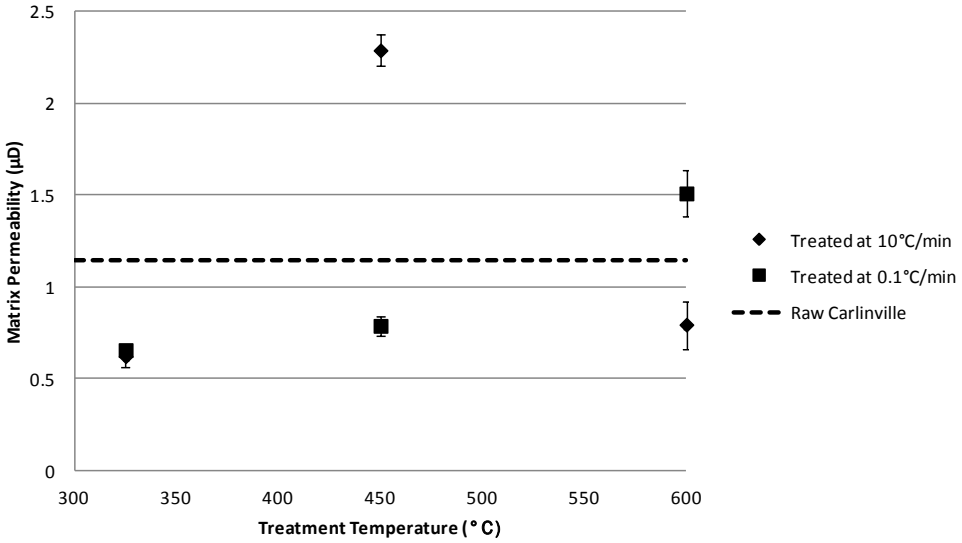

Figure 15: Permeability vs. treatment temperature for the Carlinville coal. Permeability generally increases with treatment temperature. The error bars are the standard deviation of the measurements.

Table 12: Results of the permeability measurements on the unreacted and thermally treated North Antelope coal.

Sample	Test #1 (μD)	Test #2 (μD)	Avg (μD)
Raw North Antelope	0.265	0.273	0.269
PRB 325°C @ 10°C/min	0.265	0.262	0.2635
PRB 450°C @ 10°C/min	0.575	0.576	0.5755
PRB 600°C @ 10°C/min	0.592	0.543	0.5675
PRB 325°C @ 0.1°C/min	0.353	0.356	0.3545
PRB 450°C @ 0.1°C/min	0.418	0.412	0.415
PRB 600°C @ 0.1°C/min	0.719	0.673	0.696

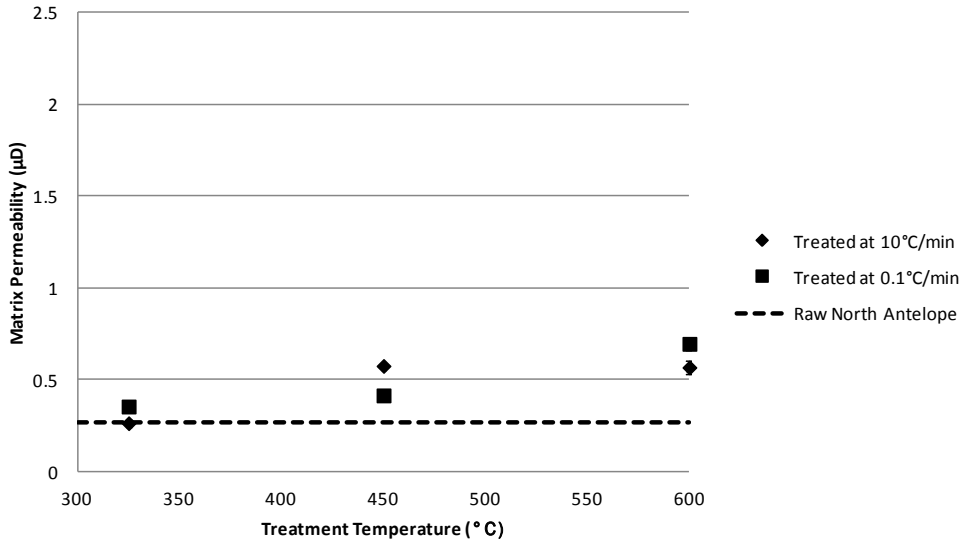

Figure 16: Permeability vs. treatment temperature for the North Antelope coal. Permeability generally increases with treatment temperature. The error bars are the standard deviation of the measurements.

CHAPTER 7

SIMULATION STUDIES

Injection simulations were done to show the effects of changes on adsorption and permeability on a larger scale. A commonly available simulation package was used, Computer Modeling Group GEM. This particular software package offers the advantage of already having enhanced coal bed methane simulations. Since CO_2 injection into a pyrolyzed coal seam is very similar to Enhanced Coal Bed Methane (ECBM) operations, the pre-existing simulations were easily modified for modeling injection into pyrolyzed coal. The template code used for the simulations can be found in Appendix A.

The purpose of this section is to briefly demonstrate some of the differences between thermally treated coals in a 100x100x9 m domain under an injection scenario using the values for adsorption and permeability determined experimentally (previous sections). Simulations were done on all the coals used in this study, however, the trends were similar across all coals, therefore, for sake of brevity it was decided to only focus on the Skyline coals treated with a heating rate of 0.1°C per minute.

Simulation Results

Injection recovery simulations were done on a 100x100x9 m domain for Skyline coals treated to 325, 450, and 600°C with a heating rate of 0.1°C/minute. The values for adsorptive capacity and permeability came from experimental results. Multicomponent adsorption was modeled using the extended Langmuir equation. For the first 60 days of

these simulations, methane was produced without the injection of CO_2. After 60 days, CO_2 was injected at a rate of 6000 m^3/day to displace the adsorbed methane in a process very similar to enhanced coal bed methane. Carbon dioxide was injected until the 365^{th} day, the end of the simulation. The results of the Skyline injection simulations can be found in Figure 17.

From Figure 17, it can be seen that the coal treated to the higher temperature has a larger amount of initial methane and at the 1 year mark only about 43% initial methane recovery. Even though the recovery percentage for the 600°C simulation is less than the others in Figure 17, the actual volume of methane recovered is greater for the 600°C simulation than the others. Since CO_2 was injected at the same rate for each simulation the amount of CO_2 stored in the formation was similar for each simulation.

Early CO_2 breakthrough was seen with all simulations, this was due to permeability through the cleats being several orders of magnitude greater than that of the matrix permeability.

Conclusions

Simulation studies were done to compare how thermally induced changes in the properties of adsorption and permeability would affect methane recovery and CO_2 injection. Simulations were done using values from all the coals that were experimented with, but all of the simulations showed the same trend. Coals treated to 600°C had more initial methane, a lower fraction of recovered methane, and a larger volume of recovered methane. Coals treated to 325°C showed trends inverse of the 600°C samples.

For all the simulations, early CO_2 breakthrough was observed due to the cleat permeability being orders of magnitude greater than the matrix permeability.

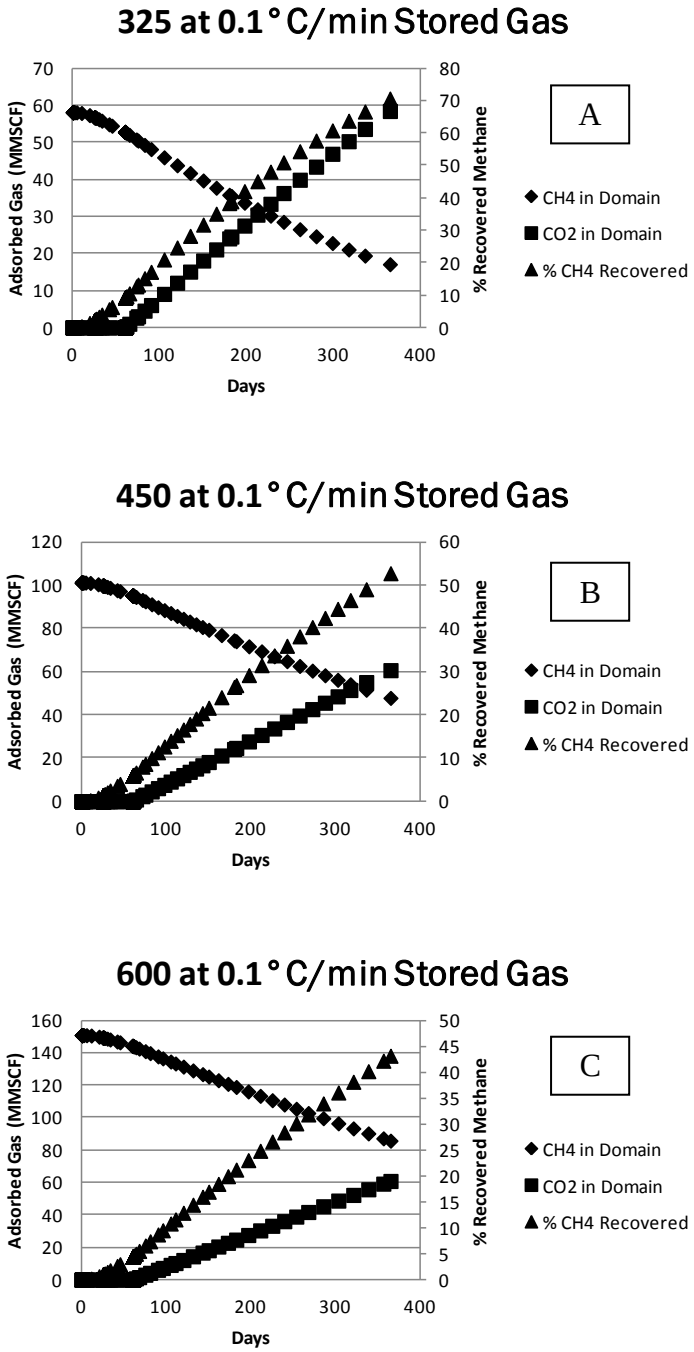

Figure 17: Formation gas content for injection / recovery simulations using adsorption and permeability determined experimentally. Values used were for Skyline coals treated with a heating rate of 0.1°C/minute. The trends in this figure were also seen with simulations on the other coals.

CHAPTER 8

CONCLUSIONS

The works in the first volume of this dissertation represent a comprehensive investigation into coals thermally treated with slow heating rates as it pertains to the Underground Coal Thermal Treatment (UCTT) process. UCTT is a process that draws similarities to other *in situ* processing technologies like Enhanced Coal Bed Methane (ECBM), Underground Coal Gasification (UCG), and oil shale pyrolysis. Like ECBM, UCG, and oil shale pyrolysis, the remnants of the UCTT process may serve as a potential sequestration repository for carbon dioxide. This dissertation focuses on properties that affect CO_2 sequestration in a pyrolyzed coal seam.

Like other *in situ* processes, determining the amount of CO_2 that can be sequestered and the injection/recovery scheme relies on computational reservoir modelling. Reservoir simulators rely on adsorption isotherms and permeability measurements to model CO_2 injections into coal seams. This work sought to determine adsorption isotherms for both methane and carbon dioxide on three different coal samples heated with slow heating rates. Permeabilities of treated coals were also determined.

Preliminary characterization of the porous structure led to three questions. First, what contribution do residual hydrocarbons have on the porous structure? It was noticed early in the experimental phase of this study that the trends for the surface area, pore volumes, and adsorption were similarly related to the final treatment temperature. This led to the second question: can properties of coals be related to treatment temperature or

heating rate through a single measurement? Accoutrement to the second question was: what porous regime, mesopore or micropore, has a greater effect on adsorption on thermally treated coals?

This dissertation showed evidence that answered all three questions. Furthermore, it was found that the trends answering the aforementioned questions almost always existed for all three of the coals tested; Skyline bituminous, Carlinville bituminous, and North Antelope subbituminous. This means that the trends noticed throughout this work are not coal specific.

Key Results

Surface area measurements on the fresh and thermally treated coals were done using BET analysis. In order to determine the effect of residual hydrocarbons on the surface area, sohxlet extraction was used to remove said hydrocarbon and the samples were re-run. All coals treated to a final treatment temperature of 325°C showed lesser or similar surface areas to the unreacted coals. The surface areas of the coals increased with the final treatment temperature but there was little relationship with the heating rate. Results of the solvent extraction showed reduction in surface areas for the coals treated to the lowest temperature. Coals treated to higher temperatures showed evidence that a portion of the developed surface area was attributable to residuals.

Pore size distributions for micro- and mesopores with and without solvent extraction gave more insight into the nature of the pores and pore development through the thermal treatment process. Micropores were characterized using the DFT approach while mesopores were BJH. Like the surface area measurements, the pore volumes for coals treated to 325°C were less than that of the unheated coals. After solvent extraction,

it was revealed that the reduction in pore volumes was due to a combination of residuals blocking pores and plastic deformation collapsing pores. Mesopore and micropore volumes tended to increase with increasing treatment temperature. Coals that were treated to 450°C with a heating rate of 10°C/minute showed little influence of residual tars while coals treated to the same temperature at 0.1°C/minute showed increases in pore volume after solvent extraction. This means that for the 450°C samples treated with the slow heating rate, tars were blocking access to some of the pores. Coals treated to 600°C showed the largest increase in pore volumes. Solvent extraction on the coals treated to this temperature showed differing results with some samples exhibiting new pores in the tar phase and other samples showing tar blockage.

Surface area and pore size distributions were performed before and after high pressure isotherm experiments to assess if exposure to methane or CO_2 at elevated pressures would cause change. It was found that for the thermally treated coals, there was little to no change after exposure. Dubinin-Radushkevich micropore analysis was performed on all samples but the results offered little insight.

High pressure adsorption isotherms were performed volumetrically on the coals using methane and carbon dioxide. Trends for the high pressure adsorption measurements were very similar to those previously shown. Coals treated to 325°C showed reduced capacity when compared to the untreated coals. It was also noticed that adsorptive capacity generally increased with treatment temperature. The effect of heating rate was not obvious with the high pressure adsorption measurements. Correlations between micropores or mesopores and adsorptive capacity found strong relationships for the Skyline and North Antelope coals. The Skyline coals showed a stronger correlation

with mesopores while the relationship was equally significant for meso- and micropores on the North Antelope coals. Correlations between adsorption and pores were similar with different analysis gases and different isotherm temperatures.

Permeability of the treated coal samples was done using the pressure decay method. Once again, similar trends were noticed; permeability was reduced when treated to the lowest temperature and increased with increasing treatment temperature.

It was determined that the best measurement to relate to the other measurements was the pore size distributions. Using pore size distributions indirectly accounts for the surface area contribution of pores, adsorption in pores, and transport through larger pores.

Preliminary CO_2 injection simulations were done using the experimentally determined values for adsorption and permeability. The CO_2 injection simulations were done in a manner very similar to how one would model ECBM. The results of the simulations found that coals treated to the highest temperature had the largest amounts of initial methane and the best methane recovery.

Implications

This extensive work shows the importance of understanding the pore structure of thermally treated coals as it pertains to UCTT. In the past, with ECBM operations, multitudes of high pressure isotherms were required to characterize the reservoir. Now, at least with UCTT, it may be possible to develop correlations between just a few high pressure isotherm measurements and pore size distributions and from there use the pore sizes to estimate the adsorptive capacity. This has the benefit of pore size distributions being much less expensive and time consuming. The pore size distributions on the coals also showed the influence of residual hydrocarbons and how residual hydrocarbons could

serve as potential adsorption sites, a concept new to the science community.

High pressure isotherms have not been done on thermally treated coals. Also being able to relate the results of high pressure isotherms and permeability measurements to treatment temperature gives insight into the roles that small pores play. The high pressure adsorption isotherms and permeability measurements can be used to help estimate the CO_2 storage potential of the UCTT process.

Future Work

All of the measurements in this study were performed on coals that were pyrolyzed at atmospheric pressure. It would be interesting to see what changes to the pore structure, and the properties related to pores structure, would result from performing the thermal treatment on coals with confining and hydrostatic pressures.

Also, it has been well documented that coals expand during high pressure measurements. It is recommended that some dilatrometry measurements be performed on thermally treated coals to determine the magnitude of this phenomenon.

Due to lack of time and resources, multicomponent isotherms were not performed on these thermally treated coals. It would be interesting to see how the extended Langmuir equation differs from true multicomponent measurements on these coals.

PART II

INVESTIGATION OF THE INTERACTIONS BETWEEN CO_2 AND PYROLYZED OIL SHALE IN THE LIQUID AND GAS PHASE

LEAD-IN

This is the second part of this two part dissertation. This part, like the previous part, examines the prospects of long-term storage of CO_2 in a geologic formation that has undergone some sort of pyrolysis. This volume focuses on the storage of CO_2 in a pyrolyzed oil shale formation and due to some of the difference in production there are some differences in terminology such as terms "retorted" being interchanged with "pyrolyzed" or "thermally treated." CO_2 sequestration in pyrolyzed oil shale differs from storage in coal in that there are mineralization reactions in addition to adsorption and volumetric storage. Like the previous volume, this volume stands as a unique work related to the other but has its own abstract, literature review, and results.

Just as the prospects for oil have changed over the decades, so has the attention being paid towards climate change. Of particular interest in the climate change debate are the effects of anthropogenic CO_2. The *in situ* retorting of oil shale has an energy requirement that is greater than conventional liquid fuels production thus resulting in comparatively larger CO_2 emissions. This work focuses on determining the prospects for sequestering CO_2 into a spent oil shale formation with liquid and gas phase experiments as well as some modeling. The results of liquid phase experiments showed that the pyrolyzed shale in the presence of brine and CO_2 provided the necessary environment for geochemical reactions to occur as evidenced by a plethora of mineral phase changes. The gas phase experiments showed little reaction for most experiments. Temperature step-down experiments showed a slight reduction in the net carbonation and also showed the

precipitation of newly formed calcite. Probability density modeling was done in order to gauge the effect of three of the four CO_2 storage mechanisms: adsorption, volumetric storage, and mineralization. When all of the variables are realized, the most common result predicted a capacity of 40 kg CO_2 per tonne of shale.

CHAPTER 9

INTRODUCTION

With the ever increasing attention to global energy concerns, unconventional energy resources are quickly evolving into a major energy supply. One of the technologies used as an unconventional source for liquid petroleum fuels is retorting oil shale. Although the concept of retorting oil shale dates back to the 19th century, fiscal and technological barriers have prevented this technology from becoming more widely adopted. With increasing prices for crude oil as well as decades of technological advancement, it seems that once again oil shale may be involved in our energy picture.

Just as the prospects for oil have changed over the decades, so has the attention being paid towards climate change. Of particular interest in the climate change debate are the effects of anthropogenic CO_2. The retorting process has an energy requirement that is greater than conventional liquid fuels production thus resulting in comparatively larger CO_2 emissions. Therefore, to mitigate the net CO_2 emissions from oil shale retorting, it has been proposed that long-term geologic storage of CO_2 within *in situ* pyrolyzed oil shale be investigated.

Previous investigators have studied the potential of long-term storage under a variety of geologic conditions such as shales, deep-saline aquifers, and carbonates. Kaszuba et al. [138] has shown that a shale aquitard can be involved in the sequestration process. Mandalaparty [139, 140] has performed experiments pertaining to CO_2 mineralization in spent shale from the Green River formation. Mandalaparty showed that

spent shale has the potential to initiate and sustain CO_2 mineralization.

This study expands on the works of Mandalaparty for a different retorted shale. Experiments were carried out at steady state temperatures of 120, 160, and 200°C with durations of 2, 5, and 10 weeks. The effects of ramping down the temperature were also examined over the course of 4 weeks. The step-down experiments were initiated at temperatures of 160°C or 120°C and ended at a temperature of either 120°C or 80°C, respectively. The intent of reducing the temperature was to approximate what happens when CO_2 is injected into a reservoir that is still warm from the retorting process.

What differentiates this study from those done previously is that this study examines the effect of all of the underground CO_2 storage mechanisms: dissolution into the brine, mineralization, storage in the pore volume, and adsorption. Pyrolyzed oil shale is unique in that all of the four aforementioned sequestration mechanisms are relevant, compared to a situation like aquifer storage where adsorption is insignificant or enhanced coal bed methane where the effects of geochemistry can be neglected.

Two sets of experiments were conducted with the shale being in direct contact with either the liquid brine or the gaseous CO_2 phase. Gas phase experiments were executed since CO_2 would likely exist in the supercritical phase or gaseous phase in part of the storage reservoir. A small amount of water vapor was allowed to remain in the gas phase experiments since a real injection environment would also likely have water vapor in the CO_2 phase.

The results of the liquid phase experiments showed that the pyrolyzed shale in the presence of brine and CO_2 provided the necessary environment for geochemical reactions to occur as evidenced by a plethora of mineral phase changes. Pyrrhotite in the starting

material dissolved releasing sulfur and iron ions, the presence of anhydrite in the reacted materials was one of the possible fates for the sulfur. Accompanying the precipitation of anhydrite was the precipitation of siderite for temperatures exceeding 160°C and durations longer than 5 weeks. Na-feldspar growth and cation exchange in the clays have also been observed in the liquid phase experiments. For liquid phase experiments, the net amount of carbonates initially decreases and then increases after 5 weeks for experiments conducted at 160°C and 200°C; the 120°C experiments showed no evidence of net carbonation in these experiments.

The gas phase experiments showed little reaction for most experiments. CO_2 acting as a corrosive gas was evidenced by etching patterns on the shale surfaces at higher temperatures. Pyrrhotite dissolution was observed at temperatures 160°C or less; siderite precipitation was also seen at similar temperatures. Evidence gathered from the gas phase experiments showed mineralization reactions occurring at temperatures less than 160°C. Temperature step-down experiments showed a slight reduction in the net carbonation and also showed the precipitation of newly formed calcite.

The computer simulation packages PHREEQC and Geochemist's Workbench (GWB) were used to model some of the geochemical processes expected in the experiments. Inverse modeling in PHREEQC was used to determine if there would be a positive or negative change on each mineral in the reactor. Inverse modeling found that the likely precipitates for the liquid phase experiments should be albite, dolomite, K-feldspar, illite, gypsum, siderite, and kaolinite. Smectite, analcime, calcite, pyrite, and quartz were expected to dissolve.

Geochemist's Workbench was used to simulate the equilibrium products that

would be expected for the liquid phase experiments. The GWB simulations predicted stable phases for dolomite, quartz, calcite, siderite, pyrrhotite, and kaolinite.

Probability density modeling was done in order to gauge the effect of three of the four CO_2 storage mechanisms: adsorption, volumetric storage, and mineralization. Mineralization results from the aforementioned experiments were combined with experimentally determined ranges of adsorption and porosity. Shale density and reservoir temperature were varied as well. When all of the variables are realized, the most common simulation result predicted a capacity of 40 kg CO_2 per tonne of shale.

In this study, we were able to examine all four mechanisms for underground CO_2 sequestration providing preliminary insight into a unique sequestration scenario.

CHAPTER 10

LITERATURE REVIEW

This section is intended to provide some background information into the aspects of CO_2 mineralization. This section focuses mainly on CO_2 sequestration in shale and addresses prominent previous works with CO_2-water-brine equilibrium, experimental studies, simulation studies, kinetic studies, and field sequestration studies.

As we move further into the 21st century, it is becoming more and more evident that unconventional resources are going to be needed to satisfy global energy demands.[141] Indeed, as the promises of renewable energy are coming closer to fruition, it is undeniable that fossil fuels are going to continue playing a role by bridging the gap towards a new energy economy. In helping bridge said gap, oil shale may prove to be a necessary source of liquid fuel, especially as more economical liquid petroleum sources become depleted. Liquids from oil shale are typically recovered by heating the shale (retorting), breaking down the kerogen in the shale into oil.

Further complicating the future's energy outlook is the potential for global climate change resulting from emissions from various industrial processes, the retorting process being included. Carbon dioxide (CO_2) has been implicated as a major contributor to global climate change.[142] In an effort to reduce the environmental impact of retorting oil shale *in situ*, it has been hypothesized that a pyrolyzed oil shale formation may provide a suitable repository for CO_2; furthermore, CO_2 sequestration by these means

may be economically attractive with Cap and Tax.

There are four distinct modes of underground CO_2 sequestration:

1. Volumetric storage in the pore space of the rock
2. Dissolution into connate water in the formation
3. Adsorption on surfaces in the formation
4. Geochemical

Of the four ways to sequester CO_2 listed above, the first three occur relatively quickly compared to geochemical reactions. Regardless, all four mechanisms should be considered when estimating the capacity of a subsurface repository; in certain situations there are orders of magnitude differences between the influences of mechanisms. For example, one would expect that the influence of adsorption would play a greater role on sequestration via Enhanced Coal Bed Methane (ECBM)[38, 66] than it would on sequestration in a deep-saline aquifer.[143] In the case of oil shale, all of the aforementioned means of sequestration play some sort of role. Removing kerogen from the rock matrix by means of pyrolysis increases the pore volume and thus the volumetric storage capacity of the rock. Connate water in the formation may dissolve CO_2: for which the extent of CO_2 dissolution depends mainly on the salinity of the water.[144] The char on the surface of the pyrolyzed oil shale can provide active sites to facilitate adsorption of CO_2.[145, 146] Although the net effect of adsorption on the pyrolyzed product amounts to tens of kilograms CO_2 per tonne rock, it is nonetheless important to account for this effect when calculating the total capacity in a repository. Geochemical reactions provide a means for long-term CO_2 sequestration with a reduced potential for CO_2 release, in contrast to the first three methods.

It is important to be able to apply what is learned with small scale experiments and have those results be extrapolated to larger volumes. Middleton et al.[147] outlined scaling CO_2 sequestration systems from the pore scale to the regional scale.

CO_2 Solubility in Brine

There have been multiple developments in calculating the solubility of CO_2 into an aqueous mixture as well as the fugacity of water in a supercritical CO_2 phase.[148] In order to calculate the solubility of CO_2 in brine, an equation of state or an empirical relationship must be used. Early models used for predicting CO_2 solubility in brine were based on the Peng-Robinson Equation of State (EOS). Other models include the Harvey-Prausnitz EOS[149] and work by Zuo and Guo.[150] For the purpose of this study, it was found that the work of Duan and Sun[151] provide an accurate prediction[152] for CO_2 solubility. The CO_2 solubility model of Duan and Sun can be used with the work of Duan et al.[153] to iteratively calculate liquid/gas phase partitioning.

Experimental Mineralization Studies

Abundant literature exists for experimental studies of geologic sequestration of CO_2 by geochemical reactions: Kaszuba et al.,[138] Carroll and Knauss,[154] Hellevang et al.,[155] and Hänchen et al.[156] are all highly relevant experimental investigators.

Kaszuba et al.[138] investigated the extent of brine/rock interactions at 200°C and 200 bars (2900 psi). The goal of Kaszuba and colleagues was to simulate the conditions of an aquifer being used for CO_2 storage: the study sought to examine not only the interaction between the fluid phases and the aquifer minerals but also the minerals making up the aquitard. The aquifer mineral was artificial arkose sandstone made up of

equal parts Minas Gerias quartz, oligoclase, and microcline. The aquitard was simulated by Silurian Maplewood Shale from New York, USA. The shale contained mostly illite, silty quartz, feldspar, sericite, and calcite with traces of pyrite, zircon, magnetite, and leucoxene. The temperature of 200°C was chosen to accelerate an otherwise slow kinetic process. The pressure of 200 bars was chosen to approximate the pressure in the full scale process.

The minerals in the experiments of Kaszuba et al. reacted with CO_2 and brine in a flexible Au-Ti reactor; the benefit of such a reactor is that it allows for sampling of the brine without disturbing the temperature and pressure of the system, a disadvantage is that removing the brine will cause the ratio of brine to rock to change. The brine was equilibrated with the rocks for 59 days after which CO_2 was injected and allowed to react with the system for an additional 80 days. Liquid samples were analyzed with ICP-ES/MS and dissolved ion chromatography. Solid materials were examined with X-Ray Diffraction (XRD), Scanning Electron Microscopy (SEM), and Energy Dispersive Spectrometry (EDS).

Experimental results showed increases and then decreases of Cl^-, Na^+, K^+, Mg^{2+}, Fe, and Ca^{2+} post CO_2 injection. The concentration of SO_4^{2-} decreased with the introduction of CO_2 and continued decreasing throughout the duration of the experiment. The injection of CO_2 into the system caused a rapid decrease in the pH from about 4.7 to 3.4. Solid phase changes included the etching of quartz grains and the formation of magnesite rosettes. The precipitation of analcime was also observed.

Kaszuba et al.[157] expanded on their previous work by reacting the same synthetic Arkose and Silurian Maplewood shale with 5.5 molal NaCl brine and supercritical CO_2 in

the same manner as previously discussed. The purpose of these experiments was to show the influence of CO_2 by having two identical reaction systems, one in the presence of CO_2 and the other without. From the fluid analysis, it was found that the concentrations of ionic Na^+ and Cl^- are suppressed by the presence of CO_2. It was also found that the concentrations of SiO_2, Mg^{2+}, Mn^{2+}, and Fe were higher in the experiment with CO_2 compared to the experiment without, suggesting that the carbonic acid from CO_2 promotes the dissolution of minerals. The precipitation of magnesite and siderite were noticed in the experiment with CO_2. The precipitation of analcime was observed in experiments with and without CO_2. An increase in the aqueous concentrations of Mg^{2+}, Fe, and Mn^{2+} were observed following the injection of CO_2; the concentration of said minerals subsequently decreased as carbonate phases precipitated.

Wigand et al.[158] continued the work of Kaszuba by experimenting on the effects of supercritical CO_2 on wellbore cement. Instead of using powdered shale/arkose, a fractured cement core was used. The experiments were conducted at 54°C and 2880 psi for 113 days. Calcite growth was observed in the fracture of the cement. As CO_2 saturated brine penetrated into the core, it formed carbonate rich bands which reduced the porosity of the cement.

Bertier et al.[159] investigated the reactions between CO_2, water, and rock on sandstone cores from Westphalia, Germany and Buntsandstein sandstone. Mineralogy was done with XRD, EPMA, and SEM-EDS. Sandstone cores were placed in a long, tubular vessel and allowed to interact with the CO_2 for 8 months. A system temperature of 80°C was used in order to speed up the reactions. Monthly analysis of the brine allowed the investigators to identify 25 chemical species that are indicative of CO_2-water-

rock interactions. Bartier et al. concluded that in their experiments there was an initial dissolution of carbonates, shown by increases in the Ca^{2+} and Mg^{2+} concentrations, followed by the precipitation of carbonates, signified by a reduction in Ca^{2+} and Mg^{2+}. Illitic needles were also observed as precipitates as well as kaolinite and pyrite.

Rosenbauer et al.[160] performed experiments to investigate the interactions between supercritical CO_2, natural brine, synthetic brine, and arkosic sandstone with and without the presence of limestone. Rosenbauer et al. used similar Ti-Au reaction vessels to those used by Kaszuba et al. Experiments were performed at 25°C or 120°C and at pressures raging from 1450 psi to 8700 psi. Brine sourced from the Paradox Valley in Colorado was used in the experiments as well as synthetic brine which was simply the product of reacting Paradox Valley brine with Leadville limestone (Colorado), Mount Tom arkosic sandstone (Massechusits), and banded sandstone (Coconio, Arizona). Liquid samples were analyzed with ICP-MS, ICP-AES, or ion chromatography. Solid samples were analyzed with XRD.

Rosenbauer et al. found that the presence of limestone can enhance the solubility of CO_2. As the dissolved CO_2 becomes carbonic acid, the limestone reacts and forms bicarbonate complexes. The increase in CO_2 dissolution ranged from 5.7% to 8.8%, decreasing with temperature. The precipitation of anhydrite and dolomite were found to be reaction products in experiments with limestone. Without the presence of limestone, the investigators concluded that the final fate of CO_2 was carbonates such as siderite. The concentrations Fe, Mg^{2+}, and Ca^{2+} showed similar trends to that observed by Kaszuba et al., where the concentration increases as a result of dissolution in the presence of carbonic acid and then decreases as carbonates precipitate.

Carroll et al.[161] examined Mount Simon sandstone and the Eau Claire (Wisconsin) shale in the presence of CO_2. The experimental apparatus and sample analysis were similar to those used by Kaszuba et al.[138] The sandstone and the shale showed the presences of quartz, K-feldspar, kaolinite, illite/smectite, iron bearing clays and magnesium bearing clays. As expected, the CO_2 interacted differently with the sandstone and the shale; however, the concentrations of calcium and magnesium varied little regardless of the presence of CO_2. PHREEQC was used to create 3000 realizations of this system with a near fit to the experimental data being achieved.

Yu et al.[162] studied the reactivity of CO_2 with flooded core experiments from the Qing 1 formation in China. XRD of the initial core showed that the mineral makeup was 58% quartz, 4% K-feldspar, 33% albite, 2% calcite, and 4% clay. The introduction of CO_2 saturated brine caused the dissolution of feldspars. The pH of the system increased with the introduction of CO_2 and then tapered off; ionic concentrations of Na^+, K^+, Al, Ca^{2+}, Mg^{2+}, and Fe all showed similar trends. The increase in the concentrations of Ca^{2+}, Fe, and Mg^{2+} were associated with the dissolution of carbonates. Porosity and permeability measurements on the core after completion of the experiment revealed that the porosity decreased on the upstream portions of the core and the permeability decreased with flow direction. The decrease in the porosity was attributed to the possibility of the precipitation of kaolinite.

Simulation Studies

In addition to the experimental studies regarding CO_2 mineralization, there have been computational investigations into the ultimate fate of the injected gas. The advantage of simulations is that they can examine a much larger system over geologic

time scales. Simulator packages such as TOUGHREACT[163] can be used to model subsurface flow with thermodynamics and geochemistry over very long periods of time.

Gundogan et al.[164] made a comparison of the most common numerical packages used for simulating the storage of CO_2. The first package they examined was PHREEQC; a free program from the United States Geological Service. The investigators also evaluated GEM, a software package from the Computer Modelling Group, and TOUGHREACT from Lawrence Berkley National Labs. Gundogan et al. found that the amount of dissolved CO_2 varied between the models, however, the pH was in good agreement. The variation in the concentration for the aqueous species was attributed to the different thermodynamic databases. Due to the discrepancies between the numerical packages, the authors suggest that the results of simulations of CO_2 storage only be interpreted as qualitative results rather than quantitative.

Gaus et al.[165] modeled the injection of CO_2 into the Sleipner area of the North Sea (Norway). The aquifer being modeled is Mio-Pliocene Utsira Sand consisting mostly of mica/illite (24.7%), quartz (21.5), kaolinite (18.0%), plagioclase (12.3%), smectite (8.8%), as well as lesser amounts of calcite, chlorite, k-feldspar, pyrite, and siderite. The brine in the aquifer is slightly basic (pH 7.67) with substantial concentrations of Ca^{2+}, Cl^{-}, Mg^{2+}, and Na^{+}. Both batch and reactive models were created to represent the aquifer at 37°C and 1470 psi. CO_2 fugacity was calculated using the methods presented by Duan at al.[166]

With the presence of abundant albite, Gaus et al. found that the principal mechanism for CO_2 mineralization was the formation of calcite, chalcedony, and kaolinite (Eqn. 1).

$$2NaAlSi_3O_8 + CO_2 + 2H_2O + Ca^{2+} \rightarrow 4SiO_2 + CaCO_3 + Al_2Si_2O_5(OH)_4 + 2Na^+ \quad (15)$$

After the Ca^{2+} ion becomes depleted form solution, it was proposed that the formation of dawsonite took over as the main means for CO_2 mineralization (Eqn. 2).

$$NaAlSi_3O_8 + CO_2 + H_2O \rightarrow 4SiO_2 + NaAlCO_3(OH)_2 \quad (16)$$

Anorthite has also been found to be a possible source of minerals necessary for CO_2 mineralization, playing a similar role to albite in Eqn. 1.[167]

$$CaAl_2(SiO_4)_2 + CO_2 + 2H_2O \rightarrow CaCO_3 + Al_2Si_2O_5(OH)_4 \quad (17)$$

Plagioclase was also examined for its possible reaction with CO_2 and water to form chalcedony, dawsonite, calcite, and kaolinite

$$5Na_{0.8}Ca_{0.2}Al_{1.2}Si_{2.8}O_8 + 5CO_2 + 6H_2O \rightarrow 10SiO_2 + 4NaAlCO_3(OH)_2 + CaCO_3 + Al_2Si_2O_5(OH)_4 \quad (18)$$

It is important to note that a secondary product of all of the four mechanisms Gaus et al. examined for CO_2 mineralization is kaolinite.

Gunter et al.[168] modeled the disposal of CO_2 as well as hydrogen sulfide and sulfuric acid in the deep saline aquifers of the Alberta Basin (Canada). These investigators used PATHARC to simulate the geochemistry in their model. Gunter et al. simulated that nearly all of the CO_2 mineralization occurred as siderite. Annite (mica) reacts with carbon dioxide to produce muscovite (an analogue for illite), siderite, and quartz (Eqn. 5). Gunter et al. also predicted the dissolution of kaolinite to produce muscovite.

$$3KFe_3^{2+}AlSi_3O_{10}(OH,F)_2 + 11CO_2 \rightarrow KAl_2(AlSi_3O_{10})(F,OH)_2 + 9\,FeCO_3 + 6SiO_2 + H_2O + 2K^+ + 2HCO_3^- \quad (19)$$

Zerai et al.[169] simulated the storage of CO_2 in the Rose Run sandstone (Ohio, USA). Equilibrium models, reaction path models, and kinetic models (Geochemists

Work Bench) were all used in investigating this deep saline aquifer's potential for long-term CO_2 storage. Zerai et al. proposed that most of the mineralization would occur as either siderite or dawsonite. The dissolution of albite, K-feldspar, and glauconite provided the necessary aqueous conditions to facilitate said precipitation. Zerai et al., much like Gunter et al., predicted the dissolution of kaolinite, in contrast to Gaus et al.

Xu et al.[170] modeled a sandstone-shale system using TOUGHREACT to study the mass transfer between the sandstone and shale zones as well as CO_2 mineralization. TOUGHREACT is an improvement on the multiphase flow simulator TOUGH2. In addition to modeling geologic reactive transport, TOUGHREACT can also model changes in porosity and permeability. Xu et al. found that the dissolution of chlorite and oligoclase provided the necessary cations for the precipitation of ankerite and siderite. Over time, Na^+ diffuses from the shale from the dissolution of albite thereby facilitating the conditions needed for the precipitation of dawsonite.

The injection of CO_2 into the Altensalzwedel gas reservoir was studied by Beyer et al.[171] In order to undertake this task, the coupled multiphase and multicomponent aspects were handled using OpenGeoSysChemApp. Mineral phases examined by the authors included: calcite, anhydrite, albite, K-feldspar, hematite, illite, dolomite, magnesite, dawsonite, siderite, halite, kaolinite, chamsonite, Ca-montmorillonite, and amorphous silica. The simulated brine was initialized with high concentrations of Na^+, Cl^-, and Ca^{2+}. CO_2 partitioning between the gas phase and the aqueous phase was assumed to be quicker than mineralogical reactions and was modeled using principles outlined by Duan and Sun.[151] Simulation results showed an increase in calcite, kaolinite, and Ca-montmorillonite with reductions of albite and illite.

Kinetic Studies

To better model temporal influence of reaction kinetics in a sequestration experiment as well as *in situ*, it is important to have adequate knowledge of the kinetic parameters of the reactions in the system. For most of the computational studies previously cited, the most important parameters are the equilibrium constant, *k*, the activation energy E_a, and the surface area; these parameters can be used with the Arrhenius equation to determine the reactions dependence on temperature.[172] Eqn. 6 shows the Arrhenius equation; wherein k_{25} is the rate constant at 25°C, *R* is the ideal gas constant, and *T* is the temperature.

$$k = k_{25}\exp\left[\frac{-E_a}{R}\left(\frac{1}{T} - \frac{1}{298.15}\right)\right] \tag{20}$$

For mineral dissolution and precipitation, a general rate law can be used [172, 173] (Eqn. 7).

$$r = \pm kA\alpha^{n}{}_{H+}\left|\left[\left(\frac{Q}{K}\right)^{\mu} - 1\right]\right|^{v} \tag{21}$$

where *A* is the specific reactive surface area, α_{H+} is the activity of hydrogen ions, *n* is the order of the reaction, *K* is the equilibrium constant for a mineral-water system defined as the destruction of one mole of mineral, *Q* is the reaction quotient, μ and *v* are fitting parameters determined by experiment. The term *Q/K* is also called the saturation index, a value for the saturation index greater than zero means that the mineral should precipitate, a value less than zero and the mineral should dissolve. Table 13 is an example of some of the rate parameters used by Xu et al.[170] Because of lack of kinetic data at the time the study was done, Xu et al. approximated some kinetics with like minerals.

The presence of kaolinite in experiments and simulations has a profound effect on the storage capacity for CO_2 in a variety of situations. Carroll and Walther[174] sought to determine the dissolution rate of kaolinite at 25, 60, and 80°C. The investigators found

that the dissolution rates are primarily dependent on surface area and pH.

The dissolution rate for kaolinite was minimal near a neutral pH and increased with deviation in either acidity or alkalinity. Ganor et al.[175] found that the dissolution rate of kaolinite is proportional to pH at a range from 3 to 4.

Carroll and Knauss[154] investigated the dissolution rates for Ca-silicates in the presence of CO_2 equilibrated with aquifer water. The Ca-silicate being investigated was labradorite. The investigators hypothesized that calcium liberated from the dissolution of labradorite could be used in the formation of calcite or dolomite. They found that the concentration has minimal effect on dissolution and also found the precipitation of aluminum phases.

Dissolution kinetics for dolomite, calcite, and magnesite under pressure and in the presence of CO_2 were determined by Pokrovsky et al.[176] The authors showed that the pressure of CO_2 in the system only has a minor effect on dissolution rates at a pH of 3 to 4.

Kumar et al.[177] attempted to model pore-level trapping, dissolution, and storage by precipitation. Simulation studies were carried out using the GEM, a Computer Modelling Group software, over a time span of up to 100,000 years. The mineral assemblage in the model included calcite, anorthite, kaolinite, siderite, and glauconite. The authors argued that capillary trapping has the potential to safely store CO_2 with reduced chances of migration. Mineralization of the CO_2 occurred on the order of 10^4 years.

In situ Studies

CO_2-rock-brine interactions in actual field situations are the ultimate coal for most of the studies regarding *in situ* storage of CO_2. Lu et al.[178] examined the geochemistry at the Cranfield CO_2 Enhanced Oil Recovery operation in Mississippi. It was expected that the change in pH due to the presence of CO_2 causes mineral changes in the form of dissolution/precipitation. Since there was approximately 40 years of equilibration with the brine, it was argued that the oil field would be analogous to a deep saline aquifer. The sampling in the field occurred over 21 months following injection; 11 brine, 37 core samples, and 830 gas samples were collected. Laboratory experiments were done using similar equipment to Kaszuba et al.[138] The mineralogy of the reservoir as determined by XRD was mostly quartz (avg. 79%), followed by chlorite (avg. 12%), kaolinite (avg. 3%), anatase (avg. 3%), illite (1%), calcite (1%), and small amounts of albite and dolomite.

Lu et al. found that the field measurements and the lab experiments were consistent. It was found that the brine chemistry had little change with little correlation between CO_2 abundance and aqueous concentrations. In field measurements and lab experiments, the pH of the systems decreased and then increased due to mineral buffering. Reservoir characterization found that most of the reactive minerals imperative for CO_2 mineralization have been depleted via diagenesis. Due to the lack of geochemical activity, the authors hypothesize that the primary mechanism of capture is CO_2 dissolution in the brine.

Kharaka et al.[179] investigated the CO_2 sequestration capability of the Frio "C" sandstone formation in the U.S. Gulf Coast. The sandstone of interest was a subarkosic

with quartz and sandstone. Fluids used during this study were adulterated with the tracer Rhodamine WT to differentiate from pristine brine. It was found that the injection of CO_2 displaces roughly 50% of the pore volume. Rapid dissolution of the calcite as well as iron oxyhydroxides was evidenced through fluid sampling. Concerns for the integrity of the reservoir arose from the rapid dissolution of said minerals, however, after 6 months little CO_2 leakage was observed.

Originality of This Work

This work represents an original contribution to the scientific community. There has been some previous attention paid to CO_2 sequestration in depleted oil shale reservoirs.[180] What makes this work stand apart is that it takes experimental results and attempts to estimate the CO_2 storage capacity of a spent shale reservoir with respect to the combined effects of mineralization, pore volumes, and adsorption. This work also expands on previous works on mineralization in shale dominated reservoirs.

Table 13: Kinetic rate parameters adapted from Xu et al.[170] * Denotes parameters identical to siderite, # for parameters identical to K-feldspar, ° for kaolinite, and • for pyrite.

Mineral	k_{25} ($mol^{-1}m^{-2}s^{-1}$)	E_a (kJ/mol)	N	A (cm^2/g)	Reference
Quartz	1.26E-14	87.50	0	9.8	[181]
K-feldspar	1.00E-10	57.78	0	9.8	[167]
Kaolinite	1.00E-13	62.76	0	151.6	[182]
Magnesite	4.47E-10	62.76	0	9.8	[183]
Siderite	1.26E-9	62.76	0	9.8	[184]
Dolomite*	1.26E-9	62.76	0	9.8	[184]
Ankerite*	1.26E-9	62.76	0	9.8	[184]
Dawsonite*	1.26E-9	62.76	0	9.8	[184]
Oligoclase#	1.00E-12	57.78	0	10	[167]
Albite-low	1.00E-12	67.83	0	9.8	[167]
Na-smectite°	1.00E-13	62.76	0	151.6	[182]
Ca-smectite°	1.00E-13	62.76	0	151.6	[182]
Illite°	1.00E-13	62.76	0	151.6	[182]
Pyrite	4.00E-11	62.76	0	12.9	[185]
Hematite•	4.00E-11	62.76	0	12.9	[185]
Chlorite	2.51E-12	62.76	0	9.8	[186]

CHAPTER 11

EXPERIMENTAL APPARATUSES AND METHODOLOGY

The purpose of this section is to provide the necessary information about the apparatuses and procedures used throughout this study in order to facilitate the reproduction of this study's results by other researchers.

Shale Sample Selection and Storage

Retorted (pyrolyzed) oil shale was provided by American Shale Oil, LLC. The shale was from the middle section of the R1 interval of the Garden Gulch member of the Green River Formation. It was retorted in a semi-open 10 kg autoclave (Batch Retort) by heating at 2^{o}C/hr up to 425^{o}C. Oil vapors escaped the reactor through the top and through a backpressure regulator set at 425 psi, achieving an oil yield of 66% of Fischer Assay

The shale samples were received in 1 centimeter chunks. Samples for analysis and experimentation were ground using a SPEX grinding mill and were sieved to have particles ranging from 88 to 120 μm. Ground samples were cone and quartered and stored in airtight jars to prevent contamination.

Brine Preparation

A 2% by weight sodium chloride brine was used in all experiments. The concentration for the brine was chosen because it is representative of the brines found in the Green River formation.[29] A bulk brine batch was made in a 1 liter volumetric flask using Fischer Scientific NaCl and water filtered with reverse osmosis to a resistance of 18 MΩ. The purpose of using highly filtered water was to prevent contamination from dissolved solids. The brine was stored in the volumetric flash and was sealed with a glass stopcock and parafilm to prevent evaporation.

Experimental Equipment

The purpose of this section is to describe in detail the primary equipment and supporting equipment used in this study. A procedure for operating the primary equipment is in the following section. All mineral materials were subject to the following analytical methods; X-Ray Diffraction (XRD), Scanning Electron Microscopy and Energy Dispersive X-Ray Spectroscopy (SEM/EDX); likewise all brine samples were examined with Inductively Coupled Mass Spectrometry (ICP-MS). Some samples were independently analyzed for organic carbon and inorganic carbon.

Geochemical Reaction Apparatus

Reactions between brine, retorted shale, and CO2 were conducted in 40 ml batch reactors. The design of the batch reactors was done with safety being the number one priority, followed by ease of use, and durability. The overall schematic of the reactors is similar in concept to that used by Ueda et al.[187] The entire experimental system was fabricated out of 316 stainless steel using Swagelok fittings. The reactor portion of the

system was a 1 inch (outside diameter) tube rated to 6,000 psi. A "K" type 1/8th inch thermocouple ran longitudinally through the reactor penetrating about half of the length. The thermocouple within the reactor served as the input for the temperature control system. The reactor was wrapped in a 24 inch 1300 watt heat trace rated to 1200°C. Needle valves were used to confine the contents of the reactor. Pressure was monitored with Honeywell pressure transducers and analog pressure gauges. A pressure relief valve was included in the reactor design as a means of preventing catastrophic failure due to temperature controller runaway. Pressurizing of the CO2 was done with a Teledyne Isco 500D syringe pump. The Isco pump used had special, corrosion resistant seals to handle exposure to high pressure CO2. The system was controlled using a personal computer running SPECVIEW. Power was supplied to the heaters using Omega SSR330DC10 solid state relays. A Schematic of the apparatus can be found in Figure 18 and a process diagram can be found in Figure 19.

Experiments in the liquid and gas phase were performed in this study. In order to facilitate gas phase experiments, the shale was suspended above the aqueous phase in a manner that was not restrictive to mass transfer. This was accomplished using a wire mesh (70μm) basket to hold the rock sample. The basket was prevented from slipping into the bottom of the reactor with glass beads. An illustration of this can be found in Figure 20.

There are several advantages and disadvantages to this experimental setup. The best way to outline some of these benefits and short comings is to compare this system with what is generally considered the standard for batch geochemical experimentation, the flexible Au-Ti reaction system.[138, 188] Advantages of this system over the Au-Ti

system are that the brine/rock ratio remains constant throughout the duration of the experiment, the apparatus is inexpensive, and has simple operation. Disadvantages are not being able to measure brine concentrations/pH throughout the experiment as well as mineralogical changes during the depressurization of the reaction vessel.

Supporting Equipment

X-Ray diffraction. X-Ray Diffraction was done at the University of Utah Energy and Geosciences Institute (EGI). EGI performed whole-rock and clay analysis on all samples submitted using a Bruker D8 Advance X-Ray diffractometer. Quantification of mineral phases via the Reitveld method was done using TOPAS software. TOPAS is a Bruker software package used for single line fitting, whole powder decomposition, Reitveld structure refinement, and quantitative Reitveld analysis.[189] Reitveld analysis uses a least squares approach to fit the observed XRD pattern to species from a library of crystalline XRD signatures. Peak profiles and crystal structures are varied to minimize the differences between calculated and observed patterns.

The XRD was operated using Cu-K-α radiation at 40kV and 40mA with a 0.02° 2Θ step size. The time for each step was 0.4 seconds for clay and 0.6 seconds for whole-rock. Clay samples were analyzed from 2 to 45° 2Θ while whole-rock samples were analyzed from 4 to 65° 2Θ. A lynx eye detector was used which collects data over 2.6mm rather than at point, thereby increasing detector counts while reducing data acquisition time.

Whole-rock sample preparation was done using the following procedure:

- Sample is pulverized with a mortar and pestle.
- Pulverized powder is mixed with deionized water, ground in a

micronizing mill and sieved to less than 44μm.

- The sample is homogenized with a rolling mill in order to randomly orient the grains.
- The rock is placed in a sample holder and smoothed with a razor blade.

Sample preparation for clay analysis was done according to the following procedure:

- Samples are pulverized with a mortar and pestle.
- Pulverized powder is mixed with deionized water, ground in a micronizing mill and sieved to less than 44μm.
- The fraction of material less than 2μm is removed by suspending them in water and decanting them off.
- A centrifuge is used to remove the remaining fraction of water.
- The sample is mixed using an ultrasonic homogenizer.
- The sample is applied to glass slides.
- The sample is air dried and a XRD scan is performed.
- After the first scan, the sample is exposed to ethylene glycol vapors for 12 hours at 65°C in order to induce clay swelling. After treatment, another scan is performed.
- Clay scans are compared using the methodology outlined by Moore and Reynolds.[190]

In order to maintain consistency between XRD interpretations, all spectra were analyzed by the same user using the same fitting criteria.

Scanning electron microscopy / Energy dispersive spectra. SEM/EDS microscopy was done in the Material Sciences and Engineering department at the University of Utah.

The scanning electron microscope used was a Hitachi S3000-N Scanning Electron Microscope (SEM) at 20kV under vacuum. An Energy Dispersive Spectrometer (EDS) unit was attached to the SEM allowing for identification of some elements. Resolution on this particular SEM was good to about 20μm. Before a sample could be examined with the SEM, the sample needed to be adhered to carbon tape and coated with gold. The carbon tape and gold coating served to make the sample conductive.

Inductively coupled plasma mass spectrometry. Inductively Coupled Mass Spectrometry (ICP-MS or just ICP) analysis was done at the Geology department at the University of Utah. Brine samples were delivered with some rock particles still in suspension and samples were filtered upon delivery.

Carbon analysis. Total carbon, organic carbon, and inorganic carbon analysis was done on some of the samples by Huffman Labs in Golden, CO. Total carbon was determined using a Leco CR 12 Carbon Analyzer. The sample is combusted in a furnace at 1350°C in an oxygen environment making CO_2. The CO_2 from combustion is quantified using infrared detection.[191]

Inorganic carbon was determined using a UIC/Coulometrics System 140 Carbonate Carbon Analyzer. The inorganic carbon analysis involves dissolving all the carbonate in 0.1N perchloric acid and quantifying the evolved CO_2 using coulometric titration.[192] The total organic carbon in the sample is the difference between the total carbon and the inorganic carbon.

Experimental Methodology

This section is supposed to provide the operating procedure for setting up, taking down, and sampling from the geochemical reactor. This section also discusses some of

the computer models used in this study. The goal of this section is to be detailed so that others can reproduce the experiments and to provide insight into some of the operations performed. In order to maintain consistency between experiments as well as ensuring quality of the data, strict guidelines were followed in sample handling and experimentation.

Geochemical Reactor

Throughout every phase of the procedure, the experimentalist avoided contamination of the system; this included always wearing gloves, maintaining a sterile work area free of clutter and dust, sonicating all tools, and rinsing all equipment three times with 18MΩ deionized water.

Before each experimental run, the entire reactor vessel was broken down and polished with alumina powder. Alumina polishing ensured the same clean and smooth surface for every experiment. After polishing, the reactor was sonicated, rinsed multiple times with deionized water and allowed to air dry. Polishing was impractical on the other parts of the apparatus; they were extensively rinsed with deionized water and allowed to dry.

The reaction vessel was loaded according to the following procedure. First, a cap is attached to the bottom of the reaction vessel. Next, 5.00 grams of pyrolyzed shale is positioned in the bottom of the vessel or in a basket if doing a gas phase experiment. The top cap is then used to seal off the vessel. The entire system is pressure tested to 1500 psi with nitrogen by placing the pressurized system in a basin of water and checking for leaks. Nitrogen also serves the purpose of flushing any air from the system. The brine, 20.00ml for aqueous experiments or 5.00ml for gas experiments, is injected through the

1/4 inch fitting in the bottom cap.

The brine and rock are allowed to come to equilibrium over the course of several weeks. Many previous geochemistry investigators noticed brine changed by leeching, dissolution, and ion-exchange in the time preceding CO_2 injection.[157, 160] After equilibration, CO_2 is injected and the system is allowed to remain undisturbed for the appropriate time span. Upon completion, the vessel is cooled, removed from the rest of the apparatus, and disassembled to remove samples.

Computer Simulations

Geochemists workbench. Geochemists Workbench (GWB) is a software package with several modules with different capabilities. This study utilized two of the available packages: "Act2" and "React," React is useful for modeling mineralogical changes over the course of a reaction, in the case that it was used for these studies initial amounts of the starting material (Chapter 4) and initial amounts of brine (Chapter 5) were programmed to come to equilibrium at a defined temperature and pressure of CO_2.

Act2 is a useful tool for producing phase stability diagrams. For this study, all mineral species were included with experimentally measured brine concentrations. Probable mineral stabilities were examined with respect to changes in temperature and changes in pH.

PHREEQC. PHREEQC is free software from the United States Geological Service (USGS). This software is a versatile tool in that it is capable of modeling reactive transport, equilibrium reactions, and important to this study: inverse modeling. The inverse modelling used was based on the models outlined in Apello and Postma.[173] Inverse modeling starts with defining the amounts of the starting mineral in the presence

of the original brine under a predefined pressure of carbon dioxide. Next, a temperature is defined with an experimentally determined brine concentration. Iterations are then run that run likely mass and charge balances that would provide the defined final brine concentrations. Sporadic nonconverging iterations were manually screened.

Sensitivity study. A sensitivity study was done to determine the effects of adsorption, mineralization, and volumetric storage of CO_2 in a pyrolyzed oil shale reservoir. A volumetric and mass balance was done on a hypothetical reservoir. This mass balance took into account changes in pore space due to dissolution and precipitation of carbonates. Experimentally determined values for adsorption and carbonates were used. Estimates for the range of porosity and carbonate density were also used.

MATLAB R2009b was used to randomly change variables in the mass/volume balance multiple iterations. The iterations were organized into probability bins and histograms were made to find the most likely amount of CO_2 stored per mass of rock. Constraints were defined on the amount of carbonate, the amount of adsorption, and the pore volume to gauge the effects of different storage mechanisms.

Experimental Matrix

The effects of reaction time and temperature are being examined in this study. In order to assess the response of these variables, most of the liquid phase and gas phase experiments were conducted following an experimental matrix. The temperatures used in this study were 120, 160, and 200°C; the experimental durations were 2 weeks, 5 weeks, and 10 weeks. Furthermore, to aid in the precision of this study, each individual experiment was duplicated. The experimental matrix is Table 14.

The result of this was 36 experiments encompassing about 2 years of work. Some

experiments also had more than two runs. Other experiments included the temperature step-down study wherein the system started at a temperature of either 160°C or 120°C and was reduced by 10°C/week over the course of 4 weeks. The purpose of the step-down experiments was to initialize dissolution at a high temperature and then promote precipitation with a lower temperature. The step-down experiments were also intended to simulate what would happen if CO_2 were injected into an oil shale formation cooling down after pyrolysis.

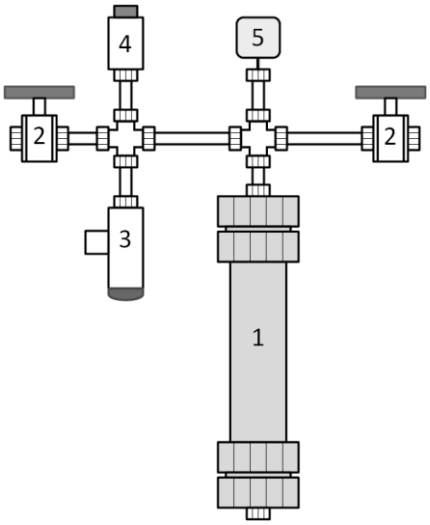

Figure 18: Schematic for the reactor apparatus used in the spent shale-brine-CO2 mineralization experiments. 1) Reaction vessel. 2) Needle valves. 3) Pressure relief valve 4) Pressure transducer 5) Thermocouple

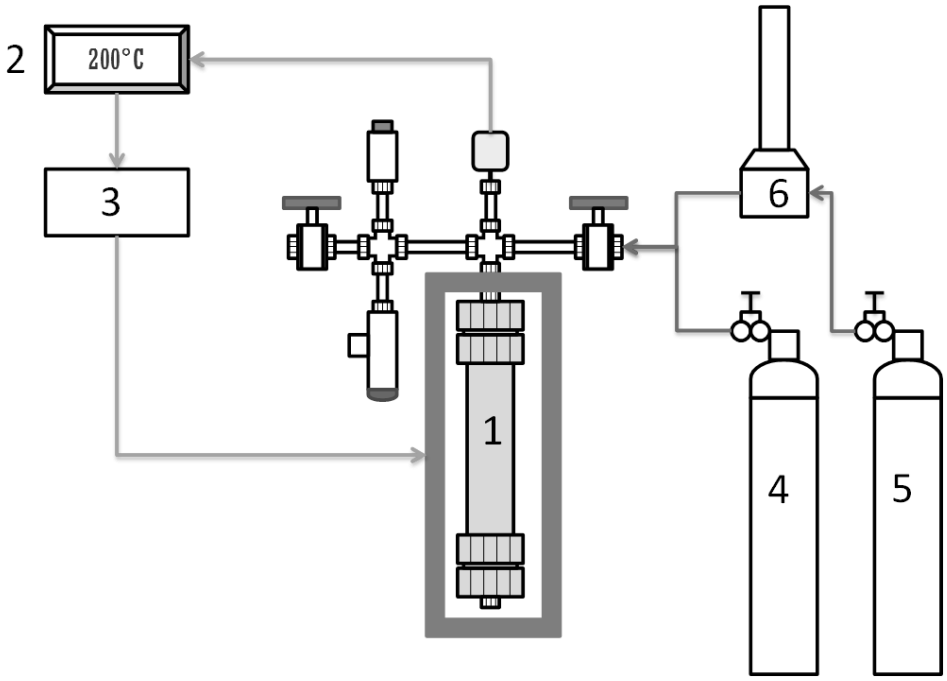

Figure 19: Extended view of the experimental apparatus. 1) Reactor vessel. 2) Temperature controller. 3) Solid state relay. 4) Nitrogen tank. 5) CO_2 tank. 6) Isco pump

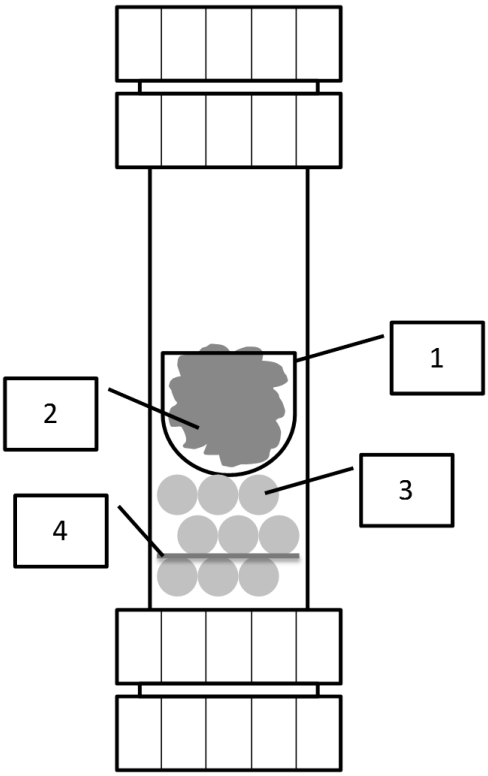

Figure 20: Configuration of reactor for gas phase experiments. 1) Mesh basket. 2) Shale sample. 3) Glass beads. 4) Water line.

Table 14: Outline of the experimental matrix used to study the effects of temperature and duration.

Duration [weeks]	Temperature [°C]		
-	120	160	200
2	Two experiments →		
5	↓	↘	
10			

CHAPTER 12

ANALYSIS OF STARTING MATERIALS

The purpose of this section is to provide a concise and accurate description of the mineralogy of the shale used as well as the ionic composition of the brine. XRD was used to identify the mineral phases in the retorted shale and ICP-MS was used to identify the ions in the starting brine.

Retorted Shale Analysis

XRD was conducted on the retorted oil shale used in the experiments according to the outlined procedure. The Reitveld analysis of the material was narrowed down to the following 13 constituents: illite, illite/smectite, albite, analcime, dolomite, quartz, orthoclase, calcite, buddingtonite, siderite, pyrrhotite, anhydrite, and halite. These species were chosen because of their omnipresence in the samples or their significance to geochemistry as it pertains to CO_2 mineralization. A summary of the XRD results for the starting material can be found in Table 15.

. The results presented in Table 15 are the average of three different XRD analyses, however little differences between analysis were observed.

From Table 15, it can be seen that the majority of the mineral content is quartz, illite, dolomite, and interlayered illite/smectite. Pyrite was present in the samples before pyrolysis, however, thermal treatment converted most into pyrrhotite[193, 194]; all other

minerals are considered to be unchanged from heating.

Brine Analysis

ICP-MS analysis was done on the starting brine, showing mostly the presence of Na^+ and Cl^-. Some other ions were found in the analysis, but their concentrations were hardly above the lower detection limit (L.O.D.). Analytical results of the initial brine can be found in Table 16.

Table 15: Mineral composition of the pyrolyzed shale before reaction with CO_2. Average of three different analyses

Species	*Wt. %*	*Species*	*Wt. %*	*Species*	*Wt. %*
illite/smectite	9.9	orthoclase	4.3	siderite	0.7
illite	27.5	quartz	26.0	pyrrhotite	2.6
analcime	2.1	Calcite	2.2	anhydrite	0.5
albite	3.3	buddingtonite	6.9	halite	~ 0.0
dolomite	14.0				

Table 16: Initial brine concentration as determined by ICP-MS

Species	Na^+	Mg^{2+}	Al	K^+	Ca^{2+}	Mn^{2+}	Fe	Ba^{2+}	Si	S	Cl^-
Units	mg/l	mg/l	mg/l	mg/l	mg/l	mg/l	mg/l	mg/l	µg/l	µg/l	mg/l
L.O.D	1	0.01	0.00005	1	0.2	0.0003	0.03	0.0005	2	65	96
Conc.	7910	0.10	0.01	<LOD	0.50	<LOD	<LOD	<LOD	4	<LOD	14688

CHAPTER 13

BRINE EQUILIBRIUM

This section discusses some of the calculations in determining the partitioning of water between the aqueous and vapor phase in these experiments. These calculations were used later to determine the starting conditions for simulations. The results presented here fill a gap in information that is commonly overlooked. Most researchers neglect the effects of phase change in the closed reactors. Evaporation of the water into the gas phase increases the concentration of ions in the brine. The significance of water vapor in the gas phase experiments will be later discussed.

NaCl-CO_2-H_2O Equilibrium

Equilibrium partitioning for the starting materials was calculated in order to best describe the *in situ* amounts of NaCl, CO_2, and H_2O in each phase. Work by the Duan research group[151, 153, 195] served as the equations of state for determining the densities of gas and liquid phases as well as phase equilibrium concentrations.

The reactor vessel is a closed system, as water evaporates from the aqueous phase as a result of heating, the volumes and densities of the aqueous phase and the gas phase change accordingly; likewise, as CO_2 dissolves into the aqueous phase partitioning changes are expected. In order to solve for equilibrium, the mass balance for the entire system must be computed iteratively until convergence with the initial mass is achieved. Each iteration begins with changing the volume of the aqueous phase. Then vapor-liquid

phase equilibrium calculations are performed. Using the results of the phase equilibrium calculations, densities of each phase are changed and a mass balance is performed. The results of the phase equilibrium calculations as a function of temperature and initial brine volume (20ml for liquid experiments, 5ml for gas) can be found in Table 17.

Volumetric increase of the aqueous phase results from reductions in density due to thermal expansion and CO_2 dissolution. The gas phase experiments have nearly twice the mass of water in the vapor phase due to the larger available volume compared to the liquid phase experiments, but the concentration of water in the vapor phase is nearly the same, for example, if one were to compare a 120°C liquid type experiment with a 120°C gas type.

Table 17: Results of phase equilibrium calculations

Exp. Type	T , °C	CO_2 (l), grams	CO_2 (v), grams	H_2O (l), grams	H_2O (v), grams	Liquid, ml	Vapor, ml
Liquid	120	0.445	1.741	19.784	0.043	21.44	16.97
Liquid	160	0.407	1.303	19.726	0.100	22.14	16.27
Liquid	200	0.384	0.927	19.668	0.158	23.11	15.30
Gas	120	0.110	3.398	4.873	0.083	5.28	33.13
Gas	160	0.098	2.650	4.752	0.204	5.34	33.07
Gas	200	0.090	2.000	4.613	0.341	5.42	32.99

CHAPTER 14

LIQUID PHASE EXPERIMENTS

This chapter focuses on experiments where the rock was in direct contact with the brine. Having the rock in contact with the brine is common practice for geochemical experiments. In this section, the effects of time and temperature are examined for changes in mineral phases and brine concentrations. For these experiments, XRD, ICP-MS, and SEM analysis are combined to describe an environment that is difficult to sample directly.

Liquid Phase Experiments

In an underground CO_2 repository, there is a region where brine occupies the majority of the pore space and there is a region where CO_2 occupies most of the pore space. In the case of underground retort, there is the possibility that thermal treatment will remove some of the initial connate water. In order to investigate the geochemical interactions in the brine filled volume of rock, liquid phase experiments were conducted according to the experimental matrix outlined in Table 14.

Experiments were done at three different temperatures: 120, 160, and 200°C for three different durations, 2 weeks, 5 weeks, or 10 weeks. Duplicates were done for each experiment per the aforementioned experimental procedure. In order to quantify reactions with the reactor material, a reactor stability study was done.[196] The reactor stability study found a slight increase in the concentrations of Fe and Mg^{2+} in the brine

and that over a range of conditions that the reactor remained stable.

The Na^+ concentration over all temperatures decreased throughout the entire duration of the experiments with the greatest decrease in the first 2 weeks, as seen in Figure 21. Temperatures of 120 and 160°C showed a more rapid decline in the Na^+ concentration than the 200°C experiment. Some of the reduction in the Na^+ concentration may be the result of cation exchange between the illite and smectite layers.[197] The measured concentrations for Na^+ and Cl^- can be found in Figure 21.

The amount of illite found in the liquid experiments remained relatively stable for the experiments at 120 and 160°C (Figure 22). The experiments performed at 200°C showed a 13% increase by 2 weeks and then a drop of 26% by 10 weeks. The drop in the amount of illite may be due to dissolution. The measured quantity of interlayered illite/smectite increased in the first 2 weeks with experiments at 120 and 160°C and then fell to about initial quantities.

The amount of illite/smectite in the 200°C experiments decreased throughout the experiments. The observed increase and decrease in the 120°C and 160°C may be the result of different cations in the layers of the clays. If Na^+ is exchanged with other cations, the measured XRD patterns for illite/smectite can differ, showing an increase in said phases due to clay swelling. The different patterns of smectite have been extensively studied by Sakharov et al.[198] The reduction of illite/smectite in the 200°C experiments may be the result of dissolution.

Dissolution of illite would cause an increase in the amount of K^+; likewise, the dissolution of orthoclase feldspar would cause a similar response. In all liquid phase experiments, an increase in the concentration of K^+ was noticed, followed by a decrease.

The decrease in the K^+ concentration may be the result of biotite precipitation, however, XRD analysis did not see a noticeable amount of biotite. Figure 23 shows dissolution patterns on illite/smectite from a 5 week 160°C experiment.

In all experiments, there is net dissolution of calcite and dolomite by 2 weeks, as shown by Figure 24. Also, in all of the experiments, the amount of dolomite increased somewhat by 5 weeks. At 10 weeks, the quantity of dolomite decreased in the 120°C and 200°C experiments while dolomite continued to increase for the 160°C experiments. The amount of calcite increased by 5 weeks for experiments at 120 and 160°C and then decreased again by 10 weeks. The amount of calcite in the 200°C experiments decreased until 5 weeks and then increased sharply to about double the amount found in the initial shale. The decrease followed by an increase in dolomite abundance had also been noticed by Mandalaparty[196]; Mandalaparty hypothesized that the initial acidification of the brine causes rapid dissolution of carbonate minerals. As the brine becomes more saturated with Mg^{2+} and Ca^{2+} from dissolution of slower dissolving minerals, carbonate phases should precipitate.

It would be expected that the dissolution of calcite and dolomite would cause an increase in the brine concentration of Ca^{2+} and Mg^{2+} (Figure 25). Likewise, the dissolution of other minerals and ion exchange should also cause an increase in these concentrations. The trend in the Ca^{2+} experiments is evidence of the trends in the amount of dolomite with respect to dissolution followed by precipitation for the experiments conducted at 160 and 200°C. Likewise, the trends in the concentration of Mg^{2+} further show this.

Examination of some of the samples using scanning electron microscopy revealed

some dissolution of the initial dolomite. Figure 26 is an image from a 2 week 160°C liquid phase experiment showing acidic etching patterns on a dolomite grain. Verification that the grain was dolomite was confirmed with an EDS scan. The precipitation of calcite was found in a 5 week 120°C experiment, shown in Figure 27. The calcite seen in Figure 27 does not have a well formed crystalline structure, meaning that it could have formed during the degassing stage of the experiment due to the desiccation of the brine, which is inevitable in that step of the experimental procedure.

Newly formed anhydrite crystals were common in almost all liquid phase experiments. The source of the sulfur for the anhydrite was attributed to the dissolution of pyrrhotite. From GWB modelling of the Ca^{2+} ion under reactor conditions and in the presence of other minerals, it was determined that anhydrite is the most stable phase for Ca^{2+}, explaining why anhydrite was commonly observed in SEM-EDS analysis. Some of the anhydrite growths found in the SEM-EDS analysis were well structured and had lengths exceeding 250μm, as seen in Figure 28. Anhydrite precipitation was also observed by Rosenbauer et al.[160]

With the dissolution of the pyrrhotite, iron ions are released into the brine, which serves to form the carbonate mineral siderite. XRD trends for siderite and dolomite support this claim, as seen in Figure 29. All liquid phase experiments showed pyrrhotite dissolution by 5 weeks, with the 120 and 200°C experiments showing a slight increase by 10 weeks. Siderite quantities for all experiments decreased by 2 weeks, which can be attributed to dissolution due to the initial acidification of the brine. As time progressed, experiments at 160°C and 200°C showed increases in siderite to amounts greater than that in the initial shale.

GWB analysis for iron found that Fe^{2+} is the prominent form of iron under temperatures used in the experiments. If the temperature is reduced, ferrous bicarbonate becomes stable. It can therefore be inferred that siderite may have precipitated as the reactors were cooled at the end of the experiments.

Since CO_2 would likely be injected into a formation that is still hot from the retorting process and subsequently cools thereafter, it stands to reason that one of the primary mechanisms for CO_2 sequestration via mineralization would involve siderite. This, among other reasons, served a justification for the temperature step-down experiments. Kaszuba et al.[157] suggested that siderite would also play an important role in sequestration. They also showed that early precipitates of calcite are not in equilibrium and undergo dissolution; our experiments showed well formed calcite crystals with etching, but it was impossible to determine if those crystals were there initially or were formed during the experiment.

The total amount of carbonate in the liquid experiments showed an initial decrease for all temperatures by 2 weeks followed by a rebound in carbonate abundance by 5 weeks. By 10 weeks, the experiments at 200°C showed a net gain in carbonate; the experiments at 160°C showed a negligible change from the initial amount of carbonate; and the experiments at 120°C showed a net decrease. Total carbonate was calculated as the sum of calcite, siderite, magnesite, and dolomite. Figure 30 shows the total carbonate amounts.

Some of the liquid phase experiments had enough sample remaining after SEM-EDS and XRD to have total carbon analysis done on them by Huffman Labs in Golden, CO. The results of this external analysis shows that the carbonate decreases at the 5 week

mark for the 120°C experiments and continues to decrease until 10 weeks; a result that is inconsistent to that shown in Figure 30. The experiments at 160°C showed a substantial decrease in carbonate by 2 weeks and a rebound in carbonate amounts by 10 weeks, but not nearly to starting amounts.

Kaszuba et al.[157] showed that analcime would precipitate in the presence of a Na^+ rich brine with and without the presence of CO_2 and that the presence of CO_2 increases the rate of analcime precipitation. XRD analysis of the reacted products showed little change in the amount of analcime; however, SEM-EDS analysis found newly formed analcime crystals. Good specimens of analcime growth were found in the 2 weeks 160°C experiments.

Other mineral phases in the liquid experiments such as quartz, albite, and buddingtonite showed little change. SEM analysis did find some silica zeolite and amorphous silica.

Conclusions

The liquid phase experiments showed a plethora of geochemical interactions that show potential for the long-term storage of CO_2. An initial decrease in the amount of carbonate in the system was found for all temperatures. With the exception of the 120°C experiments, the total amount of carbonate recovered to at least near initial quantities. For the higher temperature experiments, the dissolution of pyrrhotite and the precipitation of siderite can be considered to play a major factor in the potential for CO_2 storage. With the dissolution of pyrrhotite, the precipitation of well formed anhydrite was observed.

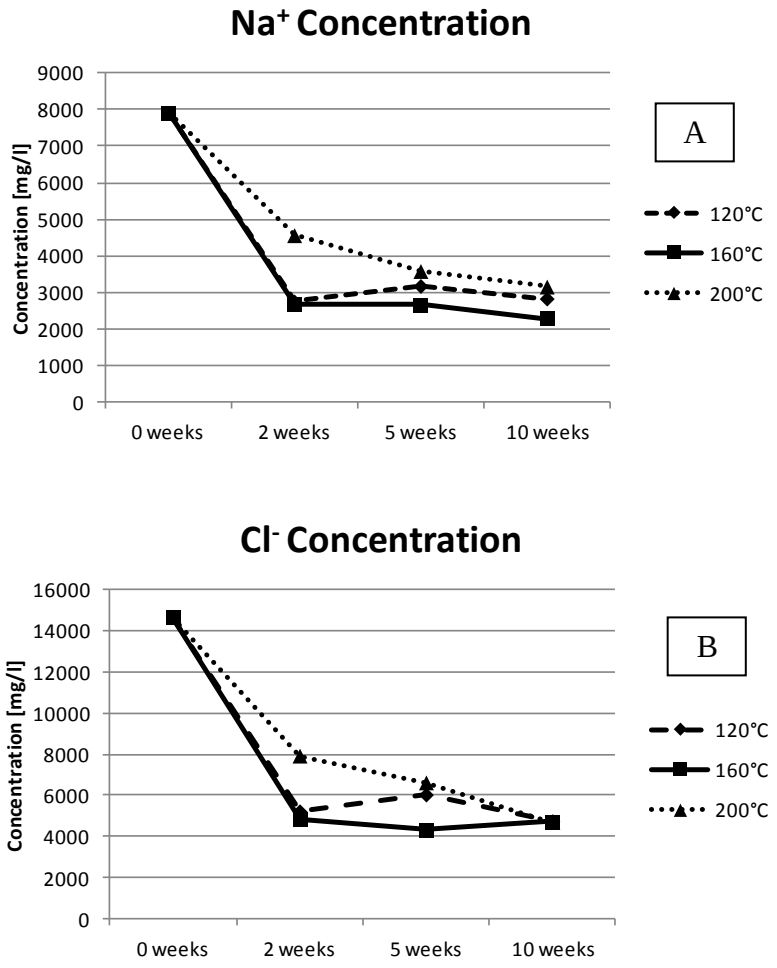

Figure 21: Na^+ and Cl^- concentrations for the liquid phase experiments. A) The reduction in the Na^+ concentration may be the result of cation exchange between the illite/smectite layers. B) Cl^- also reduce with time.

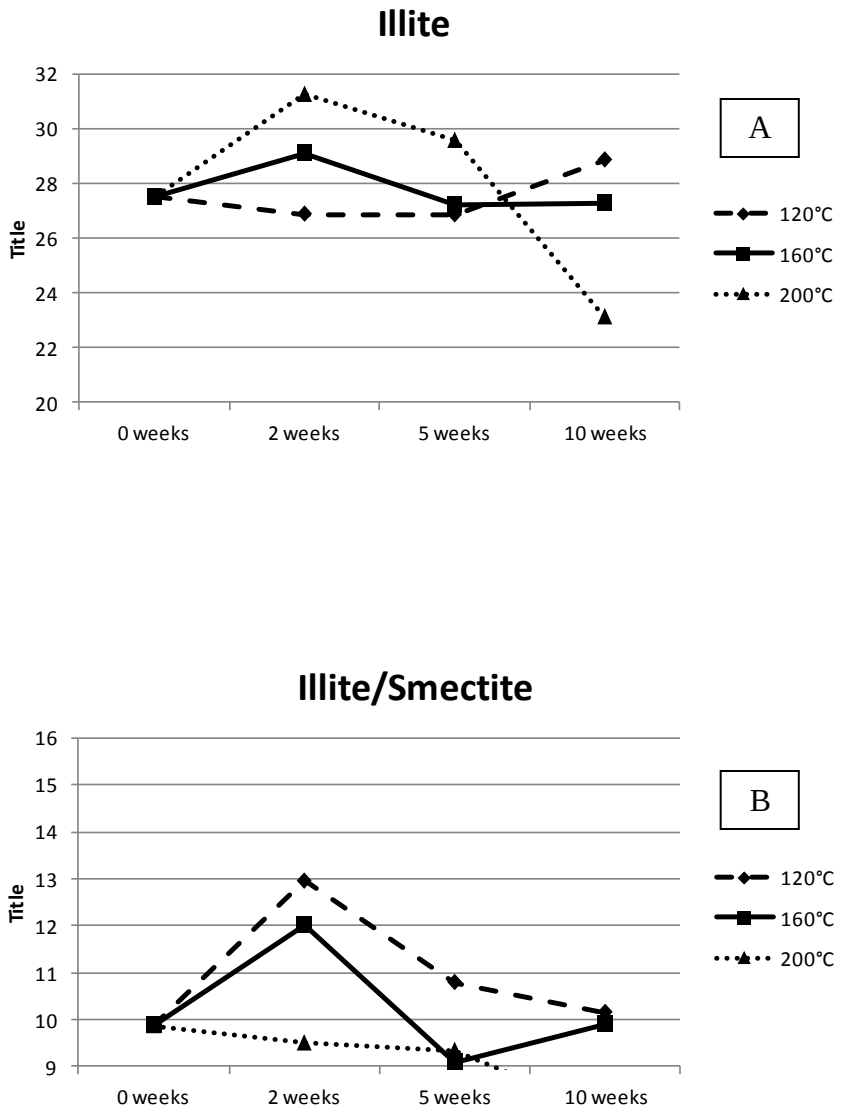

Figure 22: Illite and illite/smectite weight percentages for the liquid phase experiments. Dissolution may be responsible for the reduction of illite and illite/smectite in the 200°C experiments. A) Experimental illite amounts. B) Different cations between the layers of clay may have resulted in the XRD patterns showing an increase in the amount of illite/smectite in the lower temperature experiments.

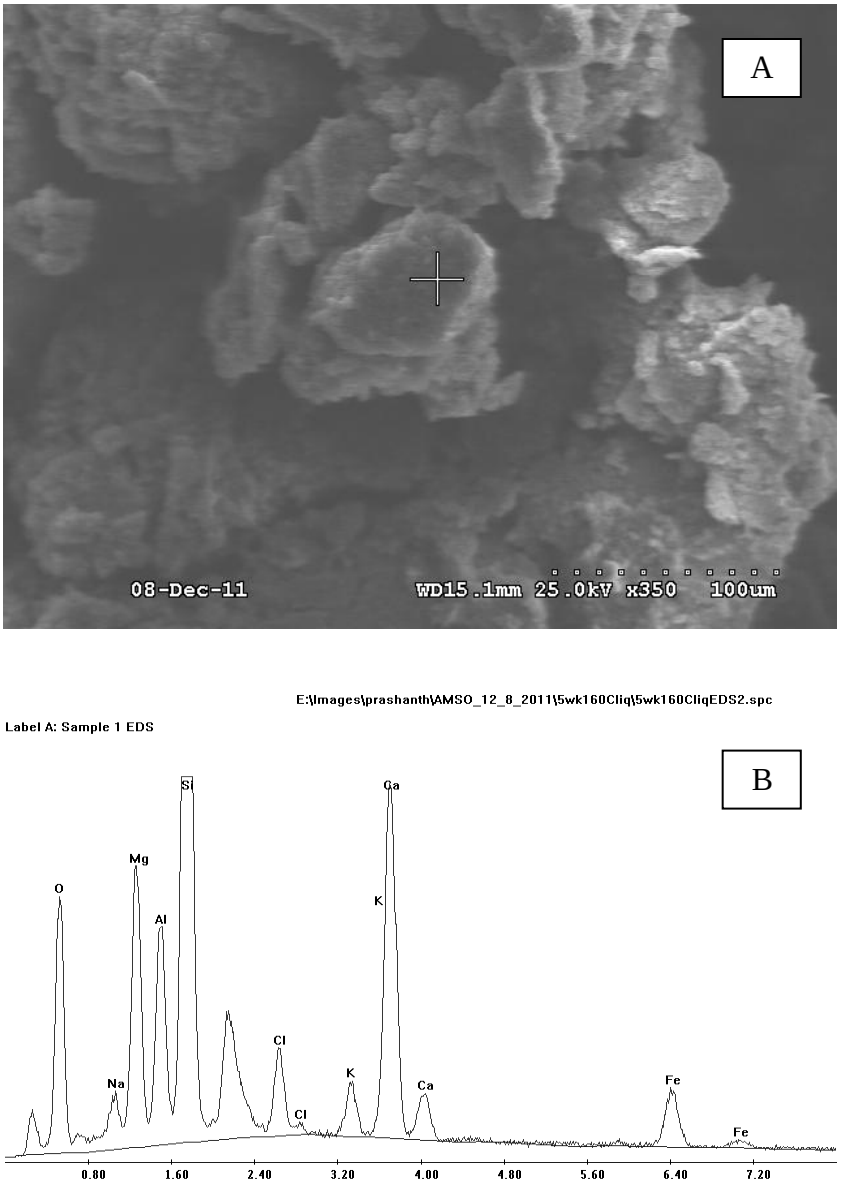

Figure 23: Interlayered illite/smectite from a 5 week 160°C experiment. A) Interlayered illite/smectite showing some etching on the edges. B) EDS of the clay verifying that it is illite/smectite.

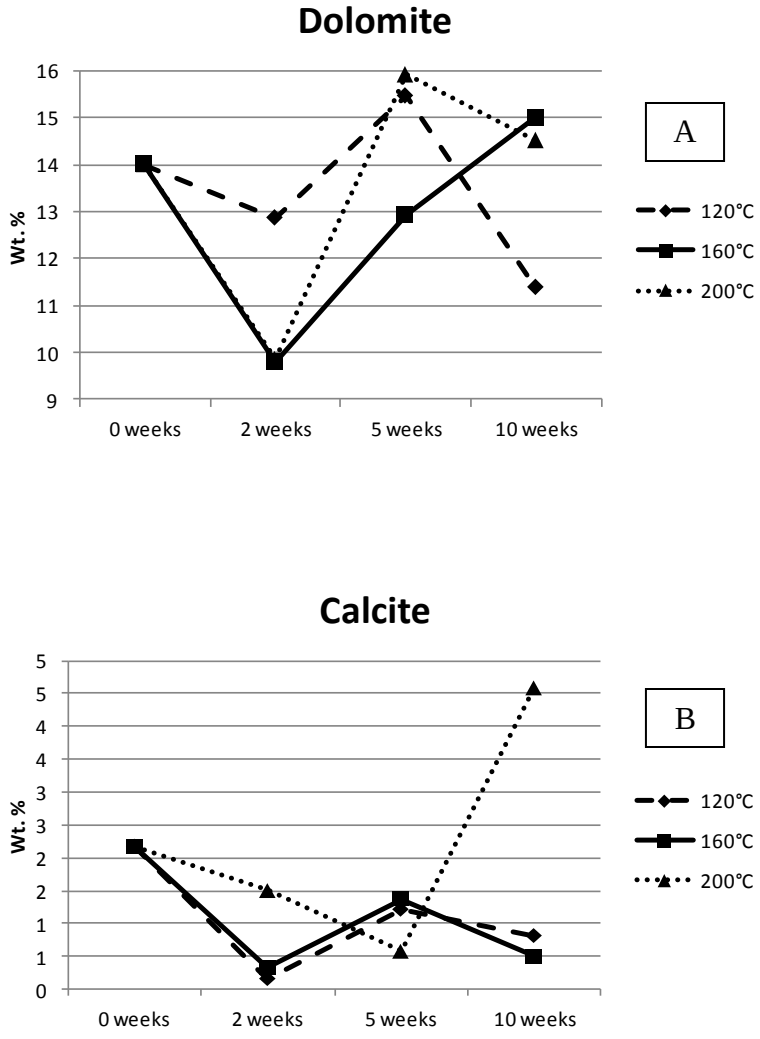

Figure 24: Abundances of dolomite and calcite in the liquid phase experiments. The quantity of these carbonates all showed dissolution by 2 weeks with some experiments showing precipitation thereafter. A) Dolomite amounts. B) Calcite amounts.

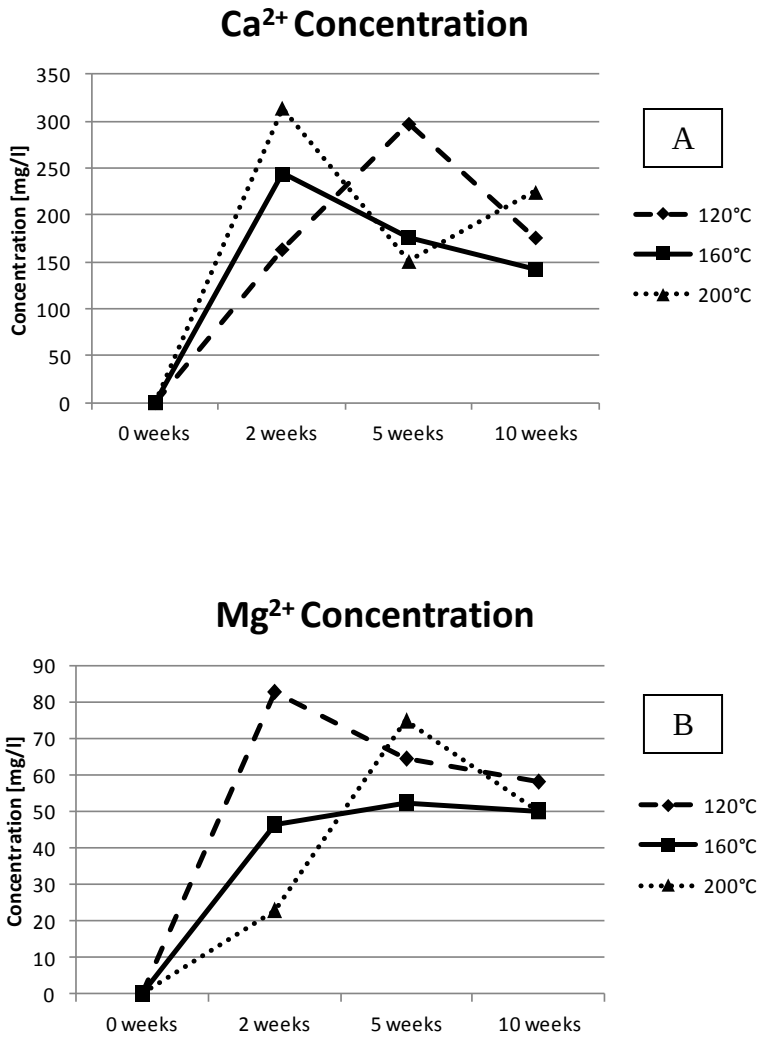

Figure 25: Ca^{2+} and Mg^{2+} concentrations in the liquid phase experiments. The concentrations of these ions support the evidence that dolomite and calcite are initially dissolving and in some instances precipitating. A) Changes in calcium concentration from changes in abundances in calcite and dolomite. B) Changes in magnesium concentration.

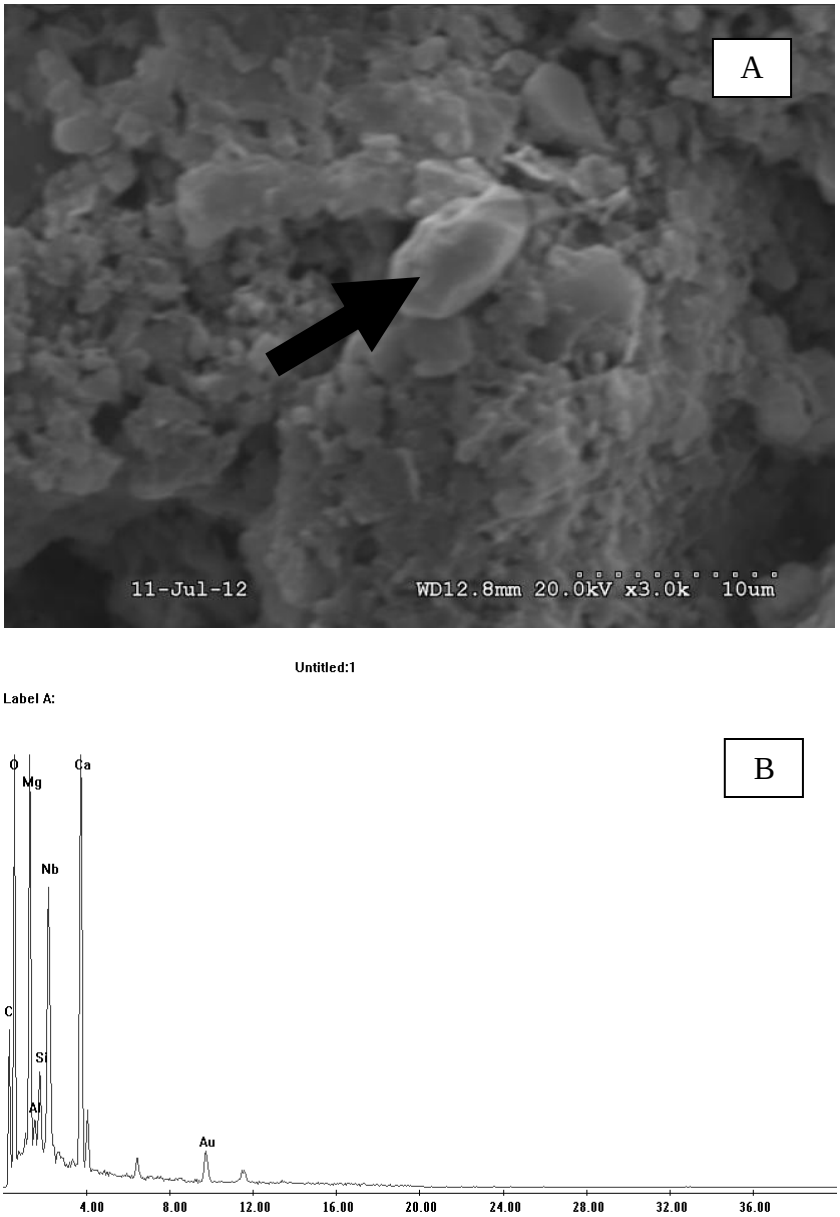

Figure 26: Dolomite grain in a 2 week 160°C experiment. A) SEM image of a dolomite grain found; designated by the arrow. B) EDS scan of the dolomite grain in the picture showing Ca, Mg, C, and O.

Figure 27: Calcite precipitation in one of the 5 week 120°C experiments. A) Calcite crystal. B) EDS scan of the newly formed mineral verifying it as calcite. This calcite may have been the result of degassing the reactor.

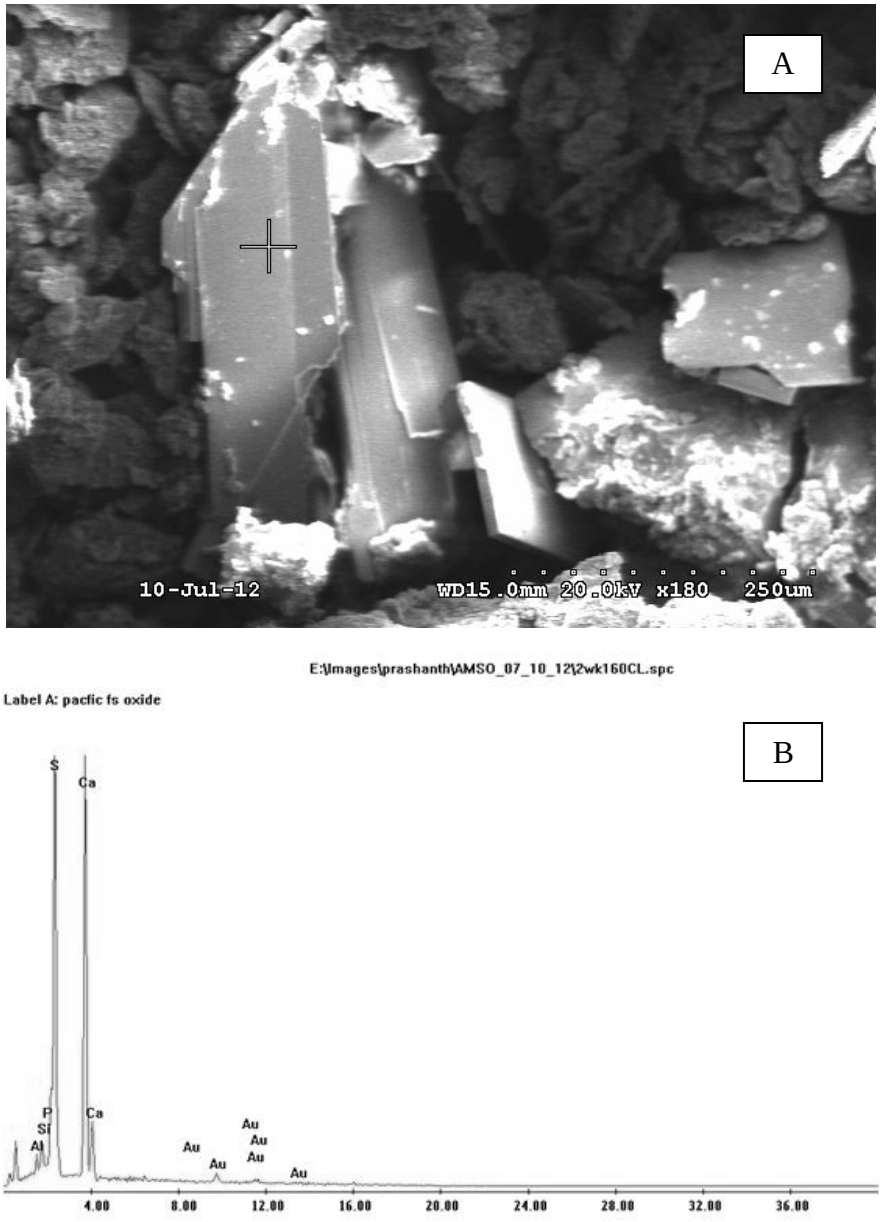

Figure 28: Anhydrite precipitation in a 2 week 160°C experiment with a well formed structure and size. A) SEM image of a commonly observed anhydrite crystal. B) EDS of the crystal verifying that it is anhydrite.

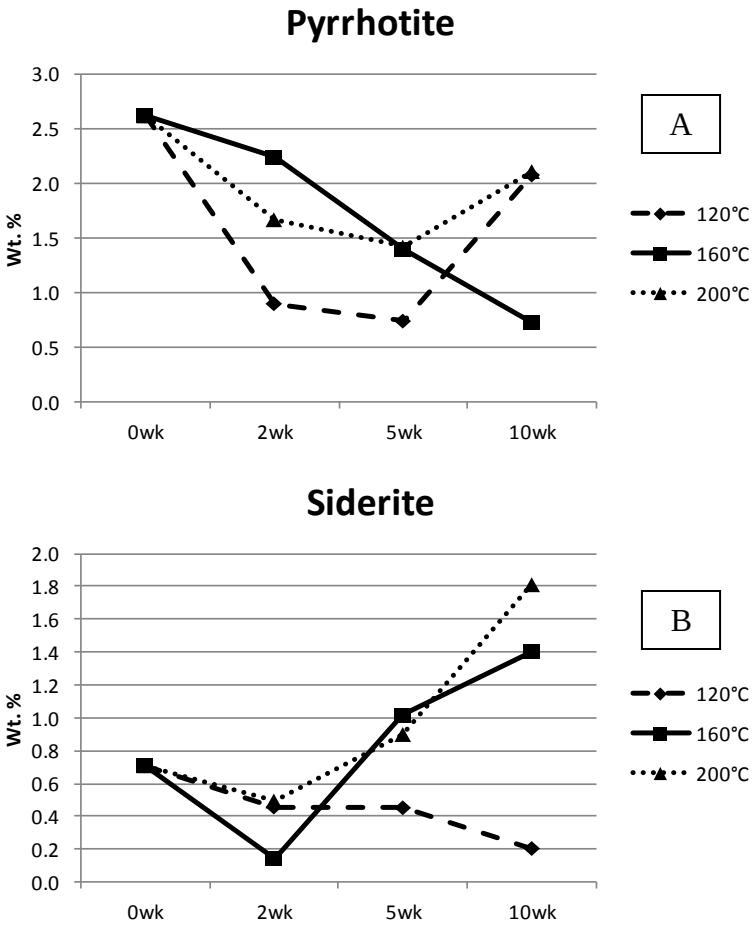

Figure 29: XRD analysis for pyrrhotite and siderite in the liquid phase experiments. A) As pyrrhotite dissolves, iron is released into the brine which precipitates out as B) siderite.

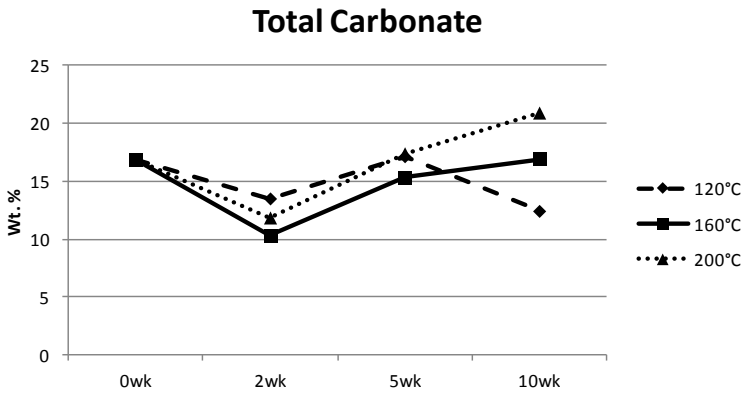

Figure 30: Total carbonate amounts for the liquid phase experiments. By 10 weeks, experiments at 200°C showed a net increase in the total amount of carbonate, experiments at 160°C showed little change, and experiments at 120°C showed a net decrease in carbonates.

CHAPTER 15

GAS PHASE EXPERIMENTS

Experiments were done with the rock exposed to gas phase CO_2, a configuration not as commonly seen in the literature as experiments having the rock in direct contact with the brine. The purpose of these experiments was to investigate the effects of CO_2 directly on the retorted oil shale. Most of what one would expect with exposing a rock to a corrosive gas is etching. Also observed were some reactions that can only take place in the presence of liquid water, which was attributed to water vapors condensing in cooler parts of the apparatus and percolating through the rock sample.

Gas Phase Experiments

Gas phase experiments were executed to determine the interactions between gaseous phase CO_2 and the retorted oil shale. As the injected CO_2 migrates from the point of injection, the initial brine in the pore space is displaced.[187, 199] Due to the CO_2 being less dense than the brine, it should migrate to the top of the repository creating a CO_2 rich region as opposed to brine rich region. The environmental differences between the gas region and the brine filled region are stark; mainly, there is little or no liquid water to facilitate aqueous geochemical reactions.

In actual injection scenarios, it is safe to assume that some of the preexisting brine that was not removed by thermal treatment would remain trapped in the pores of the rock. Within these pores geochemical reactions would inevitably occur, however, said

reactions would be limited to the minerals that the retained brine would remain in contact with.

Unconsidered during the design of the experimental apparatus was the possibility of water evaporating from the brine below the shale basket and subsequently condensing in the cooler top of the reactor, the freshly distilled water percolated through the shale basket providing the water necessary for aqueous geochemical reactions. The percolation of water was not necessarily a bad thing; in an *in situ* injection there is the likelihood of the top of the formation being cooler than the rest of the formation which could cause refluxing of water. The effects of percolation were noticeable in experiments at 160°C and were very noticeable in experiments at 120°C.

Most of the gas phase experiments had little or no recoverable brine after the experiments thus preventing ICP-MS analysis. All knowledge about reactions in the gas phase experiments had to be inferred using XRD and SEM.

In all of the gas phase experiments, the effects of the corrosiveness of CO_2 were noticed. Corrosion of the initial material was noticed on anhydrite, plagioclase feldspar, illite, smectite, and in some instances quartz. Figure 31 is an array of SEM images that serve as examples of some of the observed dissolution. Even with the dissolution observed with SEM, the XRD analysis showed inconclusive differentiation between the reacted samples and the original material with the aforementioned minerals. This leads to the conclusion that the extent of corrosion from the supercritical CO_2 in the gas phase experiments was minimal. Another observation with the SEM analysis was the presence of particles much smaller than the original material littered throughout all the samples.

EDS analysis of these particles found that many of them are either illite or

illite/smectite, suggesting that the CO_2 caused some disintegration of the clays with minimal dissolution. Zhou et al.[200] tested confined shale cores from the Pierre Shale, North Dakota, and found that if the shale was initially saturated with water and then exposed to CO_2, that significant disintegration occurred; they provided the possible explanation that as CO_2 reacted with water, the ionic balance is perturbed so greatly that the rock is weathered severely.

The amount of dolomite in the gas samples remained relatively unchanged in the 120°C experiments. With the 160°C experiments, dolomite decreased by 5 weeks and then increased by 10 weeks. The 200°C experiments showed a decrease in dolomite by 5 weeks which then stabilized by 10 weeks.

The amount of calcite increased slightly throughout the duration of the 200°C experiments. With the 160°C experiments, there is an insignificant increase in calcite by 2 weeks, a substantial decrease by 5 weeks, followed by a nearly equal increase by 10 weeks. The 120°C experiments showed an increase in calcite by 2 weeks. Following the initial increase in the 120°C experiments was a continuous decline in calcite throughout the remainder of the experiments. The decline may be the result of water saturated with carbonic acid percolating through the shale. By the same logic, it would be expected that the calcite would not increase by the 2 week mark. If the corrosion of the minerals by CO_2 is fast, it may be possible that the percolating water is capable of dissolving Ca^{2+} and precipitating calcite. As further percolation occurs, the acidity of the solution dissolves the newly formed calcite and deposits the cations in the aqueous phase below. Albeit without enough sample for ICP-MS, the aforementioned argument is entirely hypothetical but serves as justification into further experiments studying the interaction

of gas phase or supercritical phase CO_2 and rock with implications for CO_2 sequestration. One would also expect that if percolation of water is causing calcite dissolution in the 120°C experiments that it would also cause dissolution of dolomite over the same time span. Trends in dolomite and calcite can be found in Figure 32.

Although little evidence for net carbonation reaction was seen with calcite and dolomite, the trends observed with pyrrhotite and siderite suggests a possible mechanism for carbon storage. In the 120°C and the 160°C experiments, there is a net reduction of pyrrhotite over a 10 week duration with the change in the 200°C experiments being negligible. With the dissolution of pyrrhotite, iron and sulfur ions are available for other reactions, mainly the formation of siderite and anhydrite. The amount of siderite observed in the 120°C and the 160°C experiments decreased slightly by 2 weeks and increased steadily thereafter. The amount of siderite in the 200°C experiments decreased by 2 weeks and remained suppressed through the rest of the experiments (Figure 33).

Freshly precipitated siderite was difficult to locate using SEM-EDS; anhydrite, which is a product of a side reaction, was commonly observed. The presence of newly formed anhydrite serves as evidence that the conditions needed for aqueous geochemical reactions were present, likely the result of percolation in the reaction system. Figure 34 shows an example of precipitated anhydrite, this particular example is from a 2 week 160°C experiment.

Even though the formation of siderite showed promise for net CO_2 mineralization, the magnitude of siderite precipitation was less than that of dolomite, which in turn resulted in total carbonate values being more following the trend of dolomite (Figure 35).

Experiments that had enough remaining sample for further analysis were sent to

Huffman Labs in Golden, CO for carbon analysis. External carbon analysis for some of the gas phase experiments can be found in Table 18. There are definite consistencies in the trends seen in Table 18 and the trends in Figure 35.

Conclusions

Overall, the gas phase experiments showed only minor CO_2 mineralization, even though the precipitation of newly formed siderite was found in the XRD analysis. The disintegration patterns of the shale may have implication for the geomechanical stability of the system; however, more tests would have to be performed to assuage that possibility.

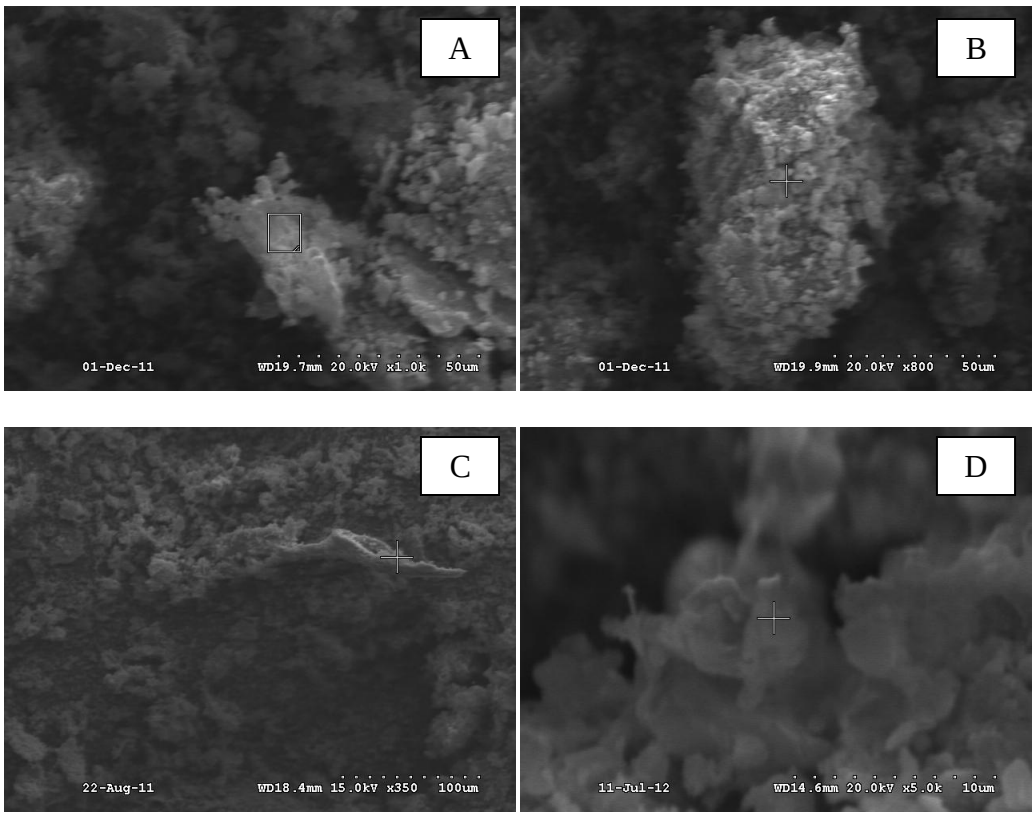

Figure 31: Examples of the observed dissolution patterns in the gas phase experiments. Ordered clockwise from the top left image: A) Dissolution on an anhydrite grain from a 2 week 160°C experiment. B) From the same specimen a grain showing plagioclase feldspar dissolution. C) Illite dissolution found in a 2 week 200°C experiment. D) Dissolution of interlayered illite/smectite found in a 10 week 120°C experiment.

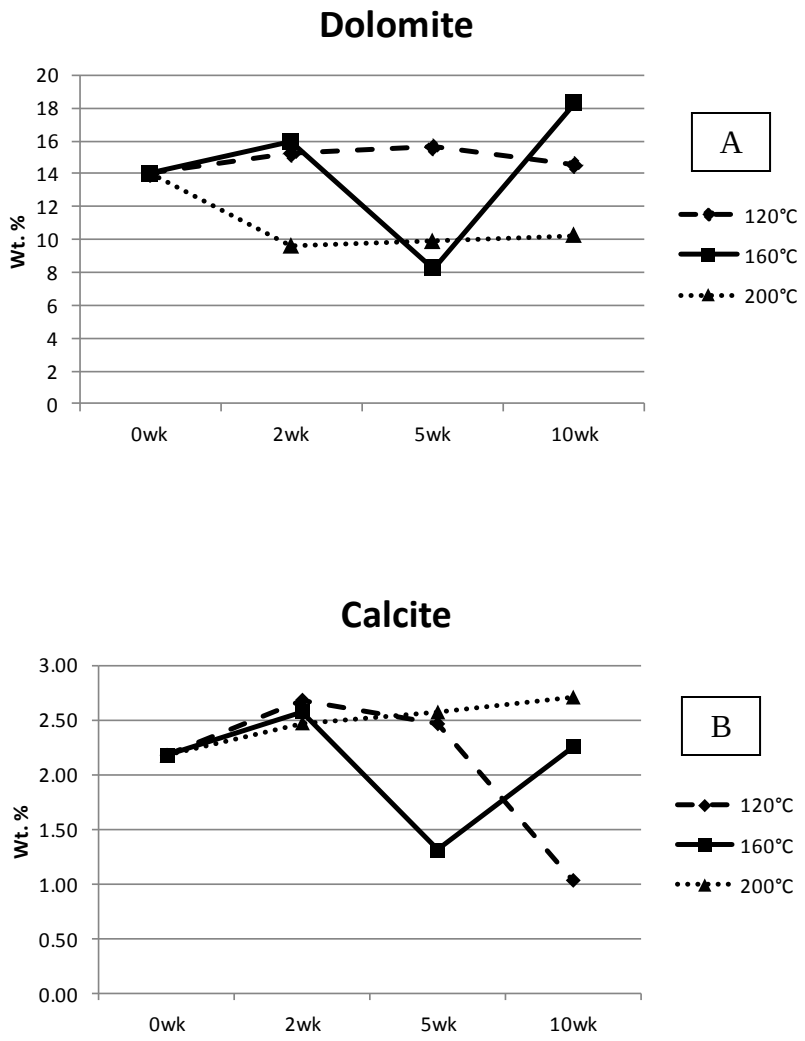

Figure 32: Dolomite and calcite trends as determined by XRD for the gas phase experiments. A) The 160°C experiments showed a slight increase in the amount of dolomite by 10 weeks. B) Calcite showing an increase then a decrease.

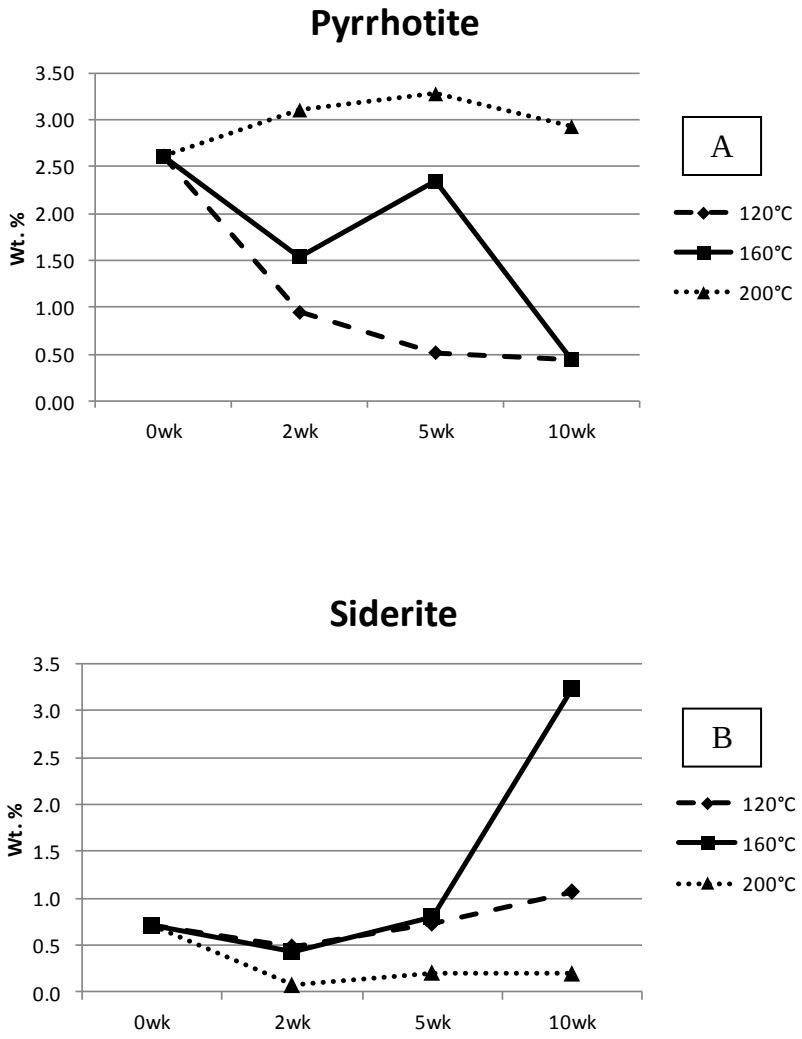

Figure 33: Pyrrhotite and siderite amounts in the gas phase experiments. A) Reduction of the pyrrhotite amounts. B) As pyrrhotite is dissolved in the 120°C and 160°C runs, siderite is precipitated. The 200°C experiments showed little change of pyrrhotite and a small decline of siderite.

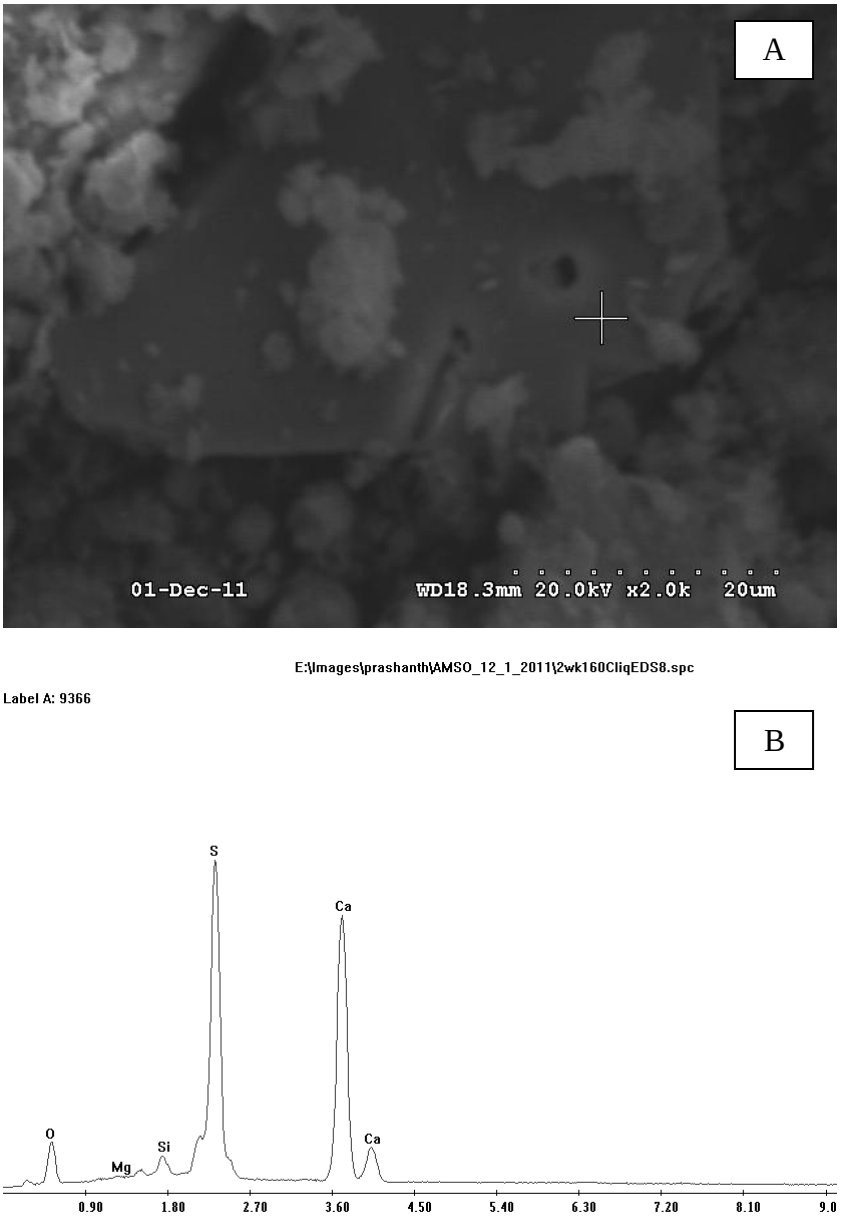

Figure 34: Anhydrite growth found in a 2 week 160°C gas phase experiment. A) Newly formed anhydrite is evidence that there is pyrrhotite dissolution as well as an aqueous phase present for geochemical reactions to occur. B) EDS scan verifying it as anhydrite.

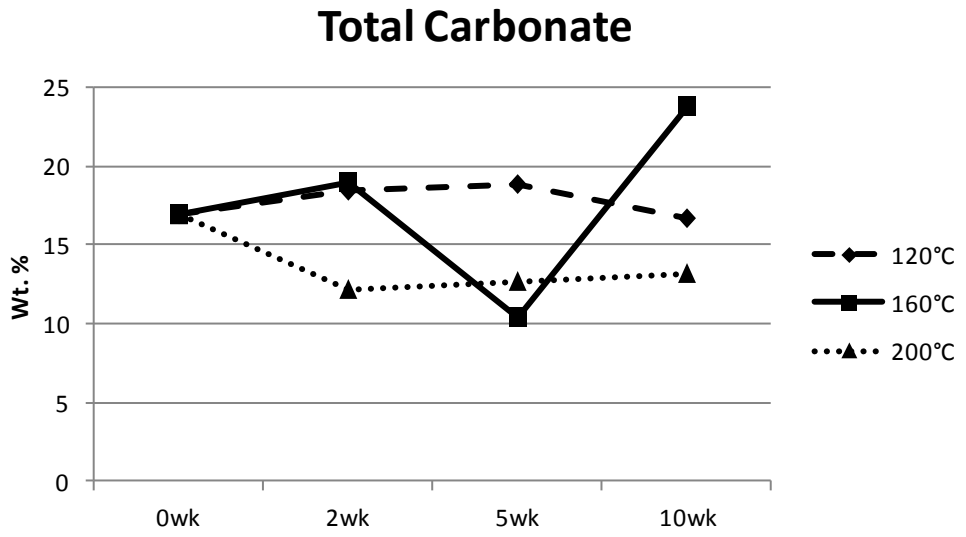

Figure 35: Sum of all carbonate minerals in the gas phase experiments. Since the change in dolomite was much larger in these experiments compared to other carbonates, the trend of total carbonate follows the dolomite trend.

Table 18: Total carbon, mineral carbon, and organic carbon for the gas phase experiments. Values reported as wt. % of bulk sample.

Time	*Temp*	*Phase*	*Run No.*	*Mineral C*
5 weeks	120°C	vapor	2	2.14
5 weeks	120°C	vapor	1	2.16
10 weeks	120°C	vapor	1	2.09
10 weeks	120°C	vapor	2	1.85
5 weeks	160°C	vapor	1	1.42
10 weeks	200°C	vapor	2	1.48
	Retorted R1 Shale		-	2.11

CHAPTER 16

STEP-DOWN EXPERIMENTS

A few experiments were performed where the temperature of the reaction vessel was reduced over the course of 4 weeks. There were two reasons for doing experiments with an unstable temperature. The first reason was that there is a likelihood that CO_2 would be injected into the pyrolyzed oil shale cooling down from the retort process. The second reason was to increase the dissolution of mineral phases at high temperatures and promote the precipitation of new minerals at the lower temperatures.

Temperature Step-Down Experiments

Two sets of aqueous phase temperature step-down experiments were performed to approximate what would happen if CO_2 were injected into a hot spent shale repository which then began to cool to prepyrolysis temperatures. The first experiment set started at 160°C and then cooled to 120°C over the course of 4 weeks; the second set started at 120°C and cooled to 80°C over the same time span. The optimal benefit for these experiments promoting carbonation reactions was that the initial high temperature would promote dissolution and therefore promote the release of cations into the brine and that the lower temperature would promote the precipitation of carbonate phases.

XRD analysis of the samples from both sets of temperature step-down experiments showed that there were minor increases in the analcime, quartz, albite, illite, and smectite phases. The amounts of calcite, siderite, pyrrhotite, buddingtonite,

orthoclase, and dolomite decreased in both sets while dolomite remained relatively unchanged.

XRD analysis for the step-down experiments also showed a decrease in the total amount of carbonate in the reacted samples. The average total carbonate in the original sample was measured as 16.89%, the average for the 160 to 120°C experiments was 16.14%, and the average for the 120 to 80°C experiments was 16.09%. The slight decrease in carbonate was also noticed in the external analysis by Huffman labs, as seen in Table 19.

EDS of the 160 to 120°C experiments identified well developed calcite growths (Figure 36) as well as the precipitation of halite and some zeolite. Throughout all of the temperature step-down experiments, the surfaces of precipitated minerals were littered with flakes of illite or illite/smectite.

Conclusions

Although the XRD analysis and the carbon analysis are in agreement that there was a slight reduction in the mineral carbonate amounts for the step-down experiments, the precipitation of well formed calcite as found in the SEM analysis shows that the conditions are met for mineralization reactions.

Table 19: Total carbon, mineral carbon, and organic carbon for the temperature step-down experiments. Reported as wt. % of total bulk material

Time	*Temp*	*Phase*	*Run No.*	*Total C*	*Mineral C*	*Organic C*
4 weeks	160 to 120°C	liquid	2	8.83	2.10	6.73
4 weeks	160 to 120°C	liquid	1	8.83	1.94	6.89
4weeks	120 to 80°C	liquid	1	8.84	1.95	6.89
Average Bart-2-02 unreacted			-	8.82	2.11	6.71

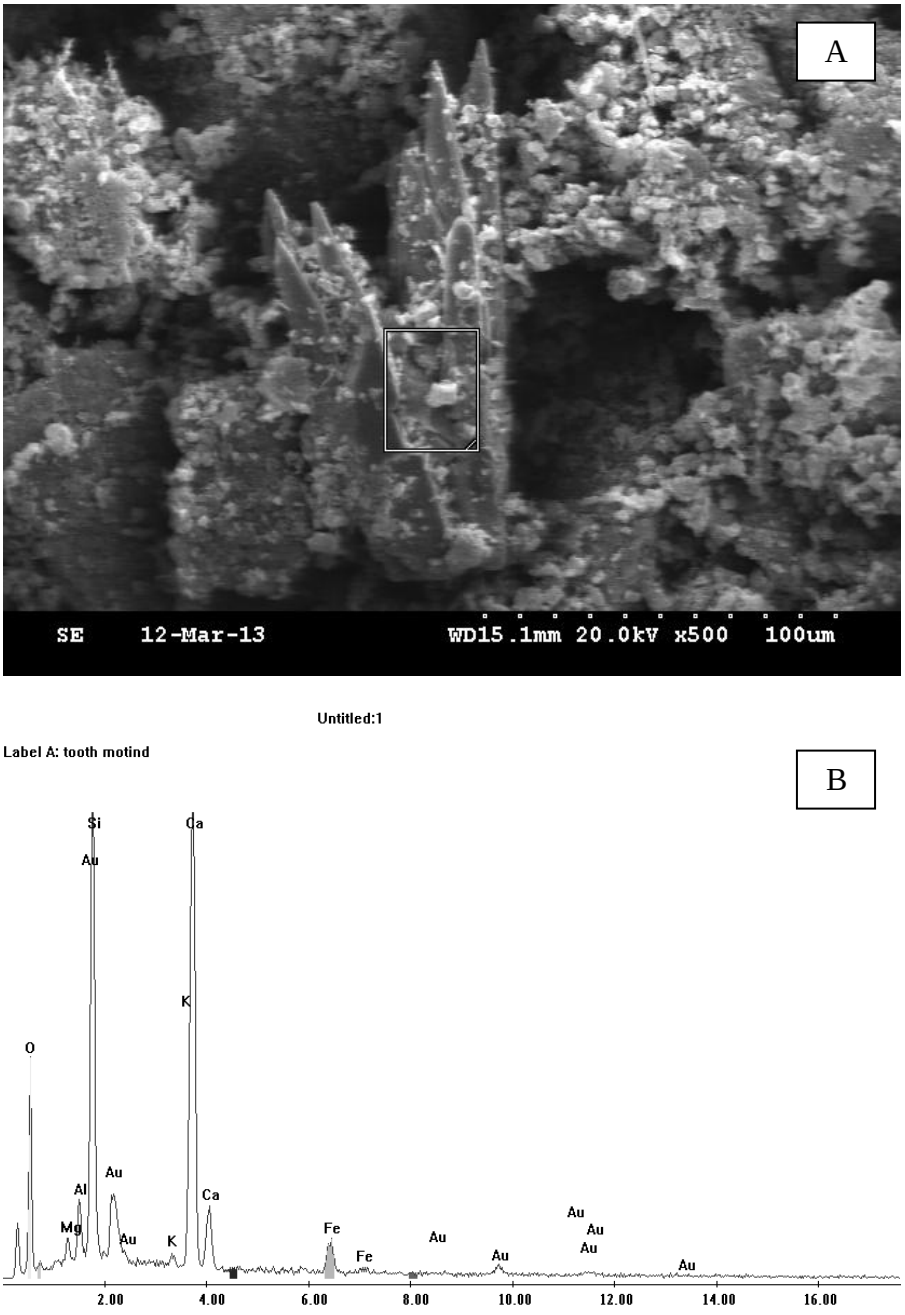

Figure 36: Calcite growth found in the 160 to 120°C temperature step down experiments. A) The small particles atop the calcite are illite. B) EDS scan verifying those particles as illite.

CHAPTER 17

SIMULATIONS

Computer simulations ended up being a useful tool in helping to validate some of the experimental observations. Computer simulations were also used in determine the relative effect of different carbon storage mechanisms. Simulations have their drawbacks however, such as one simulator package not being to model a certain property or not having particular kinetic data. With this in mind, some assumptions had to be made when doing these simulations. The purpose of this chapter is to discuss the results of the simulations and the assumptions used when performing them.

Equilibrium Studies

Using Geochemist's Workbench (GWB), equilibrium studies were performed on the experimental system in an effort to determine how close to equilibrium the experiments were. Using the simulation subpackage "React," the initial brine concentrations were used as well as the initial number of moles of dolomite, calcite, siderite, pyrrhotite, quartz, and gypsum (replacement for anhydrite). The results of the React simulations can be seen in Figure 37. Some of the other phases were not included as they were prone to causing the program to not reach convergence because of too many possible phases. For the clays, the ionic exchange was approximated. Equilibrium was calculated using the Debye-Hückel equations. The CO_2 fugacity and reacting minerals were added stepwise in the React simulations; the final result represents the whole system

in equilibrium.

Results of the reaction simulations were similar for the three different temperatures. The amount of CO_2 in the reactor was determined using the methodology outlined by Duan and Sun.[151] The predicted phases with the mineralogical input were dolomite, quartz, calcite, siderite, pyrrhotite, and kaolinite (except in the 200°C experiments where beidellite is predicted). These results are in disagreement with the experimental results on a few phases: mainly, the experimental results found that in almost every case, that there was dissolution of pyrrhotite. Agreement with the simulation was seen with the prediction of kaolinite and siderite.

Inverse Modeling

To better understand the thermodynamics of the reactor vessel, for liquid phase experiments, PHREEQC was used to perform inverse calculations on the mineralogical changes in the system. Inverse calculations were done on the center of the experimental matrix, being 5 weeks and 160°C. Inverse modeling involved in putting the initial brine concentrations and minerals then back calculating the mineral changes for the changes in the brine concentration. Over 2000 realizations were performed for the inverse modeling. Realizations were screened for improbable (thermodynamically unlikely) results, such as those predicting the mass dissolution of quartz. The results of the PHREEQC modeling found that the likely precipitates for this system should be albite, dolomite, K-feldspar, illite, gypsum, siderite, and kaolinite; dissolution was found for smectite, analcime, calcite, pyrite, and quartz.

PHREEQC was also used to calculate the pH in the reactors as a function of the fugacity of CO_2 and ionic concentrations in the brine. The results of the PHREEQC pH

calculations can be seen in Figure 38. The calculated pH for the experiments was highly dependent on the temperature and less dependent on the composition.

Mineral Phase Equilibrium

The Geochemist's Workbench package "Act2" can be used to determine the likely phases with respect to each species in the brine. The base case for iron Act2 studies was the 5 week 120°C liquid phase experiments. PHREEQC was used to determine the pH of the brine in equilibrium with CO_2, which was calculated to be 3.92 for these experiments.

"Act 2" simulations for the stability of iron show that when reactor is at temperatures above 120°C (Figure 39) that stable formation of iron carbonates cannot occur. However, if the temperature of the system is reduced to 60°C, iron bicarbonate can now be formed.

A similar trend to the iron was noticed with respect to Ca^{2+} when a temperature shift was applied. Using the brine concentrations from the 120°C experiments, a model was constructed similar to that of the previous exercise (Figure 40). The results of the model found that at the elevated temperatures of the reactor system calcium is most stable as anhydrite; anhydrite was found in almost every liquid phase experiment.

However, if the temperature is reduced to 60°C, Ca^{2+} is preferred. Figure 40 makes two important points about the fate of Ca^{2+}; that for this system the precipitation of anhydrite removes Ca^{2+} from the brine and that at reservoir-like temperatures the Ca^{2+} may not be available for carbonation reactions such as the precipitation of calcite or dolomite.

Iron and calcium were the only carbonate specific cations examined that had

shown such temperature dependence on speciation for these experimental conditions; having negative implications for producing newly formed siderite and calcite. Contrary to the GWB simulations, the existence of new siderite was found with XRD for the 120°C and 160°C experiments and the precipitation of calcite was seen in the 5 week 120°C experiments, although the calcite in the 5 week 120°C experiments may have resulted from the desiccation of the reactor during the degassing of the experiment. The calcite observed via SEM-EDS in the 160 to 120°C experiments may be evidence of the phenomena seen in Figure 40 occurring at other temperatures. Since *in situ* brine measurements are unavailable with our experimental apparatus, modeling such a shift with GWB would only be hypothetical. If one were able to perform the temperature step-down experiments with the ability to measure brine concentrations in a manner similar to Kaszuba et al.[138], some useful insight regarding injecting into a hot reservoir may be revealed.

Sensitivity Analysis

A sensitivity analysis was done on an imaginary model retorted oil shale reservoir in order to assess the influences of three of the four carbonate storage mechanisms: pore space storage, mineralization, and adsorption.

The heating of the oil shale will likely remove part of the connate water, without knowing how much water would remain; it was decided to not include water saturations in the computations. The sensitivity analysis used not only ranges for net carbonation from these experiments but also the effects of porosity change, initial porosity after pyrolysis, shale density, the amount of CO_2 adsorbed onto the shale, and the injection temperature (correlated to CO_2 density). Carbonate ranges were taken as the minimum

and maximum net carbonate from the experiments. Adsorption isotherms were conducted at Weatherford Labs in Golden, CO. Data provided by Weatherford Labs served to define the range of adsorption capacities and the range of porosity that would be used in the parameter sensitivity study.

The constants were a reservoir pressure of 1000 psi and the density of carbonate. The sensitivity calculations were done on a volumetric basis using a reference volume of 1 meter. The simulations took into account changes in porosity due to precipitation/dissolution. The ranges for the variables and the values of the constants can be found in Table 20.

Values for the variables were assigned using a random number generator and were subsequently entered into the governing mass balance equation in order to create a simple Probability Density Function (PDF). Over 1000 realizations of the PDF were done. Realization of all the variables created a Gaussian distribution. The most probable realization predicted a CO_2 storage capacity of 40 kg CO_2 per tonne of shale. The majority of realizations fell between 0 kg/tonne and 50 kg/tonne. The results of the realizations are represented graphically in Figure 41.

Some variables were set as constants to determine their overall influence on the CO_2 capacity of the system. The first example has the net carbonation being set to only positive values. Figure 42 shows the result of 1000 realizations for said constraint. From Figure 42, it can be seen that the range of the histogram tightens but that the probability bin with the highest number of occurrences remained at 45 kg CO_2/tonne.

For the PDF examining a scenario with no net carbonation, the histogram was shifted to the left. The most probabilistic bin for CO_2 capacity was 25 kg/tonne. The

occupied bins ranged from a minimum of 10 to a maximum of 40 kg/tonne CO_2. The narrow range of the bins is evidence of the influence that carbonate reactions have on the CO_2 sequestration capacity.

The straight volumetric capacity range of the reservoir was examined by setting the net CO_2 mineralization reactions to zero as well as the net adsorption. The result of the PDF found that without the adsorptive capacity of the pyrolyzed oil shale, the range of the CO_2 storage capacity shifted further left with the most probable bin being 15 kg/tonne. The range for the CO_2 sequestration capacity also narrowed to 10 to 25 kg/tonne.

Conclusions

Computer models were able to help understand the geochemistry in the system as well as show the relative effects of some of the CO_2 storage mechanisms. Mineral phases predicted with the GWB package "React" were dolomite, quartz, calcite, siderite, pyrrhotite, and kaolinite; which were for the most part similar to experimental observations.

Inverse modeling using PHREEQC predicted precipitation of albite, dolomite, K-feldspar, illite, gypsum, siderite, and kaolinite; dissolution was found for smectite, analcime, calcite, pyrite, and quartz. The results of the inverse modeling were more in line with the experimental observations than results from "React." This was likely due to two things; one, PHREEQC lets the user match mineralogical changes to brine observations, and two, there is a larger amount of kinetic data in PHREECQ thus allowing better modeling of different phase changes and intermediates. PHREEQC was also successfully used to determine the pH in the reactor.

Phase equilibria studies performed using the GWB package "Act2" were able to validate some of the results seen in experimentation and were able to show, at least theoretically, the benefit of performing temperature step-down experiments and thereby the benefit of injecting CO_2 into a formation still warm from the retort process.

The overall results of the PDF sensitivity analysis shows that there is a wide range for the potential for CO_2 capacity using the variables and constants outlined in Table 20. The wide range in simulation results is mainly attributed to the range of net carbonation results seen with the geochemical experiments. When all of the variables are realized, the most common simulation result predicted a capacity of 40 kg CO_2 per tonne of shale. If only net-positive carbonation is assumed, the range of outcomes is narrowed but the most likely outcomes remains about the same. Pure volumetric analysis (no carbonation and no adsorption) found that most common realization was 15 kg CO_2 per tonne shale, thus without the adsorptive potential and mineralization, the capacity of the retorted shale is greatly diminished.

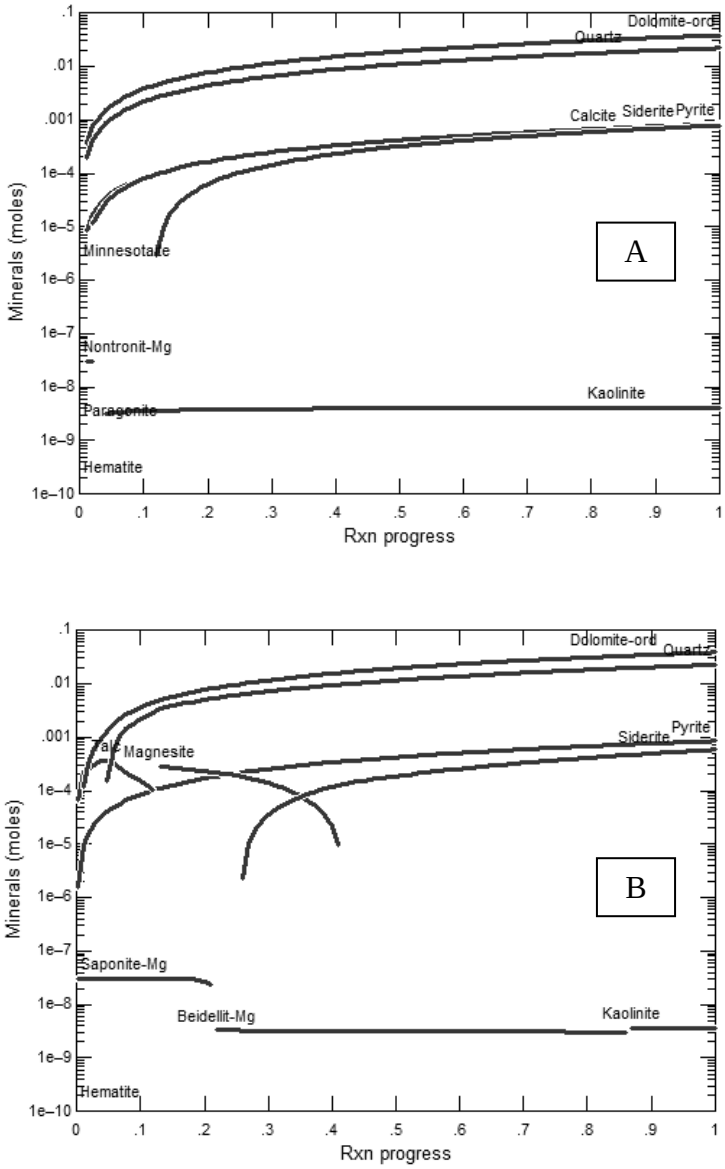

Figure 37: The results of the react simulation using the initial brine concentrations and the initial number of moles of rock at 120°C. A) The predicted dominant phases are dolomite, quartz, siderite, calcite, pyrrhotite, and kaolinite. B) The same simulation for equilibration at 160°C with similar results to the 120°C experiments. Same initial concentrations for the 200°C experiments, with the main difference being the presence of beidellite rather than kaolinite.

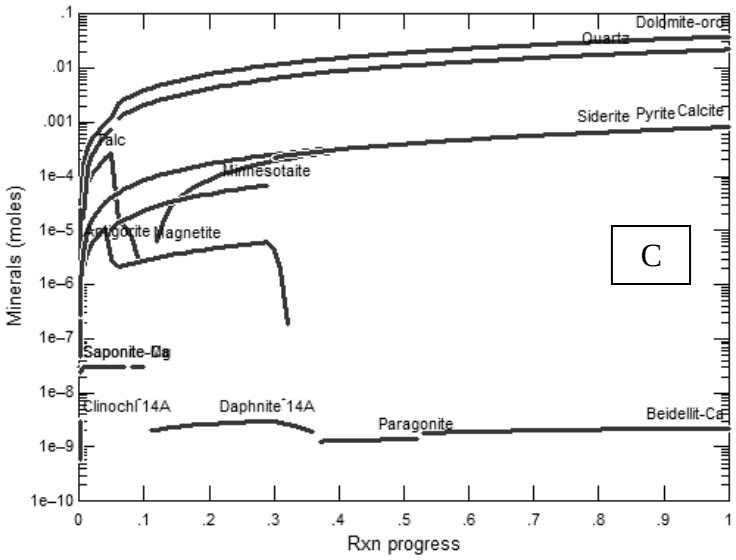

Figure 37 continued

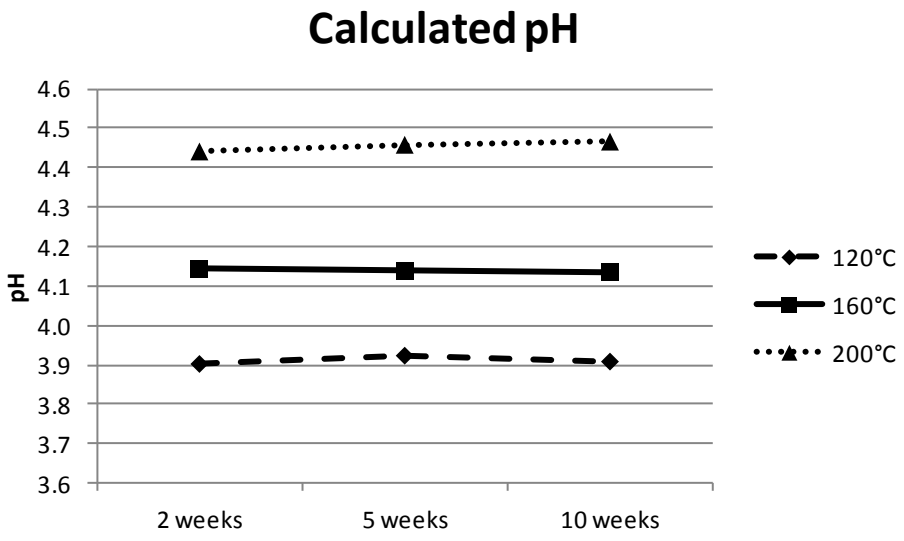

Figure 38: pH for the liquid phase experiments calculated using PHREEQC.

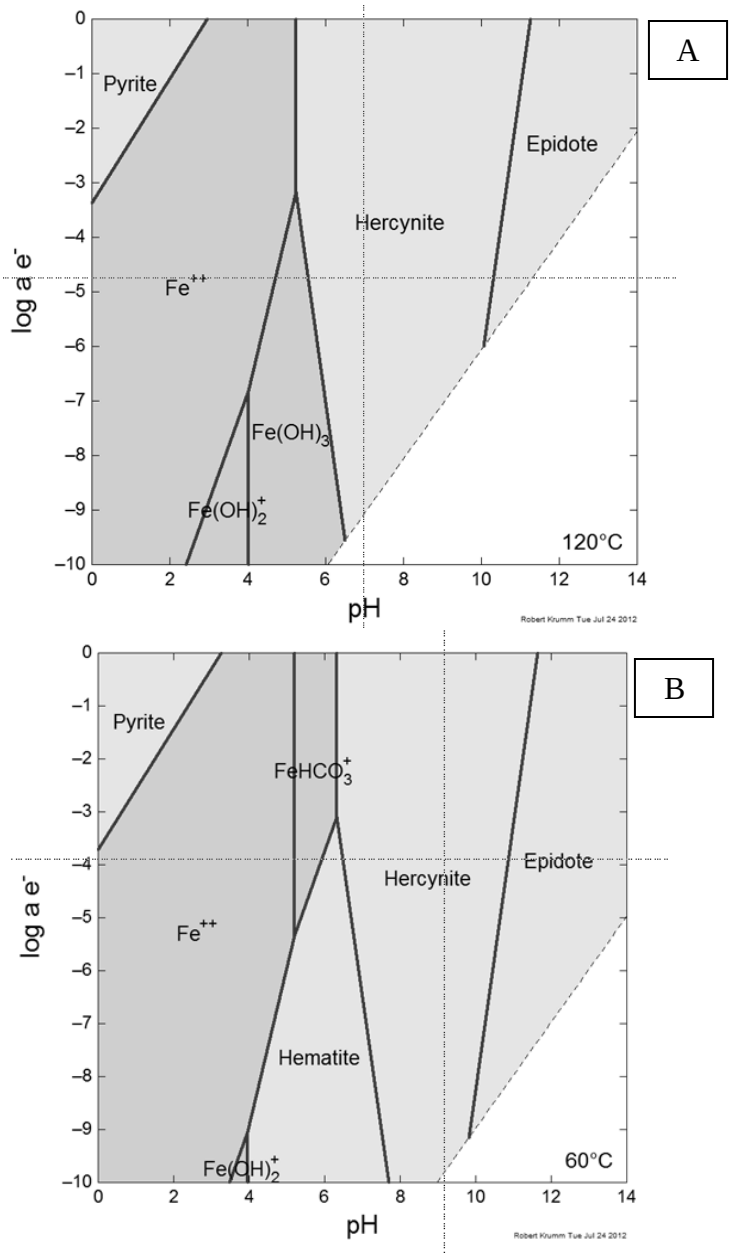

Figure 39: Act2 simulations with brine from the 120°C liquid phase experiments. A) Showing that Fe^{2+} is the dominant form of iron in the system. When the temperature for the simulation on the left is reduced to 60°C (B), iron bicarbonate becomes stable. PHREEQC calculations put the pH at about 3.92 and in a reductive environment.

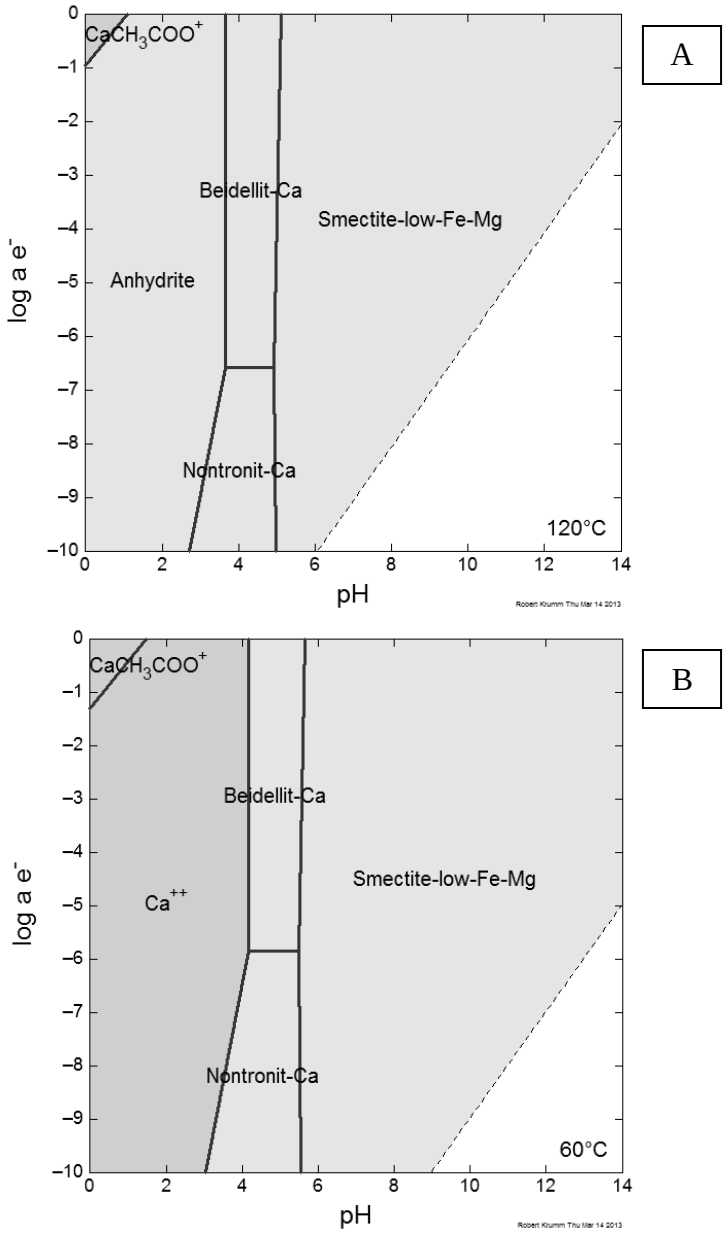

Figure 40: Act2 simulations with brine modeled from the ICP-MS results for the 5 week 120°C experiments. A) Stable calcium phases at 120°C. The simulation shows that anhydrite is a definite possibility, which explains why it was commonly found in the liquid phase experiments. B) The same brine concentrations at 60°C, Ca^{2+} is available for other reactions.

Table 20: Variables and constants used in the sensitivity analysis

Vairable	*Minimum*	*Maximum*
Carbonate [kg/tonne]	-42	37.8
ρ_{shale} [tonne/m^3]	2.4	2.8
Adsorption [wt. %]	0	2.3
ρ_{CO2} (1000psi, 50°C to 150°C) [kg/m^3]	168.13	95.78
$\Phi_{initial\ after\ treatment}$ [%]	20	30

Constant	*Value*
Pressure [psi]	1000
$\rho_{carbonate}$ [tonne/m^3]	2.8

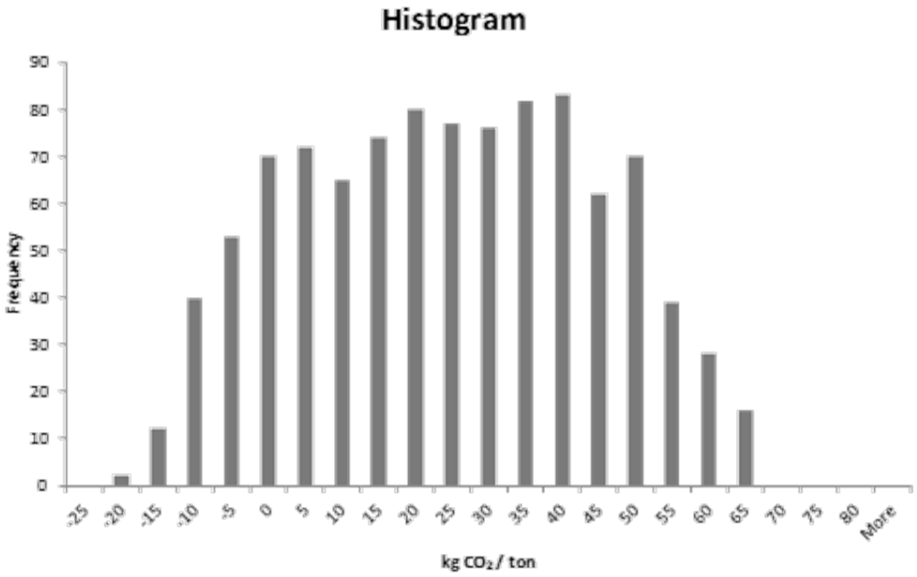

Figure 41: Histogram of the Probability Density Function (PDF) for the 1000 realizations of the total of the volumetric, mineral, and adsorptive capacity of the retorted oil shale.

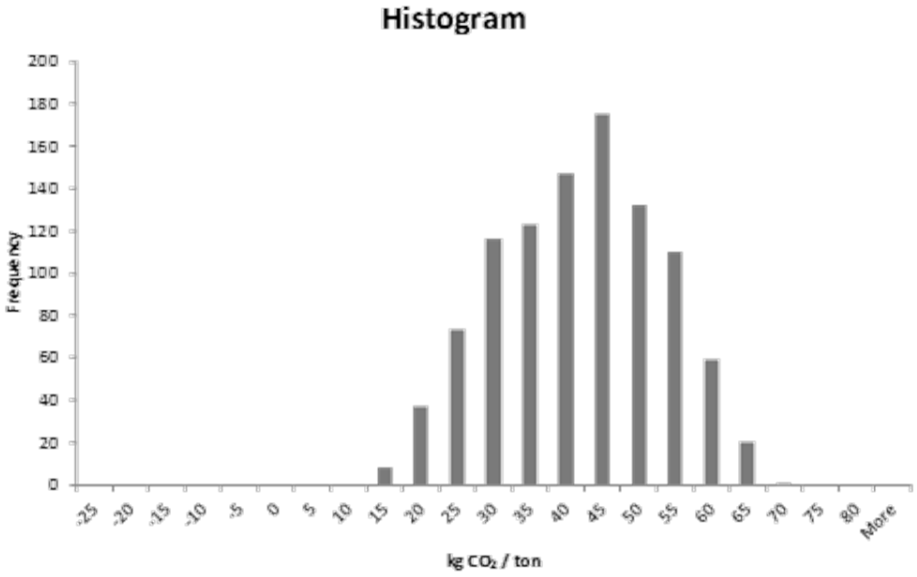

Figure 42: PDF of the volumetric CO_2 capacity calculations for the pyrolyzed oil shale with the net carbonate reactions were all positive.

CHAPTER 18

CONCLUSIONS

Pyrolyzed oil shale provides a unique CO_2 storage repository in that it demonstrates all of the CO_2 sequestration storage modes: dissolution in the connate water, adsorption onto the shale, geochemical reactions forming carbonates, and volumetric storage in the pore space.

Liquid phase and gas phase experiments were done on pyrolyzed oil shale at 1000 psi and at temperatures of either 120, 160, or 200°C for durations of 2, 5, or 10 weeks in an effort to determine the CO_2-brine-shale interactions. Liquid phase experiments all showed an initial reduction in the total carbonate by 2 weeks, with the experiments at 160 and 200°C showing total carbonate amounts near the initial values by 10 weeks. The initial decline in the carbonate amount is most likely due to the introduction of CO_2 into the system which forms carbonic acid and dissolves the carbonate. As time progressed, the solution became more saturated with cations and new carbonate phases could precipitate.

Of particular significance found in the results of the liquid phase experiments were the precipitation of pyrrhotite and the precipitation of siderite. It is hypothesized that the dissolution of pyrrhotite provided the necessary iron to facilitate the precipitation of siderite. The 160 and 200°C experiments both saw an increase in siderite, as determined by XRD. With the dissolution of pyrrhotite, sulfate ions were released into

the brine which then precipitated as anhydrite.

Gas phase experiments showed etching and disintegration of the clays in all instances, which may have geomechanical implications. The low temperature gas phase experiments may have had some percolation, wherein water vapors condense and collect in the cooler parts of the apparatus and drip through the basket containing the shale sample. This percolated water provided the medium for some geochemical reactions to occur. Similar to the liquid phase experiments, the precipitation of siderite was noticed in the XRD analysis, differences in the quantity of dolomite were large enough to negate any appreciable change in the other carbonates. Overall, there was little change in the amount of carbonate in the 120 and 200°C gas phase experiments. The 160°C gas phase experiments showed a slight decrease in carbonate by 5 weeks and then an increase by 10 weeks, largely due to the dissolution/precipitation of dolomite.

Temperature step-down experiments were done in order to better approximate what would happen geochemically if CO_2 were injected into a formation that was still hot from the retorting process. The hypothesis justifying these experiments was that the initial high temperatures would favor the kinetics for dissolution and the lower temperatures would cause a shift in the solubility constants for carbonates and promote precipitation.

Overall, the temperature step-down experiments found a slight reduction in mineral carbonate. Calcite was observed, however, as one of the products. The lack of new carbonate growth may have resulted from the decreasing temperatures having lower pH in the brine due to more CO_2 dissolution. Modeling the brine for the liquid phase experiments using PHREEQC revealed the pH trend, which would stand to reason would

also hold true for the temperature step-down experiments.

Inverse modeling in PHREEQC was used to determine if there would be a positive or negative change on each mineral in the reactor. Over 2000 PHREEQC inverse modeling realizations were analyzed and it was found that the likely precipitates for this system should be albite, dolomite, K-feldspar, illite, gypsum, siderite, and kaolinite; dissolution was predicted for smectite, analcime, calcite, pyrite, and quartz.

Geochemist's Workbench was used to simulate the equilibrium products that would be expected for the liquid phase experiments. The GWB simulations found that the predicted phases were dolomite, quartz, calcite, siderite, pyrrhotite, and kaolinite. The GWB results had some disagreements with the experimental results, mainly the precipitation of pyrrhotite.

Species specific modelling for Mg^{2+} and Fe^{2+} using Act2 in GWB found that at the elevated temperatures used in the experiments the carbonate forms of these cations were not favorable. If the temperature was reduced to a value more representative of *in situ* temperature and the brine/mineral amounts were maintained, the precipitation of carbonates then became feasible. It was also found that under experimental conditions the Ca^{2+} is consumed in the precipitation of anhydrite thereby making it unavailable for the precipitation of calcite or dolomite.

Probability density modeling was done in order to estimate the CO_2 storage capacity of the reservoir taking into account not only mineral carbonation but also changes in adsorption, porosity, shale density, and reservoir temperature. When all variables were realized, a wide range of CO_2 storage capacities were predicted; this was attributed to the wide range of net carbonation results seen in the experiments. When all

of the variables are realized, the most common simulation result predicted a capacity of 40 kg CO_2 per tonne of shale. If only net-positive carbonation is assumed, the range of outcomes is narrowed but the most likely outcomes remains about the same.

APPENDIX A

ANNOTATED GEM SIMULATION CODE

The purpose of this appendix is to provide the computer code used for the injection simulations used in this study. The code has been annotated to help readers understand what each input means with the hope that this code could be used by others to perform their own CO_2 injection simulations regarding coals thermally treated *in situ* with slow heating rates. The simulation code written was built on the GEM example GMSMO04.DAT.

GEM Injection Code

```
** Note the using the "**" is used to block out that line
**----------------------------------------------------------------------  **
** UCTT CO2 Injection Sample File                                         **
**----------------------------------------------------------------------  **
**----------------------------------------------------------------------  **
**                                                                       **
** FILE:  UCTTCO2.DAT                                                    **
**                                                                       **
**----------------------------------------------------------------------  **

**The next four lines of code define filenames and outputs

*RESULTS *SIMULATOR *GEM
*FILENAMES *OUTPUT *SRFOUT *RESTARTOUT *INDEX-OUT
*MAINRESULTSOUT
*TITLE1 'ECBM Problem'
**Defines input and output in SI units

*INUNIT *SI
```

```
**The next lines define what is written to the simulation results file.
**Dot not change unless necessary

*WSRF *GRID 1
*WSRF *WELL 1
*WPRN *GRID *TIME
*WPRN *WELL 1
*WRST  0
*OUTSRF *RES  *ALL

*OUTSRF *GRID *PRES *SW *SG *Y 'C1' *Y 'CO2' *DENW *DENG *VISG
        *ADS 'C1' *ADS 'CO2'
*OUTPRN *RES  *ALL
*OUTPRN *GRID *IMPL *PRES *SW *SG *Y 'C1' *Y 'CO2' *DENW *DENG *VISG
        *ADS 'C1' *ADS 'CO2'
*OUTPRN *WELL *ALL

**------------------------------------------------RESERVOIR DATA------
**define Cartesian grid domain, x=10, y=10, z=1 (blocks, not meters)
*GRID *CART 10 10 1
**the direction for the depth
*KDIR *DOWN

**defines that we are using a dual porosity model
*DUALPOR

**defines the block length=10m, width=10m, depth=9m
*DI *CON 10.0
*DJ *CON 10.0
*DK *CON  9.0
**defines the depth of the formation, 1000m
*PAYDEPTH *CON 1000.0

**defines fracture spacing
*DIFRAC *CON  2.0
*DJFRAC *CON  2.0
*DKFRAC *CON  2.0

**defines matrix and fracture porosity
*POR *FRACTURE *CON   0.001
*POR *MATRIX   *CON   0.005

**defines fracture permeability in each direction
**default values were used
*PERMI *FRACTURE *CON 4.0
```

```
*PERMJ *FRACTURE *CON 4.0
*PERMK *FRACTURE *CON 4.0

**defines matrix permeability in each direction
**values obtained from this study were used here
*PERMI *MATRIX   *CON 0.0001
*PERMJ *MATRIX   *CON 0.0001
*PERMK *MATRIX   *CON 0.0001

**defines matrix and fracture compressibility
**default values were used
*CPOR  *MATRIX   1.45E-7
*CPOR  *FRACTURE 1.45E-7
*PRPOR *MATRIX   7650.0
*PRPOR *FRACTURE 7650.0

**Fluid component data was computer using WINPROP
**default values were used
**-------------------------------------------------FLUID COMPONENT DATA
**Insert file written by WINPROP based on library components

** PVT UNITS CONSISTENT WITH *INUNIT *SI

*MODEL   *PR
*NC    2    2
*TRES         45.000
*PVC3  1.2000000E+00
*COMPNAME
'C1' 'CO2'
*SG        3.0000000E-01  8.1800000E-01
*TB       -1.6145000E+02 -7.8450000E+01
*PCRIT     4.5400000E+01  7.2800000E+01
*VCRIT     9.9000000E-02  9.4000000E-02
*TCRIT     1.9060000E+02  3.0420000E+02
*AC        8.0000000E-03  2.2500000E-01
*MW        1.6043000E+01  4.4010000E+01
*HCFLAG    0  0
*BIN
    1.0300000E-01
*VSHIFT
    0.0000000E+00  0.0000000E+00
*VISCOR *HZYT
*MIXVC     1.0000000E+00
*VISVC
    9.9000000E-02  9.4000000E-02
*VISCOEFF
```

```
    1.0230000E-01  2.3364000E-02  5.8533000E-02 -4.0758000E-02  9.3324000E-03
*OMEGA
    4.5723553E-01  4.5723553E-01
*OMEGB
    7.7796074E-02  7.7796074E-02
*PCHOR
    7.7000000E+01  7.8000000E+01
*ENTHCOEF
   -5.5811400E+00  5.6483400E-01 -2.8297300E-04  4.1739900E-07 -1.5255760E-10
    1.9588570E-14
    4.7780500E+00  1.1443300E-01  1.0113200E-04 -2.6494000E-08  3.4706000E-12
   -1.3140000E-16

**reference pressure for water density
*REFPW 101.325
**density of water
*DENW 990.0
**water compressibility
*CW 5.8E-07
**water viscosity
*VISW 0.607

**This section has the relative permeabilities of different fluids
**since this study did not examine these
**default values were used
**----------------------------------------------------ROCK FLUID----------
*ROCKFLUID
*RPT 1

**oil water relative permeability
*SWT
**   Sw        Krw       Krow
  0.00000    0.0000    0.00001
  0.05000    0.0006    *int
  0.10000    0.0013    *int
  0.15000    0.0020    *int
  0.20000    0.0070    *int
  0.25000    0.0150    *int
  0.30000    0.0240    *int
  0.35000    0.0350    *int
  0.40000    0.0490    *int
  0.45000    0.0670    *int
  0.50000    0.0880    *int
  0.55000    0.1160    *int
  0.60000    0.1540    *int
  0.65000    0.2000    *int
```

```
  0.70000    0.2510    *int
  0.75000    0.3120    *int
  0.80000    0.3920    *int
  0.85000    0.4900    *int
  0.90000    0.6010    *int
  0.95000    0.7310    *int
  0.97500    0.8140    *int
  1.00000    1.0000    0.0000

**liquid gas relative permeability
*SLT
**   Sl       Krg       Krog
  0.00000    1.0000    0.0000
  0.05000    0.8350    *int
  0.10000    0.7200    *int
  0.15000    0.6270    *int
  0.20000    0.5370    *int
  0.25000    0.4660    *int
  0.30000    0.4010    *int
  0.35000    0.3420    *int
  0.40000    0.2950    *int
  0.45000    0.2530    *int
  0.50000    0.2160    *int
  0.55000    0.1800    *int
  0.60000    0.1470    *int
  0.65000    0.1180    *int
  0.70000    0.0900    *int
  0.75000    0.0700    *int
  0.80000    0.0510    *int
  0.85000    0.0330    *int
  0.90000    0.0180    *int
  0.95000    0.0070    *int
  0.97500    0.0035    *int
  1.00000    0.0000    0.00001

*RPT 2
*SGT
  0.01 0.0   1.0    0.0
  1.00 1.0   0.0    0.0
*SWT
 0.00  0.0    1.0   0.0
 1.00  1.0    0.0   0.0

**defines two different rock types, matrix and fracture
*RTYPE *MATRIX   *CON 1
*RTYPE *FRACTURE *CON 2
```

```
**density of the coal
*ROCKDEN *MATRIX   *CON 1435.0
*ROCKDEN *FRACTURE *CON 1435.0

**Langmuir adsorption coefficients
**experimental data was used here
*ADGMAXC 'C1'  *MATRIX   *CON 0.5000    ** gmol/kg of rock
*ADGMAXC 'CO2' *MATRIX   *CON 1.0000    ** gmol/kg of rock
*ADGCSTC 'C1'  *MATRIX   *CON 2.000E-04 ** 1/kPa
*ADGCSTC 'CO2' *MATRIX   *CON 5.000E-04 ** 1/kPa

**no adsorption in cleats
*ADGMAXC 'C1'  *FRACTURE *CON 0.0
*ADGMAXC 'CO2' *FRACTURE *CON 0.0
*ADGCSTC 'C1'  *FRACTURE *CON 0.0
*ADGCSTC 'CO2' *FRACTURE *CON 0.0

**diffusion coefficients for the gasses
**default values were used
*COAL-DIF-TIME 'CO2' *MATRIX *CON 100.0
*COAL-DIF-TIME 'C1'  *MATRIX *CON 100.0

**------------------------------------------------INITIAL CONDITION---

**defines region, depth, and fluid composition in the coal
*INITIAL
*VERTICAL *COMP
*NREGIONS 2
*REFPRES  7650.0  5000.0
*REFDEPTH 1000.0  1000.0
*ZDEPTH 1 1000.0 1.0 0.0
       2 1000.0 1.0 0.0
*DWOC 100 100
*SWOC 0.9999 0.592
*CDEPTH 9999. 9999.
*ITYPE *FRACTURE *CON 1
*ITYPE *MATRIX   *CON 2
*SEPARATOR 101.325 15.0

**------------------------------------------------NUMERICAL-----------
**do not change
*NUMERICAL

**------------------------------------------------WELL DATA-----------
```

```
**start run and define arbitrary start date, default was used
*RUN
*DATE 2000 1 1
**implicit permanent formulations,
**do not change
*AIMSET *FRACTURE *CON 3
*AIMSET *MATRIX   *CON 3
*DTWELL 1.0E-6
*DTMIN  0.1E-06

**defines the well operating conditions
**defines a production well
      *WELL 1 'PRODUCER'
**well name
      *PRODUCER 1
**operation condition
**maximum surface water rate
      *OPERATE *MAX *STW  2.0
**minimum bore hole pressure
      *OPERATE *MIN *BHP 100.
**defines the well geometry
**diameter, skin factor, etc
      *GEOMETRY *K
         0.0365  0.249   1.000    0.0
**defines perforation zones and Cartesian location
      *PERF *GEO 1
         1 1 1 1.0

*after 25 days, the well changes operating conditions
*TIME 25.0
      *PRODUCER 1
**higher surface rates and higher bore hole pressures
      *OPERATE *MAX *STG 25000.0
      *OPERATE *MIN *BHP 275.

**time steps for writing data to results file
*TIME 30.0
*TIME 45.0
*TIME 60.0

**define a second injector well
      *WELL 2 'INJECTOR'
**well name
      *INJECTOR 2
**what the well is injecting and its composition
      *INCOMP *SOLVENT  0.0 1.0
```

```
**operating parameters
      *OPERATE *MAX *STG 6000.0
      *OPERATE *MAX *BHP 15000.0
**well geometry and location
      *GEOMETRY *K
         0.0365  0.249   1.000    0.0
      *PERF *GEO 2
         10 10 1 1.0

**time steps for recording data
*TIME 75.0
*TIME 90.0
*TIME 105.0
*TIME 120.0
*TIME 150.0
*TIME 182.5
*TIME 365.0

**end simulation
*STOP
```

APPENDIX B

CARLINVILLE ISOTHERMS

The purpose of this appendix is to provide the adsorption isotherm plots of the untreated and thermally treated Carlinville coals. This section also contains the Langmuir fitting parameters for aforementioned coal. The Langmuir fitting parameters can be found in Table 21, isotherms can be found in Figures 43 and 44.

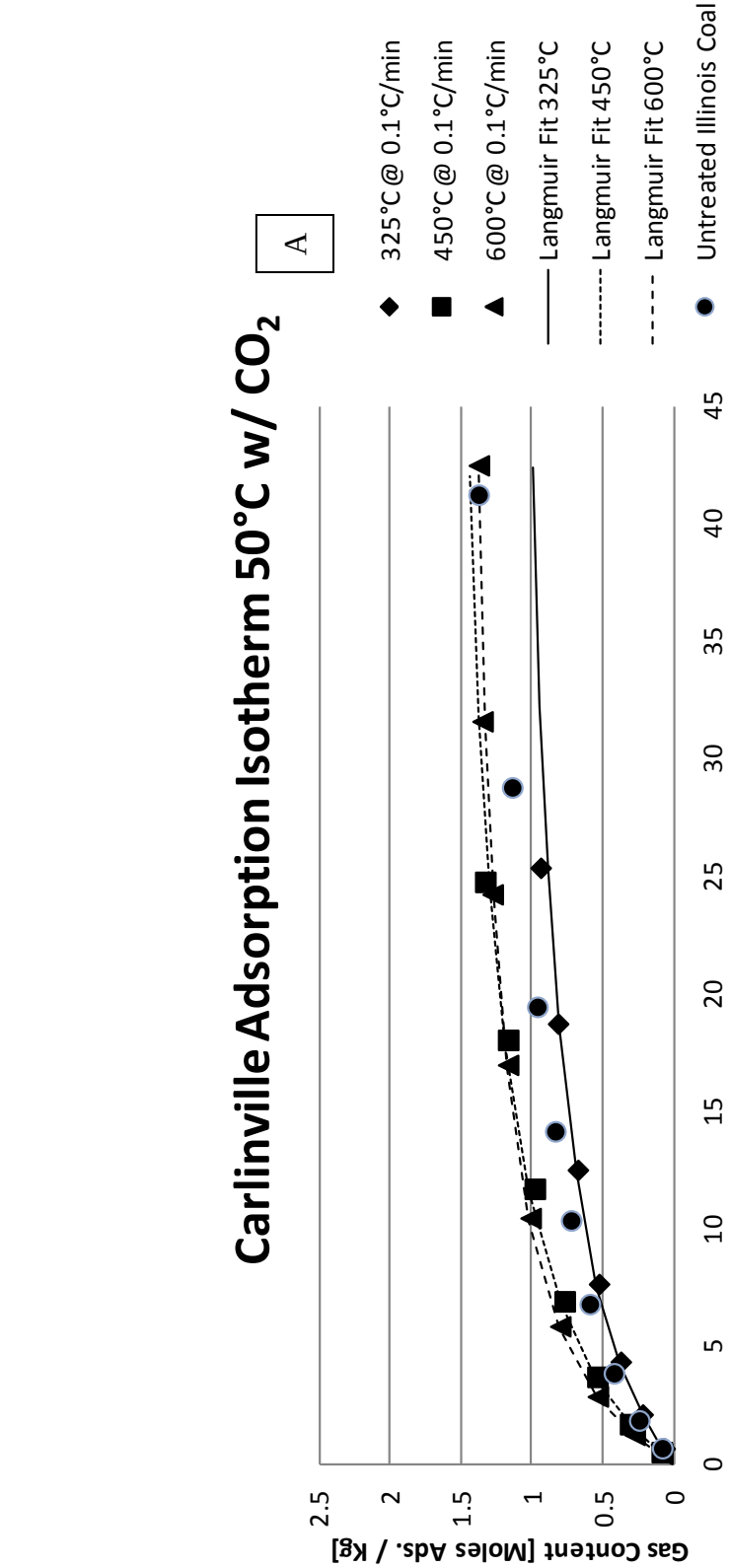

Figure 43: Adsorption isotherms for thermally treated Carlinville coal thermally treated at 0.1 °C/minute. A) CO_2 isotherms measured at 50 °C. B) CH_4 isotherms measured at 50 °C. C) CO_2 isotherms measured at 70 °C. D) CH_4 isotherms measured at 70 °C on coals.

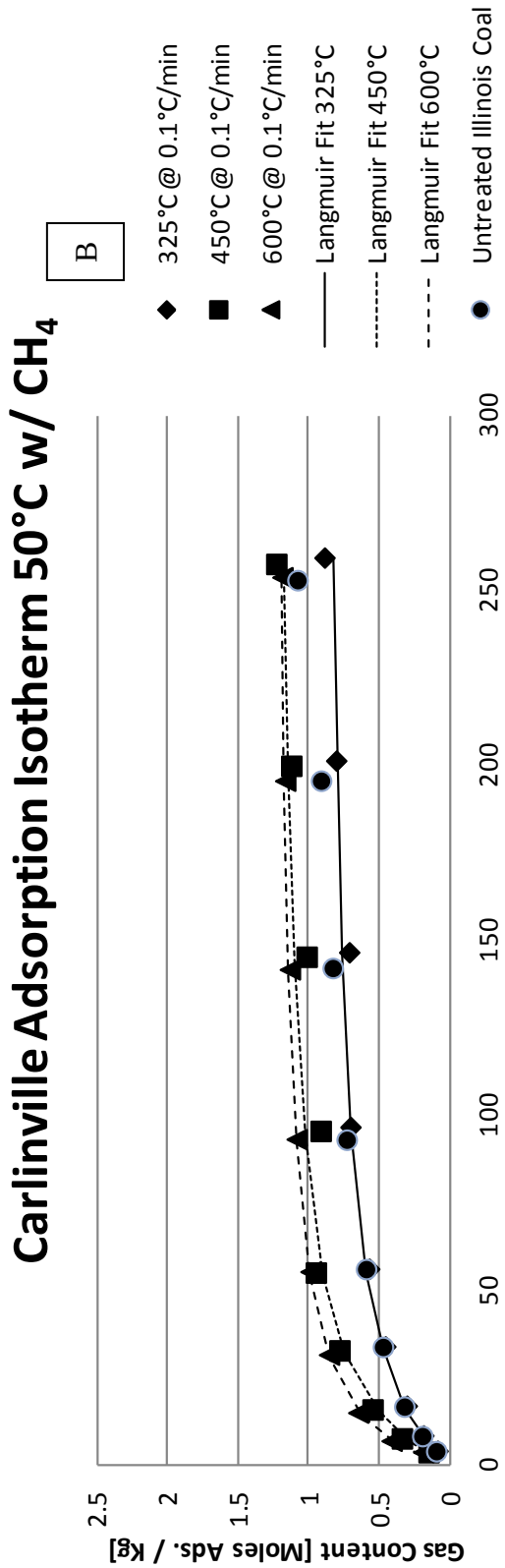

Figure 43 continued

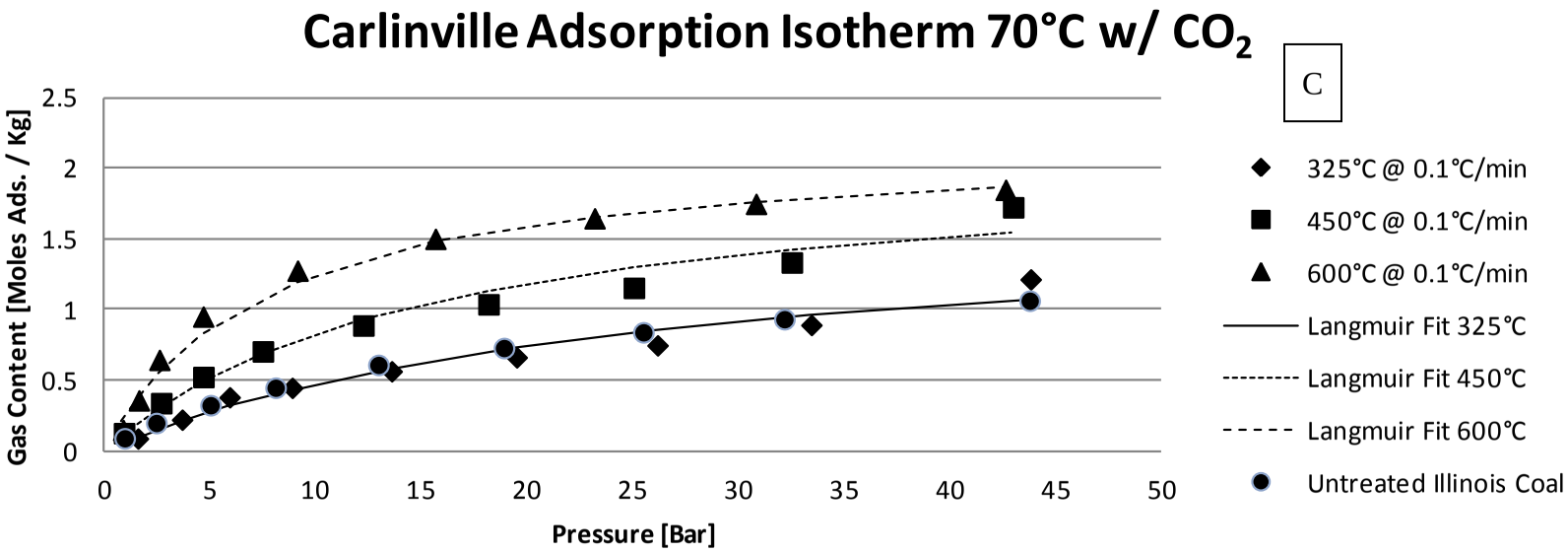

Figure 43 continued

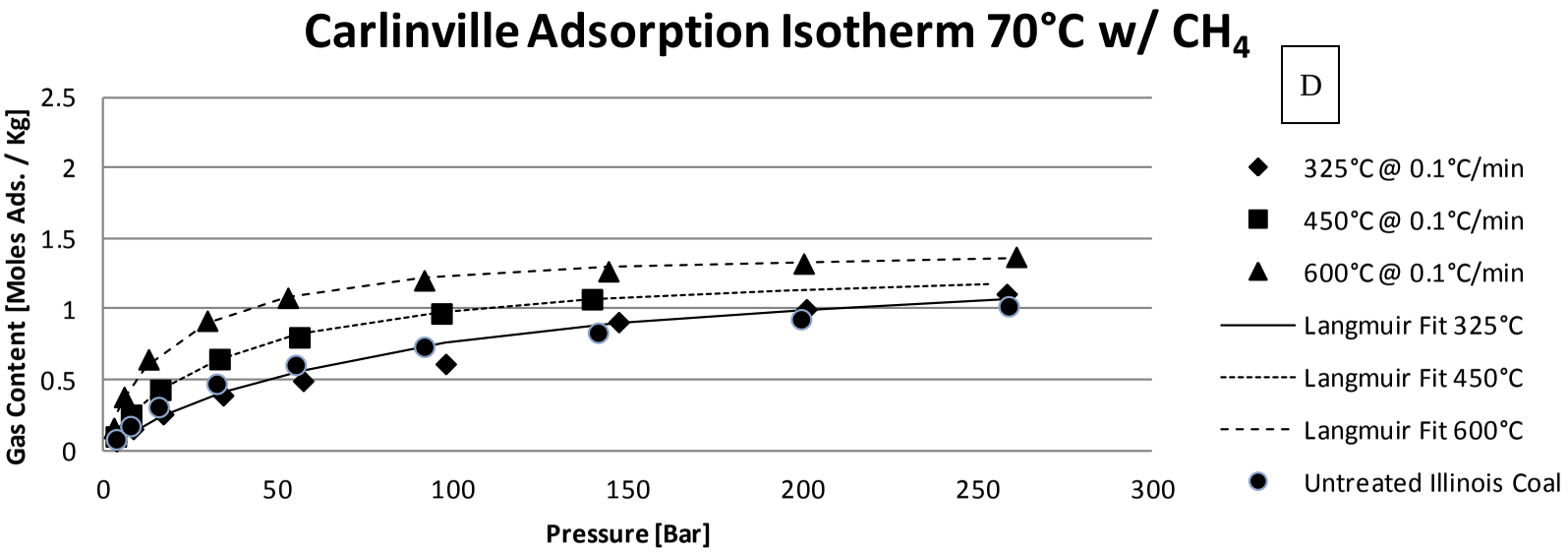

Figure 43 continued

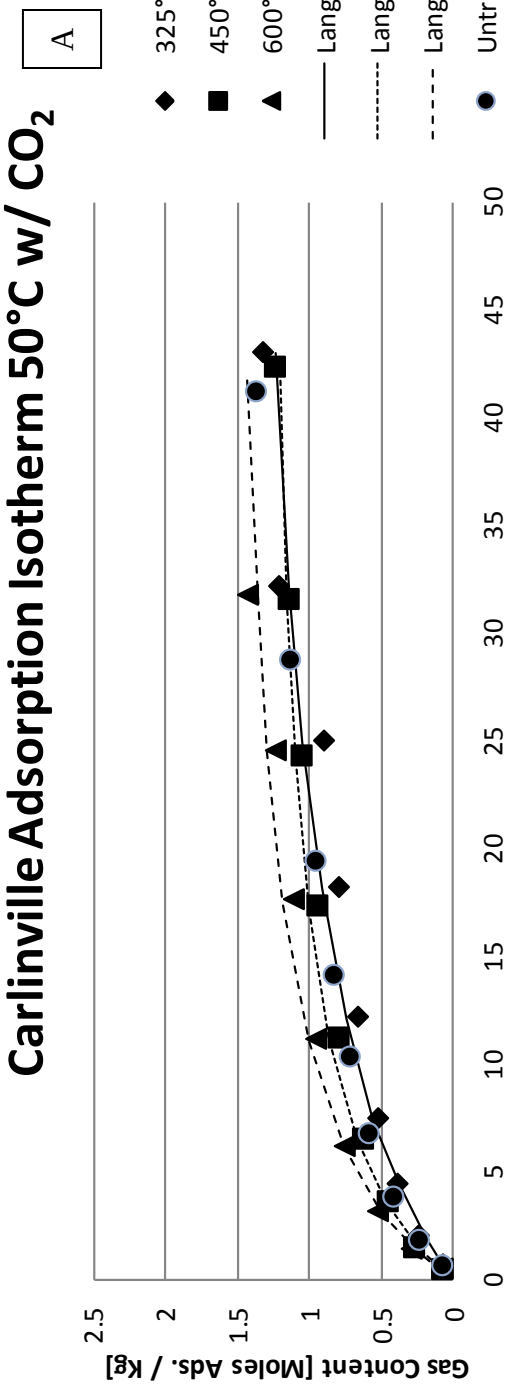

Figure 44: Adsorption isotherms on untreated and thermally treated Carlinville coals treated with a heating rate of 10°C/minute. A) CO_2 isotherms measured at 50° C0. B) CH_4 isotherms measured at 50° C. C) CO_2 isotherms measured at 70° C. D) CH_4 isotherms measured at 70° C.

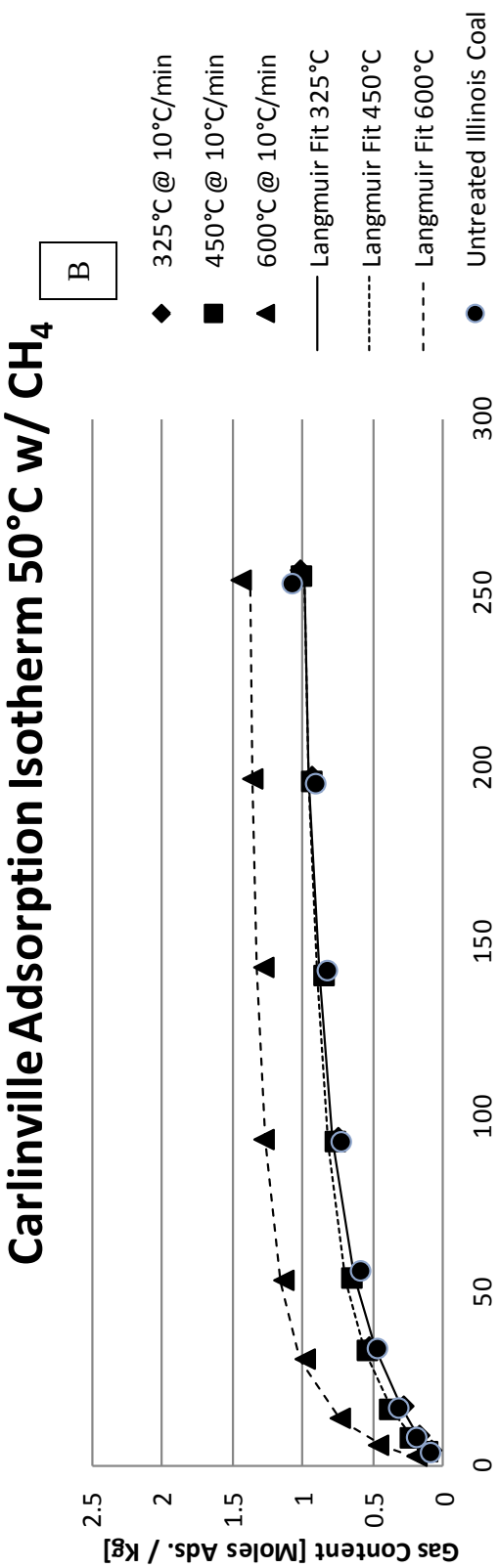

Figure 44 continued

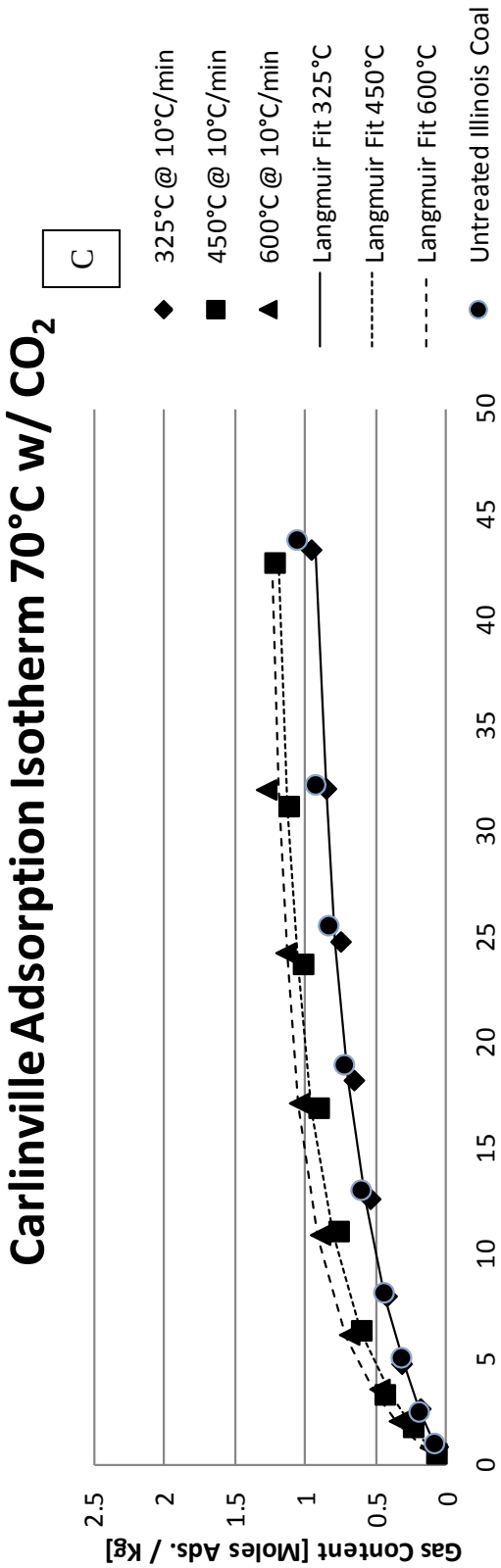

Figure 44 continued

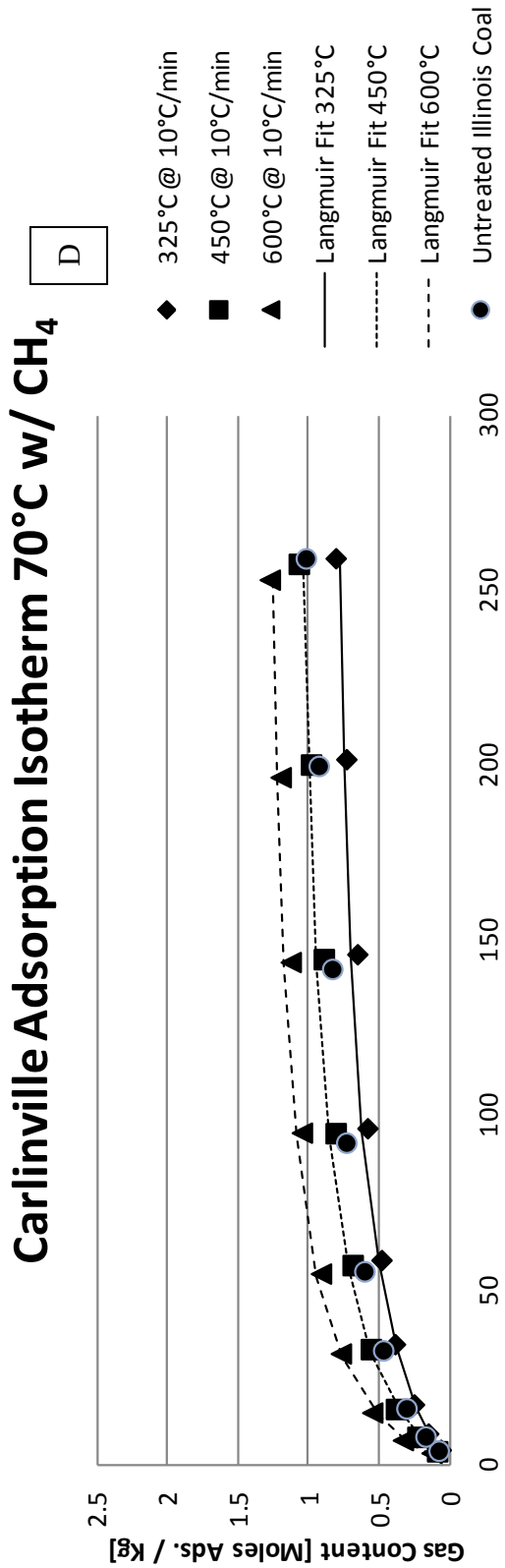

Figure 44 continued

Table 21: Langmuir equation parameters for treated and untreated Carlinville coals. Units of V∞ are moles adsorbed per kilogram of coal. Units of β are 1/bar.

Coal	*Langmuir Fit*	*CH_4 @ 50°C*	*CH_4 @ 70°C*	*CO_2 @ 50°C*	*CO_2 @ 70°C*
Carlinville	V∞	1.059	1.396	1.684	1.742
	β	2.717E-02	2.133E-02	8.224E-02	6.396E-02
325@0.1	V∞	0.923	1.404	1.218	1.712
	β	3.159E-02	1.195E-02	1.054E-01	3.786E-02
450@0.1	V∞	1.274	1.332	1.704	2.086
	β	4.343E-02	2.863E-02	1.293E-01	6.560E-02
600@0.1	V∞	1.252	1.451	1.548	2.199
	β	7.123E-02	5.634E-02	1.867E-01	1.304E-01

Coal	*Langmuir Fit*	*CH_4 @ 50°C*	*CH_4 @ 70°C*	*CO_2 @ 50°C*	*CO_2 @ 70°C*
Carlinville	V∞	1.059	1.396	1.684	1.742
	β	2.717E-02	2.133E-02	8.224E-02	6.396E-02
325@10	V∞	1.180	0.921	1.676	1.254
	β	2.090E-02	2.104E-02	6.595E-02	6.721E-02
450@10	V∞	1.106	1.180	1.417	1.424
	β	3.102E-02	2.734E-02	1.381E-01	1.196E-01
600@10	V∞	1.441	1.364	1.687	1.420
	β	7.936E-02	4.143E-02	1.323E-01	1.632E-01

APPENDIX C

NORTH ANTELOPE ISOTHERMS

The purpose of this appendix is to provide the adsorption isotherm plots of the untreated and thermally treated North Antelope coals (Figures 45 and 46). This section also contains the Langmuir fitting parameters for aforementioned coal in table 22.

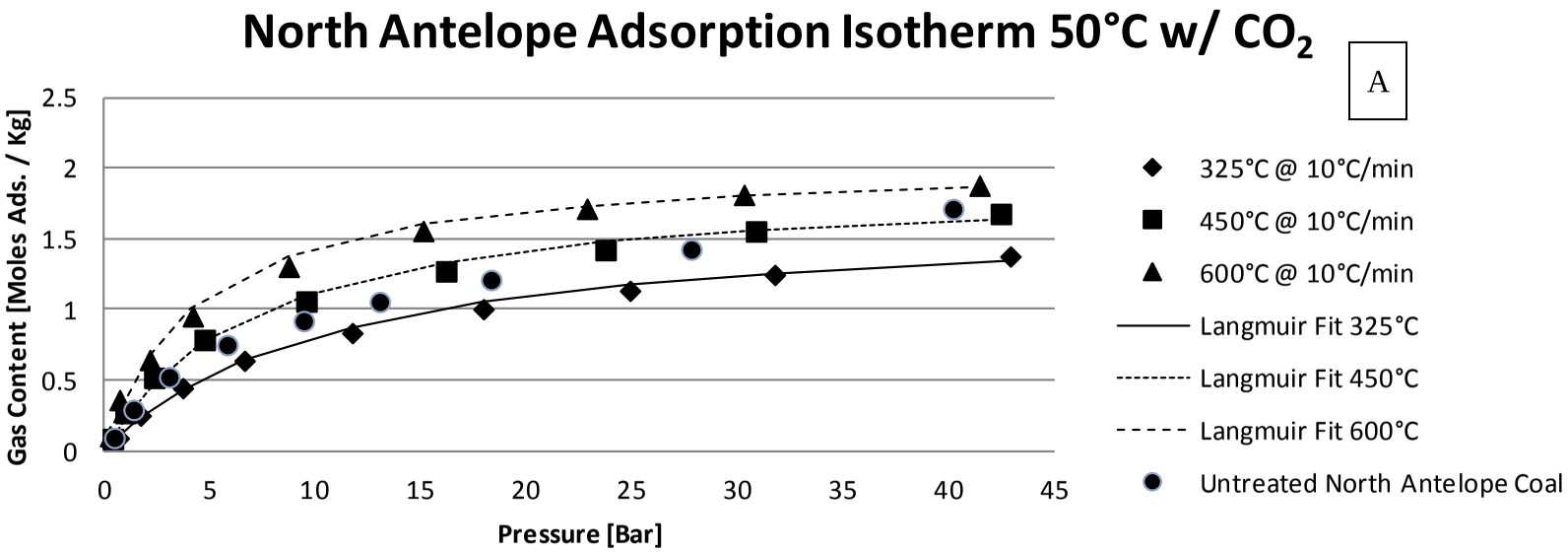

Figure 45: Adsorption isotherms on untreated and thermally treated North Antelope coals treated with a heating rate of 10°C/minute. A) CO_2 isotherms measured at 50°C. B) CH_4 isotherms measured at 50°C. C) CO_2 isotherms measured at 70°C. D) CH_4 isotherms measured at 70°C.

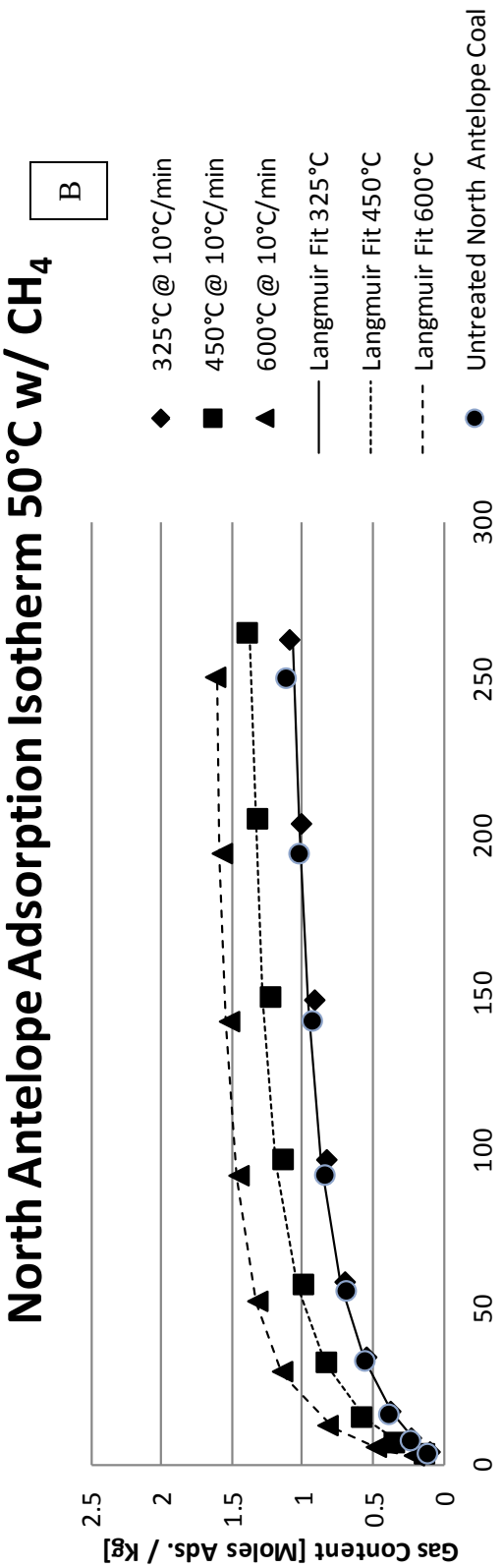

Figure 45 continued

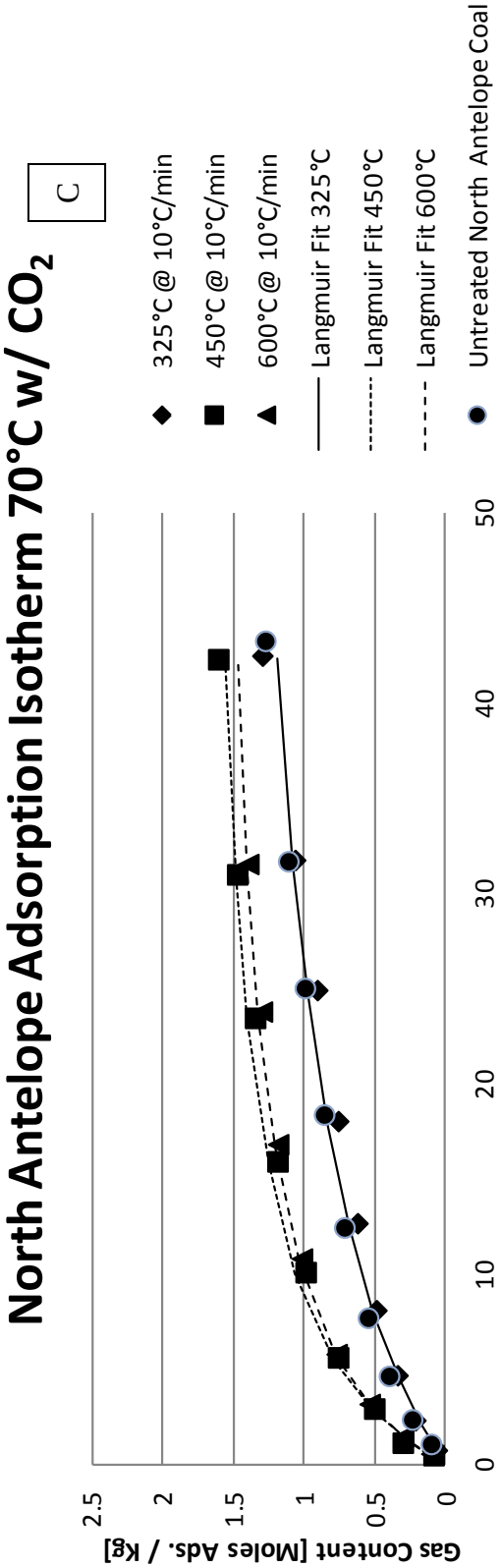

Figure 45 continued

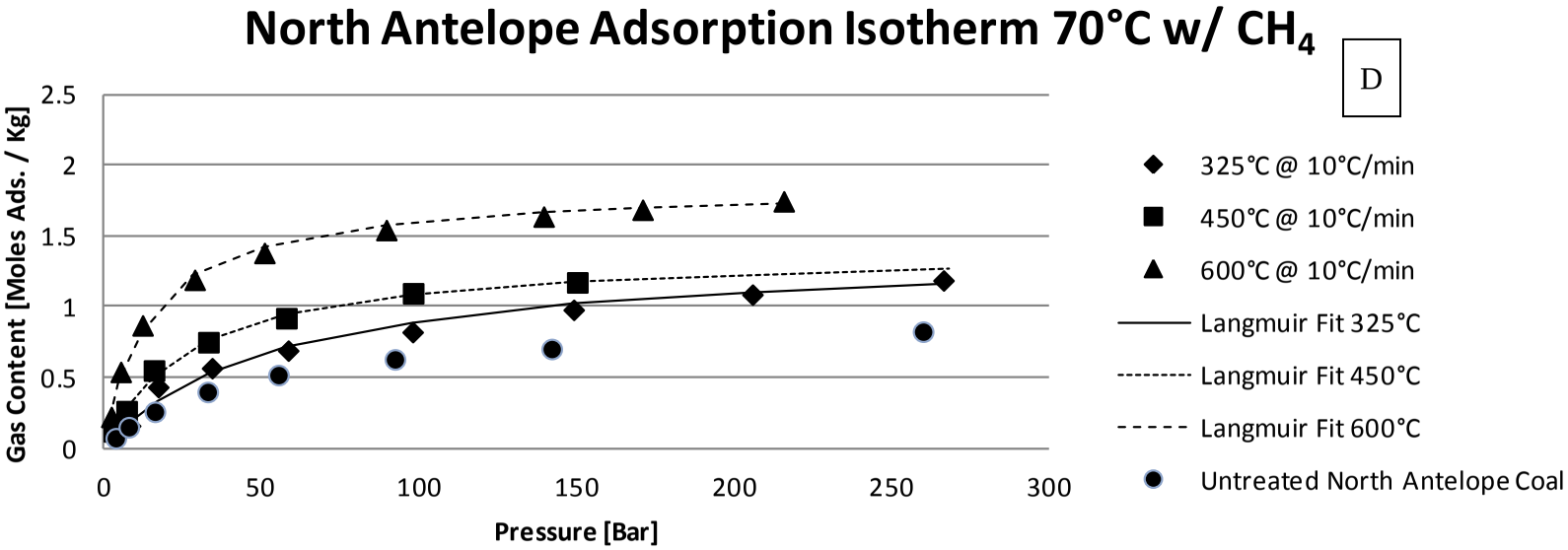

Figure 45 continued

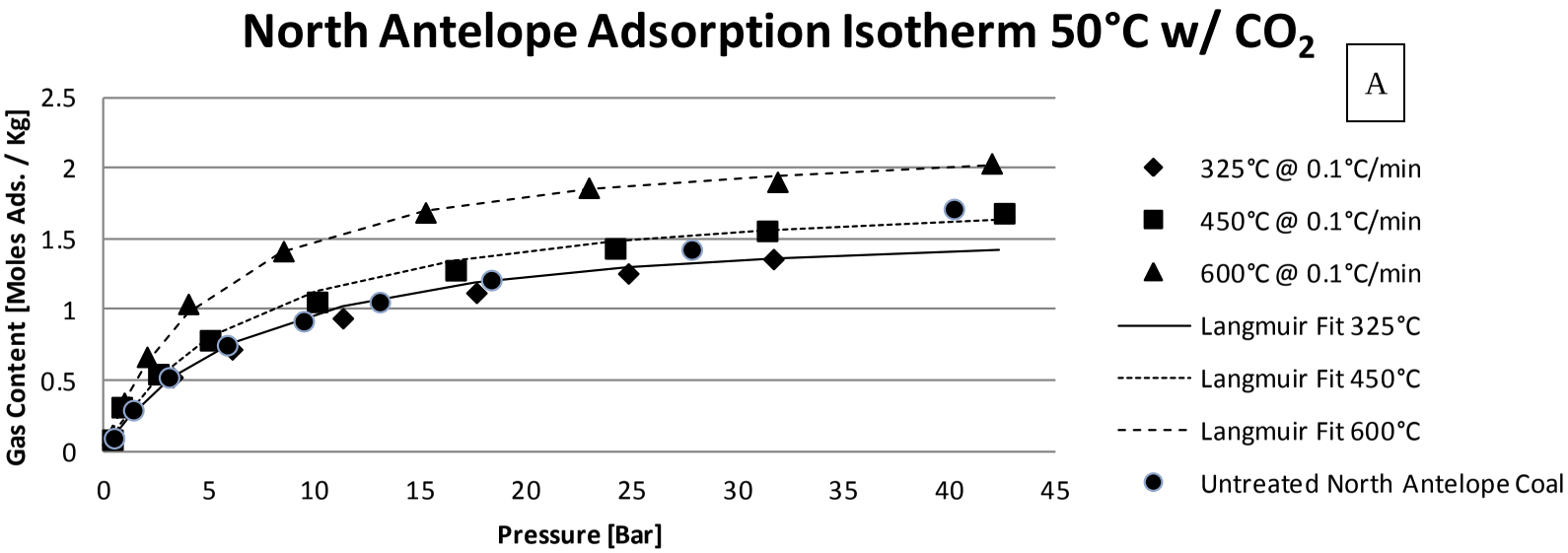

Figure 46: Adsorption isotherms on untreated and thermally treated North Antelope coals treated with a heating rate of 0.1°C/minute. A) CO_2 isotherms measured at 50° C. B) CH_4 isotherms measured at 50° C. C) CO_2 isotherms measured at 70° C. D) CH_4 isotherms measured at 70° C.

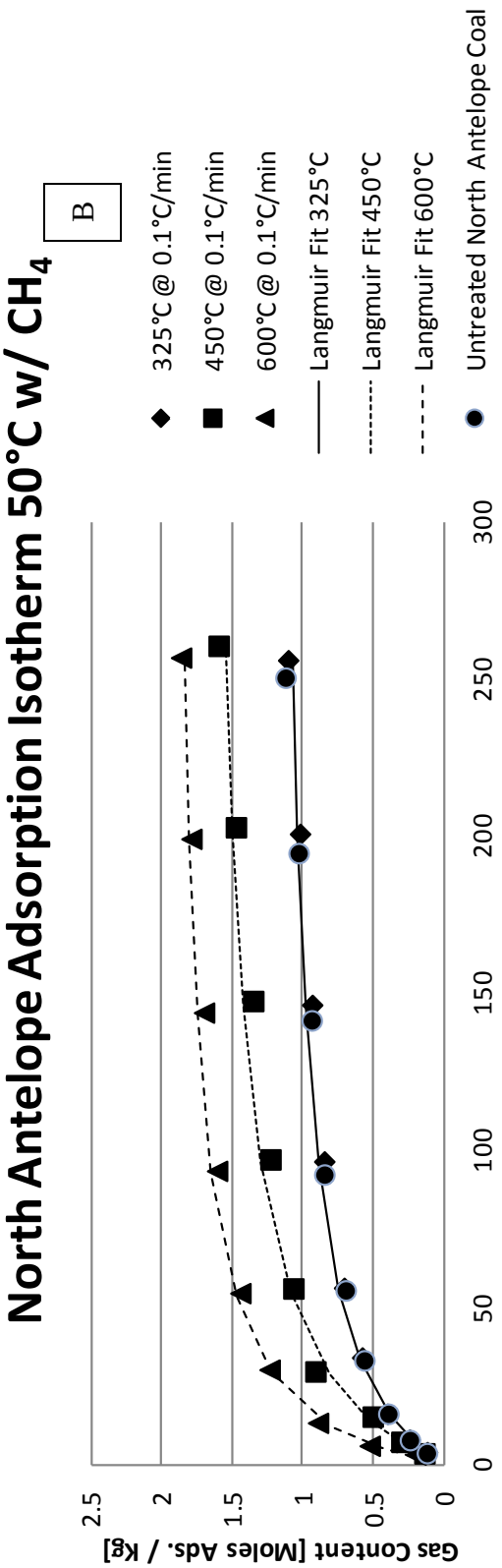

Figure 46 continued

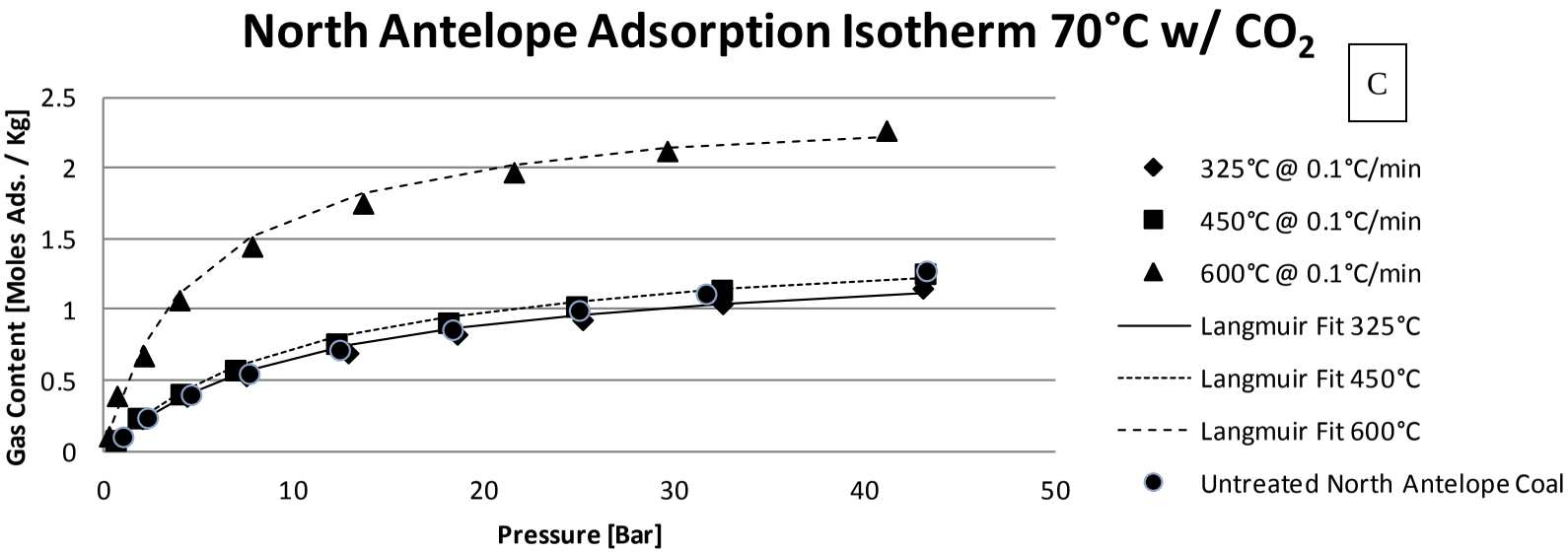

Figure 46 continued

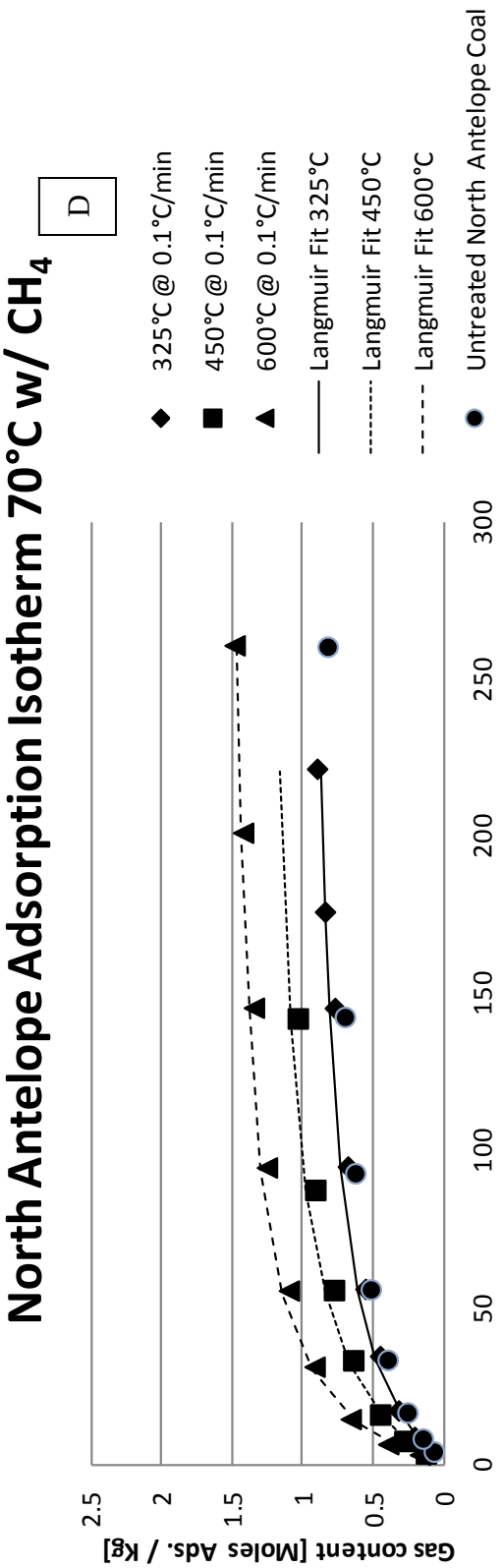

Figure 46 continued

Table 22: Langmuir equation parameters for treated and untreated North Antelope coals. Units of V∞ are moles adsorbed per kilogram of coal. Units of β are 1/bar

Coal	*Langmuir Fit*	*CH_4 @ 50°C*	*CH_4 @ 70°C*	*CO_2 @ 50°C*	*CO_2 @ 70°C*
North Antelope	V∞	1.230	0.872	1.528	1.377
	β	2.867E-02	2.617E-02	1.683E-01	8.970E-02
325@0.1	V∞	1.207	1.017	1.668	1.393
	β	2.937E-02	2.635E-02	1.403E-01	9.035E-02
450@0.1	V∞	1.746	1.317	1.893	1.530
	β	2.957E-02	3.195E-02	1.497E-01	9.074E-02
600@0.1	V∞	1.966	1.578	2.262	2.490
	β	5.516E-02	4.804E-02	1.954E-01	2.030E-01

Coal	*Langmuir Fit*	*CH_4 @ 50°C*	*CH_4 @ 70°C*	*CO_2 @ 50°C*	*CO_2 @ 70°C*
North Antelope	V∞	1.230	0.872	1.528	1.377
	β	2.867E-02	2.617E-02	1.683E-01	8.970E-02
325@10	V∞	1.221	1.392	1.677	1.732
	β	2.556E-02	1.802E-02	9.295E-02	5.229E-02
450@10	V∞	1.501	1.392	1.906	1.833
	β	3.874E-02	3.618E-02	1.445E-01	1.365E-01
600@10	V∞	1.698	1.836	2.057	1.696
	β	7.130E-02	6.900E-02	2.329E-01	1.484E-01

REFERENCES

1. Upadhye, R.; Burton, E.; Friedmann, J. *Science and technology gaps in underground coal gasification*; Technical Report, UCRL-TR-222523, Lawrence Livermore National Laboratory, University of California, Berkeley, CA: 2006.

2. Reeves, S. In *Geological Sequestration of CO_2 in Deep, Unmineable Coalbeds: An Integrated Research and Commerical-Scale Field Demonstration Project*, SPE Annual Technical Conference and Exhibition, 2001.

3. Karanikas, J. M.; Wellington, S. L.; Vinegar, H. J.; De Rouffignac, E. P.; Berchenko, I. E.; Stegemeier, G. L.; Zhang, E.; Fowler, T. D.; Ryan, R. C. In Situ thermal processing of a coal formation to control product composition. U.S. Patent No. 6,588,503, 8 Jul. 2003.

4. Krumm, R. L.; Deo, M.; Petrick, M. Direct Thermal and Catalytic Treatment of Paraffinic Crude Oils and Heavy Fractions. *Energy & Fuels* **2011,** *26* (5), 2663-2671.

5. Brandt, A. R. Converting oil shale to liquid fuels: Energy inputs and greenhouse gas emissions of the Shell in situ conversion process. *Environmental Science & Technology* **2008,** *42* (19), 7489-7495.

6. Karanikas, J. M.; Vinegar, H. J.; Wellington, S. L.; De Rouffignac, E. P.; Berchenko, I. E.; Stegemeier, G. L.; Zhang, E.; Fowler, T. D.; Ryan, R. C. In situ thermal processing of a coal formation using a relatively slow heating rate. Google Patents: 2004.

7. Gneshin, K. W.; Eddings, E. G. In *Development of porosity in a bituminous coal under conditions that mimic underground coal pyrolysis*. Abstracts of papers for the American Chemical Society, Amer Chemical Soc 1155.

8. Vinegar, H. J.; Wellington, S. L.; De Rouffignac, E. P.; Karanikas, J. M.; Berchenko, I. E.; Stegemeier, G. L.; Shahin Jr, G. T.; Maher, K. A.; Zhang, E.; Fowler, T. D. In situ thermal processing of a coal formation to increase a permeability/porosity of the formation. U.S. Patent No. 6,866,097, March 15, 2005.

9. Vinegar, H. J.; Wellington, S. L.; De Rouffignac, E. P.; Berchenko, I. E. In situ thermal processing of a coal formation to form a substantially uniform, relatively high permeable formation. U.S. Patent No. 6,742,587, June 1, 2004.

10. Maroto-Valer, M. M.; Tang, Z.; Zhang, Y. CO_2 capture by activated and impregnated anthracites. *Fuel Processing Technology* **2005,** *86* (14–15), 1487-1502.

11. Brunauer, S.; Emmett, P. H.; Teller, E., Adsorption of Gases in Multimolecular Layers. *Journal of the American Chemical Society* **1938,** *60* (2), 309-319.

12. Gregg, S. J.; Sing, K. S. W. Adsorption Surface Area and Porosity. *J. Electrochem. Soc.* **1967,** *114* (11), 279.

13. Ruthven, D. M. *Principles of Adsorbtion and Adsorbtion Processes*. John Wiley: New York, 1984.

14. Yang, R. T. *Gas Separation by Adsorption Processes*. Butterworth Publishers: Stoneham, 1986.

15. Keller, J.; Staudt, R. *Gas Adsorption Equilibria*. Springer: New York, 2005.

16. Pakseresht, S.; Kazemeini, M.; Akbarnejad, M. M. Equilibrium isotherms for CO, CO_2, CH_4 and C_2H_4 on the 5A molecular sieve by a simple volumetric apparatus. *Separation and Purification Technology* **2002,** *28* (1), 53-60.

17. Belmabkhout, Y.; Frère, M.; Weireld, G. D. High-pressure adsorption measurements. A comparative study of the volumetric and gravimetric methods. *Measurement Science and Technology* **2004,** *15* (5), 848.

18. Lastoskie, C.; Gubbins, K. E.; Quirke, N. Pore size distribution analysis of microporous carbons: A density functional theory approach. *The Journal of Physical Chemistry* **1993,** *97* (18), 4786-4796.

19. Jiang, S.; Rhykerd, C. L.; Gubbins, K. E. Layering, freezing transitions, capillary condensation and diffusion of methane in slit carbon pores. *Molecular Physics* **1993,** *79* (2), 373-391.

20. Barrett, E. P.; Joyner, L. G.; Halenda, P. P. The Determination of Pore Volume and Area Distributions in Porous Substances. I. Computations from Nitrogen Isotherms. *Journal of the American Chemical Society* **1951,** *73* (1), 373-380.

21. Clarkson, C.; Bustin, R. The effect of pore structure and gas pressure upon the transport properties of coal: A laboratory and modeling study. 1. Isotherms and pore volume distributions. *Fuel* **1999,** *78* (11), 1333-1344.

22. Krishna, R. A unified approach to the modelling of intraparticle diffusion in adsorption processes. *Gas Separation and Purification* **1993,** *7* (2).

23. Langmuir, I. The Adsorption of Gases on Plane Surfaces of Glass, Mica, and Platinum. *Journal of the American Chemical Society* **1918,** *40* (9), 1361-1403.

24. Keller, J. U.; Staudt, R.; Tomalla, M. Volume-Gravimetric Measurements of Binary Gas Adsorption Equilibria. *Berichte der Bunsengesellschaft für physikalische Chemie* **1992,** *96* (1), 28-32.

25. Keller, J. U.; Rave, H.; Staudt, R. Measurement of gas absorption in a swelling polymeric material by a combined gravimetric-dynamic method. *Macromolecular Chemistry and Physics* **1999,** *200* (10), 2269-2275.

26. Keller, J. U.; Robens, E.; Hohenesche, C. d. F. v. Thermogravimetric and sorption measurement techniques/instruments. In *Studies in Surface Science and Catalysis*, F. Rodriguez-Reinoso, B. M. J. R.; Unger, K., Eds. Elsevier: 2002; Vol. Volume 144, pp 387-394.

27. Dreisbach, F.; Lösch, H. W.; Harting, P. Highest Pressure Adsorption Equilibria Data: Measurement with Magnetic Suspension Balance and Analysis with a New Adsorbent/Adsorbate-Volume. *Adsorption* **2002,** *8* (2), 95-109.

28. Dreisbach, F.; Staudt, R.; Keller, J. U. High Pressure Adsorption Data of Methane, Nitrogen, Carbon Dioxide and their Binary and Ternary Mixtures on Activated Carbon. *Adsorption* **1999,** *5* (3), 215-227.

29. Humayun, R.; Tomasko, D. L. High-resolution adsorption isotherms of supercritical carbon dioxide on activated carbon. *AIChE Journal* **2000,** *46* (10), 2065-2075.

30. M.J. Mavor, L. B. O., T.J. Pratt. Measurement and Evaluation of Coal Sorption Isotherm Data. In *Society of Petroleum Engineers Annual Technical Conference and Exhibition*, Soceity of Petroleum Engineers: New Orleans, Louisiana, 1990; pp 157--170.

31. Clarkson, C. R.; Bustin, R. M. Binary gas adsorption/desorption isotherms: effect of moisture and coal composition upon carbon dioxide selectivity over methane. *International Journal of Coal Geology* **2000,** *42* (4), 241-271.

32. Yu, H.; Zhou, L.; Guo, W.; Cheng, J.; Hu, Q. Predictions of the adsorption equilibrium of methane/carbon dioxide binary gas on coals using Langmuir and ideal adsorbed solution theory under feed gas conditions. *International Journal of Coal Geology* **2008,** *73* (2), 115-129.

33. Bae, J.-S.; Bhatia, S. K.; Massarotto, P.; Rudolph, V.; Shin, C. H. In *Gas Adsorption Measurement on Coals for CO_2-ECBM*, Proceedings of 2009 Asia Pacific Coalbed Methane Symposium and 2009 China Coalbed Symposium, Xozhou, Xozhou, 2009.

34. Bae, J.-S.; Bhatia, S. K.; Rudolph, V.; Massarotto, P. Pore Accessibility of Methane and Carbon Dioxide in Coals. *Energy & Fuels* **2009,** *23*, 3319-3327.

35. Hall, F. E.; Zhou, C.; Gasem, K. A. M.; Robinson, R. L.; Yee, D. In *Adsorption of Pure Methane, Nitrogen, and Carbon Dioxide and Their Binary Mixtures on Wet Fruitland Coal*, 1994 Eastern Regional Conference & Exhibition, Charleston, SPE: Charleston, 1994; pp 329-344.

36. Li, D.; Liu, Q.; Weniger, P.; Gensterblum, Y.; Busch, A.; Krooss, B. M. High-pressure sorption isotherms and sorption kinetics of CH_4 and CO_2 on coals. *Fuel* **2010,** *89*, 569-580.

37. Stanton, R.; Flores, R.; Warwick, P. D.; Gluskoter, H.; Stricker, G. D. *Coal Bed Sequestration of Carbon Dioxide*. United States Department of Energy: Washington D.C., 2001.

38. Gale, J.; Freund, P. Coal-Bed Methane Enhancement with CO_2 Sequestration Worldwide Potential. *Environmental Geosciences* **2008,** *8* (3), 210-216.

39. Arri, L. E.; Yee, D.; Morgan, W. D.; Jeansonne, M. W. In *Modeling Coalbed Methane Production With Binary Gas Sorption*, SPE Rocky Mountain Regional Meeting, Casper, Society of Petroleum Engineers: Casper, 1992; pp 459-471.

40. Bae, J.-S.; Bhatia, S. K. High-pressure Adsorption of Methane and Carbon Dioxide on Coal. *Energy & Fuels* **2006,** *20*, 2599-2607.

41. Tóth, J. Uniform interpretation of gas/solid adsorption. *Advances in Colloid and Interface Science* **1995,** *55* (0), 1-239.

42. Terzyk, A. P.; Chatłas, J.; Gauden, P. A.; Rychlicki, G.; Kowalczyk, P. Developing the solution analogue of the Toth adsorption isotherm equation. *Journal of Colloid and Interface Science* **2003,** *266* (2), 473-476.

43. Himeno, S.; Komatsu, T.; Fujita, S. High-Pressure Adsorption Equilibria of Methane and Carbon Dioxide on Several Activated Carbons. *Journal of Chemical & Engineering Data* **2005,** *50* (2), 369-376.

44. Siemons, N.; Busch, A. Measurement and interpretation of supercritical CO_2 sorption on various coals. *International Journal of Coal Geology* **2007,** *69* (4), 229-242.

45. Span, R.; Wagner, W. A New Equation of State for Carbon Dioxide Covering the Fluid Region from the Triple-Point Temperature to 1100 K at Pressures up to 800 MPa. *Journal of Physical and Chemical Reference Data; 25 (6);* pp. 1509-1596.

46. Ozdemir, E.; Morsi, B. I.; Schroeder, K. Importance of Volume Effects to Adsorption Isotherms of Carbon Dioxide on Coals. *Langmuir* **2003,** *19*, 9764-9773.

47. DeBarr, J. A.; Lizzio, A. A.; Daley, M. A. Adsorption of SO_2 on Bituminous Coal Char and Activated Carbon Fiber. *Energy & Fuels* **1997,** *11* (2), 267-271.

48. Lorenc-Grabowska, E.; Gryglewicz, G. Adsorption characteristics of Congo Red on coal-based mesoporous activated carbon. *Dyes and Pigments* **2007,** *74* (1), 34-40.

49. Sun, J.; Rood, M. J.; Rostam-Abadi, M.; Lizzio, A. A. Natural gas storage with activated carbon from a bituminous coal. *Gas Separation & and Purification* **1996,** *10* (2), 91-96.

50. Teng, H.; Lin, H.-C. Activated carbon production from low ash subbituminous coal with CO2 activation. *AIChE Journal* **1998,** *44* (5), 1170-1177.

51. Teng, H.; Yeh, T.-S.; Hsu, L.-Y. Preparation of activated carbon from bituminous coal with phosphoric acid activation. *Carbon* **1998,** *36* (9), 1387-1395.

52. Yoshizawa, N.; Yamada, Y.; Furuta, T.; Shiraishi, M.; Kojima, S.; Tamai, H.; Yasuda, H. Coal-Based Activated Carbons Prepared with Organometallics and Their Mesoporous Structure. *Energy & Fuels* **1997,** *11* (2), 327-330.

53. Izquierdo, M. a. T.; Rubio, B.; Mayoral, C.; Andrés, J. M. Low cost coal-based carbons for combined SO_2 and NO removal from exhaust gas. *Fuel* **2003,** *82* (2), 147-151.

54. Hsi, H.-C.; Chen, S.; Rostam-Abadi, M.; Rood, M. J.; Richardson, C. F.; Carey, T. R.; Chang, R. Preparation and Evaluation of Coal-Derived Activated Carbons for Removal of Mercury Vapor from Simulated Coal Combustion Flue Gases. *Energy & Fuels* **1998,** *12* (6), 1061-1070.

55. Yang, R. T.; Saunders, J. T. Adsorption of gases on coals and heattreated coals at elevated temperature and pressure: 1. Adsorption from hydrogen and methane as single gases. *Fuel* **1985,** *64* (5), 616-620.

56. Gavalas, G. R.; Wilks, K. A. Intraparticle mass transfer in coal pyrolysis. *AIChE Journal* **1980,** *26* (2), 201-212.

57. Elliott, M. A. *Chemistry of Coal Utilization. Second Supplementary Volume*. 1981; Pages: 2395.

58. Shafirovich, E.; Varma, A. Underground coal gasification: A brief review of current status. *Industrial & Engineering Chemistry Research* **2009,** *48* (17), 7865-7875.

59. White, C. M.; Smith, D. H.; Jones, K. L.; Goodman, A. L.; Jikich, S. A.; LaCount, R. B.; DuBose, S. B.; Ozdemir, E.; Morsi, B. I.; Schroeder, K. T., Sequestration of carbon dioxide in coal with enhanced coalbed methane recovery: A review. *Energy & Fuels* **2005,** *19* (3), 659-724.

60. Zhang, E.; Vinegar, H. J.; Wellington, S. L.; De Rouffignac, E. P.; Karanikas, J. M.; Berchenko, I. E.; Stegemeier, G. L.; Maher, K. A.; Fowler, T. D.; Ryan, R. C.

In situ thermal processing of a coal formation with a selected vitrinite reflectance. U.S. Patent No. 6,591,907, July 15, 2003.

61. Howard, J. B. Fundamentals of Coal Pyrolysis and Hydropyrolysis. In *Chemistry of Coal Utilization*, John Wiley & Sons: New York, 1981; p 703.

62. Price, P. H.; Headlee, A. J. W. Natural coal gas in West Virginia. *AAPG Bulletin* **1943,** *27* (4), 529-537.

63. Institute, G. T. North American coalbed methane resource map. Institute, G. T., Ed. 2001.

64. Ayers, W. B. Coalbed gas systems, resources, and production and a review of contrasting cases from the San Juan and Powder River basins. *AAPG Bulletin* **2002,** *86* (11), 1853-1890.

65. McKee, C.; Bumb, A.; Koenig, R. Stress-dependent permeability and porosity of coal and other geologic formations. *SPE Formation Evaluation* **1988,** *3* (1), 81-91.

66. White, C. M.; Smith, D. H.; Jones, K. L.; Goodman, A. L.; Jikich, S. A.; LaCount, R. B.; Dubose, S. B.; Ozdemir, E.; Morsi, B. I.; Schroeder, K. T. Sequestration of Carbon Dioxide in Coal with Enhanced Coalbed Methane Recovery-A Reviey. *Energy & Fuels* **2005,** *19* (3), 659-724.

67. Crawford, P.; Biglarbigi, K.; Dammer, A.; Knaus, E. In *Advances in World Oil-Shale Production Technologies*, SPE Annual Technical Conference and Exhibition, 2008.

68. Burnham, A. K.; Day, R. L.; Hardy, M. P.; Wallman, P. H. AMSO's Novel Approach to *In Situ* Oil Shale Recovery. Oxford University Press: New York, NY, USA: 2010; pp 149-160.

69. Dyni, J. R. *Geology and resources of some world oil-shale deposits*. US Department of The Interior, US Geological Survey: 2006.

70. Vinegar, H. In *Shell's In situ conversion process*, 26th Oil Shale Symposium, Golden, Colorado, October 16, 2006; p 2006.

71. Hill, D. A.; Pearson, D. J.; Motley, E. P.; Beard, T. N.; Farrell, J. L. Recovery system for oil shale deposits. Google Patents: 1977.

72. Mastalerz, M.; Drobniak, A.; Rupp, J. Meso- and Micropore Characteristics of Coal Lithotypes: Implications for CO_2 Adsorption. *Energy & Fuels* **2008,** *22* (6), 4049-4061.

73. Orr, C. Treatise on Analytical Chemistry, Part 3, Vol. 4, edited by IM Kolthoff, PJ Elving, FH Stross. New York: John Wiley & Sons: 1977.

74. Clarkson, C.; Bustin, R. The effect of pore structure and gas pressure upon the transport properties of coal: A laboratory and modeling study. 2. Adsorption rate modeling. *Fuel* **1999,** *78* (11), 1345-1362.

75. Krishna, R. Problems and pitfals in the use of the Fick formulation for intraparticle diffusion. *Chemical Engineering Science* **1992,** *48* (5).

76. Clarkson, C. R. The Effect of Coal Composition Upon Gas Sorption and Transmissibility of Bituminous Coal. University of British Columbia, Vancouver, 1992. MS Thesis.

77. Amarasekera, G.; Scarlett, M.; Mainwaring, D. Micropore size distributions and specific interactions in coals. *Fuel* **1995,** *74* (1), 115-118.

78. Cai, Y.; Liu, D.; Pan, Z.; Yao, Y.; Li, J.; Qiu, Y. Pore structure and its impact on CH4 adsorption capacity and flow capability of bituminous and subbituminous coals from Northeast China. *Fuel* **2012**.

79. Gan, H.; Nandi, S.; Walker Jr, P. Nature of the porosity in American coals. *Fuel* **1972,** *51* (4), 272-277.

80. Zhang, S.; Tang, S.; Tang, D.; Pan, Z.; Yang, F. The characteristics of coal reservoir pores and coal facies in Liulin district, Hedong Coal Field of China. *International Journal of Coal Geology* **2010,** *81* (2), 117-127.

81. Diessel, C. In *On the correlation between coal facies and depositional environments*, Proc 20th Symp Dep Geol, Univ. Newcastle, NSW, 1986; pp 19-22.

82. Zhao, Y.; Jiang, C.; Chu, W. Methane adsorption behavior on coal having different pore structures. *International Journal of Mining Science and Technology* **2012**.

83. Mosher, K.; He, J.; Liu, Y.; Rupp, E.; Wilcox, J. Molecular Simulation of Adsorption in Micro-and Mesoporous Carbons with Applications to Coal and Gas Shale Systems. *International Journal of Coal Geology* **2013**.

84. Lowell, S.; Shields, J. E.; Thomas, M. A.; Thommes, M. *Characterization of Porous Solids and Powders: Surface Area, Pore Size and Density*. Springer: 2006; Vol. 16.

85. Wilcox, J. *Carbon Capture*. Springer: 2012.

86. Ottiger, S.; Pini, R.; Storti, G.; Mazzotti, M.; Bencini, R.; Quattrocchi, F.; Sardu, G.; Deriu, G. Adsorption of pure carbon dioxide and methane on dry coal from the Sulcis Coal Province (SW Sardinia, Italy). *Environmental Progress* **2006,** *25* (4), 355-364.

87. Gil, A.; Grange, P. Application of the Dubinin-Radushkevich and Dubinin-Astakhov equations in the characterization of microporous solids. *Colloids and Surfaces A: Physicochemical and Engineering Aspects* **1996,** *113* (1–2), 39-50.

88. Dubinin, M.; Radushkevich, L. Equation of the characteristic curve of activated charcoal. *Chem. Zentr* **1947,** *1* (1), 875.

89. Dubinin, M.; Astakhov, V. Description of adsorption equilibria of vapors on zeolites over wide ranges of temperature and pressure. *Adv. Chem. Ser* **1971,** *102*, 69-85.

90. Polanyi, M. Section III.—Theories of the adsorption of gases. A general survey and some additional remarks. Introductory paper to section III. *Transactions of the Faraday Society* **1932,** *28*, 316-333.

91. Nguyen, C.; Do, D. D. The Dubinin–Radushkevich equation and the underlying microscopic adsorption description. *Carbon* **2001,** *39* (9), 1327-1336.

92. Scherdel, C.; Reichenauer, G.; Wiener, M. Relationship between pore volumes and surface areas derived from the evaluation of N_2-sorption data by DR-, BET- and t-plot. *Microporous and Mesoporous Materials* **2010,** *132* (3), 572-575.

93. Lippens, B.; De Boer, J. Studies on pore systems in catalysts: V. The t method. *Journal of Catalysis* **1965,** *4* (3), 319-323.

94. Harkins, W. D.; Jura, G. Surfaces of solids. XIII. A vapor adsorption method for the determination of the area of a solid without the assumption of a molecular area, and the areas occupied by nitrogen and other molecules on the surface of a solid. *Journal of the American Chemical Society* **1944,** *66* (8), 1366-1373.

95. Carrasco-Marin, F.; Lopez-Ramon, M.; Moreno-Castilla, C. Applicability of the Dubinin-Radushkevich equation to carbon dioxide adsorption on activated carbons. *Langmuir* **1993,** *9* (11), 2758-2760.

96. Landers, J.; Gor, G. Y.; Neimark, A. V. Density Functional Theory Methods for Characterization of Porous Materials. *Colloids and Surfaces A: Physicochemical and Engineering Aspects* **2013**.

97. Dombrowski, R. J.; Hyduke, D. R.; Lastoskie, C. M. Pore size analysis of activated carbons from argon and nitrogen porosimetry using density functional theory. *Langmuir* **2000,** *16* (11), 5041-5050.

98. Jagiello, J.; Thommes, M. Comparison of DFT characterization methods based on N_2, Ar, CO_2, and H_2 adsorption applied to carbons with various pore size distributions. *Carbon* **2004,** *42* (7), 1227-1232.

99. Jagiello, J. Stable numerical solution of the adsorption integral equation using splines. *Langmuir* **1994,** *10* (8), 2778-2785.

100. Neimark, A. V.; Lin, Y.; Ravikovitch, P. I.; Thommes, M. Quenched solid density functional theory and pore size analysis of micro-mesoporous carbons. *Carbon* **2009,** *47* (7), 1617-1628.

101. Franz, M.; Arafat, H. A.; Pinto, N. G. Effect of chemical surface heterogeneity on the adsorption mechanism of dissolved aromatics on activated carbon. *Carbon* **2000,** *38* (13), 1807-1819.

102. Larsen, J. W. The effects of dissolved CO_2 on coal structure and properties. *International Journal of Coal Geology* **2004,** *57* (1), 63-70.

103. Chaback, J.; Morgan, W.; Yee, D. Sorption of nitrogen, methane, carbon dioxide and their mixtures on bituminous coals at in situ conditions. *Fluid Phase Equilibria* **1996,** *117* (1), 289-296.

104. Clarkson, C.; Bustin, R.; Levy, J. Application of the mono/multilayer and adsorption potential theories to coal methane adsorption isotherms at elevated temperature and pressure. *Carbon* **1997,** *35* (12), 1689-1705.

105. Martin-Martinez, J.; Torregrosa-Macia, R.; Mittelmeijer-Hazeleger, M. Mechanisms of adsorption of CO_2 in the micropores of activated anthracite. *Fuel* **1995,** *74* (1), 111-114.

106. Ozdemir, E. Chemistry of the Adsorption of Carbon Dioxide by Argonne Premium Coals and a Model to Simulate CO_2 Sequestration in Coal Seams. University of Pittsburgh, 2005.

107. Liu, Y.; Wilcox, J. CO2 adsorption on carbon models of organic constituents of gas shale and coal. *Environmental Science & Technology* **2010,** *45* (2), 809-814.

108. Bustin, R.; Clarkson, C. Geological controls on coalbed methane reservoir capacity and gas content. *International Journal of Coal Geology* **1998,** *38* (1), 3-26.

109. Garnier, C.; Finqueneisel, G.; Zimny, T.; Pokryszka, Z.; Lafortune, S.; Défossez, P. D. C.; Gaucher, E. C. Selection of coals of different maturities for CO2 Storage by modelling of CH_4 and CO_2 adsorption isotherms. *International Journal of Coal Geology* **2011,** *87* (2), 80-86.

110. Dake, L. P. *Fundamentals of Reservoir Engineering*. Vol. 8. Elsevier: Amsterdam, 2006;

111. Ahmed, T. *Reservoir Engineering Handbook*. Gulf Professional Publishing: 2006.

112. Grant, M. A.; Bixley, P. F. *Geothermal Reservoir Engineering*. Academic Press: 2011.

113. Ottiger, S.; Pini, R.; Storti, G.; Mazzotti, M. Competitive adsorption equilibria of CO_2 and CH_4 on a dry coal. *Adsorption* **2008,** *14* (4-5), 539-556.

114. Krooss, B.; Van Bergen, F.; Gensterblum, Y.; Siemons, N.; Pagnier, H.; David, P. High-pressure methane and carbon dioxide adsorption on dry and moisture-equilibrated Pennsylvanian coals. *International Journal of Coal Geology* **2002,** *51* (2), 69-92.

115. Levy, J.; Killingley, J.; Day, S. In *Measurement of Coalbed Methane Isotherms for Australian Coals*, Proc. of the Symp. Coalbed Methane Research and Development in Australia, 1992; pp 1-8.

116. ASTM, Standard Test Method for Equilibrium Moisture of Coal at 96 to 97 Percent Relative Humidity and 30C. ASTM International: 1993; Vol. ASTM D 1412-93.

117. Švábová, M.; Weishauptová, Z.; Přibyl, O. The effect of moisture on the sorption process of CO_2 on coal. *Fuel* **2012,** *92* (1), 187-196.

118. Wang, G. X.; Wei, X. R.; Wang, K.; Massarotto, P.; Rudolph, V. Sorption-induced swelling/shrinkage and permeability of coal under stressed adsorption/desorption conditions. *International Journal of Coal Geology* **2010,** *83* (1), 46-54.

119. Mazumder, S.; Wolf, K. H., Differential swelling and permeability change of coal in response to CO_2 injection for ECBM. *International Journal of Coal Geology* **2008,** *74* (2), 123-138.

120. Pan, Z.; Connell, L. D. A theoretical model for gas adsorption-induced coal swelling. *International Journal of Coal Geology* **2007,** *69* (4), 243-252.

121. Levine, J. R. Model study of the influence of matrix shrinkage on absolute permeability of coal bed reservoirs. *Geological Society, London, Special Publications* **1996,** *109* (1), 197-212.

122. Van Krevelen, D.; Huntjens, F.; Dormans, H. Chemical structure and properties of coal. XVI. Plastic behavior on heating. *Fuel* **1956,** *35*, 462-475.

123. Garrido, J.; Linares-Solano, A.; Martin-Martinez, J.; Molina-Sabio, M.; Rodriguez-Reinoso, F.; Torregrosa, R. Use of nitrogen vs. carbon dioxide in the characterization of activated carbons. *Langmuir* **1987,** *3* (1), 76-81.

124. Yeom, I. T.; Ghosh, M. M.; Cox, C. D.; Robinson, K. G. Micellar solubilization of polynuclear aromatic hydrocarbons in coal tar-contaminated soils. *Environmental Science & Technology* **1995,** *29* (12), 3015-3021.

125. Larsen, J. W.; Mohammadi, M. Structural changes in coals due to pyridine extraction. *Energy & Fuels* **1990,** *4* (1), 107-110.

126. Tinni, A.; Fathi, E.; Agarwal, R.; Sondergeld, C.; Akkutlu, I. Y.; Rai, C. In *Shale Permeability Measurements on Plugs and Crushed Samples*, SPE Canadian Unconventional Resources Conference, 2012.

127. Handwerger, D.; Keller, J.; Vaughn, K. In *Improved Petrophysical Core Measurements on Tight Shale Reservoirs Using Retort and Crushed Samples*, SPE Annual Technical Conference and Exhibition, 2011.

128. Culp, S. J.; Gaylor, D. W.; Sheldon, W. G.; Goldstein, L. S.; Beland, F. A. A comparison of the tumors induced by coal tar and benzo [a] pyrene in a 2-year bioassay. *Carcinogenesis* **1998,** *19* (1), 117-124.

129. Goodman, A. L.; Busch, A.; Duffy, G. J.; Fitzgerald, J. E.; Gasem, K. A. M.; Gensterblum, Y.; Krooss, B. M.; Levy, J.; Ozdemir, E.; Pan, Z.; Robinson, R. L.; Schroeder, K.; Sudibandriyo, M.; White, C. M. An Inter-laboratory Comparison of CO_2 Isotherms Measured on Argonne Premium Coal Samples. *Energy & Fuels* **2004,** *18* (4), 1175-1182.

130. Mavor, M. J., Hartman, C., and Pratt, T.J. In *Uncertainty in Sorption Isotherm Measurements*, International Coalbed Methane Symposium, Tuscaloosa, Tuscaloosa, 2004.

131. Rouquerol F., R. J., Sing K.S.W. *Adsorption by Powders and Porous Solids*. Acedemic Press: Sand Diego, 1999.

132. Reeves, S.; Gonzalez, R.; Harpalani, S.; Gasem, K. Results, status and future activities of the coal-seq consortium. *Energy Procedia* **2009,** *1* (1), 1719-1726.

133. Clarkson, C. Application of a new multicomponent gas adsorption model to coal gas adsorption systems. *SPE Journal* **2003,** *8* (3), 236-251.

134. Solomon, P.; Fletcher, T.; Pugmire, R. Progress in coal pyrolysis. *Fuel* **1993,** *72* (5), 587-597.

135. Di Nola, G.; De Jong, W.; Spliethoff, H. TG-FTIR characterization of coal and biomass single fuels and blends under slow heating rate conditions: Partitioning of the fuel-bound nitrogen. *Fuel Processing Technology* **2010,** *91* (1), 103-115.

136. Cui, X.; Bustin, A.; Bustin, R. M. Measurements of gas permeability and diffusivity of tight reservoir rocks: different approaches and their applications. *Geofluids* **2009,** *9* (3), 208-223.

137. Lee, C. W.; Jenkins, R. G.; Schobert, H. H. Structure and reactivity of char from elevated pressure pyrolysis of Illinois No. 6 bituminous coal. *Energy & Fuels* **1992,** *6* (1), 40-47.

138. Kaszuba, J. P.; Janecky, D. R.; Snow, M. G. Carbon dioxide reaction processes in a model brine aquifer at 200C and 200 bar: Implications for geologic sequestration of carbon. *Applied Geochemistry* **2003,** *18* (7), 1065-1080.

139. Mandalaparty, P.; Deo, M.; Moore, J. In *CO_2 Sequestration: Temperature and Gas Compositional Effects on the Kinetics of Mineralogical Reactions*, SPE Annual Technical Conference and Exhibition, 2009.

140. Mandalaparty, P.; Deo, M.; Moore, J.Gas-Compositional Effects on Mineralogical Reactions in Carbon Dioxide Sequestration. *SPE Journal* **2011,** *16* (4), 949-958.

141. Rogner, H. H. Energy resources. *Energy for Development* **2012**, 149-160.

142. Cox, P. M.; Betts, R. A.; Jones, C. D.; Spall, S. A.; Totterdell, I. J. Acceleration of global warming due to carbon-cycle feedbacks in a coupled climate model. *Acc. Chem. Res* **1995,** *28*, 37-44.

143. White, D. C. M.; Strazisar, B. R.; Granite, E. J.; Hoffman, J. S.; Pennline, H. W. Separation and capture of CO_2 from large stationary sources and sequestration in geological formations—coalbeds and deep saline aquifers. *Journal of the Air & Waste Management Association* **2003,** *53* (6), 645-715.

144. Duan, Z.; Sun, R.; Zhu, C.; Chou, I. An improved model for the calculation of CO2 solubility in aqueous solutions containing Na^+, K^+, Ca^{2+}, Mg^{2+}, Cl^-, and SO_4^{2-}. *Marine Chemistry* **2006,** *98* (2), 131-139.

145. Soni, Y.; Thomson, W. J. Oxidation Kinetics of Oil Shale Char. *Industrial & Engineering Chemistry Process Design and Development* **1979,** *18* (4), 661-667.

146. Külaots, I.; Goldfarb, J. L.; Suuberg, E. M. Characterization of Chinese, American and Estonian oil shale semicokes and their sorptive potential. *Fuel* **2010,** *89* (11), 3300-3306.

147. Middleton, R. S.; Keating, G. N.; Stauffer, P. H.; Jordan, A. B.; Viswanathan, H. S.; Kang, Q. J.; Carey, J. W.; Mulkey, M. L.; Sullivan, E. J.; Chu, S. P. The cross-scale science of CO_2 capture and storage: From pore scale to regional scale. *Energy & Environmental Science* **2012**.

148. Luigi, M. Chapter 3 Carbon dioxide and CO_2–H_2O mixtures. In *Developments in Geochemistry*, Ed. Elsevier: 2006; Vol. Volume 11, pp 27-51.

149. Harvey, A. H.; Prausnitz, J. M. Thermodynamics of high-pressure aqueous systems containing gases and salts. *AIChE Journal* **1989,** *35* (4), 635-644.

150. Zuo, Y. X.; Guo, T. M. Extension of the Patel—Teja equation of state to the prediction of the solubility of natural gas in formation water. *Chemical Engineering Science* **1991,** *46* (12), 3251-3258.

151. Duan, Z.; Sun, R. An improved model calculating CO_2 solubility in pure water and aqueous NaCl solutions from 273 to 533 K and from 0 to 2000 bar. *Chemical Geology* **2003,** *193* (3), 257-271.

152. Spycher, N.; Pruess, K. CO_2-H_2O mixtures in the geological sequestration of CO2. II. Partitioning in chloride brines at 12–100° C and up to 600 bar. *Geochimica et Cosmochimica Acta* **2005,** *69* (13), 3309-3320.

153. Duan, Z.; Hu, J.; Li, D.; Mao, S. Densities of the CO_2–H_2O and CO_2–H_2O–NaCl Systems up to 647 K and 100 MPa. *Energy & Fuels* **2008,** *22* (3), 1666-1674.

154. Carroll, S. A.; Knauss, K. G. In *Experimental Determination of Ca-silicate Dissolution Rates: A Source of Calcium for Geologic CO_2 Sequestration*, First National Conference on Carbon Sequestration. National Energy Technology Laboratory, Washington, DC, 2001.

155. Hellevang, H.; Aagaard, P.; Oelkers, E. H.; Kvamme, B. Can Dawsonite Permanently Trap CO_2? *Environmental Science & Technology* **2005,** *39* (21), 8281-8287.

156. Hänchen, M.; Prigiobbe, V.; Baciocchi, R.; Mazzotti, M. Precipitation in the Mg-carbonate system—effects of temperature and CO_2 pressure. *Chemical Engineering Science* **2008,** *63* (4), 1012-1028.

157. Kaszuba, J. P.; Janecky, D. R.; Snow, M. G. Experimental evaluation of mixed fluid reactions between supercritical carbon dioxide and NaCl brine: Relevance to the integrity of a geologic carbon repository. *Chemical Geology* **2005,** *217* (3), 277-293.

158. Wigand, M.; Kaszuba, J. P.; Hollis, W. K. Geochemical effects of CO_2 sequestration in fractured wellbore cement at the cement/ caprock interface. *Chemical Geology* **2009,** (265), 122-133.

159. Bertier, P.; Swennen, R.; Laenen, B.; Lagrou, D.; Dreesen, R. Experimental identification of CO_2-water-rock interactions caused by sequestration of CO_2 in Westphalian and Buntsandstein sandstones of the Campine Basin (NE-Belgium). *Journal of Geochemical Exploration* **2006,** *89*, 10-14.

160. Rosenbauer, R. J.; Koksalan, T.; Palandri, J. L. Experimental investigation of CO_2-brine-rock interations at elevated temperature and pressure: Implications for CO_2 sequestration in deep-saline aquifers. *Fuel Processing Technology* **2005,** *86* (14-15).

161. Carroll, S.; McNab, W. W.; Dai, Z.; Torres, S. C. Reactivity of Mt. Simon sandstone and the Eau Claire shale under CO_2 storage conditions. *Environmental Science & Technology* **2012**.

162. Yu, Z.; Liu, L.; Yang, S.; Li, S.; Yang, Y. An experimental study of CO_2–brine–rock interaction at in situ pressure–temperature reservoir conditions. *Chemical Geology* **2012**.

163. Xu, T.; Sonnenthal, E.; Spycher, N.; Pruess, K. TOUGHREACT—A simulation program for non-isothermal multiphase reactive geochemical transport in variably saturated geologic media: Applications to geothermal injectivity and CO_2 geological sequestration. *Computers & Geosciences* **2006,** *32* (2), 145-165.

164. Gundogan, O.; Mackay, E.; Todd, A. Comparison of numerical codes for geochemical modelling of CO_2 storage in target sandstone reservoirs. *Chemical Engineering Research and Design* **2011,** *89* (9), 1805-1816.

165. Gaus, I.; Azaroual, M.; Czernichowski-Lauriol, I. Reactive transport modelling of the impact of CO_2 injection on the clayey cap rock at Sleipner (North Sea). *Chemical Geology* **2005,** *217* (3), 319-337.

166. Duan, Z.; Møller, N.; Weare, J. H. An equation of state for the CH_4-CO_2-H_2O system: I. Pure systems from 0 to 1000° C and 0 to 8000 bar. *Geochimica et Cosmochimica Acta* **1992,** *56* (7), 2605-2617.

167. Blum, A. E.; Stillings, L. L. Feldspar dissolution kinetics. *Reviews in Mineralogy and Geochemistry* **1995,** *31* (1), 291-351.

168. Gunter, W. D.; Perkins, E. H.; Hutcheon, I. Aquifer disposal of acid gases: modelling of water-rock reactions for trapping of acid wastes. *Applied Geochemistry* **2000,** *15*, 1085-1095.

169. Zerai, B.; Saylor, B. Z.; Matisoff, G. Computer simulation of CO_2 trapped through mineral precipitation in the Rose Run Sandstone, Ohio. *Applied Geochemistry* **2006,** *21* (2), 223-240.

170. Xu, T.; Apps, J. A.; Pruess, K. Mineral sequestration of carbon dioxide in a sandstone–shale system. *Chemical Geology* **2005,** *217* (3), 295-318.

171. Beyer, C.; Li, D.; De Lucia, M.; Kuehn, M.; Bauer, S. Modelling CO_2-induced fluid-rock interactions in the Altensalzwedel gas reservoir. Part II-Coupled Reactive Transport Simulations. *Environmental Earth Sciences. v67* **2012**.

172. Lasaga, A. C. Chemical kinetics of water-rock interactions. *Journal of Geophysical Research* **1984,** *89* (B6), 4009-4025.

173. Appelo, C. A. J.; Postma, D. *Geochemistry, Groundwater and Pollution*. Taylor & Francis: 2005.

174. Carroll, S. A.; Walther, J. V. Kaolinite dissolution at 25, 60, and 80 C. *Am. J. Sci* **1990,** *290* (7), 797-810.

175. Ganor, J.; Mogollón, J. L.; Lasaga, A. C. The effect of pH on kaolinite dissolution rates and on activation energy. *Geochimica et Cosmochimica Acta* **1995,** *59* (6), 1037-1052.

176. Pokrovsky, O. S.; Golubev, S. V.; Schott, J. Dissolution kinetics of calcite, dolomite and magnesite at 25° C and 0 to 50 atm pCO_2. *Chemical Geology* **2005,** *217* (3), 239-255.

177. Kumar, A.; Noh, M.; Pope, G.; Sepehrnoori, K.; Bryant, S.; Lake, L. In *Reservoir Simulation of CO_2 Storage in Deep Saline Aquifers*, SPE/DOE Symposium on Improved Oil Recovery, 2004.

178. Lu, J.; Kharaka, Y. K.; Thordsen, J. J.; Horita, J.; Karamalidis, A.; Griffith, C.; Hakala, J. A.; Ambats, G.; Cole, D. R.; Phelps, T. J. CO_2-rock-brine interactions in Lower Tuscaloosa Formation at Cranfield CO2 sequestration site, Mississippi, USA. *Chemical Geology* **2011**.

179. Kharaka, Y.; Cole, D.; Hovorka, S.; Gunter, W.; Knauss, K.; Freifeld, B. Gas-water-rock interactions in Frio Formation following CO_2 injection: Implications for the storage of greenhouse gases in sedimentary basins. *Geology* **2006,** *34* (7), 577-580.

180. Burnham, A. K.; Carroll, S. A. Carbon Sequestration in Depleted Oil Shale Deposits. U.S. Patent Application 13/121,550 September 30, 2009,

181. Tester, J. W.; Worley, W. G.; Robinson, B. A.; Grigsby, C. O.; Feerer, J. L. Correlating quartz dissolution kinetics in pure water from 25 to 625 C. *Geochimica et Cosmochimica Acta* **1994,** *58* (11), 2407-2420.

182. Nagy, K. Dissolution and precipitation kinetics of sheet silicates. *Reviews in Mineralogy and Geochemistry* **1995,** *31* (1), 173-233.

183. Chou, L.; Garrels, R. M.; Wollast, R. Comparative study of the kinetics and mechanisms of dissolution of carbonate minerals. *Chemical Geology* **1989,** *78* (3), 269-282.

184. Steefel, C., CRUNCH. *Lawrence Livermore National Laboratory, Livermore, CA* **2001**.

185. Ague, J. J.; Brimhall, G. H. Geochemical modeling of steady state fluid flow and chemical reaction during supergene enrichment of porphyry copper deposits. *Economic Geology* **1989,** *84* (3), 506-528.

186. Malmström, M.; Banwart, S.; Lewenhagen, J.; Duro, L.; Bruno, J. The dissolution of biotite and chlorite at 25 C in the near-neutral pH region. *Journal of Contaminant Hydrology* **1996,** *21* (1), 201-213.

187. Ueda, A.; Kato, K.; Ohsumi, T.; Yajima, T.; Ito, H.; Kaieda, H.; Metcalfe, R.; Takase, H. Experimental studies of CO_2-rock interaction at elevated temperatures under hydrothermal conditions. *Geochemical Journal* **2005,** *39* (5), 417-425.

188. Seyfried Jr, W.; Janecky, D.; Berndt, M. Rocking autoclaves for hydrothermal experiments, II. The flexible reaction-cell system. *Hydrothermal Experimental Techniques* **1987**, 216-239.

189. Bruker. TOPAS V3: General profile and structure analysis software for powder diffraction data. *Bruker AXS, Karlsruhe, Germany* **2005**.

190. Moore, D. M.; Reynolds Jr, R. C. *X-ray Diffraction and the Identification and Analysis of Clay Minerals*. Oxford University Press (OUP): 1989.

191. ASTM D5373-08. In *Standard Test Methods for Instrumental Determination of Carbon, Hydrogen, and Nitrogen in Laboratory Samples of Coal* West Conshohocken, PA, 2008.

192. International, A., ASTM D513-92(1996). In *Standard Test Methods for Total and Dissolved Carbon Dioxide in Water*, West Conshohocken, PA, 1996.

193. Maes, I. I.; Yperman, J.; Van den Rul, H.; Franco, D. V.; Mullens, J.; Van Poucke, L. C.; Gryglewicz, G.; Wilk, P. Study of coal-derived pyrite and its conversion products using atmospheric pressure temperature-programmed reduction (AP-TPR). *Energy & Fuels* **1995,** *9* (6), 950-955.

194. Burnham, A.; Bey, N. K.; Koskinas, G. In *Hydrogen Sulfide Evolution from Colorado Oil Shale*, ACS Symposium Series, ACS Publications: 1981; p 61.

195. Mao, S.; Duan, Z.; Hu, W. A vapor–liquid phase equilibrium model for binary CO_2–H_2O and CH_4–H_2O systems above 523K for application to fluid inclusions. *Journal of Supercritical Fluids* **2009,** *50* (1), 13.

196. Mandalaparty, P. Reaction Chemistry in Carbon Dioxide Sequestration. Dissertation, University of Utah, Salt Lake City, 2012.

197. Morgan, D. J.; Eslinger, E. V.; Eberl, D. D.; Karlinger, M. R. Chemistry of illite/smectite and end-member illite. *Clays and Clay Minerals* **1986,** *34* (4), 368-378.

198. Sakharov, B. A.; Lindgreen, H.; Salyn, A.; Drits, V. A. Determination of illite-smectite structures using multispecimen X-ray diffraction profile fitting. *Clays and Clay Minerals* **1999,** *47* (5), 555-566.

199. Xu, T.; Pruess, K.; Apps, J. In *Numerical Studies of Fluid-Rock Interactions in Enhanced Geothermal Systems (EGS) with CO_2 as Working Fluid*, Proceedings, Thirty-third Workshop on Geothermal Reservoir Engineering Stanford University, Stanford, California, January, 2008; pp 28-30.

200. Zhou, X.; Zeng, Z.; Liu, H. In *Laboratory Testing On Pierre Shale For CO_2 Sequestration Under Clayey Caprock*, 44th US Rock Mechanics Symposium and 5th US-Canada Rock Mechanics Symposium, 2010.